Abstract

Title: Can Polyamines be used to deliver chemotherapeutic drugs?

Author: Vicki Emms

The naturally occurring polyamines putrescine, spermidine and spermine are found in almost all living cells. They are crucial to cell viability and play a key role in proliferation. As cancer cells exhibit an upregulated polyamine transport system (PTS) polyamine-drug conjugates are potential cancer-selective chemotherapeutics. This thesis describes the synthesis and biological evaluation of a series of polyamine conjugated 1,2,3-pyridyl triazole transition metal complexes, and efforts to tune the photophysical properties of these complexes for use in confocal microscopy.

Cationic rhenium(I) tricarbonyl complexes with substituted pyridyl triazole ligands were synthesised to improve the performance of these probes for use in confocal microscopy. An electron withdrawing trifluoromethyl group significantly red-shifted the emission and increased the emission lifetime of the complexes with respect to the parent compound. A cationic rhenium spermine conjugate was found to have an IC_{50} of 7 μM cisplatin resistant A2780R ovarian cancer cells.

Cyclometallated iridium polyamine conjugates were readily taken up by A549 lung adenocarcinoma cells and accumulated in the mitochondria, but not by polyamine transport deficient A549R cells. Similar results were seen with H157 cells and the PTS deficient cell line H157R. A triethylene glycol iridium conjugate was taken up similarly in both cell lines lending further support to the notion that uptake of the polyamine conjugates occurs via the PTS. Although iridium complexes were well tolerated in the dark, illumination led to rapid cell death by apoptosis, and may have potential for photodynamic therapy

Acknowledgements

As they say “regret what you have done not what you haven’t” now I can no longer say that I regret not doing a PhD (I may just regret not doing it sooner!). So, I first extend my thanks to one of my former students Kirk for planting the seed of an idea in my head! I would also like to express my gratitude to Mark and Paul for taking me on, thanks for being there to guide me on my journey!

Many thanks are extended to Mick Lee for mass spec analysis, Dr Gerry Griffiths for the numerous VT NMRs (and training me how to run them) and Dr Vanessa Timmerman for assistance with NMR. Thanks also to Dr Meike Vogler for help with toxicity testing, and Dr Kees Straatman at the AIF for assistance with confocal microscopy. A special word of thanks goes out to Bob Cassero for sending us the polyamine resistant cell lines, and Lynne Howells and Tom Richards for helping me to get up and running with cell culture; a massive part of this work would not have been possible without your help.

Working in lab 2.14 has been a blast; thanks to all members past and present for all the fun times, I have made some truly special friends – love you guys xx

Finally, I would like to thank my family for supporting me every step of the way; especially Aaron for putting up with me you really do deserve a medal!

Thanks xx

Table of Contents

List of figures

Abbreviations

2PE: two photon excitation

Φ: quantum yield

Γ: emissive rate constant

λ: wavelength

τ: emission lifetime

µL: microlitre

µM: micromolar

µs: microsecond

ABC: ATP binding cassette

Abs: absorption

Ac-CoA: acetyl co-enzyme A

APAO: acetyl polyamine oxidase

ATP: adenosine triphosphate

AZ: antizyme

AZIn: antizyme inhibitor

AZIn: antizyme inhibitor

BEHSpm: bisethylhomospermine

BENSpm: bisethylnormspermine

BESpm: bisethylspermine

Boc: *tert*-butyloxycarbonyl

bpy: bipyridine

bq: benzoquinoline

btp: 2-(2-pyridyl)benzothiophene

cav-1: caveolin-1

CFSE: crystal field stabilisation energy

CHO: Chinese hamster ovary

CHO-MG: Chinese hamster ovary MGBG resistant

***cis*-DCBPR:** *cis*-dichlorobis(phenanthroline)rhodium(III)

CKDi: cyclin dependent kinase inhibitors

CLEM: correlative light-electron microscopy

CLL: chronic lymphocytic leukaemia

CLSM: confocal laser scanning microscopy

cm^{-1}: wavenumber

COSY: homonuclear correlation spectroscopy

C^N: cyclometallating ligand

CT: charge transfer

CuAAC: copper-catalysed Alkyne-Azide Cycloaddition

d: doublet

DAPI: 4',6-diamidino-2-phenylindole

DCA: dichloroacetate

DCM: dichloromethane

dcSAM: decarboxylated S-adenosyl methionine

dd: doublet of doublets

ddd: doublet of doublet of doublets

DFMO: α-difluoromethylornithine

DHS: deoxyhypusine synthase

DMSO: dimethylsulfoxide

dm: decimetre

DMF: dimethyl formamide

DOHH: deoxyhypusine hydrolase

dppz: dipyridophenazine

dt: doublet of triplets

ECM: extracellular matrix

EDG: electron donating

EDTA: ethylene diaminetetraacetic acid

eIF-5A: elongation factor eukaryotic translation initiation factor 5A

EM: electron microscopy

ER: endoplasmic reticulum

EtOAc: ethyl acetate

EtOH: ethanol

EWG: electron withdrawing

FCS: foetal calf serum

FLAP: fluorescence localisation after photobleaching

FLIM: fluorescence lifetime imaging

FLIP: fluorescence loss in photobleaching

FRAP: fluorescence recovery after photobleaching

Gpc-1: glypican-1

H_2SO_4: sulfuric acid

h: hour

hCE2: human carboxylesterase 2

HCl: hydrochloric acid

HDAC: Histone deacetylase

HDACi: Histone deacetylase inhibitor

HE: high energy

HEDP: hydroxyethylidine diphosphonate

HIF-1: hypoxia inducible factor-1

HMBC: heteronuclear multiple bond correlation

HOMO: highest occupied molecular orbital

HPLC: high performance liquid chromatography

HRMS: high resolution mass spectrometry

HS: heparan sulfate

HSPG: heparan sulfate proteoglycan

HSQC: heteronuclear single bond correlation

hTERT: human telomere reverse transcriptase protein

HYNIC-Spm: hydrazinonicotinamide-spermine

Hz: Hertz

I: intensity

ICP-MS: inductively coupled plasma mass spectrometry

IL: intra ligand

IL-2: interleukin-2

ILCT: intra-ligand charge transfer

IR: infrared

ISA: imidazole-1-selfonyl azide

ISC: intersystem crossing

K_2CO_3: potassium carbonate

Kir: inward rectifier potassium

k_{nr}: non radiative decay constant

LC: ligand centred

LE: lower energy

LLCT: ligand to ligand charge transfer

LTR: LysoTracker

LUMO: lowest unoccupied molecular orbital

M: molar

m: multiplet

MANT: N-methyl anthranilic acid

MAPK: mitogen activated protein kinase

MATE1: multi drug and toxin extrusion protein 1

MC: metal centred

MeOH: methanol

MGBG: methylgloxal bisguanyl hydrazone

mins: minutes

mg: milligram

mL: millilitre

mM: micromole

ms: microsecond

MLC: metal ligand complexes

MLCT: metal to ligand charge transfer

MLLCT: metal to ligand to ligand charge transfer

MMP: matrix metalloproteinase

MMP: mitochondrial membrane potential

mol: moles

mRNA: messenger RNA

ms: milliseconds

MS: mass spectrometry

MTA: 5'-deoxy,5'-methylthioadenosine

MTT: (3-(4,5-dimethylthiazol-2-yl)-2,5-diphenyl tetrazolium bromide

m/z: mass to charge ratio

$NaHCO_3$: sodium hydrogen carbonate (bicarbonate)

NIR: near infrared

nm: nanometres

NMDA: N-methyl-D-aspartate

NMR: Nuclear magnetic resonance

N^N: diimine ligand (also referred to as bisimine)

NO: nitric oxide

NOS: nitrogen oxide synthase

NOS2: nitric oxide synthase 2

ns: nanoseconds

NSCLC: non-small cell lung cancer

OCT1: Organic cation transporter 1

OCT2: Organic cation transporter 2

ODC: ornithine decarboxylase

PA/PAs: polyamine

PACT: photoactivated chemotherapy

PALM: photoactivated localisation microscopy

papy: *para*-anisyl pyridine

PBS: phosphate buffered saline

PDT: photodynamic therapy

PEG: polyethylene glycol

phen: phenanthroline

photoCORMs: photoactivated CO releasing molecules

PI3K-Akt: phosphatidylinositol 3-kinase protein kinase B

PIP2: phosphatidylinositol biphosphate

PLIM: phosphorescence lifetime imaging

$P(OEt)_3$: triethyl phosphite

ppy: phenyl pyridine

pRb: retinoblastoma protein

PS: photosensitiser

PSF: point spread function

PTIs: polyamine transport inhibitor

PTM: post-translational modification

PTS: polyamine transport system

pyta: pyta pyridyl triazole

Put: Putrescine

pyta: pyridyl triazole

RME: receptor mediated endocytosis

q: quartet

quin: quintet

ROS: reactive oxygen species

RP-HPLC: reverse phase HPLC

RuAAc: ruthenium-catalysed alkyne-azide cycloaddition

SAM: S-adenosyl methionine

SAMdc: S-adenosyl methionine decarboxylase

SMO: Spermine oxidase

SOC: spin orbit coupling

Spd: spermidine

Spd-BODIPY: spermidine boron-dipyrromethene-spermidine conjugate

SPDS: spermidine synthase

SPECT: Single photon emission computed tomography

Spm: spermine

SPMS: spermine synthase

SRM: super resolution microscopy

SSAT: spermine/spermidine acetyl transferase

STED: stimulation electron depletion

STORM: stochastic optical reconstruction microscopy

t: triplet

td: triplet of doublets

tt: triplet of triplets

Tapy: inverse click ligand

TCSPC: time correlated single photon counting

TEA: triethylamine

TEG: triethylene glycol

TEM: transomssion electron microscopy

TFA: trifluoroacetic acid

TGF-β: transforming growth factor-β

THF: tetrahydrofuran

TMS: tetramethyl silane

TPA: two photo absorption cross section

TPP: triphenylphosphonium

TsCl: tosyl chloride

UV: ultraviolet

Compound Index

Proligands

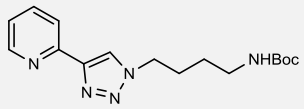

149 BocPut pyta

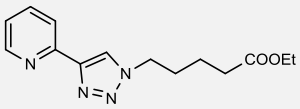

150 COOEt pyta

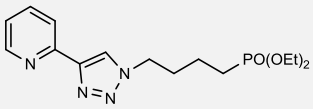

151 $PO(OEt)_2$ pyta

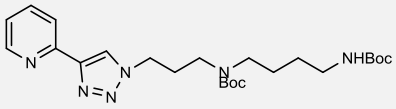

154 AP-BocPut pyta

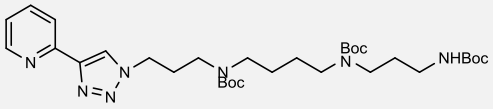

155 BocSpm pyta

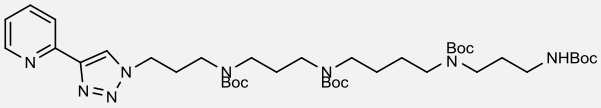

156 AP-BocSpm pyta

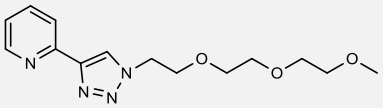

152 PEG pyta

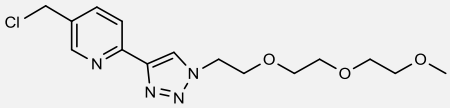

153 ClMe-PEG pyta

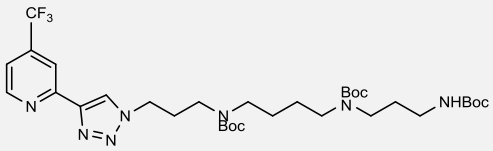

158 $4CF_3$-BocSpm pyta

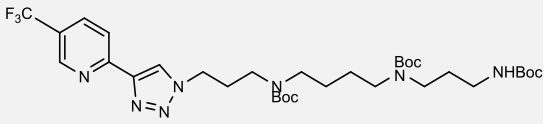

157 $5CF_3$-BocSpm pyta

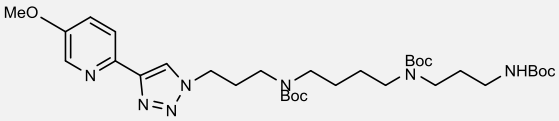

159 5OMe-BocSpm pyta

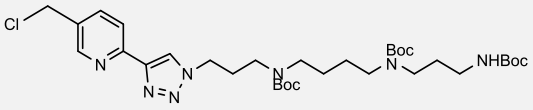

160 5ClMe-BocSpm pyta

ClRe(N^N')CO_3

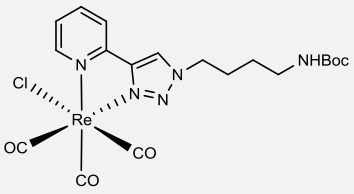

162 BocPut ClRe

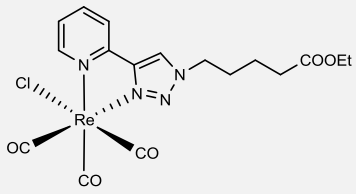

163 COOEt ClRe

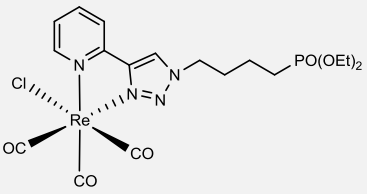

164 $PO(OEt)_2$ ClRe

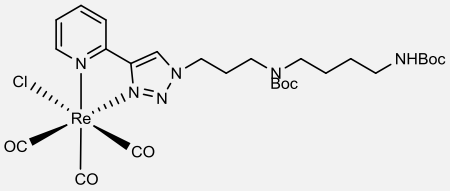

165 AP-BocPut ClRe

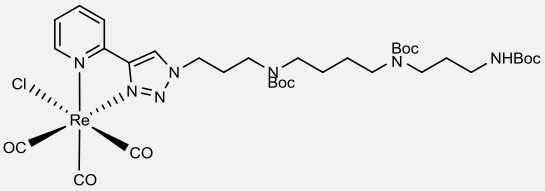

166 BocSpm ClRe

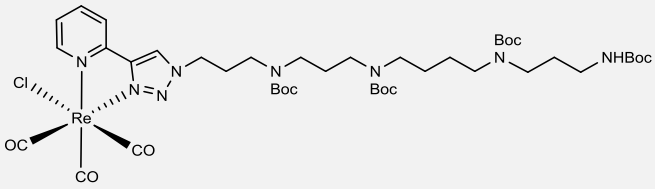

167 AP-BocSpm ClRe

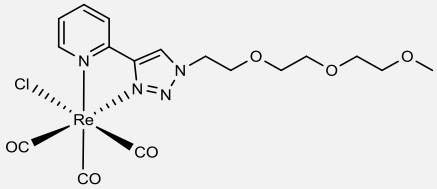

168 PEG ClRe

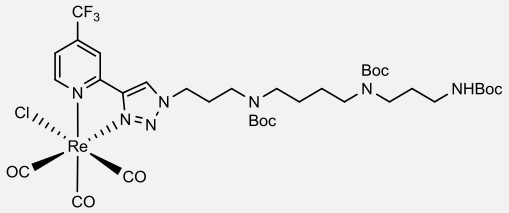

169 $4CF_3$-BocSpm ClRe

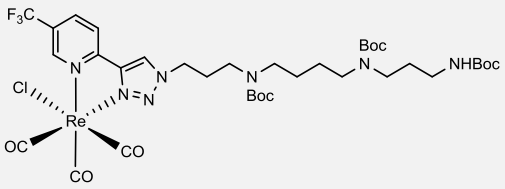

170 $5CF_3$-BocSpm ClRe

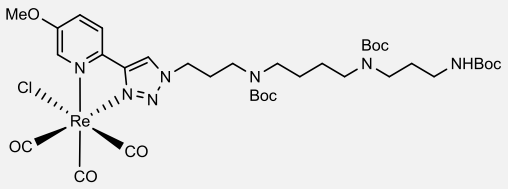

171 5OMe-BocSpm ClRe

$[PyRe(N\hat{}N')CO_3]^{n+}$

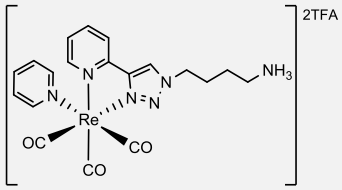

111 Put pyRe

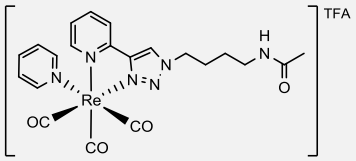

112 AcPut pyRe

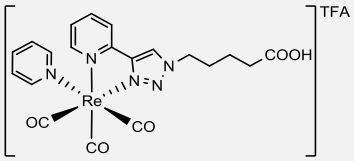

113 COOH pyRe

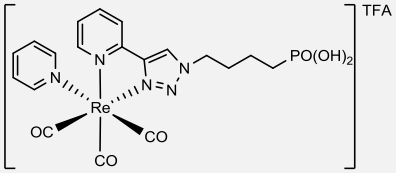

114 $PO(OH)_2$ pyRe

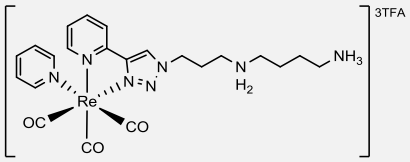

125 AP-Put pyRe

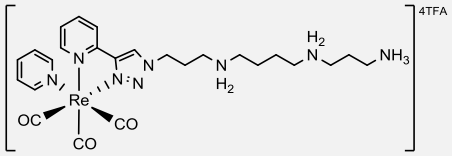

119 Spm pyRe

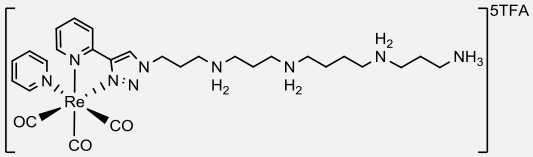

126 AP-Spm pyRe

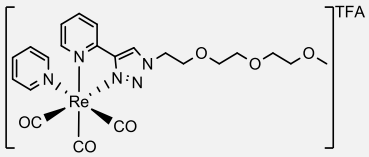

139 PEG pyRe

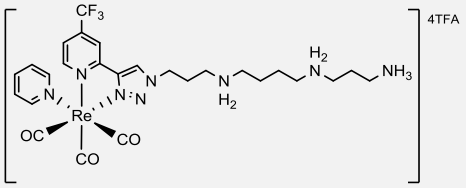

131 $4CF_3$-Spm pyRe

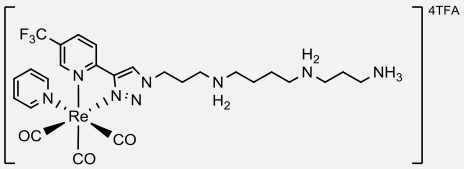

130 $5CF_3$-Spm pyRe

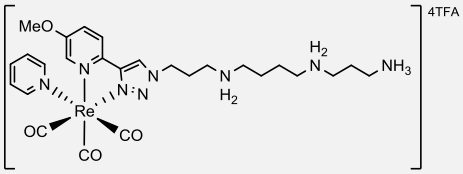

129 5OMe-Spm pyRe

Pt (N^N') $(Cl)_2$

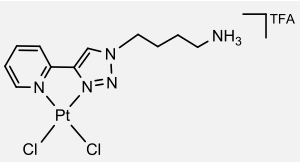

172 $PtCl_2$-Put

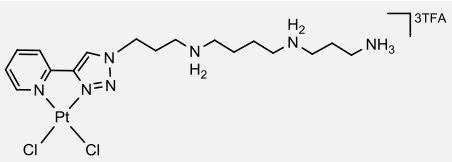

173 $PtCl_2$-Spm

$[Ir(C^N)_2(N^N')]^{n+}$

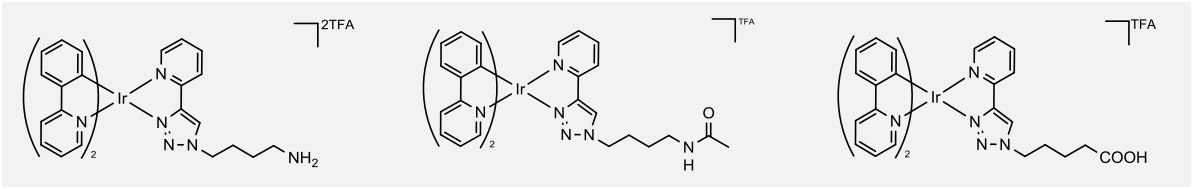

115 Ir-Put **116** Ir-AcPut **117** Ir-COOH

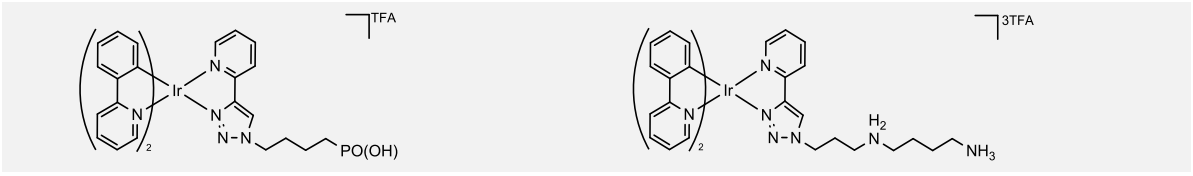

118 Ir-$PO(OH)_2$ **127** Ir-APPut

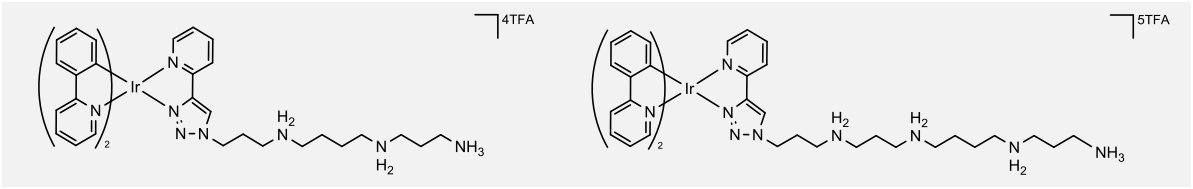

123 Ir-Spm **128** Ir-APSpm

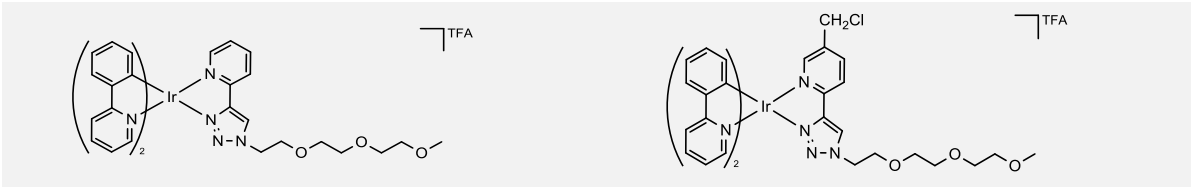

140 Ir-PEG **147** 5-ClMe-IrPEG

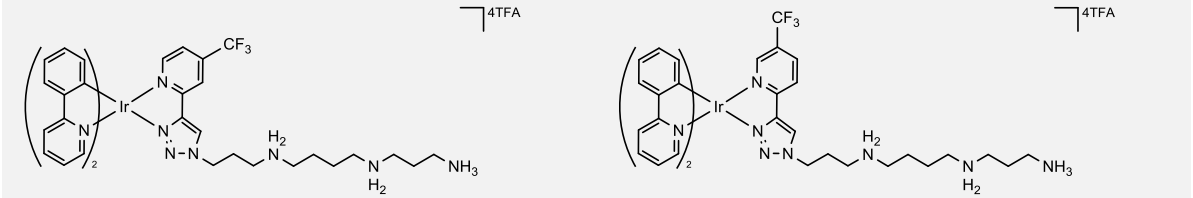

134 $4CF_3$-IrSpm **133** $5CF_3$-IrSpm

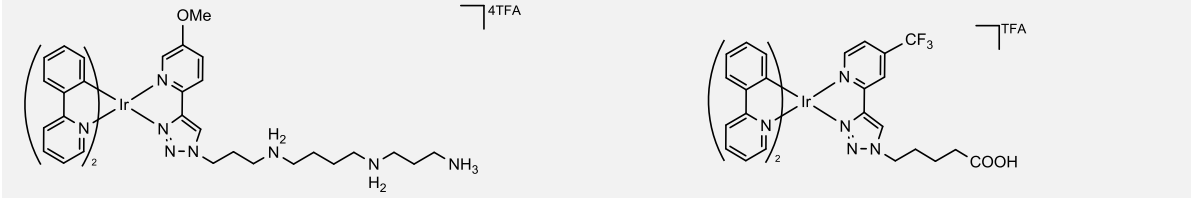

132 5OMe-IrSpm **174** $4CF_3$-IrCOOH

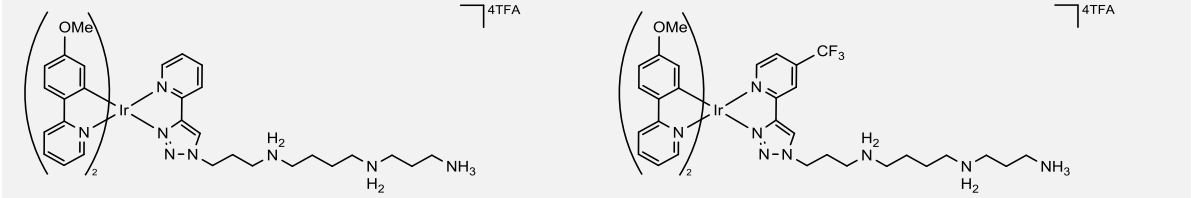

135 Ir$(papy)_2$Spm **136** Ir$(papy)_2$ $4CF_3$-Spm

Chapter 1 : Introduction

This thesis investigates the feasibility of using polyamines as a cancer specific vector for transition metal complexes. There are many examples in the literature of small organic molecules tethered to polyamines, however this approach has had limited application in the realm of bioinorganics. In this chapter, section 1.1 introduces some of the key features of polyamine biochemistry with a particular focus on their transport and their role in cancer progression, section 1.2 gives a brief snapshot of current research using luminescent metal complexes for cellular imaging whilst sections 1.3, 1.4 and 1.5 discuss therapeutic applications.

1.1: Polyamines

Polyamines are found in millimolar concentrations in almost every living cell. They are crucial to cell viability being required for growth and proliferation.[1] Mammalian cells contain the diamine precursor putrescine (**1**) from which the polyamines spermidine (**2**) and spermine (**3**) are derived, whereas polyamines (**5**)–(**9**) with alternative carbon frameworks may be found in other organisms such as thermophiles and archaea.[2] Putrescine (**1**) and the related compound cadaverine (**4**) were first identified in rotting flesh in 1885 by Ludwig Brieger,[3] and Rosenheim and co-workers isolated the phosphates of spermidine (2) and spermine(3) in the mid-1920s.[4,5,6]

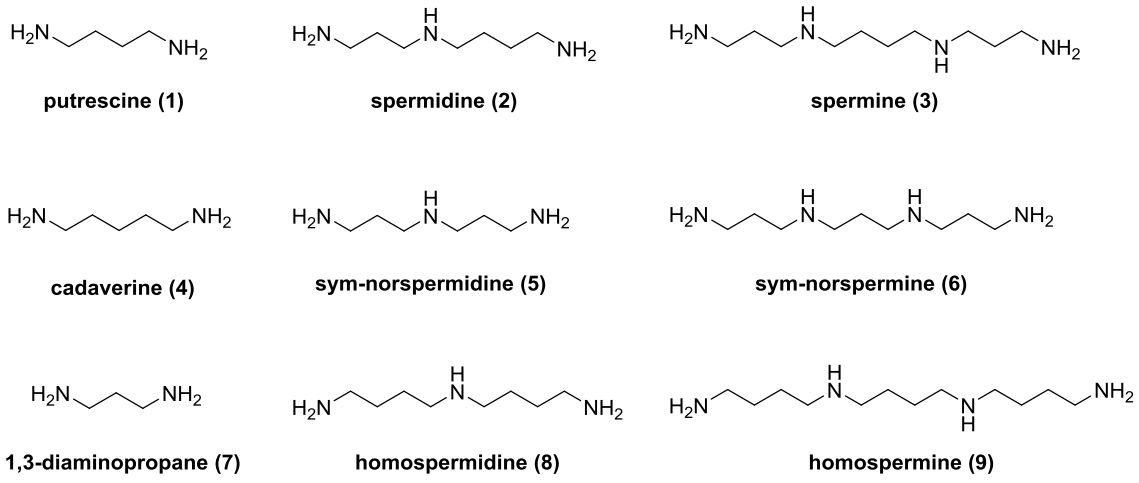

Figure 1.1: *Chemical structures of biogenic polyamines.*

1.1.1: Biological roles of the polyamines

Herbst and Snell demonstrated that putrescine was necessary for growth of *Hemophilus parainflenzae* cultures.[7] Several years later this effect was also shown to extend to mammalian cells in culture.[8] Polyamines are polycations at physiological pH as indicated by the pK_a values shown in Figure 1.2, and therefore interact with anionic macromolecules such as nucleic acids, phospholipids and proteins. Electrostatic interactions of polyamines with macromolecules can account for many of the observed effects of polyamines.[9]

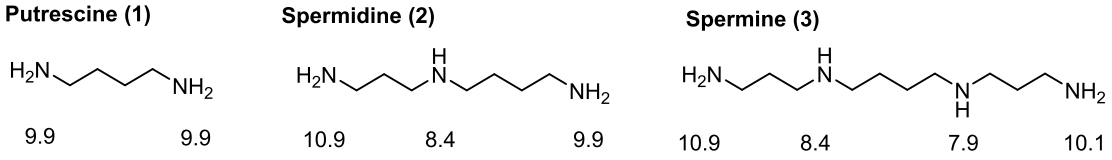

***Figure 1.2**: pKa values of the mammalian polyamines.*

Polyamines act as multivalent counterions for DNA and RNA. Spermine is highly effective at minimising repulsion between phosphate groups,[10] and can promote the transition of B-DNA to Z-DNA at micromolar concentrations.[11] This is thought to be significant for the recruitment of transcription factors.[12] Spermine also plays an important role in condensing DNA and chromatin.[13] The vast majority (around 90 %) of the cellular polyamines are found as a polyamine-RNA complex with around 1-4 equivalents of polyamine being associated per 100 equivalents of RNA phosphate.[14] Polyamine interactions with RNA have important downstream effects on gene expression and protein synthesis, imposing a regulatory effect on protein synthesis.

Protein synthesis is also affected by polyamines at the level of translation. Polyamines bind to Shine-Dalgarno sequences in mRNA to enhance translation of inefficient codons, stimulate ribosome shunting and enhancing codon read-through and frameshifting.[15] The set of genes whose translation is modified in the presence of polyamines are collectively known as the "polyamine modulon" many of which have been shown to play significant roles in cellular growth and viability.[16] Cellular polyamines

may also influence epigenetic control of gene transcription via their effects on key enzymes involved with chromatin remodelling.[17–20]

The ubiquitous elongation factor eukaryotic translation initiation factor 5A (eIF-5A) stimulates mRNA translation and promotes formation of difficult peptide bonds,[21] and is activated by a spermidine-dependant post-translational modification (PTM). Hypusine (**10**) formation activates eIF-5A and occurs in two enzymatically controlled steps, as shown in Figure 1.3. Deoxyhypusine synthase (DHS) transfers an aminobutyl moiety from spermidine (from here on in referred to as Spd) to the amino group of the lysine side chain which is subsequently hydroxylated by deoxyhypusine hydrolase (DOHH).[22] This protein is the only biological target activated in this way, and has been identified as a putative oncogene as it is commonly over expressed in a range of cancers.[23]

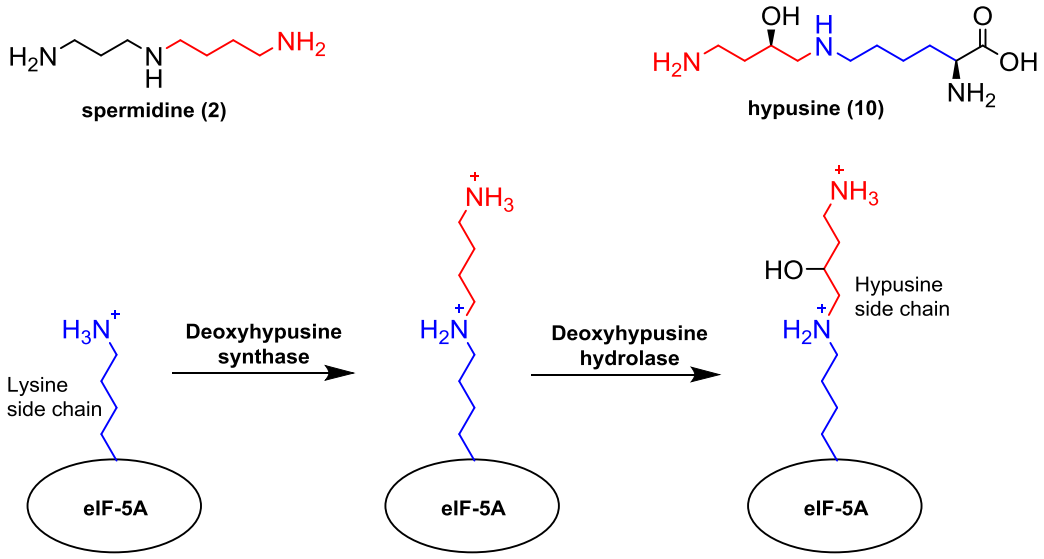

***Figure 1.3**: Biosynthesis of the unusual basic amino acid hypusine.*

Polyamines (PAs) can associate with phospholipids and stabilise membranes by minimising repulsive charges between phosphate groups in the lipid bilayer,[24,25] and promote the association of membrane bound proteins.[26] They have also been proposed to affect intracellular signalling processes via interactions with phosphatidylinositol bisphosphate (PIP2).[27] Spermine (3) which will be referred to as Spm here on in is a potent channel gating molecule for strong inward rectifier potassium (Kir) channels,[28] an allosteric modulator of the ligand gated N-methyl-D-aspartate (NMDA) receptor,[29] an

inhibitor of Ca^{2+} permeable non-NMDA glutamate receptors,[30] and can stimulate mitochondrial Ca^{2+} uptake.[31] Kinase activity is also modulated by polyamines.[32–35] Polyamines also facilitate polymerisation of microtubules and actin filaments, which both play key roles in intracellular trafficking, cell motility and migration.[36,37]

From this snapshot of the literature documenting the numerous cellular functions polyamines, it is easy to appreciate why normal cells are so heavily dependent upon polyamines for growth. In addition to their fundamental role in sustaining growth and proliferation. They have also been implicated in many additional cellular functions which, when aberrantly controlled may contribute to the progression towards a malignant phenotype.

1.1.2: Polyamine metabolism

Given their fundamental roles in the cell it is paramount that intracellular polyamine pools are stringently maintained. This is achieved via intricately balanced biosynthesis, degradation, uptake and efflux mechanisms. Polyamine metabolism and transport are highly interdependent.[38] Polyamine influx and efflux are sensitive to cellular levels of PAs and their metabolites, and there is also evidence to suggest that levels of some of the enzymes involved in polyamine metabolism exert a regulatory effect on polyamine transport.[39] Polyamine metabolism is complex; it is responsive to the cellular concentration of polyamines and may be further modulated by external signals such as hormones to exert homeostatic control. The key steps of polyamine metabolism are shown in Figure 1.4.

Several inhibitors of enzymes associated with polyamine metabolism have been developed as potential cancer drugs. As ornithine decarboxylase (ODC) is the critical rate limiting enzyme of polyamine biosynthesis the irreversible inhibitor α-difluoromethylornithine (DFMO) (**13**) was designed as an antiproliferative drug. Unfortunately, it lacked therapeutic efficacy presumably due to the upregulation of compensatory pathways. Nevertheless, it has proven to be an extremely useful research tool to probe polyamine mediated events.[40]

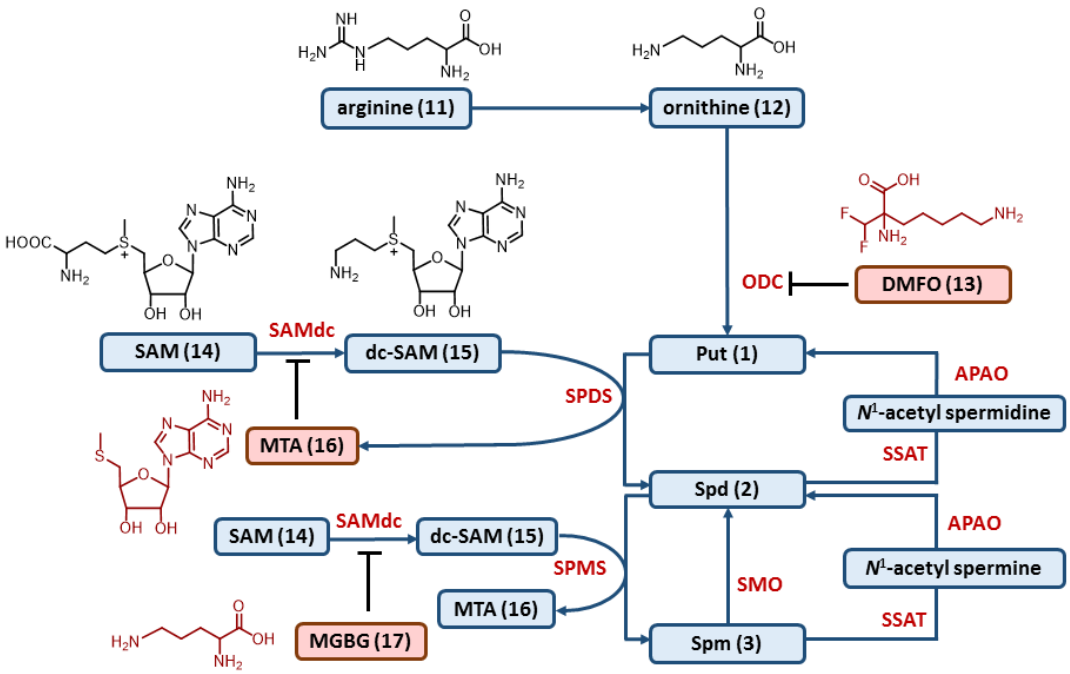

***Figure 1.4**: An overview of polyamine metabolism showing the key intermediates and the enzymes involved in biosynthesis and catabolism. ODC = ornithine decarboxylase, SPDS = spermidine synthase, SPMS = spermine synthase, APAO = acetyl polyamine oxidase, SSAT = Spermine/spermidine acetyl transferase, SMO = spermine oxidase, DMFO (**13**) (efluorithine) the suicide inhibitor of ODC. S-adenosyl methionine (SAM) (**14**), decarboxylated S-adenosyl methionine (dcSAM) (15), 5'-deoxy,5'-methylthioadenosine (MTA) (**16**) and SAMdc inhibitor MGBG (**17**) (mitoguazone).*

S-adenosyl methionine (SAM) (**14**) has a unique role in polyamine biosynthesis as a source of propylamine for the aminopropyl transferase enzymes and is shown in figure 1.4. The enzyme S-adenosyl methionine decarboxylase (SAMdc) catalyses formation of decarboxylated S-adenosyl methionine (dcSAM) (**15**),[41] and the by-product 5'-deoxy,5'-methylthioadenosine (MTA) (**16**) has moderate inhibitory activity and acts as a feedback control mechanism for these enzymes.[42] The SAMdc inhibitor methylglyoxal bisguanyl hydrazone (MGBG) (**17**) was also designed as a cancer drug.[43] Unfortunately it was found to be inefficient in clinical applications and significantly toxic,[44] however it is frequently used in research to probe polyamine transport and synthesis.

Spermine/spermidine acetyl transferase (SSAT) is the major regulatory enzyme in the catabolism of the polyamines as shown in figure 1.4.[45] The SSAT gene contains a polyamine response element (PRE) and its expression is upregulated at higher polyamine concentrations.[46] SSAT influences polyamine export as acetylated polyamines can be transported out of the cell via an efflux pump. As can be seen in figure 1.4, N^1-acetylpolyamines are also substrates for the degradative enzyme acetyl polyamine

oxidase (APAO). The fate of acetylated polyamines is regulated by the growth status of the cell; when cells are actively growing spermine is recycled, however when growth is restricted, acetylated polyamines (and synthetic polyamine analogues) are excreted.[47,48]

APAO is structurally and functionally similar to HDACs.[49] APAO oxidizes acetylated polyamines producing hydrogen peroxide and 3-acetamidopropanal.[45] The related enzyme spermine oxidase (SMO) regenerates Spd (as shown in figure 1.4) producing hydrogen peroxide and 3-aminopropanal as by-products. SMO significantly reduces Spm levels in the cell, which can lead to up-regulation of ODC. SMO expression is markedly increased in neoplasia and can be induced by Spm and spermine analogues. Polyamine analogues are poor substrates of SMO and act as competitive inhibitors.[50]

1.1.3: Polyamine transport

Polyamine metabolism is controlled by many levels of feedback which ensures polyamines are maintained at optimum cellular concentrations. Polyamine metabolism directly impacts polyamine transport and polyamine homeostasis is incredibly robust, maintaining a cellular polyamine concentration of approximately 1 mM. Spd and Spm have a similar affinity for the PTS, with a K_m of around 1 µM compared to putrescine (which will be referred to as Put from here on in) which has an affinity of around 10 µM. The PTS is a high velocity transporter and has the capacity to accumulate 5 nmol Spd or Spm per 10^6 cells per hour. This can effectively double cellular polyamine concentration in this timeframe.[51]

However, the precise mechanism by which the transporter operates remains somewhat elusive. Polyamines are cationic species and unlikely to permeate the membrane unaided. Several uptake mechanisms have been proposed in the literature, but it is highly likely that mammalian polyamine transport occurs by more than one mechanism.[52] Polyamine transport proteins have been isolated from yeast and bacteria, but as yet a mammalian homologue has not been identified.[53] The majority of evidence points to endocytosis as the major mode of polyamine transport in mammalian cells.

Early studies on the PTS determined that polyamine uptake is energy dependant and saturable, implying a carrier-mediated uptake mechanism.[54] The primary amino

group was shown to be critical to uptake.[55] The transporter was found to be surprisingly non-specific; not only can it transport a wide variety of structural analogues, but also seemingly unrelated structures such as paraquat. [56]

Aziz *et al.* were the first to report the use of fluorescent polyamine conjugates to probe polyamine uptake using confocal laser scanning microscopy (CLSM).[57] Mono-fluorescein polyamine adducts were used to probe uptake in smooth muscle cells. The probe was internalised with similar kinetic parameters to non-derivatised polyamines. Fluorescence was confined to discrete "islands" in the cytoplasm, proposed to be mitochondria. In a similar study Cullis *et al.* used site-specifically functionalised N^4-spermidine *N*-methyl anthranilic acid (MANT) (**18**).[58] Compound **18** accumulated in granular structures in the cytoplasm that colocalised with the endosomal marker Lucifer yellow (**19**), consistent with uptake via receptor mediated endocytosis (RME).[59]

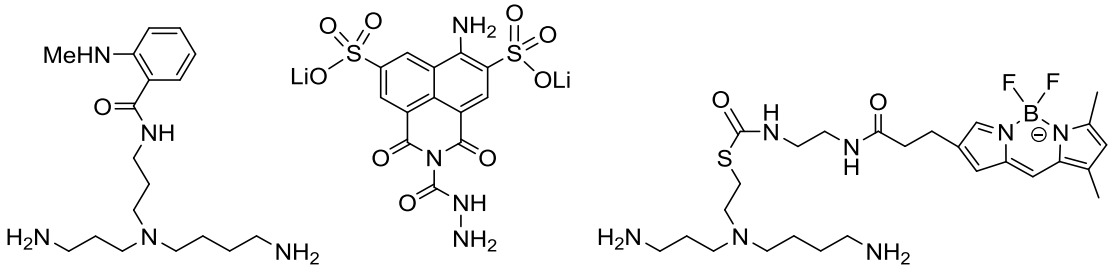

18 **19** **20**

***Figure 1.5**: Some fluorescent probes used to study uptake by the PTS, Spd-MANT (**18**), endosomal marker Lucifer Yellow (**19**) and Spd-BODIPY (**20**).*

Soulet and co-workers followed up this study using a fluorescent boron-dipyrromethene-spermidine conjugate (Spd-BODIPY) (**20**) as shown in figure 1.5 to probe uptake in RME deficient Chinese hamster ovary (CHO) cells. As the probe was taken into the cell despite the deficiency of RME they proposed that transport occurred by active transport of the conjugate via a membrane carrier followed by sequestration into acidic vesicles by a proton-dependent membrane pump, as shown in figure 1.6.

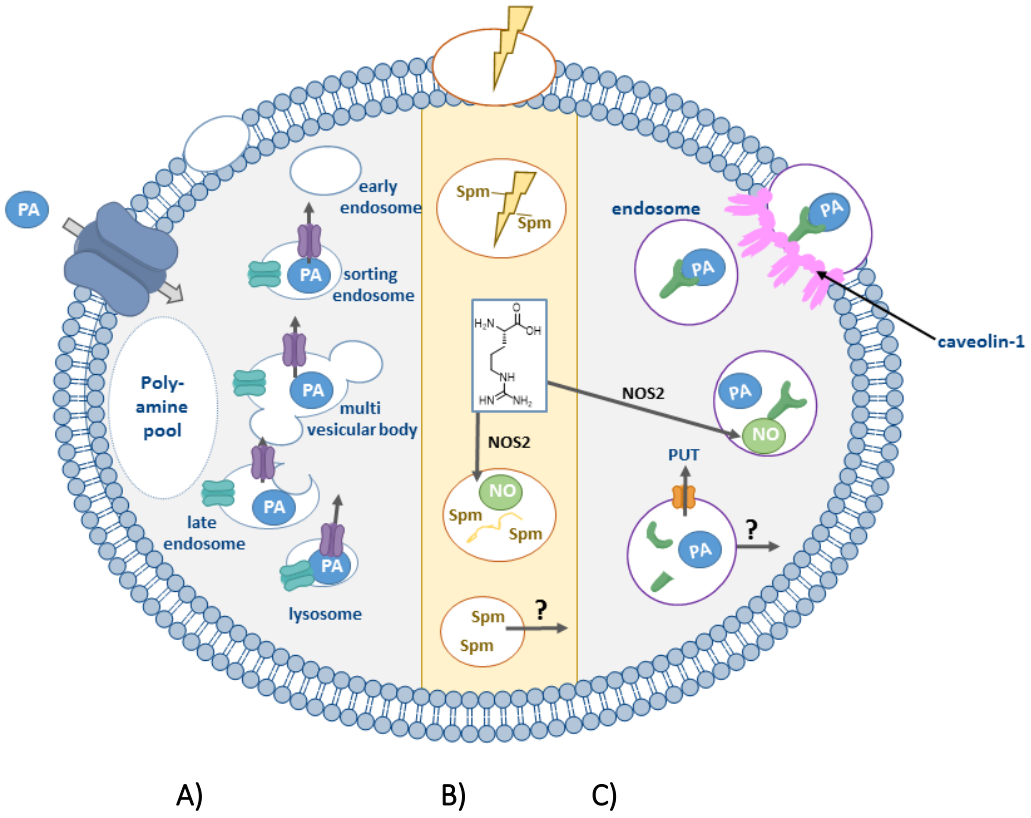

***Figure 1.6**: The proposed theories to explain experimental observations of polyamine transport in mammalian cells (adapted from Casero et al.[40]) A) Soulet's two-step mechanism of polyamine uptake and sequestration. B) Belting's glypican mediated endocytosis and C) Gerner's proposed model of uptake by caveolin mediated endocytosis.*

An alternative mechanism was proposed by Belting and co-workers, who showed that glypican-1 (Gpc-1) and nitric oxide (NO) are critical for polyamine uptake.[60] Gpc-1 is a glycosylphosphatidylinositol anchored cell-surface heparan sulfate proteoglycan (HSPG) that localises to lipid rafts and caveolae. Polyamines bind to anionic sulfate groups and are internalised by caveolar endocytosis. In response to polyamine depletion, cells synthesise a form of glypican with enhanced affinity for spermine.[61] Release of NO in the endosome cleaves the HS polyamine binding sites, liberating polyamines. Gerner *et al.* corroborated these findings using nitric oxide synthase 2 (NOS2) deficient mice, demonstrating a clear role for NO in gastrointestinal uptake of Put.[62]

Gerner *et al.* subsequently demonstrated that the uptake of polyamines occurs by caveolar endocytosis.[42] Spd uptake was found to be both energy and dynamin dependant, but also inhibited by Brefeldin A (an inhibitor of endocytosis). Upon treatment with methyl-β-cyclodextrin (an inhibitor of caveolar endocytosis) polyamine uptake was substantially reduced. Furthermore, polyamines were also found to associate

with the lipid raft cell fraction and showed similar uptake to cholera toxin which is known to be internalised by caveolar endocytosis. Taken together these findings strongly support a role for caveolar endocytosis in polyamine uptake.

Caveolae ("little caves") are flask-shaped invaginations of the cell membrane composed of lipid rafts with associated caveolin and cavin proteins.[63,64] The precise mechanism of caveolar endocytosis has not been well defined, but it is believed that Src kinase signalling triggers depolymerisation of the actin filaments that anchor the vesicle to the cytoskeleton and recruits dynamin leading to vesicle budding and internalisation upon ligand binding, as shown in figure 1.7.[65,66] A K-RAS dependant increase in cav-1 phosphorylation by Src kinase leads to a substantial increase in polyamine uptake. This is abrogated upon Src kinase inhibition and provides a causal link to the upregulation of polyamine transport by the *K-Ras* oncogene.[42] Src activity is also modulated by polyamines.[67]

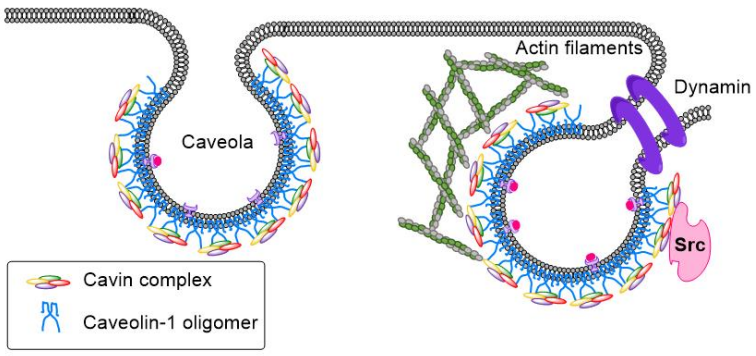

***Figure 1.7**: Structural features of caveolae (Adapted from Bastiani & Parton.[65])*

Several polyamine transporter proteins have been identified in yeast and bacteria yet only limited evidence points to polyamine transport by membrane proteins in mammalian cells.[68] The *E. coli* polyamine transporter PotE is a bidirectional Put transporter.[69] Put uptake is proton gradient-dependent whilst efflux occurs as a result of putrescine/ornithine antiporter activity.[70] In the gastrointestinal tract Put and acetylated polyamines (PAs) can be transported by the solute carrier SLC3A2 in exchange for arginine.[52] At low internal and high external Put concentrations, SLC3A2 can transport Put into the cell, and is a plausible explanation for polyamine uptake from gut flora and dietary sources.

Organic cation transporter OCT1 is a sodium independent transporter that has been linked to the membrane potential dependent transport of PAs in rats.[71] OCT2 and multi drug and toxin extrusion protein 1 (MATE1) can also transport PAs.[72,73] L-carnitine transporter hCT2 has also been linked to polyamine transport as both uptake and sensitivity to the Bleomycin-A5 polyamine conjugate (**21**) (shown in figure 1.8), is dependent on its expression levels. Testicular cancer cells strongly expressing hCT2 are more sensitive to **21**, whilst hCT2-knockdown suppresses the genotoxic effect of **21**.[74]

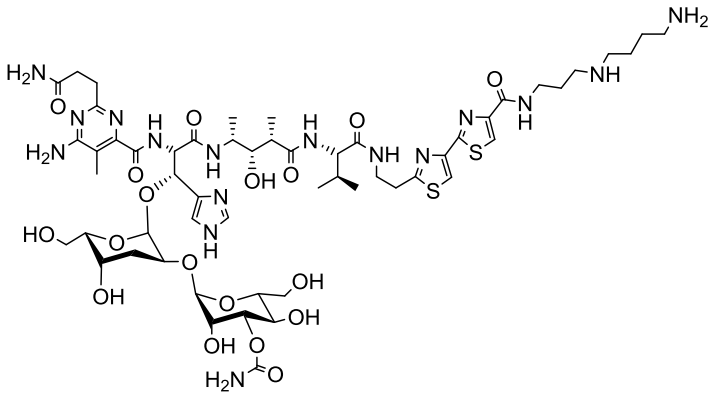

Figure 1.8: *Bleomycin-A5 (21) a polyamine conjugated glycopeptide.*

ATP binding cassette (ABC) transporters are proton pumps that utilise conformational changes fuelled by ATP to transport a single species across the membrane against the concentration gradient. Whilst no human ABC transporters with polyamine transport capabilities have been identified, two polyamine transporters belonging to the ABC family have been discovered in *E. coli*. PotD is a polyamine transporter with a substrate preference for Spd, whilst PotF is Put-specific.[69]

Despite a long history of research to discern the precise nature of the PTS there remain many unanswered questions. To date the most significant data points towards cavelolar endocytosis as the major route by which polyamines can be internalised by mammalian cells. Uptake is saturable and energy dependent. It is regulated by intracellular PA levels and largely independent of amino acid uptake although evidence suggests there is more than one mechanism of uptake. Uptake is stimulated by polyamine depletion and increases during hormonal stimulation and proliferation; however, during differentiation, uptake decreases, and it can be repressed at high PA

levels by antizyme (AZ). Polyamine efflux is repressed by an active PTS; however, when growth is restricted Spd efflux occurs.

1.1.4: Polyamine analogues.

Much of our understanding of the workings of the PTS has come from studies of cellular uptake of polyamine analogues. The precise spacing of point charges is paramount to recognition by the PTS; uncharged analogues are poor substrates of the PTS.[75] Substrates must contain at least two cationic centres separated by a four-carbon chain to be recognised by the PTS; the Put motif is the minimum requirement for polyamine transport. Additional cationic centres spaced by a minimum of three methylene units enhances affinity; Spm and Spd have an approximately ten-fold higher affinity for the PTS compared to Put.[76]

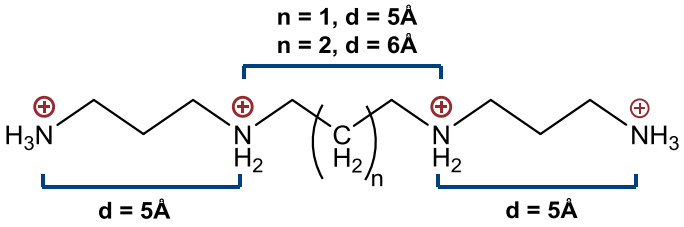

***Figure 1.9**: Charge spacings of polyamines; natural polyamines are separated by either a 3- or a 4-methylene bridge, which corresponds to 5 or 6 Å. Analogues with a charge separation corresponding to 7 methylene units may still be recognised as substrates for the PTS.*

Bisethylnormspermine (BENSpm) (**22**), bisethylspermine (BESpm) (**23**), and bisethylhomospermine (BEHSpm) (**24**) (shown in figure 1.10) are commonly used polyamine analogues.[77] Bergeron and co-workers have carried out extensive surveys of polyamine analogues in relation to their size, charge, and toxicity.[55,77–79.] It has been found that uptake of polyamine analogues is sensitive not only to the architecture of the carbon backbone but also to the size of the cargo with larger appended groups tending to reduce cellular uptake. Due to the inequivalence of the terminal amine groups, the uptake of Spd analogues is sensitive to the effect of adding N-terminal substituents. N^1-alkylspermidines show greater activity (with regards to depleting cellular polyamines) compared to their N^8-counterparts. N^1-substituted analogues can persist in the cell as they are substrates for spermine synthase and can undergo chain elongation to form N^1-spermine analogues, whereas the N^8-analogues are degraded. Whilst spermine and non-

biogenic tetraamines tend to have a greater affinity for the PTS, and are most effective at reducing the polyamine pool, Spd conjugates accumulate in the cell to a greater extent, and show a greater duration of action in perturbing polyamine homeostasis.[80]

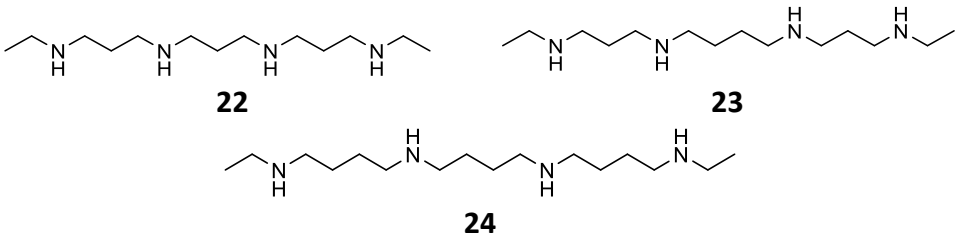

***Figure 1.10**: Bisethyl tetraamine analogues, (**22**) bisethylnorspermine (BENSpm), (**23**) bisethylspermine (BESpm) and (24) bisethylhomospermine (BEHSpm).*

Phanstiel *et al.* examined the effect of the carbon framework on uptake using fluorescent N^1-monosubstituted anthracene polyamine transport inhibitors (PTIs exemplified by compounds 25 and 26 shown in figure 1.11. [81] The polyamine transporter showed greatest affinity for the homospermine analogue 25 and hence was expected to be the most toxic; surprisingly the triamines were found to be more potent. Uptake of 26 was rapid, with significant incorporation of the homospermidine conjugate in just three minutes, however compound 25 was found to be predominantly bound to the membrane, explaining its lack of toxicity. Combination of the biosynthesis inhibitor DMFO and the trimeric homospermidine PTI 27 lead to a 30% reduction in growth of human pancreatic cancer cells over a 48 hour period.[80]

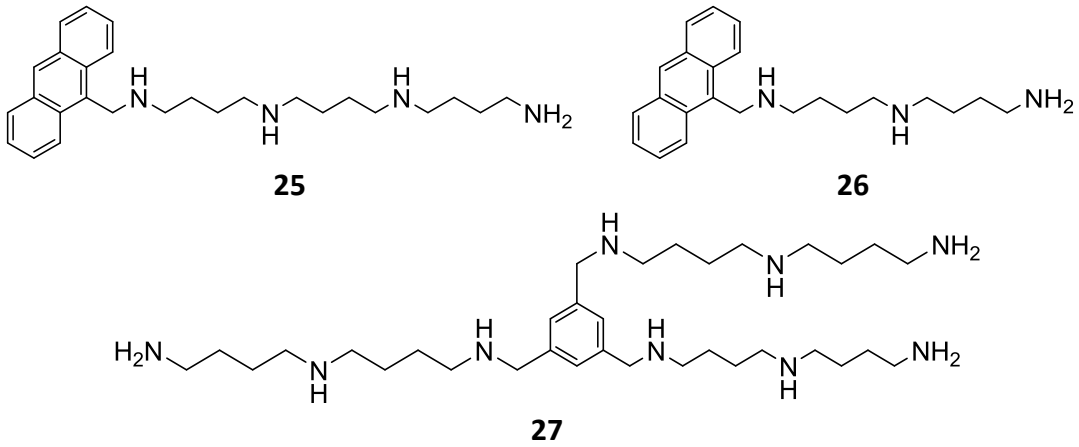

***Figure 1.11**: Polyamine conjugates based upon homospermine and homospermidine.*

Indocyanine green has been approved for clinical use for image-guided surgery, angiography and lymph node imaging.[82] A near-infrared fluorescent polyamine

conjugate of indocyanine green (28) was designed for use as a live cell probe for cancer cells (Figure 1.12). Cancer cell lines showed significant uptake of the probe, whilst non-cancer cells showed minimal accumulation. Toxicity was measured after 24 h and found to be in the low micromolar range. A derivative with the polyamine chain tethered via the sulfonyl group showed no discrimination between cancer cells and normal cells, which serves to illustrate that the point of attachment of polyamines to a molecule to achieve cancer cell specific uptake is not trivial.

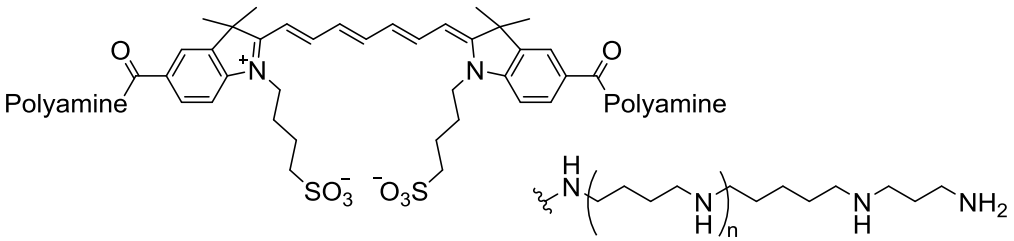

28

***Figure 1.12**: Near IR indocyanine green polyamine probe (**28**)*

1.1.5: Polyamines as drug vectors

The PTS is somewhat promiscuous and can be used to import a wide variety of cargoes into cells.[83] As the PTS in cancer cells is significantly upregulated compared to normal cells polyamine conjugation is an attractive approach to confer cancer cell selectivity or circumvent drug resistance.[58,84] One of the first examples of a polyamine drug conjugate was reported by Cullis in 1992.[85] The nitrogen mustard chlorambucil (29) is widely used in cancer chemotherapy for the treatment of ovarian carcinoma, lymphomas and chronic lymphocytic leukaemia (CLL). Conjugate 30 (shown in figure 1.13) was shown to alkylate DNA more potently owing to an additional DNA targeting action of the polyamine. Unfortunately, it showed significant neurotoxicity when tested in experimental animals. This may be as a result of its actions on ion channels given its close structural relationship to known spider and wasp venoms.[28,86] Nevertheless, this study serves as a useful proof of principle for the use of the PTS as a drug vector.[87]

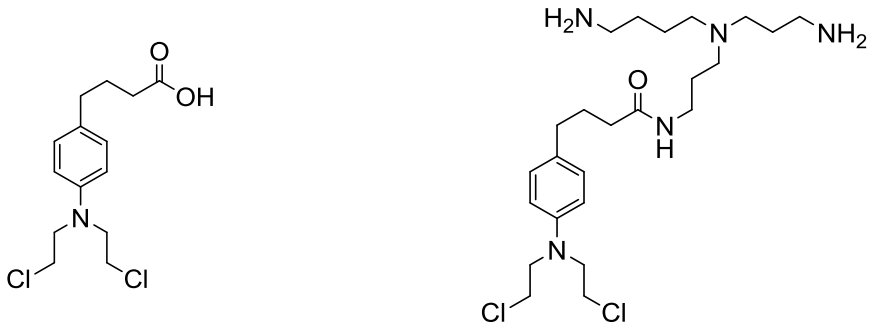

29 **30**

***Figure 1.13**: Chlorambucil (**29**) and the Spd conjugate (**30**)*

Artemisinin (**31**) is a potent antimalarial with promising cytotoxicity in cancer cells.[75] Spd conjugates (shown in figure 1.14) with different *N*-alkylation patterns were evaluated in artemisinin sensitive, PTS active HL-60 human leukaemia cells. The N^4-substituted analogue (**32**) was inactive, however terminally alkylated N^1- and N^8-conjugates (**33** and **34** respectively) were more potent than the parent drug. Conjugate **34** was the most active with low micromolar IC_{50} values. Conversely, the N^4-substituted analogue **32** was found to be the most efficacious (albeit weak) antimalarial.

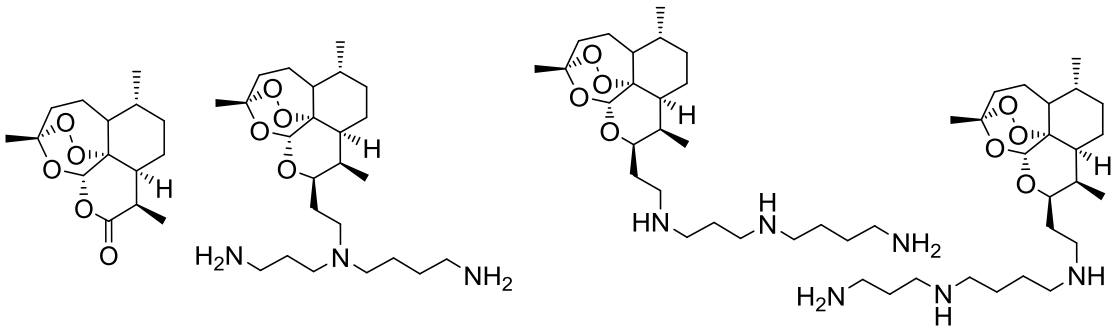

31 **32** **33** **34**

***Figure 1.14**: Artemisinin (31) and spermidine conjugates (**32–34**)*

Chloramphenicol (**35**) is a broad-spectrum antibiotic that binds to bacterial ribosomes and inhibits protein synthesis, however its clinical use is limited by its toxicity as it damages bone marrow and causes aplastic anaemia.[88] Compound **35** also targets the machinery of mitochondrial protein synthesis, therefore a cancer-selective mode of delivery has significant therapeutic potential.[89] Kalpaxis *et al* investigated both the antibacterial and anticancer activity of a range of polyamine conjugates of **35**, typified by

the spermine conjugate (36) shown in Figure 1.15. As polyamines are known to associate with ribosomes it is unsurprising that the polyamine conjugates of chloramphenicol displayed enhanced inhibition of protein synthesis and bacterial growth.

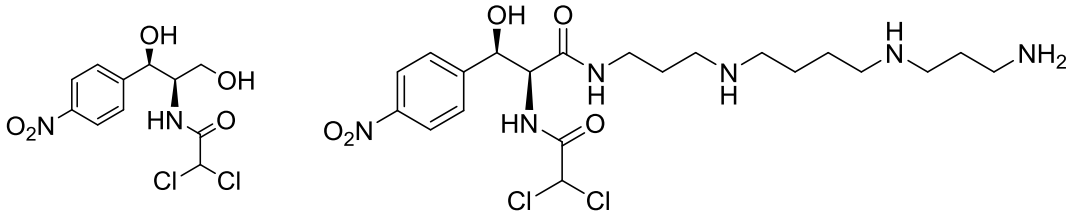

35 **36**

***Figure 1.15**: Chloramphenicol (**35**) and spermine conjugate (**36**)*

Polyamine conjugation enhanced both toxicity and cancer cell selectivity. Whilst both compounds and had little ill effect on healthy leukocytes, treatment with conjugate 36 at 60 μM induced apoptosis in lymphoma cells. The enhanced efficacy could be due mitochondrial targeting by the polyamine moiety; as the mitochondrial membrane is highly negatively charged polyamines are likely to associate with it and gain access via its own polyamine uptake system.[90]

F14512 (37) is a polyamine conjugate of the topoisomerase II inhibitor etoposide (38) (Figure 1.16) that is currently under clinical evaluation.[91,92] F14512 is an effective antiproliferative agent at low nanomolar doses in a range of human leukaemia cell lines, and more potent than 38.[93]

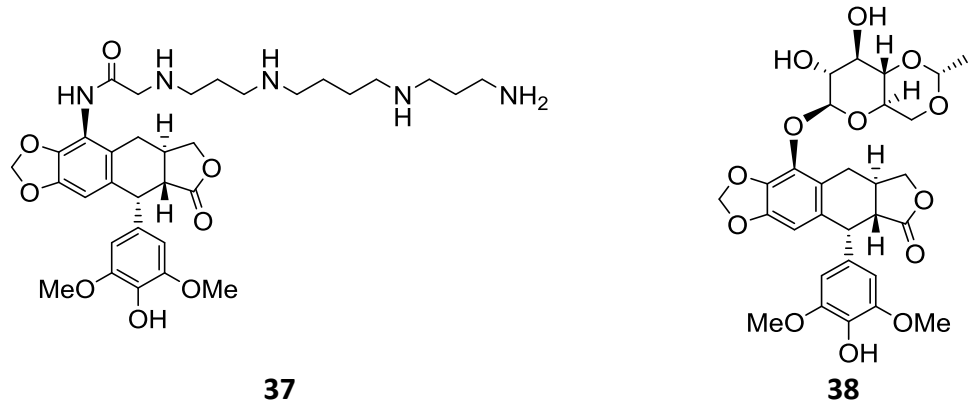

37 **38**

***Figure 1.16**: Etoposide spermine conjugate F15412 (**37**), Etopsoside (**38**).*

Amonafide (39) has interesting anticancer activity however, however clinical trials of napthalimides have so far proven unsuccessful. Tian et al. synthesised a range of

naphthalimide-polyamine conjugates and tested their anti-cancer activity in a range of human cancer cell lines. The homospermidine conjugate (40) was shown to induce production of ROS, disrupt the mitochondrial membrane potential (MMP), and lead to p53 induced apoptosis. It also inhibited tumour growth and metastasis in a mouse model.[94]

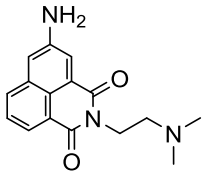

39

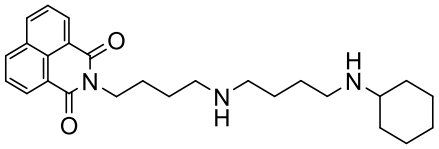

40

***Figure 1.17**: Anticancer napthalimides, amonafide (**39**) and homospermidine conjugate (**40**).*

Although polyamine conjugation has been widely used with DNA targeting cancer drugs as a strategy to enhance cancer cell selectivity; polyamine drug conjugates are yet to make a significant impact in the clinic. Polyamines have also been used to direct porphyrins to DNA to induce DNA photocleavage in photodynamic therapy (PDT).[95] Polyamine conjugates often show greater efficacy due to enhanced interaction with DNA. Despite the proven ability of polyamines to differentiate between cancer cells and non-cancerous cells *in vitro* and *in vivo* and potentiate their activity there is a significant potential for off-target effects due to their pleiotropic nature. Going forward it may prove fruitful to use cleavable linkers that release the drug at the target location. Acid labile hydrazone linkers may prove particularly useful in this respect as polyamines are sequestered in acidic vesicles following uptake.[96]

1.1.6: Polyamines in cancer

The link between polyamines and cancer was established around fifty years ago by Russel and Snyder.[97] They discovered that ODC activity in cancer cells was significantly elevated compared to normal cells. Activation of ODC is an important step in carcinogenesis, with ODC overexpression being key to malignant transformation.[98] Overexpression of SMO has also been linked to inflammatory cancers and oxidative DNA damage.[99,100] Polyamines can be used as a biomarker of cancer as cancer patients tend

to excrete high levels of polyamines in urine. High levels of polyamines often correlate with more advanced cancers, and poor prognosis.[101–103]

Polyamines not only enhance tumour growth, but they are also intricately associated with cancer-promoting functions in the cell. Polyamines have been described as the oil for the cancer engine,[104] their actions can be aligned with most of the accepted hallmarks of cancer, (shown in figure 1.18).[105] *K-RAS* and *c-Myc* are two of the most commonly activated oncogenes in cancer, both of which are closely linked to polyamine transport and metabolism.

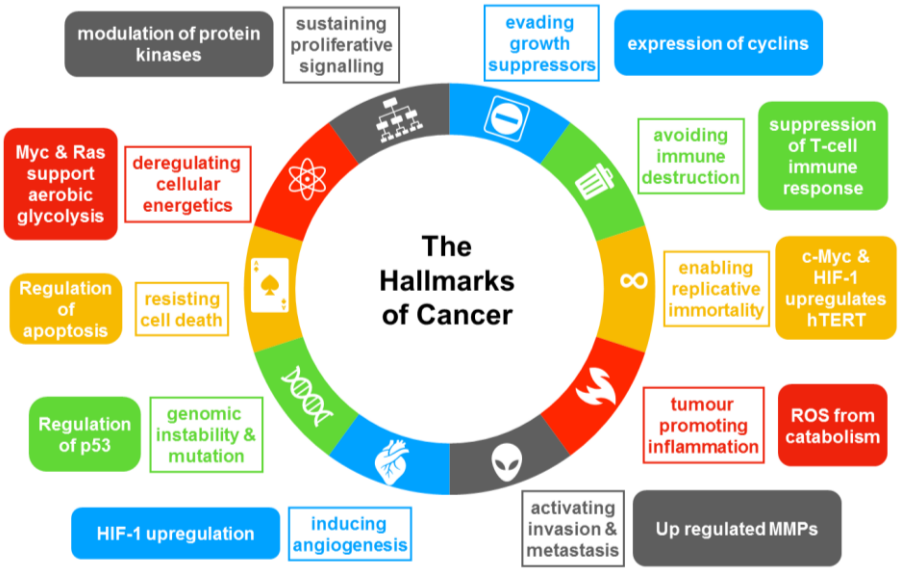

***Figure 1.18**: The roles of polyamines in the hallmarks of cancer, adapted from Hanahan & Weinberg.*[105]

1.1.6.01: Evading growth suppressors.

Polyamine biosynthesis fluctuates through the cell cycle, with ODC and SAMdc showing peaks of activity around both the G1/S and S/G2 transitions. Inhibition of polyamine biosynthesis results in rapid cell cycle arrest, implying a critical role for polyamines in cell cycle progression.[106] Retinoblastoma protein (pRb) is the "master switch of the cell cycle"[107] and its phosphorylation status determines cell fate. pRb is phosphorylated by cyclin D1/CDK4, and its phosphorylation is inhibited by the anti-growth signalling growth factor-β (TGF-β),[108] both of which are modulated by polyamines. Expression of ODC is activated at the G1/S transition which stimulates degradation of cyclin D1 by AZIn, which enables progression to the next phase.[109] Polyamines also regulate the expression of tumour suppressor p53 and the cyclin

dependent kinase inhibitors (CKDi) p21 and p27, all of which are crucial in control of the cell cycle. Polyamines are also required for cyclin B1 degradation[110] and tubulin polymerisation.[111]

1.1.6.02: Avoiding immune destruction.

Immunosuppression in tumours occurs by either exclusion of immune cells from the tumour microenvironment or by impairing their response. Polyamines suppress the immune response to cancer cells by reducing CD44 and interleukin-2 (IL-2) expression and reducing anti-tumour cytokine production.[112]

1.1.6.03: Enabling replicative immortality

The human telomere reverse transcriptase protein (hTERT) enables replicative immortality in cancerous cells. The *hTERT* gene is highly repressed in normal cells however its transcription may be activated by c-MYC, which is in turn enhanced by polyamines at the level of transcription.[113,114]

1.1.6.04: Tumour promoting inflammation

Immune responses are intimately associated with inflammatory responses, both being key drivers of cancer progression.[115–117] Arginine plays an important role in this inflammatory response.[118] Nitrogen oxide synthase (NOS) produces a high concentration of NO from arginine at the onset of the inflammatory response. Accumulation of reactive nitrogen species at the site of injury exerts an antibacterial effect. In the long term this is damaging to the surrounding tissues as NO is linked to angiogenesis, proliferation, and migration. The "arginine switch" diverts arginine to arginase, increasing production of ornithine. Accumulation of polyamines creates a pro-proliferative microenvironment facilitating wound healing and repair. However, this also leads to an increase in polyamine catabolism. APAO and SMO liberate the irritant hydrogen peroxide (H_2O_2) which sustains tumour promoting inflammation and may contribute to inflammation-induced carcinogenesis.[48]

1.1.6.05: Activating invasion and metastasis

ODC overexpression is commonly associated with a more invasive phenotype showing enhanced angiogenesis and matrix metalloproteinase (MMP) production. MMPs break down the extracellular matrix (ECM) enabling cells to escape from the

tumour, invade surrounding tissues and metastasize to other organs. The hypoxic tumour environment enhances expression of hypoxia inducible factor-1 (HIF-1), which in turn enhances transcription of genes that promote angiogenesis, anaerobic metabolism, invasion, cell survival and suppresses cellular adhesion molecules such as CD44. Polyamine uptake from the surrounding tissues is promoted, although biosynthesis is reduced.

Metastasis requires cancer cells to escape from the tumour cluster, enter the bloodstream, avoid immune destruction and establish a new colony in a secondary location. As oxygen is in plentiful supply in the bloodstream, migrating cells regain their normoxic characteristics. This bestows a selection advantage as normal adhesion characteristics of CD44 are restored which enables the cancer cell to anchor in a new site. Normoxia also restores proliferation-sustaining polyamine biosynthesis.[119]

1.1.6.06: Inducing angiogenesis

Angiogenesis is closely linked to invasion and metastasis as it also occurs in response to hypoxia. The hypoxic microenvironment flips the angiogenic switch; HIF-1 upregulates expression of growth factors, which promote neovascular growth, which is supported by high levels of polyamines.[120,121]

1.1.6.07: Genomic instability and mutation

The guardian of the genome, p53 also regulates genes linked to growth arrest, apoptosis, cellular metabolism and the response to oxidative stress.[122] Loss of tumour supressing function of p53 occurs in the vast majority of human cancers. Cancers with mutant p53 tend to display greater genomic instability and increased metastasis.[122] Expression of p53 is highly regulated by cellular polyamines.[123–125]

1.1.6.08: Resisting cell death

Polyamines are actively involved in cell death; however, studies reveal both effector and protective roles dependent upon context.[126,127] Polyamine catabolism produces H_2O_2 which is known to trigger apoptosis, however Spm can also prevent activation of the executioner caspase 3.[128] Biologically, proliferation and apoptosis are frequently interconnected as they share common regulators. One such example is the JNK/JunD pathway; it has shown to be sensitive to polyamine levels and somewhat

pleiotropic in action.[129] c-Jun N-terminal kinase (JNK) activates the transcription factor JunD, which mediates cell survival signalling by regulating expression of inhibitors of apoptosis. JunD expression is regulated by two RNA binding proteins which compete for the same binding site; polyamines regulate JunD mRNA stability by modulating this competitive binding.

1.1.6.09: Deregulating cellular energetics

Defective *Myc* and/or *Ra*s are observed in the majority of cancers and both of these oncogene families have been implicated in polyamine pathways. Myc family transcription factors are important regulators of anabolic metabolism promoting expression of genes required for glycolysis and polyamine biosynthesis. ODC, SAMdc, SPDS and SPMS are also regulated by Myc transcription factors.[130,131] Whilst Myc acts to stimulate polyamine biosythesis, Ras transcription factors serve to feed cancer cells by upregulating critical nutrient uptake pathways including polyamine transport.[42]

1.1.6.10: Sustaining proliferative signalling

Many of the commonly mutated genes can be traced to either the phosphatidylinositol 3-kinase-protein kinase B (PI3K-Akt) or Ras dependant MAPK (mitogen activated protein kinase) pathways which are both implicated in cell proliferation.[132] MAPK prevents ubiquitin dependant degradation of Myc. In addition to its role in upregulation of polyamine biosynthesis and glycolysis, Myc is also responsible for the expression of cyclins, CDKs transcription factors which drive the cell cycle. Evidence points to a role for the Ras-MAPK signalling pathway as a communicator of cellular polyamine status.[133] Phosphorylation of protein kinase CK2 is sensitive to the relative levels of polyamines and serves to modulate Ras-MAPK signalling.

Akt regulates many proteins that control cell proliferation, and hyperactivation of the PI3K-Akt pathway promotes survival and proliferation of cancer cells.[134] This pathway has also been linked to control of polyamine metabolism; Rajeeve *et al.* proposed a feedback loop whereby these two biochemical pathways control each other's activities. The PI3k/Akt pathway controls production of Spd via activation of SAMdc. However, activation of Akt is inhibited by Spd. Activated Akt enhances polyamine production which promotes proliferation, this eventually depletes spermidine which

relieves the block on Akt phosphorylation and subsequently reactivates Spd biosynthesis.[135]

Given their established role in proliferation it is easy to understand how polyamines contribute to oncogenic potential. Polyamines are known to interact with both DNA and RNA to bring about changes in gene expression and protein synthesis. They act as a molecular switch for many effector proteins via their modulatory action on protein kinases. In concert, these activities play a vital role in the sustaining the hallmarks of cancer and aiding development of the malignant phenotype.

1.2: Metal complexes for imaging

1.2.1: Luminescence and luminescent metal ligand complexes

Luminescence is a radiative process and is defined as the emission of light from an electronically excited state.[136] When light energy is absorbed by a molecule it can be used to promote an electron to an excited state. This absorbed energy must then be dissipated as the electron relaxes back to the ground state. This can occur by either radiative or non-radiative processes as represented in figure 1.19.

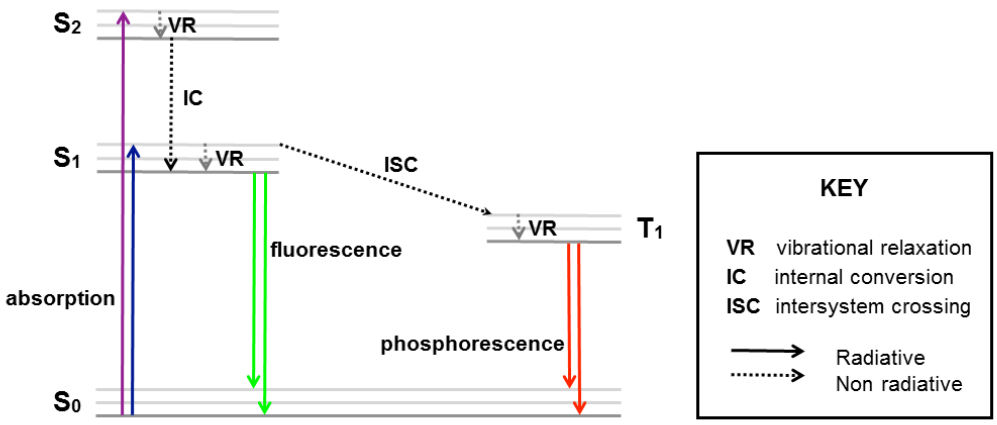

***Figure 1.19**: Jablonski diagram showing electronically excited states and interconversion processes.*

Luminescence can occur via two distinct processes depending upon the nature of the transition from the emissive excited state. Fluorescence is observed when the

excited state relaxes via a spin allowed electronic transition. Fluorescent emission is rapid with emission lifetimes in the order of 10 nanoseconds (ns). In contrast, phosphorescence arises from the radiative decay from a triplet excited state. Phosphorescence has a much longer emission lifetime, (in the millisecond range) owing to the spin forbidden nature of the electronic transition. Direct population of the triplet excited state is also spin forbidden and hence phosphorescence is only observed if intersystem crossing (ISC) is efficient. Molecules containing heavy atoms, such as iodine or transition metals, exhibit strong spin orbit coupling (SOC) which enhances ISC. Emission occurs at a lower energy (longer wavelength) than the energy of absorption. This difference between the excitation and emission maximum is quantified by the Stokes shift. As triplet excited states tend to be lower in energy than the singlet excited state, phosphorescent emission typically has a large Stokes shift.

Luminescent transition metal ligand complexes (MLCs) are emerging as a promising alternative to organic fluorophores for imaging cells.[137] Whilst the quantum yield of MLCs tends to be lower than their organic counterparts, MLCs boast a number of other useful properties which makes them highly attractive for use as biological probes. Heavy metals exhibit efficient spin-orbit coupling which gives rise to strong phosphorescence. Traditional phosphors exhibit millisecond lifetimes, however phosphorescent emission from MLCs is typically of the order of 100 ns as strong spin orbit coupling relieves the forbidden nature of the transition. The lifetime of phosphorescent emission from MLCs is much longer than the emission lifetime of typical organic fluorophores, and hence emission from MLCs may be easily distinguished from background autofluorescence using time gating techniques.

Phosphorescent emission is less prone to self-quenching upon accumulation as there is little overlap of their emission and excitation spectra due to the large Stokes shift. MLCs are also resistant to photobleaching and so are readily applicable to time lapse experiments to observe dynamic processes in live cells in real time, even with high powered lasers. Emission lifetime is often sensitive to surroundings, so MLCs are useful for phosphorescence lifetime imaging (PLIM). As the metal atoms concerned are not normally found in biological systems their uptake may be measured quantitatively by inductively coupled plasma mass spectrometry (ICP-MS).

1.2.2: Iridium probes

The archetypal cationic heteroleptic cyclometallated iridium(III) complex $[Ir(ppy)_2(bpy)]^+$ (**41**) was first reported by Watts,[138] and the photophysical properties were elaborated by Güdel.[139] A plethora of heteroleptic cationic Ir(III) complexes of the general formula $[Ir(C^N)_2(N^N)]^+$ where C^N is a cyclometallating ligand and N^N is an ancillary diimine ligand have since been reported with emission spanning the entire visible range. Heteroleptic cyclometallated iridium(III) polypyridine complexes exhibit intense phosphorescence as a result of emission from mixed excited states. Compared to $[Ru(bpy)_3]^{2+}$, the HOMO of cyclometallated iridium complexes tend to have greater ligand character due to increased aryl-π* contribution from the C^N ligands.

Red light is less damaging to tissue and shows enhanced penetration depths therefore, red-emitting luminophores are highly desirable for biological applications. Photophysical properties can be tuned by subtle modification of ligand architecture to modify the relative energies of the HOMO (N^N) and LUMO (C^N). Red-shifted emission can be achieved by decorating the C^N ligand with electron donating groups to destabilise the HOMO, for example the addition of a methoxy group *para*- to the carbon-iridium bond results in red-shifted emission.[140,141] The N^N based LUMO can be stabilised by either incorporating electron withdrawing groups, or extending the conjugation.[142] The strategies for tuning emission will be discussed in more detail in Chapter 3. The following synopsis is by no means an exhaustive review of the vast literature in this area, but more intended to illustrate some of the salient features of these complexes and how both photophysical and biological properties can be modulated by rational ligand design.

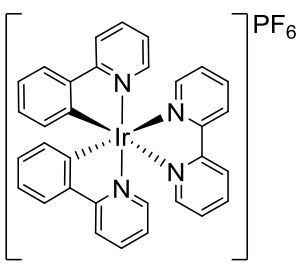

41

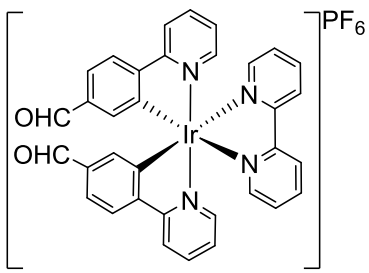

42

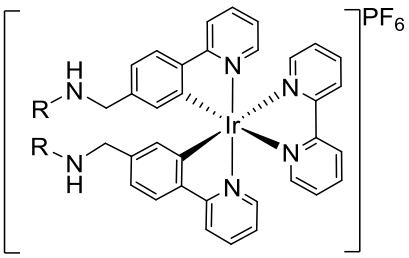

43

***Figure 1.20**: The first reported cyclometallated iridium(III) complex, (**41**) $[Ir(ppy)_2(bpy)]^+$, amine reactive parabenzaldehyde complex (**42**) and reduced Schiff base complex (**43**).*

Complexes 42 and 43 are some of the earliest reported iridium complexes for biological imaging. The complexes reported by Lo *et al* in 2004 were designed for protein labelling and incorporated amine-reactive pyridyl benzaldehyde (pba) cyclometallating ligands typified by complex 42 shown in figure 1.20.[143] Emission spectra of the complexes were found to be vibronically resolved and somewhat insensitive to solvent and temperature. Varying the extent of conjugation of the ancillary ligand was found to have very little effect on the λ_{max} of emission, pointing to a triplet excited state with significant intra-ligand character (^{3}IL). However, upon reaction with alanine and subsequent reduction to the amine the nature of the emission was found to change significantly. Emission spectra were broader and structureless; with the colour of the emission observed for each of the complexes reflecting the strength of the π-acceptor ligand used. This is consistent with a triplet excited state with significant metal to ligand charge transfer (^{3}MLCT) d π(Ir) -> π* (N^N) character.

The excited states of these complexes are often highly sensitive to their microenvironments and so luminescent MLCs can also be used as sensors for phosphorescence lifetime imaging (PLIM).[144] Many studies report applications of iridium complexes for the imaging of hypoxia which is of clinical significance for imaging ischemia, respiratory diseases and solid tumours. Phosphorescent MLCs are often readily quenched by molecular oxygen, which can cause the phosphorescent lifetime to change. However, PLIM can also be used to monitor cellular reactions and interactions in real time. As seen in the previous example, chemical reactions of ligand substituents can significantly alter photophysical properties including emission lifetime.

Complex 44 was designed as a probe to monitor human carboxylesterase 2 (hCE2) activity in cells. Upon cleavage by hCE2, the absorption and emission was largely unaffected by enzyme activity, however the phosphorescent lifetime of the product (45) increased significantly (from 338 ns to 625 ns).[145] This was rationalised as arising partly due to a reduced MLCT character of the emission from the hydrolysis product, and partly due to the reduced size of the pendant substituent having less opportunity to undergo non-radiative decay associated with its molecular motion. Whilst the reacted and

unreacted probe could not be differentiated using standard confocal microscopy, lifetime images could clearly differentiate between them.

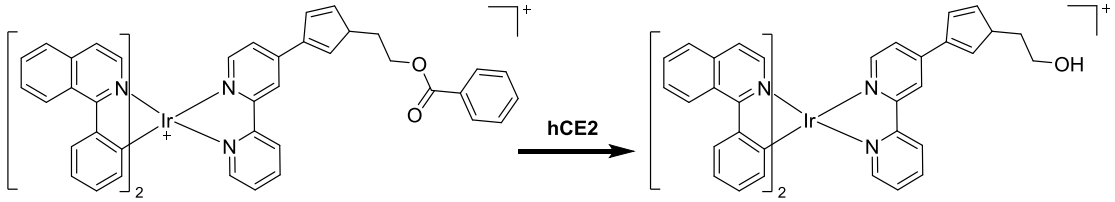

44 **45**

***Figure 1.21**: PLIM probe **44** to monitor hCE2 activity in live cells, upon esterase activity complex **45** shows a dramatic change in emission lifetime.*

Lippard *et al.* developed a dual emission iridium complex with a di(2-picolyl)amine receptor to sense zinc ions (**46**).[146] In solution the complex exhibited blue ^{3}MLCT emission from the 2-(2,4- difluorophenyl)pyridine (dfppy) cyclometallating ligands and yellow ^{3}MLCT emission from the phen ligand, which was significantly enhanced by zinc binding. In the absence of zinc, yellow emission from the $^3MLCT_{(phen)}$ is partially quenched by radiationless decay from a $^3ILCT_{(phen)}$ excited state. Zinc binding increases the energy of the $^3IL_{(phen)}$ excited state; as this route is no longer thermodynamically accessible the yellow component of emission is amplified with respect to the blue enabling zinc binding to be quantified by a ratiometric response. Ratiometric determinations are prone to error owing to background autofluorescence. This can be eliminated using time resolved techniques. Phosphorescent decay of complex **46** was found to have 3 components, the mid-range and short-lived components were unaffected by zinc (6.1 ns and 0.80 ns respectively) whereas the longer-lived component varied between 140 ns in zinc free conditions and 160 ns with zinc. Zinc binding could be quantified using PLIM in both fixed and live cells, although some cytotoxicity was noted in live cells (and attributed to singlet oxygen generation).

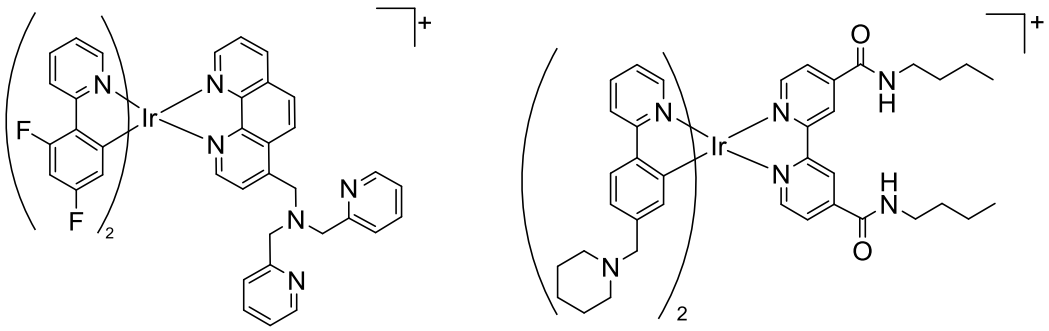

46 **47**

***Figure 1.22**: Dual emission ratiometric probes, zinc responsive probe (**46**) and oxygen sensor (**47**).*

Lo designed a dual emission phosphorescent complex (**47**) that can sense both hypoxia and hyperoxia.[147] Dual emission occurs as a result of emission from the ^{3}IL excited state at higher energy and ^{3}CT at lower energy. Emission from the higher energy ^{3}IL excited state showed a greater propensity for quenching by oxygen compared to the emission from the oxygen insensitive ^{3}CT excited state. As the emission lifetime of the ^{3}IL excited state changes in the presence of oxygen the dual emission enables a ratiometric luminescence response to be measured.

In this case it was the oxygen sensitivity of the complex that needed to be tuned to ensure sufficient sensitivity under hyperoxic conditions. Quenching efficiency was modulated by installing an electron withdrawing amide group to stabilise the π* orbital of the bpy ligand. This enhanced IC from ^{3}IL to ^{3}CT excited state, shortening emission lifetime and thus reducing quenching. Complex **47,** shown in Error! Reference source not found. has visibly different emission in nitrogen, air and oxygen. Emission under nitrogen is dominated by the ^{3}IL emission, and green in colour, whereas in oxygen red emission of predominantly ^{3}CT character is observed. In air, dual phosphorescence gives rise to an orange emission. This was attributed to charge transfer from the non-conjugated amino group lone pair on the cyclometallating ligand to the π* orbitals of the diimine ligand, a so-called triplet amine-to ligand excited state (^{3}NLCT). If the ^{3}NLCT state resides (energetically) between the ^{3}IL and ^{3}CT excited states, internal conversion between the emissive states is inhibited resulting in dual phosphorescence. Complex **47** was used to image zebra fish by CSLM and found to distinguish between hypoxia, normoxia and hyperoxia by virtue of the ratiometric response, and could be used to image hypoxia *in vivo*, in a mouse tumour.

Cationic, lipophilic compounds such as $[Ir(C^N)_2(N^N)]^+$ have a tendency to accumulate in mitochondria due to their high membrane potential.[148] Complexes can be steered to specific biological targets by incorporating pendant receptor ligands such as hormones, peptides and key nutrients, or they can be directed to specific cell compartments by controlling their physical properties such as lipophilicity, charge, or pK_a. There are many examples of Ir(III) complexes that have been designed to specifically label the nucleus, endoplasmic reticulum (ER), lysosomes and mitochondria, amongst others.[149]

The triphenylphosphonium (TPP) cation is routinely used as a mitochondria-targeting substituent. Several heteroleptic iridium complexes with a pendant TPP group show selective accumulation in mitochondria, as exemplified by complex (**48**) shown in Figure 1.24. This is by no means a fool-proof approach, as a platinum complex (**49**) with a similar TPP pendant was unexpectedly found to localise in the nucleuolus.[150] Other strategies employed include adding a reactive group to label mitochondrial proteins, such as isothiocyanate complex (**50**), and has potential to be used to characterise binding targets by mass spectrometry.[151] It should be noted that a great number of cationic iridium complexes have been shown to localise to mitochondria without the addition of a targeting functionality.

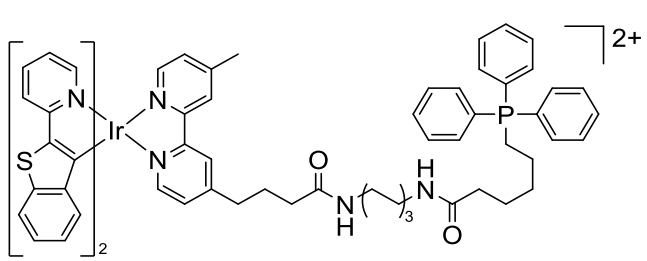

48

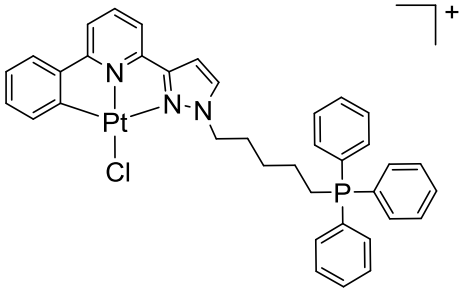

49

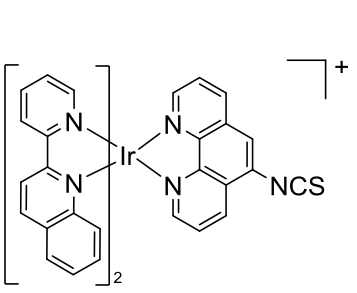

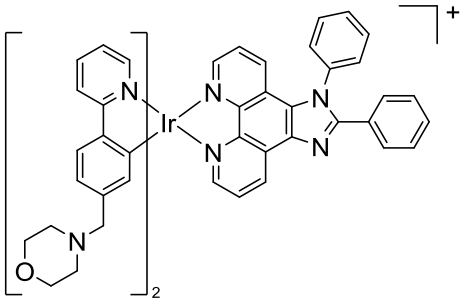

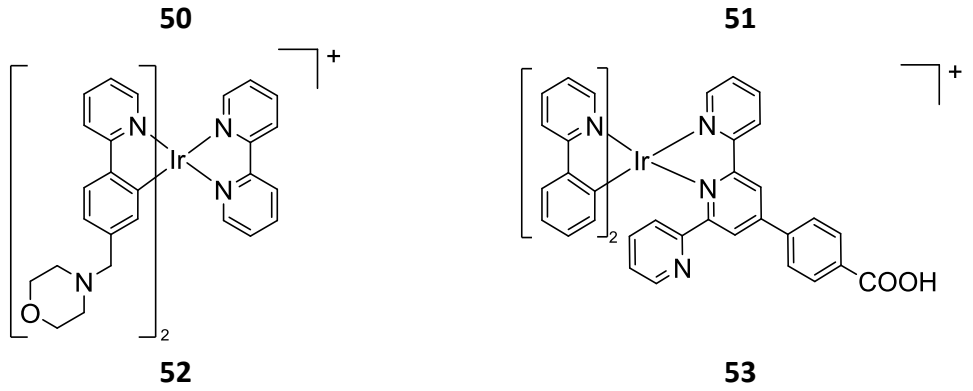

***Figure 1.23**: Mitochondria localising complex (**48**), nucleolar localising TPP platinum complex (**49**), thiol reactive complex (**50**) and lipophilic mitochondria localising complex (**51**) lysosome localising complex (**52**) and histidine sensing probe (**53**).*

Commercial probes that accumulate in lysosomes often contain morpholine groups that preferentially localise in acidic vesicles, and this approach has also been applied to direct iridium complexes to lysosomes. Lipophilic complex (51) accumulated in the mitochondria; however by decreasing lipophilicity, the complex accumulated in the lysosomes (52).[152] Horobin *et al.* propose that cations with a log P value between 0 and 5 are likely to localise in the mitochondria whereas cations with a log P value between −5 and 0 are more likely to localise in lysosomes.[153] Lipophilicity is also important for ER probes due to their highly membranous nature; heteroleptic bis-cyclometallated iridium complexes have also been demonstrated to localise to the ER.[154]

Tian *et al* designed complex 53 for use in high resolution, stimulated emission depletion (STED) microscopy.[155] Their cellular probe shown in Figure 1.23 contains a bidentate terpyridine (terpy) ancillary ligand with a free carboxylate group to sense nuclear histidine. Emission at 475 nm was proposed to have significant ^{3}LLCT character mixed with some ^{3}MLCT contribution, and efficient two-photon excitation at 780 nm. Upon binding with histidine, a significant (and histidine specific) enhancement in luminescence intensity was observed, owing to an additional contribution from a ^{3}[π(imidazole) -> π* (terpy)] excited state. Two photon microscopy revealed intense and nuclear specific staining in live and fixed cells. The iridium complex also proved to be useful as a contrast agent for electron microscopy; whilst only the nucleus was stained, the contrast was better than that observed with osmium tetroxide alone. STED microscopy using a 700 nm depletion beam produced images of the nucleus with exquisite resolution, rivalling that obtained by electron microscopy.

An example of a receptor targeted compound is the dopamine complex **54**. Non-small cell lung cancer (NSCLC) is the most common subtype of lung cancer, with a 5-year survival rate less than 15%. As dopamine receptors are overexpressed in this cell line (NCI-H69) it is a useful biomarker of disease status. Several fluorescent receptor agonists have been developed but are limited in use by their lack of photostability and short emission lifetimes. Complex **54** was designed to be used in longer-term studies to not only observe the distribution of the dopamine receptors, but also to track their dynamics *in cellulo*. Complex **54** was found to have a quantum yield of 25 % and an emission lifetime of 4.61 μs.[156] At early time points the complex was predominantly membrane bound; however, after several hours luminescence was observed inside the cell, in discrete structures consistent with uptake via endocytosis. Exogenous dopamine significantly reduced the luminescent intensity in the cell, consistent with uptake via the dopamine receptor.

A PEGylated Ir(III) complex (**55**) was also been successfully used in electron microscopy and found to enhance contrast when used in conjunction with osmium reagents.[157] Complexes were moderately soluble in water and displayed structured emission typical of a complex with some intraligand character, with a quantum yield of 0.088. Emission lifetimes in aerated water fitted a single exponential decay profile with a lifetime of 550 ns. Cells were incubated with 50 μM of the probe for 4 hours. Image analysis revealed a high level of colocalization of the probe with MitoTracker™, and super resolution images revealed that the complex binds to the mitochondrial membrane.

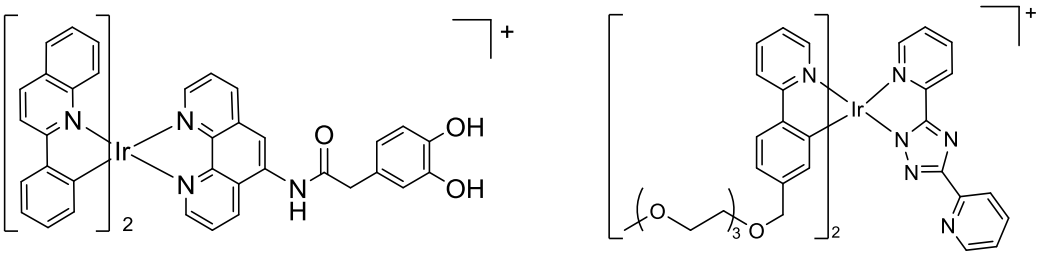

54 **55**

***Figure 1.24**: Dopamine receptor probe (**54**) and multimodal PEG complex (**55**).*

A vast array of luminescent iridium complexes have been synthesised and optimised for biological imaging as a result of slight tweaks in ligand design. The current state of play in this area has recently been extensively reviewed by Massi *et al*.[158]

1.2.3: Rhenium and technetium probes

Rhenium is often used as a non-radioactive model for the development of technetium complexes for diagnostic imaging; however, luminescent rhenium complexes are useful diagnostic tools in their own right. Luminescent rhenium complexes have been widely used for biological imaging, and their cellular uptake has been extensively researched. Rhenium tricarbonyl complexes exhibit good cellular uptake when complexed with a hydrophobic ligand, and their localisation can be controlled using targeting vectors.[159] Their low spin d^6 electron configuration bestows kinetic stability which in turn confers low toxicity in biological systems.[160] For diagnostic use, cytotoxicity can be circumvented by using strong field ligands. Such ligands give rise kinetically stable complexes due to large crystal field stabilization energies (CFSE) and are resistant to ligand exchange in the cellular environment. Rhenium(I) diimine complexes can be tuned by modifying the N^N ligand to alter the relative position of the LUMO. However, as the HOMO typically resides over the metal and carbonyl ligands, tuning opportunities are somewhat limited compared to iridium diimine complexes. Luminescence tuning will be discussed further in Chapter 3.

One of the first applications of rhenium complexes for cellular imaging was reported in 2003. A tridentate bisquinoline ligand was conjugated to formylated targeting peptide fMLF (56). The K_d of the fMLF peptide complex with the receptor was found to be similar to literature values for the free peptide, proving that the metal complex does not negatively affect binding to the receptor,[161] and the rhenium-peptide conjugate was found to localise in the same way as fluorescein-peptide conjugate.[162]

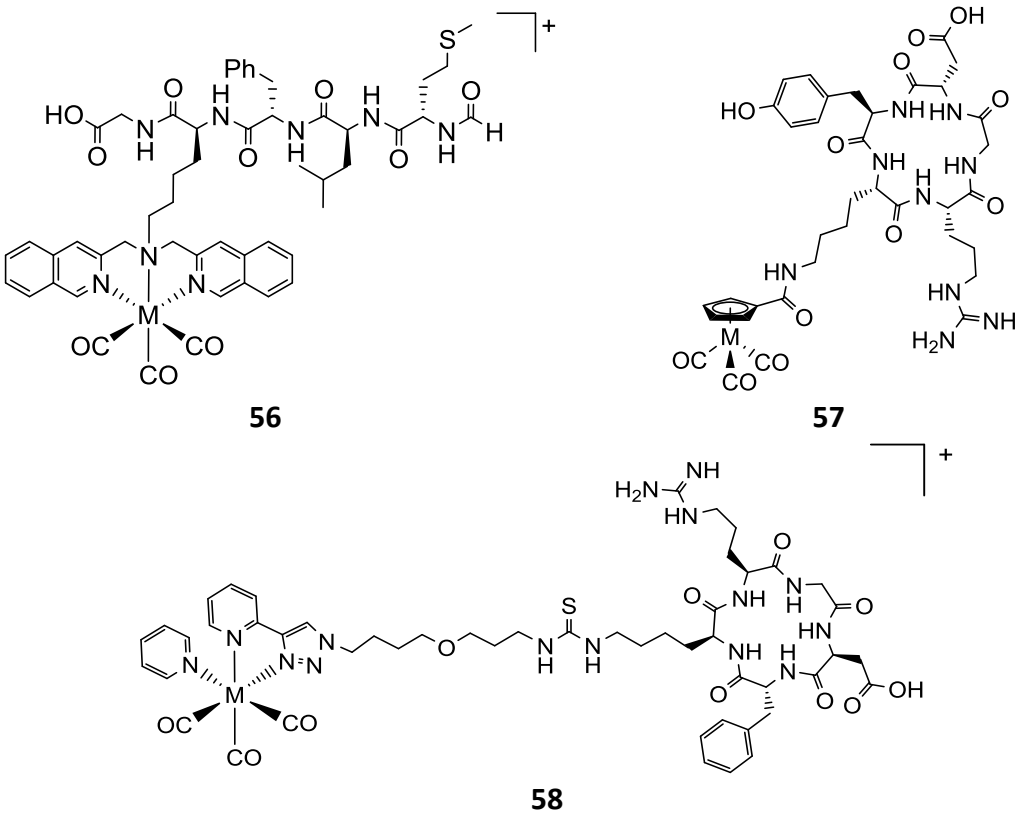

56 **57** **58**

***Figure 1.25**: Formylated targeting peptide (fMLF) bisquinonline rhenium tricarbonyl complex (**56**), cRGDfK cyclopentadienyl tricarbonyl complex (**57**) and cRGDyK pyridyl triazole complex (**58**).*

Integrins are commonly upregulated in aggressive cancers and so their ligand, cyclic RDG peptides can be used as part of a diagnostic probe. The synthesis of diagnostic Tc tricarbonyl probes (and their rhenium congeners) have been reported using both diimine (57) and cyclopentadienyl ligands (58).[163,164] Most breast cancers overexpress oestrogen receptors (ER+), therefore oestradiol conjugated tricarbonyl probes have been designed for use in SPECT to detect hormone responsive breast cancer cells that are likely to respond well to the receptor antagonist drug Tamoxifen. The neutral rhenium(I) complex 59 was shown to have a high affinity for the oestrogen receptors *in vitro*.[165] Oliveira *et al*. synthesised tridentate rhenium and technetium complexes 60 and 61. Cationic complex 60 accumulated in ER+ MCF-7 breast cancer cells to a greater extent than neutral complex 61, and whilst the probes showed good binding affinity for the oestrogen receptor uptake was not inhibited when ER were saturated, hinting at an alternative uptake mechanism.[166]

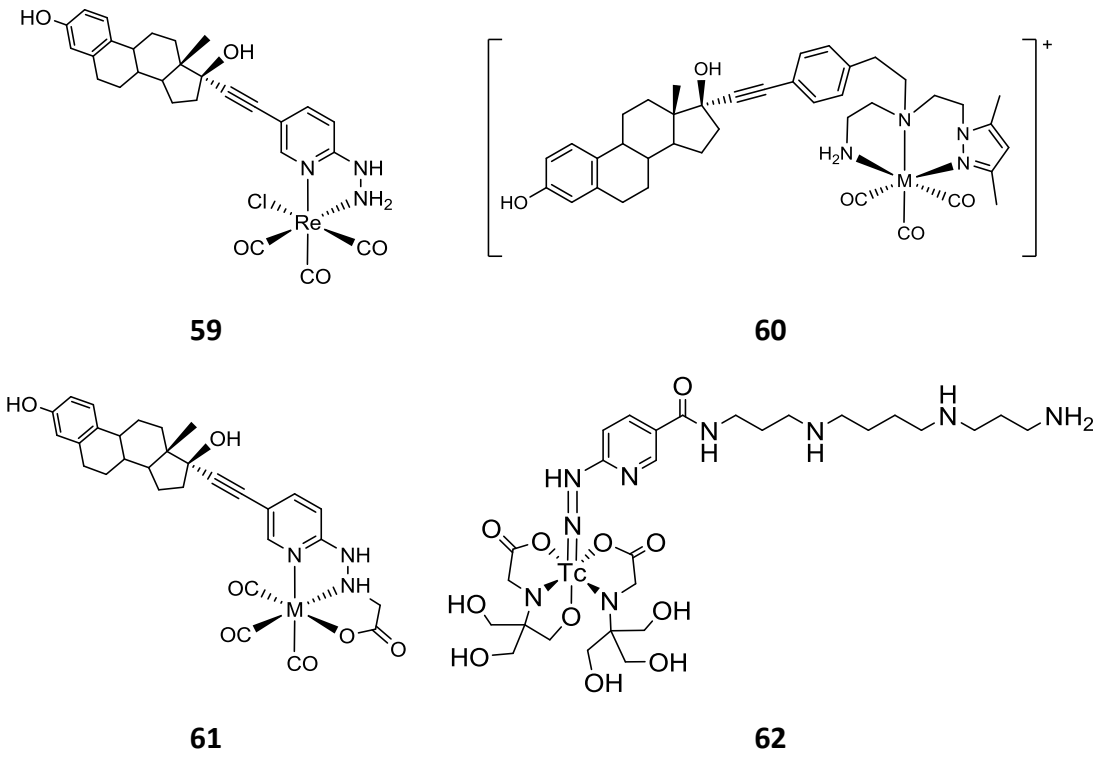

***Figure 1.26**: Rhenium and technetium complexes designed to target oestrogen receptors.*

Whilst fluorescent probes are simple to use with blood cells or cells in culture, they are much less useful for imaging solid tumours where a non-invasive imaging probe is preferable. The technetium probe (**62**) with a hydrazinonicotinamide-spermine (HYNIC-Spm) ligand was designed as a tool to evaluate polyamine transport in experimental animals used for testing the polyamine drug F14512.[167] **62** was found to preferentially accumulate in the tumour two hours post-administration (*intra-venous*), with minor localisation in the kidneys and liver due to excretion. A significant reduction of tumoral accumulation was observed when co-administered with spermine, demonstrating uptake by the PTS. This serves as a useful proof of concept that bulky MLCs can be internalised by a functional polyamine transporter.

One of the first organelle-specific MLC probes was designed by Coogan *et al.*[168] The structure of rhenium tricarbonyl complex **63** was inspired by the MitoTracker™ probes and incorporated a thiol reactive chloromethyl functionality to confer mitochondrial selectivity (Figure 1.27). As the thiol reactive group was installed on the axial pyridine ligand, subsequent reaction with a model thiol compound (glutathione) did not alter the photophysical properties. Localisation of complex **63** in MCF-7 cells was

compared to that of tetramethylrhodamine ethyl ester (64); a fluorophore known to localise in the mitochondria but lacking a chloromethyl group. As both probes had very similar emission (551 nm for 63, 588 nm for 64) colocalization was demonstrated by observing the emission generated when exciting at different wavelengths (405 nm for 63, 543 nm for 64). Luminescence from the probe was found to overlap significantly with that of 64 and did not show any signs of toxicity after cells were exposed to the complex.

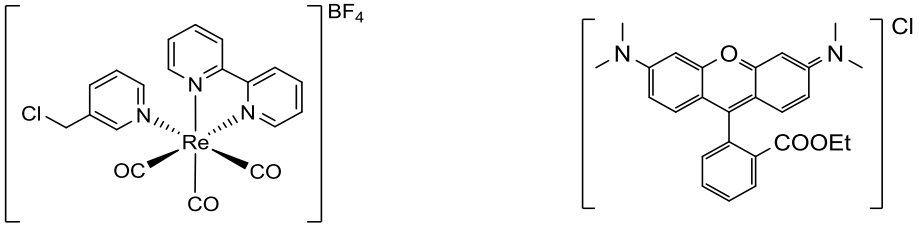

63 **64**

***Figure 1.27**: Thiol reactive mitochondrial cationic rhenium tricarbonyl complex (**63**) and mitochondria-selective probe, tetramethylrhodamine (**64**).*

The fluorescent 1,8-napthalimide scaffold exhibits solvent dependent emission as a result of intramolecular (n-π*) charge transfer. 1,8-napthalimides can be used as DNA binding probes and are amenable to luminescence tuning by varying the type and position of its substituents.[169] Pope *et al* have reported the synthesis and biological evaluation of Re(I) napthalimide complexes constructed from both a dipicolyl amine chelate (65), and using using a phen diimine ligand with an axial picolyl ligand decorated with 1,8-napthalimides (66), as shown in Figure 1.28. [170,171]

The absorption and emission spectra of complex 65 was similar to that of the ligand (albeit slightly hypsochromically shifted). The emission lifetime of the complex showed a modest increase with respect to the ligand but being less than 10 ns was fluorescent in nature.[170] The ligand was cell permeable and localised predominantly in the mitochondria of osteoarthritic cells. Upon coordination to the rhenium tricarbonyl scaffold, complex 65 showed intense cellular staining of and clear labelling of membranous structures within apoptotic cells.

Typically, the emission arising from rhenium tricarbonyl diimine complexes is phosphorescent in nature, dominated by the ^{3}MLCT (dπ(Re)-π*(N^N)) excited state with little to no contribution from the axially coordinated ligand. However, complex 65 with a

fluorogenic axial ligand exhibited emission of mixed (dπ(Re)-π*(phen)) and napthalimide (n-π*) character, as evidenced by its biexponential luminescence decay.[171] The emission lifetime was substantially shorter than expected for this type of complex, owing to quenching of the ^{3}MLCT excited state by the substituted napthalimides. The emission lifetime was approximately equal to that of the free ligand, which was attributed to the fact that the ligand possesses an absorption band at same wavelength as the ^{3}MLCT emission. In *S. pombe* yeast cells, intense DNA staining was observed when cells were treated with complex at a concentration of 100 μg/mL.

Triazoles are attractive ligands for biological probes due to the ease of conjugation to a wide variety of targeting groups using robust click chemistry. The pyta complex **67** exhibits slightly blue-shifted emission compared to bpy as the ligand centred LUMO is at a higher energy.[172] To compensate for this, Bertrand and co-workers used an inverse click reaction to modulate emission by structural variations in the ligand structure, as shown in Figure 1.28.[173] Complex **68** bearing the inverse click ligand, (tapy) showed bathochromically shifted emission, with an emission maximum at 554 nm compared to the that using the pyta ligand which has an emission maximum at 512 nm. The tapy complexes also had a greater quantum yield. In cells, the tapy derived complex gave brighter more defined images, however, these tapy complexes have been shown to be less stable than their pyta counterparts.[174]

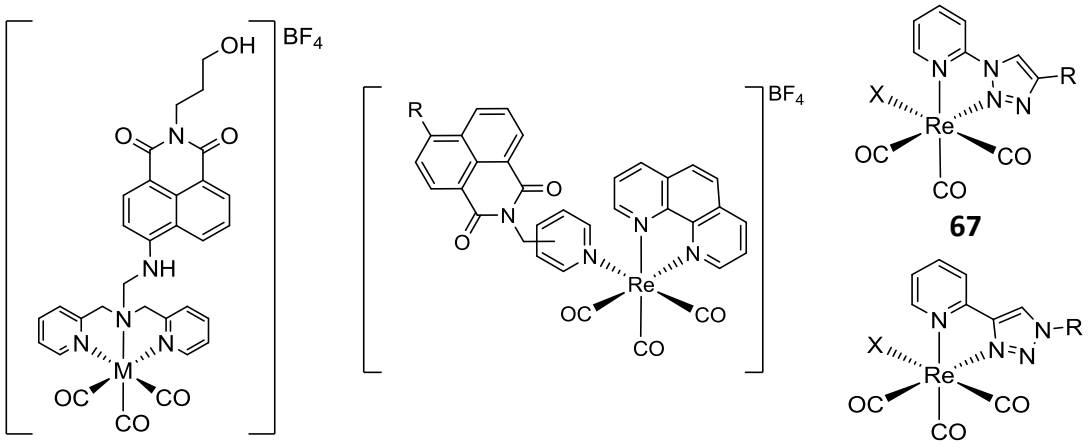

65 **66** **67** **68**

***Figure 1.28**: Rhenium napthalimide complexes (**65** & **66**), rhenium pyridyl triazole complex (**67**) and inverse click complex (**68**).*

1.2.5: Summary

The future for luminescent MLCs in biological imaging is bright! Transition metal-based probes are still not as widely used in biological imaging as their organic counterparts. A wide range of MLCs can be tailor-made to address key biological questions by rational ligand design to ensure probes have the correct photophysical and localisation properties. Continued developments in the field has enormous potential to revolutionise cellular imaging. One of the most powerful features of luminescent MLCs is their photostability, they are easier to handle as they are less sensitive to light but also can be used to track biological events over longer periods of time.

Luminescent MLCs are particularly well-suited to lifetime imaging as they have long emission lifetimes that are sensitive to their environment. MLCs have also been found to be superior alternatives to commonly used fluorophores for STED microscopy. As MLCT emission tends to be broad, overlap with the STED laser is more efficient than that of the most commonly used organic fluorophores. The probability of STED occurring is enhanced by the long emission lifetimes and photostability of these MLCs. As a result, emission depletion is more efficient which dramatically improves resolution.

1.3: Metal complexes for chemotherapy

Despite the notion that medicinal inorganic chemistry is a relatively young branch of science, metallodrugs have been in use for over 5000 years.[175,176] Cisplatin is the most famous metallodrug, and given its enormous success has sparked a wider interest in the use of metallodrugs particularly as anticancer agents.[177] Many metal-based anticancer drugs have been designed to overcome some of the difficulties experienced with cisplatin.[178,179] In addition to MLCs that are inherently cytotoxic, owing to their rich photochemistry, many MLCs are useful for photodynamic therapy (PDT) or photoactivated chemotherapy (PACT).

1.3.1: Platinum based cancer drugs

Cisplatin (69) has been used in chemotherapy since 1978 and is one of the most widely used chemotherapeutic agents, being used in around half of all chemotherapeutic regimes. It is listed by the world health organisation (WHO) as an essential medicine; however, it suffers from severe off target toxicity and resistance.[180] Cisplatin is a "classical chemotherapeutic" as its molecular target is DNA. It is thought to gain entry to the cell via several mechanisms, notably by passive diffusion and the copper transporter CRT1.[181] In the cell the chloride concentration is low, this leads to aquation which activates the drug. The aquated platinum complex is a potent electrophile and reacts at the most nucleophilic site in DNA to form N7-guanine adducts as shown in figure 1.29.

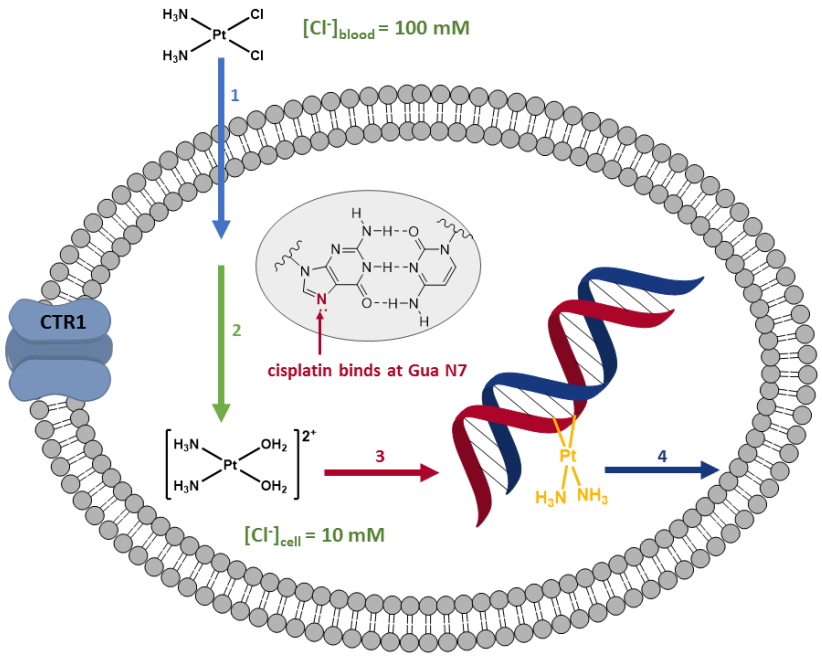

***Figure 1.29**: Mechanism of action of cisplatin: 1) cellular uptake by passive diffusion or copper transporter CTR1 2) activation by aquation in the cell at low chloride concentration 3) DNA binding to adjacent guanine residues on the same strand 4) DNA damage leads to apoptosis.*

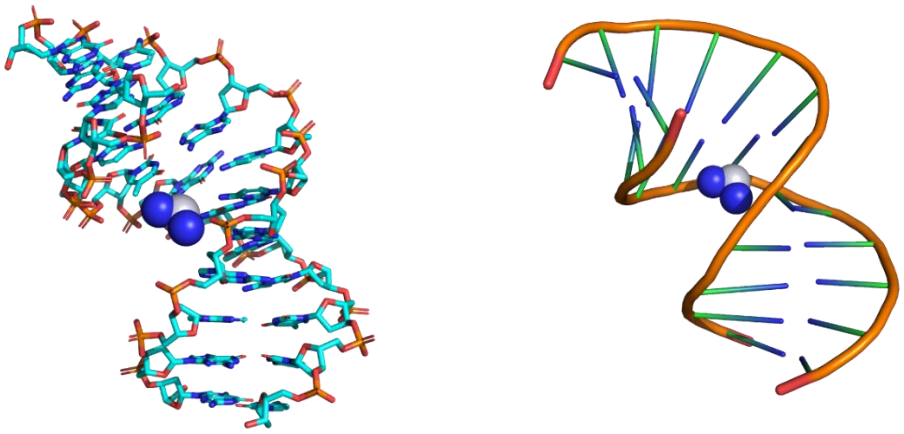

***Figure 1.30**: Intrastrand cross links caused by cisplatin distorts the DNA helix, (PDB 1AIO). Images made using PyMOL Molecular Graphics System, Version 2.0 Schrödinger, LLC.*

Cisplatin forms intra-strand cross links with adjacent guanine residues. DNA platination distorts the helical structure of DNA (as shown in Figure 1.30) ultimately leading to cell death by apoptosis. However, resistance occurs when cells become insensitive to this insult. Second generation platinum drugs have been rationally designed to circumvent the significant dose-limiting toxicity and evade cancer cell resistance. One of the major limitations of cisplatin is the indiscriminate reactivity of the chlorido ligands. In order to attenuate its toxicity, second generation platinum drugs oxaliplatin (**70**) and carboplatin (**71**) have bidentate dicarboxylato ligands in place of the labile chlorido ligands. This slows the rate of aquation enabling higher doses to be used.[182] Despite significant research, no new platinum drugs have been approved for clinical use since carboplatin in 2002. [183]

Picoplatin (**72**) (also reported as AMD473) has a 2-methylpyridine ring in place of one of the non-leaving ammine ligands. The aromatic ring sits perpendicular to the square planar complex, and positioning the methyl substituent over the platinum centre and prevents it from nucleophilic attack from glutathione or deactivating proteins.[184] The platinum(IV) prodrug Satraplatin (**73**) is a coordinatively saturated low spin d^6 complex with octahedral geometry which renders it more resistant to ligand substitution (which reduces its propensity to take part in toxic side reactions). Satraplatin is orally available and readily reduced to its active, square-planar form in the bloodstream. The axial ligands can be used to fine tune physico-chemical properties and serve as a handle for targeting groups.

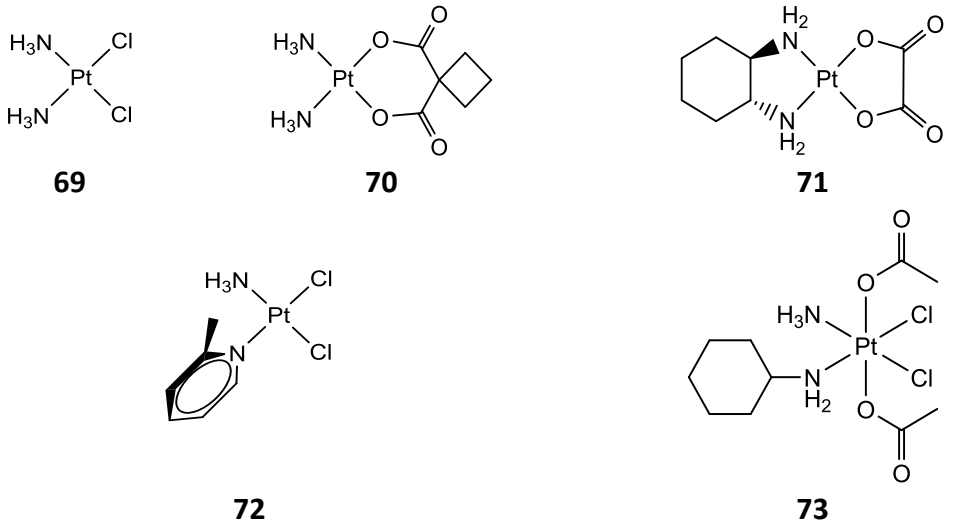

***Figure 1.31**: Platinum anticancer drugs, cisplatin (**69**), carboplatin (**70**) and oxaliplatin (**71**), and experimental drugs picoplatin (**72**) and satraplatin (**73**).*

The promise of Pt(IV) complexes has led to the development of so-called dual-threat prodrugs, whereby another anticancer agent is axially coordinated. Refinement of this approach has yielded potent complexes with nanomolar IC_{50} values.[185] Some examples of this class of drug are shown in Figure 1.33. The HDAC inhibitor (HDACi) valproic acid was chosen as the axial ligand for complex **74** in the hope it would act synergistically with oxaliplatin. HDAC inhibition leads to histone hyperacetylation which in turn increases the accessibility of DNA facilitating DNA platination. The drug was found to be more potent than oxaliplatin in both cisplatin sensitive and resistant cell lines and showed both HDAC inhibition and DNA damage.[186] Octanoato ligands (complex **75**) have a much weaker HDAC inhibitory effect however the associated increase in lipophilicity significantly enhances complex uptake (by passive diffusion) leading to a greater potency.[185]

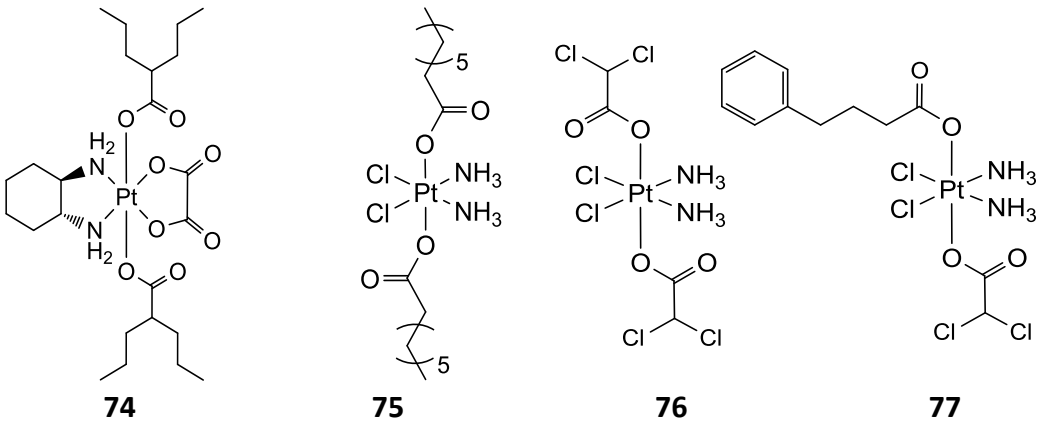

***Figure 1.32**: Multi-threat platinum(IV) complexes, HDACi/oxaliplatin complex (**74**), lipophilic HDACi (**75**), PDKi complex (**76**), and triple threat HDACi/PDKi complex (**77**).*

Mitaplatin (76) uses dichloroacetate (DCA) as the axial ligand. DCA inhibits pyruvate dehydrogenase kinase to switch off aerobic glycolysis which initiates intrinsic apoptosis; however, the effective doses of these two drugs are very poorly matched.[187] The natural progression of this approach was to use two different drugs. The combination of the HDACi phenylbutyrate and DCA gave a drug (77) with an average IC_{50} of 0.37 μM, being approximately 34-fold more potent than cisplatin.[188] Multinuclear quadruple action complexes have also been developed.[189]

Trans-platinum(II) complexes with bulky heteroaromatic ligands have also been found to be cytotoxic. Weakly trans-directing aromatic heterocyclic ligands reduce the kinetic liability of trans chloride groups rendering them more resistant to deactivation by sulfur-containing nucleophiles. This in turn enhances their propensity to form monofunctional DNA adducts.[190] Polynuclear platinum complexes containing *trans*-$[Pt(NH_3)Cl_2]$ units have shown remarkable cytotoxicity. The trinuclear platinum(II) complex BBR3464 (78) was found be around forty times more potent than cisplatin *in vitro* and could overcome cisplatin resistance presumably due to its alternative interaction with DNA. 78 binds to DNA at multiple sites and forms longer range intra- and inter-strand cross links.[191] Unfortunately, phase II clinical trials revealed severe side effects and the drug lacked efficacy at the maximum tolerated dose.[182]

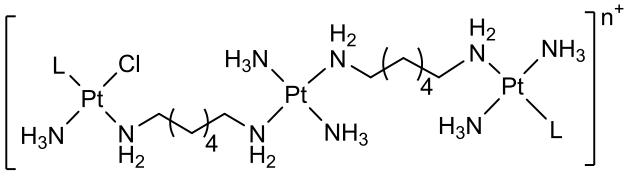

78 L = Cl (n = 4) **79** L = NH_3 (n = 6) **80** L = $NH_2(CH_2)_6NH_3$ (n = 8)

***Figure 1.33**: Polynuclear platinum complexes, BBR3464 the polynuclear platinum complex triplatin tetranitrate (**78**), and substitution inert ammine and diamine complexes **79** & **80**.*

Substitution inert analogues of 78 where chlorido ligands have been replaced with ammine (79) or diamine ligands (80) are of particular interest due to structural similarities with the polyamines. Like the polyamines, these polycationic molecules are efficient counterions and interact with the minor groove of the DNA helix (as can be seen in figure 1.35) and promote the formation of condensed B-DNA (akin to the polyamines).

Despite structural similarities, both complexes have different mechanisms of action; complex **79** induces apoptosis via a p53 dependent pathway but occurs via a p53-independent pathway for complex **80**.

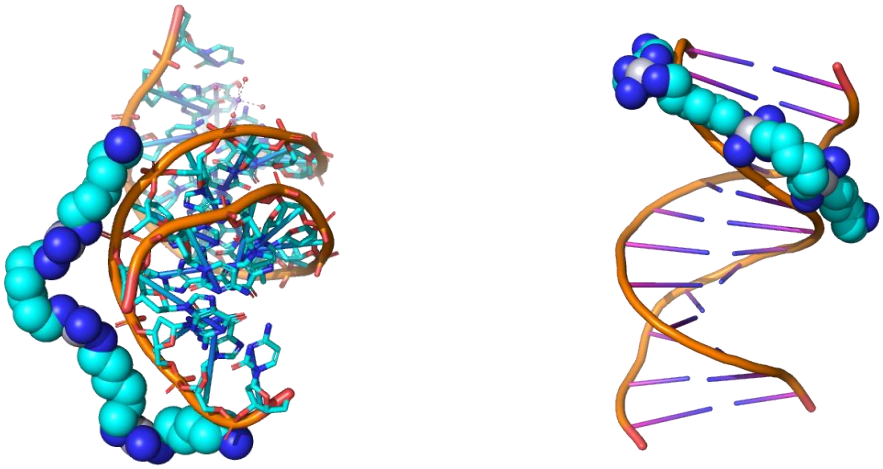

***Figure 1.34**: Crystal structure of TriplatinNC (85) with DNA (PDB 2DYW). Images made using PyMOL Molecular Graphics System, Version 2.0 Schrödinger, LLC.*

1.3.2: Iridium anticancer complexes

Iridium has been used in radiotherapy for over 100 years. Iridium-192 emits gamma radiation with a mean energy of 400 keV, and a half-life of 74 days, and has been widely used in high-dose brachytherapy to treat prostate, cervical and breast cancers.[192] However, As iridium(III) complexes are generally rather inert, they were thought to be poor substitutes for platinum-type drugs, and as such research into iridium complexes as anticancer agents has been somewhat scarce prior to 2010.[193] Half-sandwich cyclopentadienyl iridium complexes have been shown to be highly potent (sub-micromolar) anti-cancer agents,[193–196] however this review will focus on more structurally relevant cyclometallated complexes.

Complex **81** is an example of a small molecule protein-protein interaction (PPI) inhibitor that inhibits the association of p53 with the ubiquitin E3 ligase hDM2 that targets p53 for degradation.[197] **81** is an efficient PPI inhibitor with a sub-micromolar IC_{50} of in a range of cancer cell lines. Complex **82** was also shown to have a sub-micromolar IC_{50} in breast cancer cells (MCF-7) but with an alternative mechanism of action. The

authors proposed that upon entry to the cell complex **82** accumulates in the mitochondria, resulting in oxidative stress. Mitochondrial swelling and ER stress is followed by paraptotic cell death; a caspase-9 mediated nonapoptotic programmed cell death mechanism. Paraptosis is characterized by cytoplasmic vacuolation and resistance to apoptosis inhibitors.[198] As many anticancer drugs induce apoptosis a drug that kills cells via an alternative mechanism has potential to overcome multidrug resistance.

Mao *et al.* designed mitochondria-immobilised complexes **83** and **84** with thiol reactive chloromethyl functionalities installed on the N^N ligand. Both complexes displayed sub-micromolar IC_{50} in a range of cancer cell lines. Complexes **83** & **84** localised in the mitochondria and caused depolarisation of the mitochondrial membrane after incubation with the complex for 6 hours (10 μM).[199] ATP synthesis was also reduced, and a dramatic increase in production of ROS was observed. Confocal microscopy showed that the mitochondria were densely aggregated round the nucleus and both swollen and fragmented after incubation with the complexes for 6 hours. After 24 hours cells displayed morphological changes associated with apoptosis.

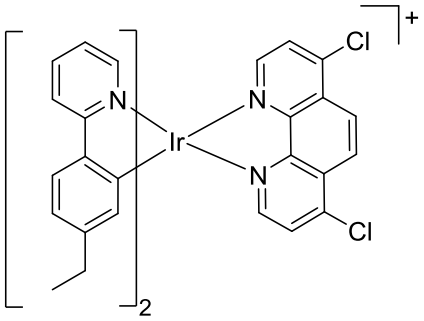

81

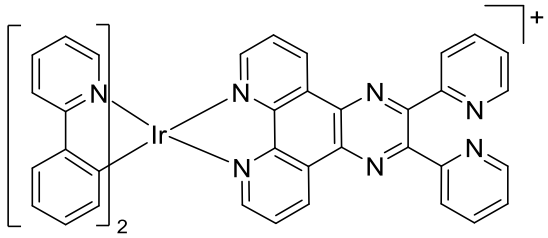

82

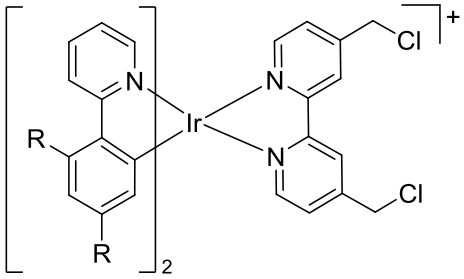

83 R = H **84** R = F

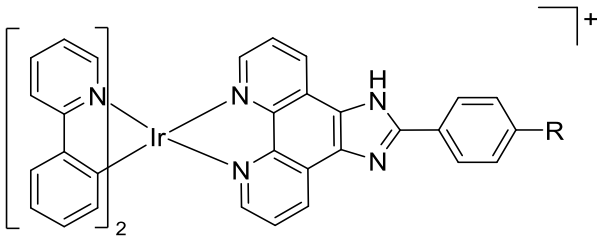

85 R = CN **86** R = OH

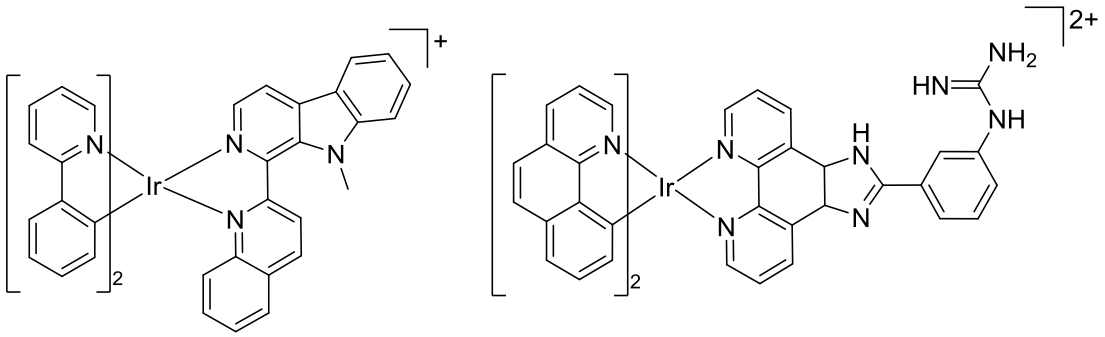

87 **88**

***Figure 1.35**: Anticancer cyclometallated iridium(III) complexes.*

Wang *et al*. investigated the antistatic potential of complex **85** in the metastatic breast cancer cell line MDA-MB-231. Complex **85** was shown to block migration in a wound healing assay, significantly reduced invasion and down-regulated ERK and AKT phosphorylation. The mitochondria-localising complex was shown to be more toxic in MDA-MB-231 cells (IC_{50} 5 μM) compared to normal LO2 liver cells (IC_{50} 40 μM) and caused cell death by intrinsic apoptosis.[200] The related complex **86**, was found to be around ten-fold more active than cisplatin in A549 cells, and showed similar activity in the cisplatin resistant A549R cell line. Cytotoxicity was attributed to enhanced ROS production followed by apoptotic cell death.

Mao *et al.* also designed and evaluated complex **87**. This complex was also found to have sub-micromolar IC_{50} in a range of cell lines. As is typical of this class of compound, **87** was found to accumulate in the mitochondria, leading to a reduction in ATP synthesis, increased production of ROS and loss of MMP. Cell morphology revealed cytoplasmic vacuoles consistent with cell death by paraptosis. In a mouse model tumour xenografts showed a significant decrease in tumour volume and a reduction in cellular proliferation, and the complex was tolerated better by experimental animals.[201]

Complex **88** bearing structural resemblance to complexes **85** and **86**, was designed by Sun *et al*. The complex incorporated a cationic guanidinium functionality to target mitochondria, and its lipophilicity was enhanced by using benzoquinoline (bq) as the cyclometallating ligand used. Despite significant mitochondrial localisation disruption of the MMP and enhanced ROS production this complex displayed only moderate anticancer activity in a range of cell lines.

1.3.4: Rhenium and technetium

^{186}Re and ^{188}Re are both beta emitters and useful reagents for radiotherapy. ^{186}Re emits beta particles with an energy of 1.07 MeV and a half-life of 3.8 days, and ^{188}Re emits beta particles with an energy of 1.97 MeV and a half-life of 16.98 h. One of the most widely used rhenium radiopharmaceuticals is the bone targeting hydroxyethylidine diphosphonate (HEDP) complex used for pain palliation of bone metastases.[202,203] Commercial generators are available that provide rhenium isotopes with high specific activity as perrhenate ions $[ReO_4]^-$ which can be readily reduced to *fac*-$[Re(H_2O)_3(CO)_3]^+$ using commercially available kits, and subsequently conjugated with a wide variety of targeting species. *fac*-$[Re(H_2O)_3(CO)_3]^+$ itself has been shown to bind to gunanine residues via the N7 atom,[204,205] and hence such complexes have the potential to act as both radio- and chemotherapeutics.

The acetonitrile complex **89** was also shown to bind to the N7 atom of 9-ethyl guanine (9-EtG) proving that rhenium tricarbonyl complexes also have the potential to be genotoxic agents.[206] Rhenium tricarbonyl complexes are also able to form non covalent interactions with DNA, for example the phendione complex **90** binds in the major grove of DNA, but it is less cytotoxic than the free ligand.[207] Tricarbonyl aqua complex **91** has a comparable IC_{50} to cisplatin in HeLa cells.[208] Akin to some of the iridium complexes discussed previously, complex **91** induced cell death with visible cytoplasmic vacuolisation, however the MMP was not disrupted and ROS production was not significantly increased.

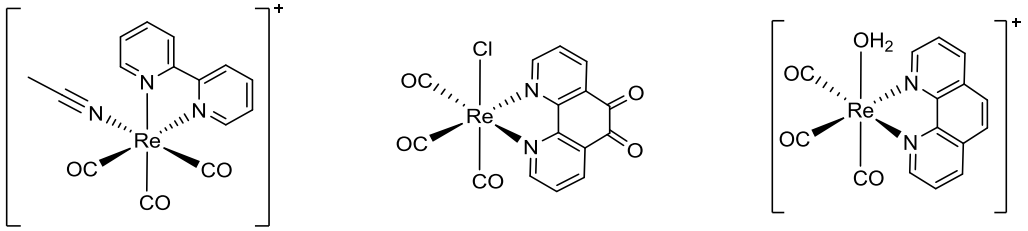

89 **90** **91**

***Figure 1.36**: Simple cytotoxic rhenium(I) tricarbonyl complexes.*

Yam *et al.* investigated the DNA binding properties of a rhenium tricarbonyl complex with a dppz diimine ligand (**92**). Like the ruthenium dppz complexes studied previously, complex **92** showed a DNA switch-on effect upon DNA binding and was

proposed as a DNA intercalator based on the hypochromic and bathochromic shifts in emission observed upon DNA binding.[209] Schanze *et al.* studied the related compound **93** which was also found to behave in an analogous fashion.[210] Complex **92** showed a sequence preference for AT binding sites and was found to induce oxygen-independent photocleavage of DNA (like related Ru complexes).[211] Complexes **94** and **95** were designed with targeting axial ligands to attempt to redirect these complexes to alternative cellular compartments.[212] Compared to complex **92**, complex **92** had a much lower affinity for DNA and was found to localise in the perinuclear region. This was attributed to the mitochondria-directing chloromethyl group. Complex **95** with a pendant myristyl chain localised within the nucleus. Complex **95** had a much higher affinity for DNA compared to **92** which was attributed to additional hydrophobic interactions with DNA.

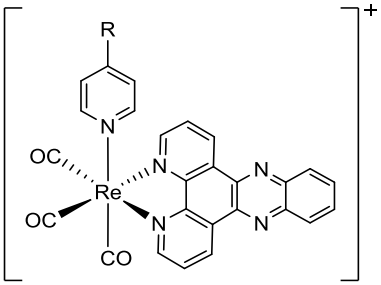

92 R = H **93** R = Me

94 R = CH_2Cl **95** R = myristyl

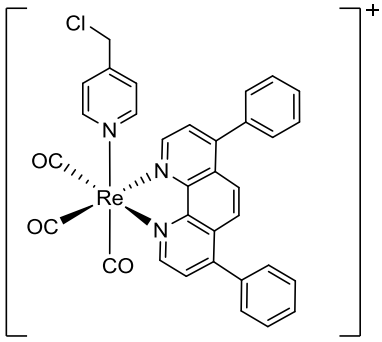

96

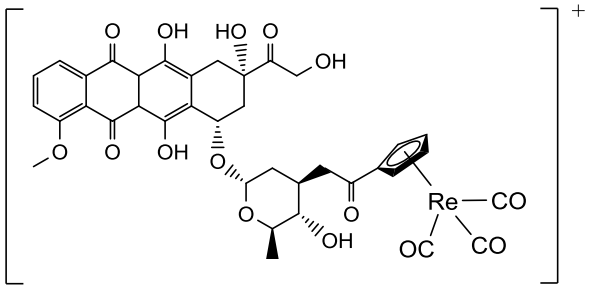

97

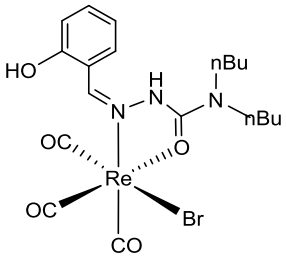

98

***Figure 1.37**: Rationally designed rhenium(I) tricarbonyl anticancer complexes.*

Complex **96** was designed by Mao *et al*. using the chloromethyl moiety previously used in complexes **63** and **94**. The diphenyl phenanthroline diimine ligand is lipophilic

and enhances cellular accumulation. The mitochondria localising complex **96** was retained in mitochondria even after washing and displayed greater cytotoxicity than control complexes. As frequently seen with these mitochondria targeting MLCS, **96** mitochondrial damage resulted in enhanced ROS production, decreased ATP production and induced caspase-dependant apoptosis.[213]

The rhenium piano stool complex **97** was used to divert the cellular localisation of the DNA intercalator doxorubicin to the mitochondria.[214] Using the fluorescence signal from the doxorubicin moiety, Alberto *et al.* demonstrated significant accumulation of **97** in the mitochondrial membranes, with loss of MMP and subsequent cell death by apoptosis, with a sub-micromolar IC_{50} value comparable to that of doxorubicin.

Salicaldehyde semicarbazone rhenium complex (**98**) displays cytotoxicity comparable to that of cisplatin towards MOLT-4 leukaemia cells whilst is relatively non-toxic towards non-cancerous fibroblasts. The hydroxyl group can form adducts with the N7 of guanine residues in DNA, whilst the bromide ligand has also been shown to be labile.[215] Polyamine metal complexes of rhenium have also been synthesised as anticancer agents. The polyamine rhenium tricarbonyl complexes shown below were evaluated as cytotoxic agents and found to have IC_{50} values in the low micromolar range. Additionally, they were found to crosslink DNA more effectively than cisplatin.[215]

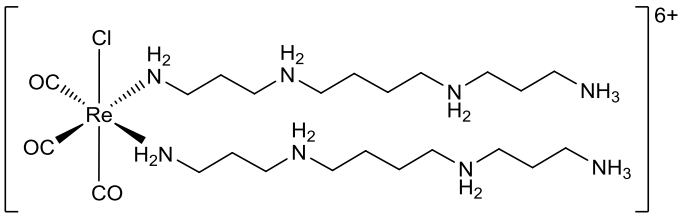

99

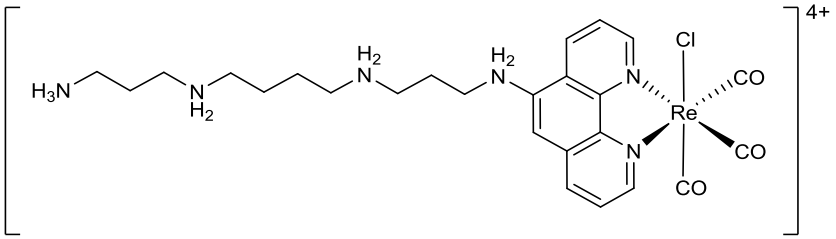

100

***Figure 1.38**: Rhenium(I) polyamine complexes*

1.4: Photodynamic therapy

Photodynamic therapy (PDT) uses a photosensitiser (PS) to generate toxic $^1O_2$ to destroy cancerous tissue without the need for surgery. It is routinely used to treat accessible cancers.[216] Visible light is used to activate the PS and generate $^1O_2$ at its target location. $^1O_2$ is a powerful electrophile and highly reactive.[217] $^1O_2$ causes severe oxidative damage leading to necrotic cell death. The ideal PS should have low dark toxicity, be cell permeable and able to localise at the biological target. For maximal tissue penetration, they must also be able absorb light within the therapeutic window of 600–900 nm. As heavy metals promote rapid ISC luminescent MLCs have great potential for use in PDT, as they are photostable with long lived triplet excited states. Although MLCs typically absorb in the UV/vis region many of these complexes exhibit two-photon excitation within the therapeutic window.[218]

Long-lived triplet excited states (T_1) persist long enough to interact with molecular oxygen. Upon collision, energy is transferred from the T_1 of the luminophore to ground state triplet oxygen ($^3O_2$). Superoxide radical anions are formed by type I processes whereas singlet oxygen $^1O_2$ is formed in type II processes (equation 1). In the type II pathway the triplet excited state of the luminophore collides with $^3O_2$, energy is transferred from the luminophore to oxygen forming $^1O_2$. The main photophysical processes are illustrated in figure 1.39.

Equation 1: $PS(T_1) + {}^3O_2 \longrightarrow PS(S_0) + {}^1O_2$

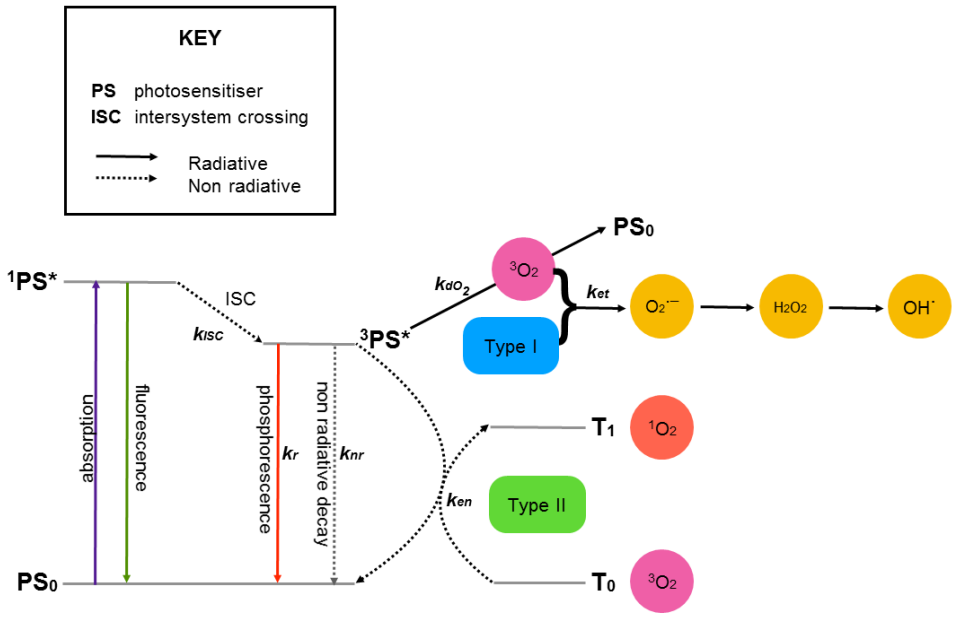

***Figure 1.39**: Photophysical processes of PDT.*

The Ru(II) sensitiser **101** (TLD1433) was entered into clinical trials in 2017 to treat bladder cancer. Although the complex absorbs around 530 nm, its high photostability means it can be used with high intensity light to improve tissue penetration. Its emission is readily quenched by oxygen and has a singlet oxygen quantum yield approaching unity.[219] Complexes with high two-photon absorption (TPA) cross-sections typically contain highly conjugated ligands, such as Ir(II) complex **102** which has emerged as a promising candidate for two photon excitation (TPE) PDT. **102** has an emission quantum yield of 0.33 and a two-photon cross-section of 112 GM at 760 nm. It has minimal dark toxicity, but an LD_{50} of 0.3 μM when illuminated at 405 nm (3.6 Jcm^{-2}). It is a good PS with a 42% yield of singlet oxygen generation. Following irradiation, an 8-fold increase in ROS was detected in treated cells.[220] Interestingly, a structural analogue derived from a 1,1′-dimethyl-2,2′-bisbenzimidazole ligand was found to be significantly cytotoxic under dark conditions.

One of the short-comings of PDT is that it requires an adequate supply of oxygen, however tumours are typically hypoxic in nature. Mitochondria targeting complex **103** was shown to be an effective PDT agent as it reduced the rate of respiration in the mitochondria, with a quantum yield of emission and singlet oxygen production of 0.13

and 0.21 respectively. Cells incubated with 5 μM complex **103** for 12 h maintained 87% cell viability, which decreased to 7.6% after irradiation (475 nm).

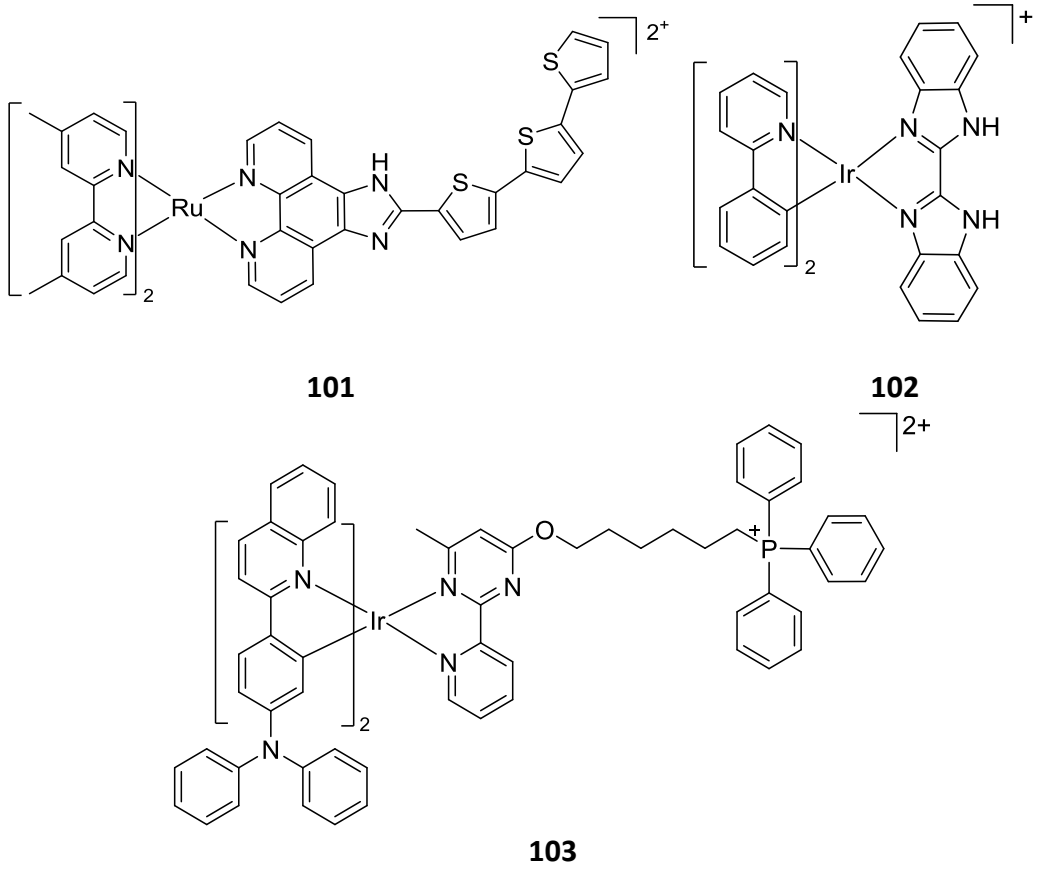

101 **102**

103

***Figure 1.40**: Assorted MLC cellular probes.*

1.5: Photoactivated chemotherapy

Although PDT is a minimally invasive technique, it is not without side-effects. The most widely used PDT agents can persist in the body for a long time and can cause severe skin photosensitivity. Additionally, as cell death occurs by necrosis, significant inflammation occurs in the surrounding tissues which can be very painful.[221] An alternative technique that is gaining popularity is photoactivated chemotherapy (PACT), whereby a prodrug with negligible toxicity is activated by a photochemical reaction at the target location, as shown in figure 1.41. Upon irradiation, triplet excited states can undergo reactions such as reduction or ligand dissociation, which reflect the nature of the reactive excited state and its closely lying states.[222] Metal-centred (MC) d-d transitions are generally weak as they are Laporte-forbidden. As the d-d excited state is antibonding in nature its presence manifests as bond lengthening and enhanced ligand substitution. If the MC excited state is the lowest energy level, the complex may be

susceptible to ligand photorelease, for example rhenium(I) photoactivated CO releasing molecules (photoCORMs). In contrast, charge transfer transitions (MLCT or LLCT) can lead to photoredox reactions, such as the reduction of Pt(IV) to Pt(II) or the generation of radicals by homolytic cleavage. Photoactivation can be used to control when and when the toxic species (metal fragment and/or ligand) is unleashed.[223]

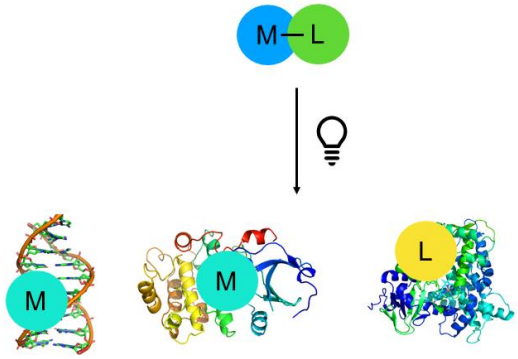

***Figure 1.41**: Photoactivated therapy with MLCs. Photochemical reactions cause the MLC to dissociate releasing a metal fragment and a ligand fragment either of which (or both) have a therapeutic effect. (Adapted from Bonnett.* [223]*)*

Complex **104** *cis*-dichlorobis(phenanthroline)rhodium(III), (cisDCBPR) is one of the first PACT agents studied, largely inspired by cisplatin.[224] Upon photoactivation, the aquated species formed at least 2 covalent adducts with calf thymus DNA (at guanine N1 and adenine N3). Sadler *et al.* developed the photoactivated Pt(IV) complex **105**. It was found to be stable in the dark and resistant to biologically relevant reducing species; however, it undergoes some photoinduced reduction. The predominant toxic species are formed by photosubstitution of the azido ligand(s) to yield highly cytotoxic *trans*-platinum species that form intrastrand cross links with DNA using red light.[225]

There has recently been a surge in interest to develop pharmaceutical PhotoCORMs as CO plays an important role in cell signalling. In addition to its role as a cytoprotective agent, it can protect against ischemic reperfusion injury in low doses, modulates MAPK signalling and exerts an anti-proliferative effect.[226] PhotoCORMs have been shown to rapidly eradicate aggressive malignant cells.[227]

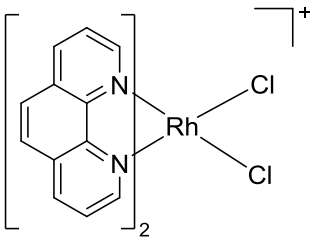

104

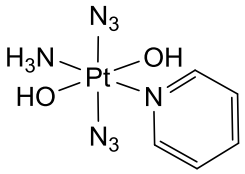

105

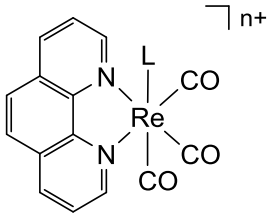

106 L = Cl^- (n = 0)
107 L = MeCN (n = 1)
108 L = PPh_3 (n = 1)
109 L = MeIm (n = 1)
110 L = CF_3SO_3 (n = 1)

***Figure 1.42**: Photoactivated metal complexes.*

Mascharak *et al.* designed a family of phenanthroline Re(I) tricarbonyl complexes (106 – 110) and investigated their photophysical properties, CO release and cellular localisation.[226] High energy UV irradiation enables the thermally accessible ^{3}MC to be populated. Complex 110 did not act as a photoCORM; however, complexes 108 and 109 with π-acceptor ligands labilise the trans carbonyl ligand; the remaining carbonyls can effectively stabilise the Re(I) state, and no further photorelease occurs. Complex 106 underwent multiple carbonyl loss as the Re(I) centre could not be stabilised with the σ-donating chlorido ligand.[227] All complexes were taken up by triple negative breast cancer cells, and localised in discrete structures within the cytoplasm. Complex 108 also showed some staining of the nucleoli. No other biological effects were reported.

1.6: Project rationale

The polyamine transport system has huge potential for targeting chemotherapeutic drugs; the aim of this project is to explore the feasibility of using the polyamine transport system to deliver therapeutic and/or theranostic MLCs to cancer cells with an active PTS. Polyamines are readily incorporated into chelating ligands using robust and versatile Click chemistry that can subsequently be coordinated to a wide variety of metal centres. The scaffold of the target complexes of this study are shown below.

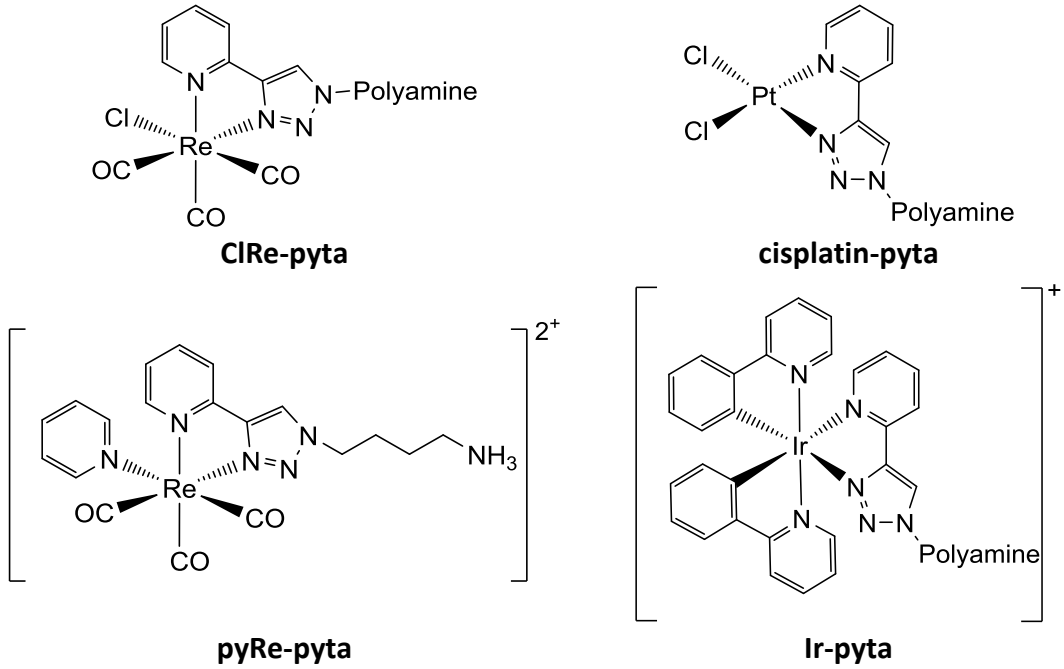

***Figure 1.43**: Polyamine MLCs*

1.7.1: Project aims

Whilst the use of polyamines as a cancer specific vector has been well researched with respect to small organic molecules, their applications in metallodrugs is extremely limited. Given that metallodrugs often exert their therapeutic action via their effects on DNA, polyamine conjugation has great potential to enhance both cancer specificity and potency. A platinum(II) pyridyl triazole complex with a pendant Spd group was made previously, however the synthetic route used resulted in extremely low yields (around 7%). In order to evaluate the therapeutic potential of this approach, the synthetic procedure needed to be optimised.

Earlier work in the Lowe/Cullis group had demonstrated that polyamine conjugates of iridium and rhenium are internalised into A549 cells and are suitable for use as luminescent probes for confocal microscopy.[96] However, whether or not this uptake is mediated by the PTS had not been established. The key aim of this project was to investigate this cellular uptake in more detail. As the PTS has been shown to be highly dependent upon charge, a series of complexes with different charges at physiological pH were designed and synthesised in order to characterise cellular uptake.

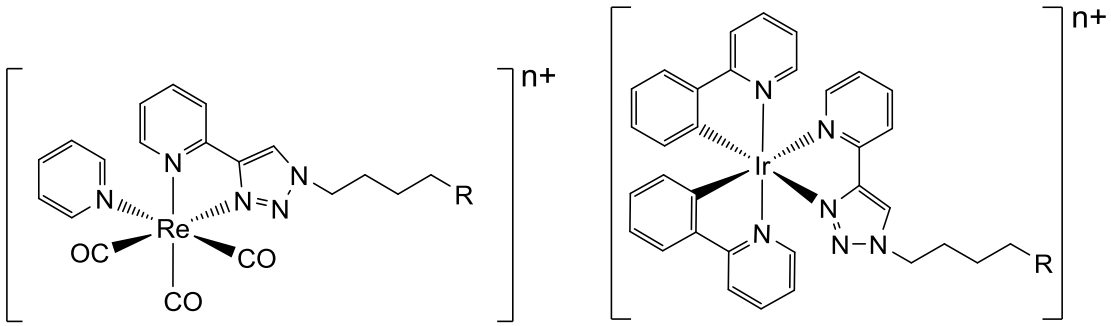

111	**pyRe-Put** (R = NH_2)	**115**	**Ir-Put** (R = NH_2)
112	**pyRe-AcPut** (R = NHAc)	**116**	**Ir-AcPut** (R = NHAc)
113	**pyRe-COOH** (R = COOH)	**117**	**Ir-COOH** (R = COOH)
114	**pyRe-PO(OH)$_2$** (R = $PO(OH)_2$)	**118**	**Ir-PO(OH)$_2$**(R=$PO(OH)_2$)

***Figure 1.44**: Control complexes designed to probe polyamine transport in cells.*

Whilst the iridium pyridyl triazole (pyta) complexes used were found to give rise to bright phosphorescence when excited at the wavelength commonly used for confocal microscopy (405 nm), the rhenium constructs show only weak emission at this excitation wavelength. A further aim of this project was to tune the photophysical properties of the complexes to improve their performance as cellular probes for confocal microscopy. Initially this was explored by incorporating either electron donating or electron withdrawing groups into the pyta ligand to assess the impact of different substituents on the photophysical properties of the complexes.

1.7.3: Thesis overview

The biological significance of the polyamines in both normal cell functions and their role in maintaining the malignant phenotype has been discussed, along with the current understanding of polyamine transport in mammalian systems, and how this knowledge can be exploited for therapeutic and/or diagnostic purposes. The use of MLCs as alternative luminescent probes in state-of-the-art microscopy techniques has been explored along with the development of MLCs for cancer treatment. In order to create theranostic molecules it is important to understand how each of these components can modified and combined to good effect. The work presented herein goes some way towards realising this aim.

Chapter 2 discusses the synthetic strategies employed to synthesise the target compounds, from synthesis of the precursors used to prepare the pyta proligands, to the chemistry of coordination to the various metal centre used in this study. Also discussed are the various methods used to functionalise the ligands for both modulation of the photophysical properties and the localisation of the target complexes. Chapter 3 explores the concepts behind tuning emission in both rhenium and iridium diimine complexes, and the photophysical properties of the complexes are presented. The development of procedures to image cells treated with the complexes designed to probe uptake are discussed in chapter 4, along with results from time-course experiments and colocalization studies using the commercial probes MitoTracker™ and LysoTracker™. Uptake was evaluated in a range of cell lines both with and without a competent PTS. The toxicological evaluation of Re(I) and Pt(II) complexes in cisplatin sensitive and cisplatin resistant ovarian carcinoma cells are presented in chapter 5.

The key findings of this study are summarised in chapter 6 and some results of some related studies that have great future potential are discussed, along with suggestions for the future direction of the research. Experimental details can be found in chapter 7.

Chapter 2 : Synthesis

2.1: The story so far.

Previous studies in the Lowe/Cullis group had shown that a range of polyamine MLCs are taken into A549 cells.[96] Analysis of live cells treated with 100 μM of rhenium(I) complexes **119** to **122** by confocal microscopy showed that complexes with an amide linkage (**121** and **122**) were less efficiently transported into the cells than the directly attached complexes (**119** and **120**). Overall, complex **119** was the most substantially internalised rhenium probe. The localisation of iridium probes **123** and **124** largely resembled that of the rhenium complexes, although the observed luminescence intensity was much greater. This is most likely to be a result of the differences in the photophysical properties of the two probes (discussed further in Chapter 3), rather than differential uptake. The straight chain analogues (**119**, **121** and **123**) were transported more efficiently into the cells compared to the branched chain analogues (**120**, **122** and **124**); however, they may be more toxic as the nucleoli of cells treated with complex **124** (75 μM) were intensely stained at early timepoints.

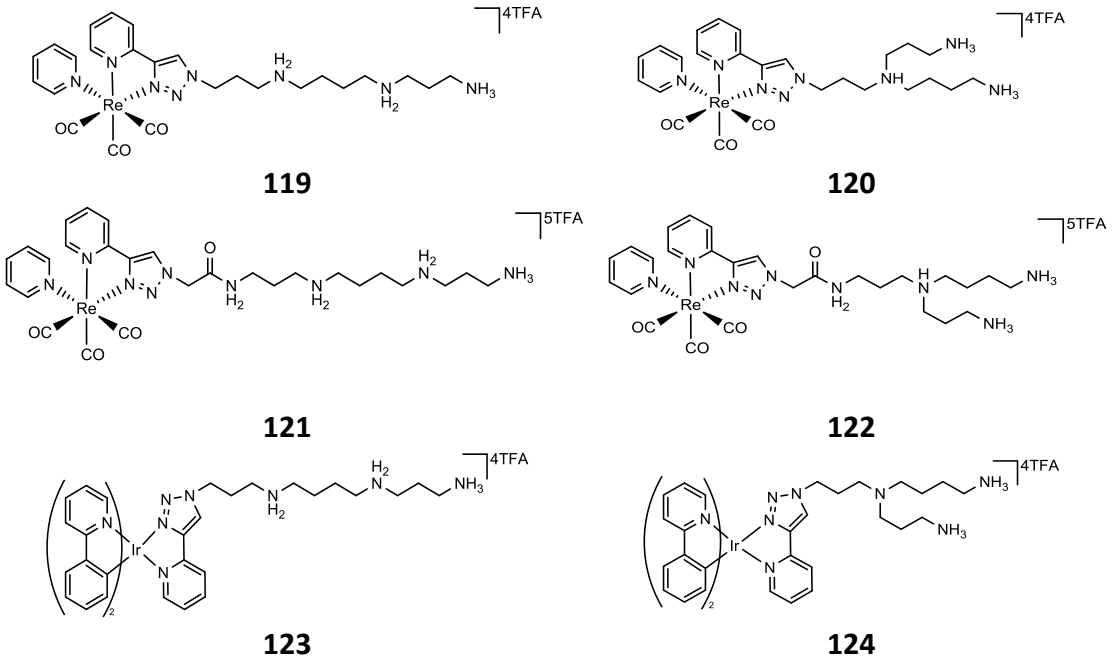

***Figure 2.1**: Complex cations used in preliminary cellular studies.*[96]

Attempts to inhibit uptake of complexes with Spd to determine if the PTS was responsible for uptake gave ambiguous results. Spd did not abrogate uptake of the complex and little difference in uptake was seen in cells treated with or without a 10-fold excess of Spd; however, as the cell culture medium used contained Put, these results should be treated with caution, the transporter may already be saturated which could explain the lack of effect.

Iridium complex **115** (Figure 2.2) with a pyta ligand derived from Put was used as a control. This monoamine complex was not expected to be taken up into the cells via the PTS. However, its uptake paralleled that of complex **123** implying a common mechanism of uptake. It is not inconceivable given the promiscuity of the PTS that this control complex could be recognised as a substrate. Although there is only one amine site that can be protonated at physiological pH; the metal centre is itself cationic and likely fulfil the criteria for recognition by the PTS. Alternatively, this could imply that the uptake of complexes occurs by an entirely different mechanism. Given that a wide variety of MLCs without a polyamine targeting vector have been shown to localise in cells this possibility cannot be ruled out, and thus the findings of these preliminary studies were largely inconclusive.

2.2: Target compounds

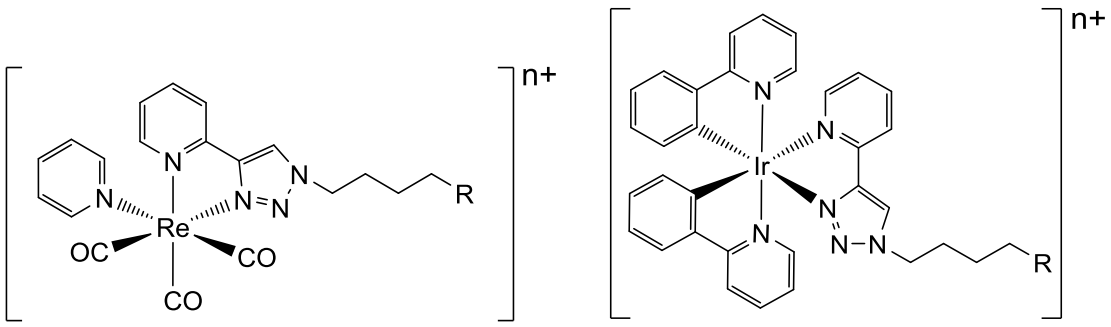

111	**pyRe-Put** (R = NH_2)	**115**	**Ir-Put** (R = NH_2)
112	**pyRe-AcPut** (R = NHAc)	**116**	**Ir-AcPut** (R = NHAc)
113	**pyRe-COOH** (R = COOH)	**117**	**Ir-COOH** (R = COOH)
114	**pyRe-PO(OH)$_2$** (R = $PO(OH)_2$)	**118**	**Ir-PO(OH)$_2$**(R=$PO(OH)_2$)

***Figure 2.2**: Charge modified complexes.*

A library of luminescent complexes **111 – 118** (as shown in Figure 2.2) were designed to probe cellular uptake in order to determine whether the PTS mediates the transport of the polyamine MLCs. These complexes were based on the same pyta ligand framework differing only in the nature of the terminal substituent at the end of the carbon chain. A synthetic route for the synthesis of complex **115** has been established previously, however complex **111** is novel but can be accessed via this methodology.[96] The acetylated complexes **112** and **115** can be prepared directly from complexes **111** and **115**. Complexes **113, 114, 117** and **118** are not derived from polyamines but are instead accessed via brominated starting materials.

In addition to these charged analogues, a series of complexes were designed with different polyamine chain lengths as shown in figure 2.3. These ligands mimic the naturally occurring polyamines as evidence from the literature points to these structures as being the most efficiently transported. Branched polyamines were not used as the preliminary data showed that they were not as well internalised as their linear counterparts;[96] this has also been documented by Vanhoutten.[228] Complexes **126** and **128** are novel complexes, and whilst complexes **125, 127**, **119** and **123** have been made previously, an alternative synthetic route was developed as part of this work.

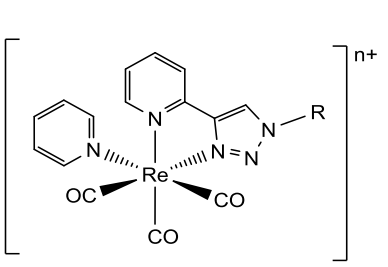

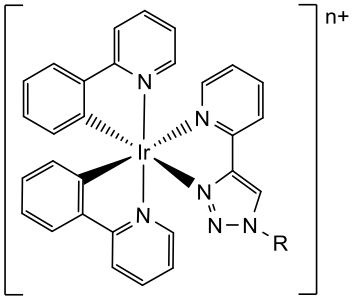

111 Butylamine (n = 2)

125 Putrescine (n = 3)

119 Spermidine (n = 4)

126 Spermine (n = 5)

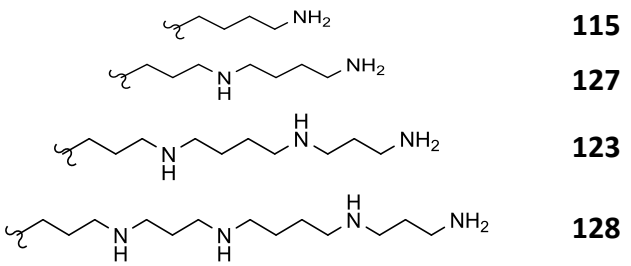

115

127

123

128

Figure 2.3: *Polyamine complex library.*

Complexes with substituted pyridyl triazoles were designed as a starting point to optimise the photophysical properties of these complexes for biological imaging. Substituted 2-ethynylpyridines are either not commercially available, or prohibitively expensive, and so these compounds were prepared via Sonogashira coupling of the substituted 2-bromopyridine compounds with ethynyltrimethylsilane. Iridium complexes with substituted cyclometallating ligands were also investigated, with cyclometallated ligands prepared by Suzuki coupling. The synthetic route is summarised in figure 2.5.

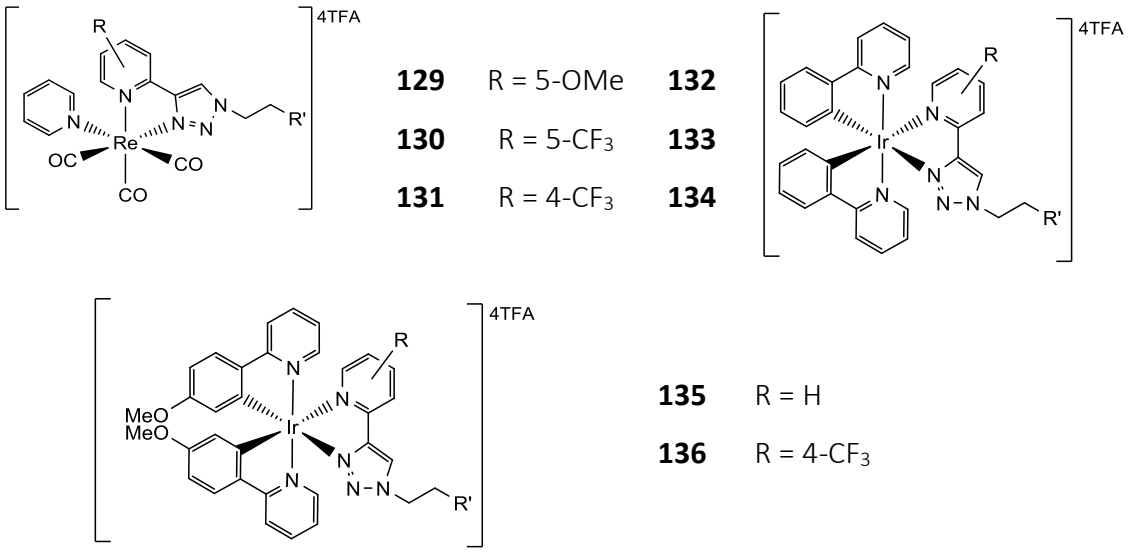

***Figure 2.4**: Substituted complexes, all substituted complexes were prepared with the Spd chain, where R' = $CH_2NH_2(CH_2)_4NH_2(CH_2)_3NH_3^{3+}$*

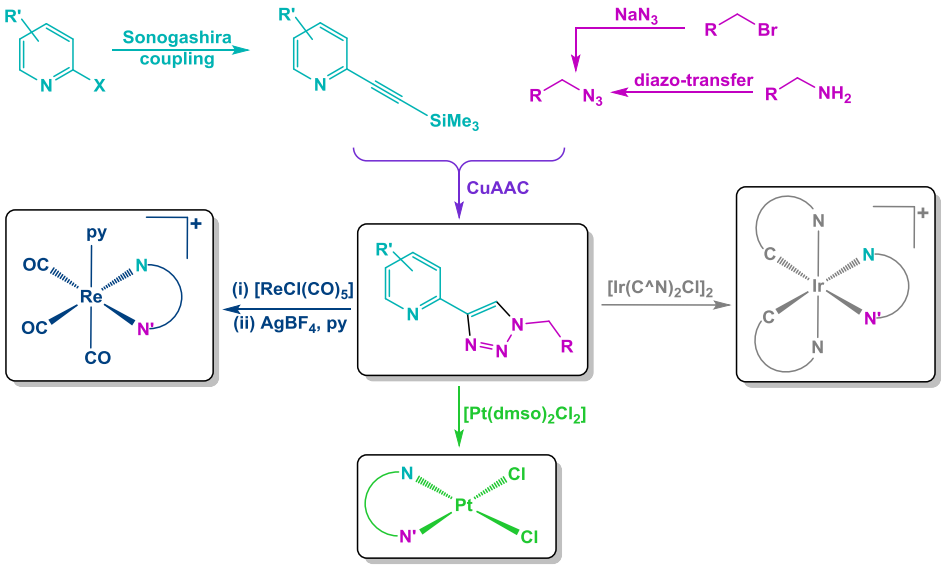

***Figure 2.5**: Proposed synthetic route for the preparation of polyamine MLCs, where C^N is ppy or p-OMe ppy (papy) and X is Br or Cl.*

2.3: Synthesis of polyamines.

In order to use polyamines as a vector for the delivery of therapeutic agents, robust synthetic techniques for the site-specific conjugation of drug molecules are vital. As biogenic polyamines are not symmetrical and contain both primary and secondary amine functionalities, careful consideration must be given to the synthetic strategies employed. It is possible to synthesise polyamine analogues from commercially available polyamines by exploiting differences in reactivities of the individual amines, particularly in the case of Spd,[229,230] however a bottom-up stepwise synthetic approach to the assembly of the polyamine chain enables a greater degree of control and can be used to create non-biogenic analogues. Both approaches have successfully been employed in the literature, and extensively reviewed elsewhere.[231]

2.3.1: Selective mono-protection of polyamines

Put (1) is a cheap and readily available starting material with two equivalent amine groups. A single primary amine group is required for conjugation, so the remaining amine group must be masked to prevent any undesired reactions and/or coordination to the metal in subsequent steps. This is particularly important for this low molecular weight compound as the subsequent step is synthesis of an azide; bis-functionalisation could lead to a potentially unstable molecule that could be dangerous, especially if accidentally isolated. The protecting group used needs to be compatible with the basic reaction conditions used in subsequent steps and stable to hydrogenation, so the *tert*-butyloxycarbonyl (Boc) protecting group is an obvious choice.

To ensure that only a single protecting group was introduced, the kinetics of the reaction were carefully controlled. The starting material di-*tert*-butyl dicarbonate (Boc_2O) was added very slowly to a three-fold excess of Put at low temperature with rapid stirring to avoid localised high concentrations developing and to help prevent the solvent freezing. The literature procedure followed reported a yield of 95 % using anhydrous dioxane.[75] The Boc-protected amine (137) was routinely prepared in yields of around 75 % using standard reagent grade dioxane and without employing rigorously anhydrous reaction conditions to yield a clean product following a simple extraction. As

the subsequent steps to prepare the target molecules were carried out on a millimolar scale, this yield was more than adequate.

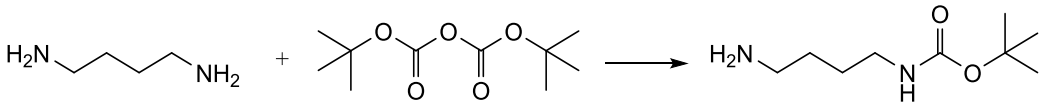

1 **137**

***Scheme 2.1**: Boc protection of putrescine (**1**). **Reaction conditions**: 1,4-Dioxane, N_2 0 °C, 4h, 20 °C, 16h (75%).*

The synthesis of Spm and Spd analogues is not amenable to this simple approach owing to the presence of both secondary and primary amines. In previous work, Spd and spermine conjugates were prepared via a systematic chain extension of a diamine precursor, as shown in scheme 2.1.[96] This method requires seven synthetic steps involving subsequent rounds of protection, chain elongation, protection and hydrogenation. In this stepwise approach, acrylonitrile is used to alkylate the primary amine, which is subsequently hydrogenated using Raney nickel. Although the individual reactions can be carried out in good to moderate yields, the overall yield of the process is low due to the large number of steps (around 30 % overall), and need to be carried out on a multi-gram scale. Given that most of the reactions require 24 hours; synthesis of Boc-protected spermine by this approach is a somewhat arduous task.

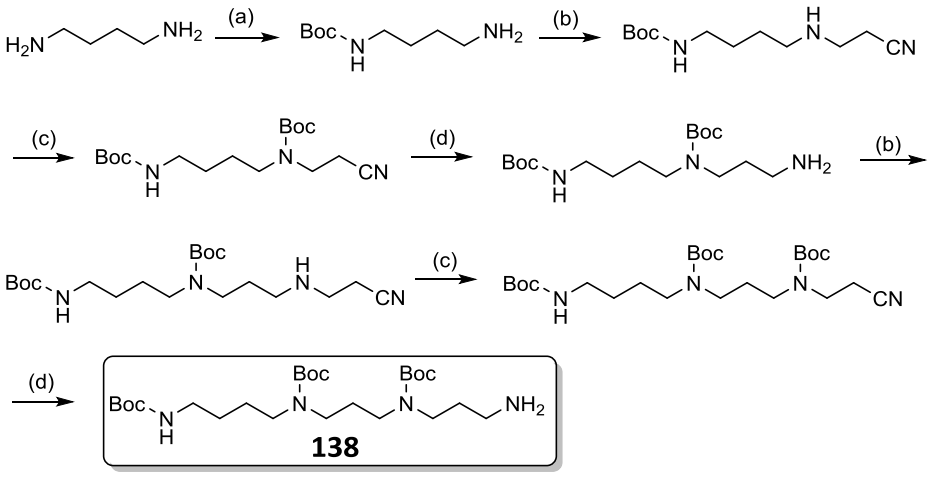

***Scheme 2.2**: Stepwise synthesis of Boc_3Spm (**138**). **Reaction conditions**: (a) Boc_2O, Dioxane, 0 °C, 16h; (b) acrylonitrile, MeOH, 20 °C, 24 h; (c) Boc_2O, Et_3N, DCM, 20 °C, 24 h; (d) H_2, Raney Ni, NaOH, aq. EtOH, 20 °C, 24 h.*

A variety of alternative methods to prepare polyamine conjugates using the free base of the biogenic polyamines are reported in the literature that employ a mixture of orthogonal protecting groups to ensure conjugation occurs reliably and at the desired nitrogen site. One such approach uses ethyl trifluoroacetate to install a temporary, primary amine selective protecting group.[232] However this method requires very low temperatures (-70 ˚C) to ensure the primary amine is alkylated selectively. The trityl protecting group has also been successfully used as a primary amine-selective protecting group for polyamines.[233] In a recent publication, Magoulas *et al.* used acid labile trityl groups to protect the primary amines and the base labile methoxycarbonyl group to protect the secondary amines.[234]

In this study Boc-protected spermine, (**138**) was prepared using the approach outlined in Scheme 2.3.[80] Salicylaldehyde is used stoichiometrically to install a single, primary amine selective protecting group. Boc_2O is then used to globally protect the remaining amines, and the imine group subsequently cleaved using methoxyamine. The distinct advantage of this approach, which is essentially a one-pot, three-step reaction; is that can be completed within 3 days giving isolated yields of around 50 %, (which is comparable with the literature method). Not only is the method much quicker but the overall yield is also significantly greater than the aforementioned step-wise approach, and is it is also more amenable to a smaller, sub-gram scale. This is a greener alternative as it negates the repeated use of the suspected carcinogen acrylonitrile and the environmental pollutant Raney nickel, which is also pyrophoric and potentially carcinogenic.

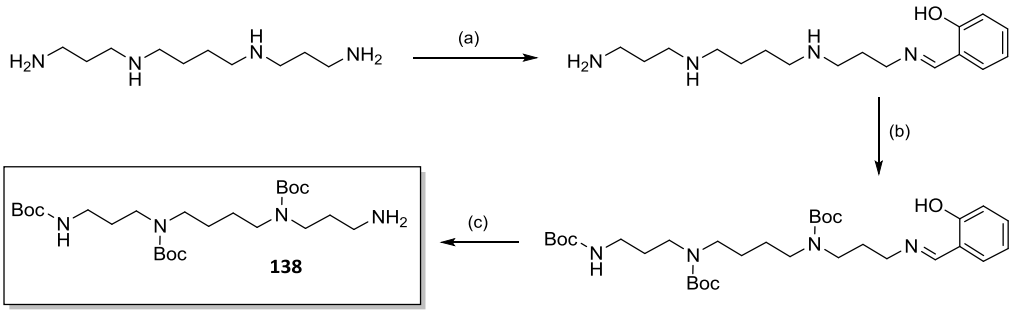

***Scheme 2.3**: Synthesis of triBocSpm (**138**) via temporary protecting group. **Reaction conditions**: (a) salicylaldehyde, Na_2SO_4, MeOH/DCM (1:3) 0 °C, 16h; (b) Boc_2O, 20 °C, 12h; (c) CH_3ONH_2, Na_2CO_3, 20 °C, 2 h, 56 % yield over 3 steps.*

In the first step of the reaction a temporary protecting group is installed on one of the terminal primary amines. Salicylaldehyde reacts preferentially with primary amines to form an imine. Similar kinetic controls were employed to favour the formation of the mono-imine intermediate. Sodium sulfate was added to the reaction mixture to remove water formed in the reaction thus preventing unwanted hydrolysis of the imine and maintaining anhydrous conditions for the subsequent step. In the second step, Boc_2O was added to globally protect the remaining amine groups. The target molecule (138) was obtained by removing the temporary imine protecting group from the primary amine *in situ* using methoxyamine.

Due to the telescopic nature of this procedure careful consideration must be given to the molar equivalents used in this reaction in order to minimise the formation of unwanted by-products. A common impurity of this reaction is the fully Boc-protected amine, which is formed if too large an excess of Boc_2O is used. Free amine formed in the final stage of the reaction may react with any excess Boc_2O, for this reason, it is important that the final step is carried out immediately prior to the work up and purification by column chromatography. The fully protected by-product is very non-polar and may be readily separated from the desired product by column chromatography. Conversely, if insufficient Boc_2O is used (or it is depleted by insufficiently anhydrous conditions) a range of under-protected compounds may form, which being more polar are harder to resolve chromatographically from the desired product.

As an abundance of possible by-products may be generated when using this procedure, it is crucial to ensure that compounds are spectroscopically pure by quantifying the signal intensities of characteristic proton resonances. Many of the methylene proton resonances appear broad due to the presence of rotamers. Slow (on the NMR timescale) rotation of the Boc groups about the carbamate nitrogen-carbon bond leads to E- and Z-tautomeric forms as shown in Figure 2.6. This gives rise to two separate sets of signals for atoms adjacent to Boc groups. In the case of ^{1}H-NMR, many of the methylene resonances (along with their rotameric forms), occur within a very narrow region of the spectrum. As a result, multiply superimposed signals manifest as broad featureless signals that are difficult to fully assign.

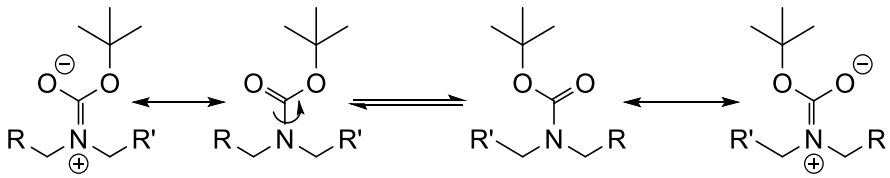

Figure 2.6: *Tautomerisation of the Boc group.*

This is remedied by acquiring NMR data at an elevated temperature. At 323K the faster rotation of the Boc groups cause the resonances to coalesce enabling the characteristic splitting patterns to be observed, and signal intensities may be measured with greater precision. In the case of ^{13}C-NMR, tautomerisation causes two discrete carbon signals to be observed for some signals at room temperature. At elevated temperatures these coalesce to form a single broadened peak.

2.3.2: Polyamine chain elongation

Upon conjugation to a molecule of interest, one of the amine functionalities (and hence cationic sites) is lost. In order to generate molecules that closely resemble Put, Spd and Spd with respect to their charged sites, the biogenic polyamines must be synthetically elongated prior to conjugation. This is carried out by the process described in scheme 2.4. Michael addition of acrylonitrile to the unmodified amine is used to extend the polyamine chain by an aminopropyl unit. It is important that the initial alkylation step is carried out under basic conditions to ensure that the amine nitrogen is sufficiently nucleophilic. Over-alkylation readily occurs, but this can be minimised by using stoichiometric quantities of the reactants; however, these by-products are easily separated by flash column chromatography. Subsequent steps in the synthesis, i.e. Boc-protection of the newly formed secondary amine followed by hydrogenation of the nitrile are both clean and high yielding reactions giving products that are typically suitable for use without further purification.

2.3.3: Branched polyamines

In this work linear polyamine conjugates have been prepared, with mono-functionalisation carried out exclusively at a single primary amine site. Another widely used strategy that is suitable for the synthesis of branched polyamine conjugates uses the primary amine selective reagent 2-(Boc-oxyimino)-2-phenylacetonitrile, commonly referred to as Boc-ON. Boc-ON can be used to selectively protect primary amines, leaving

only secondary amines free to react. This methodology is particularly well suited to the preparation of branched Spd conjugates. The strategy outlined in Scheme 2.2 can then be used to introduce a linker for conjugation to the molecule of interest, and has been used (by others) to synthesise Spd-drug conjugates and fluorescent probes.[235–237]

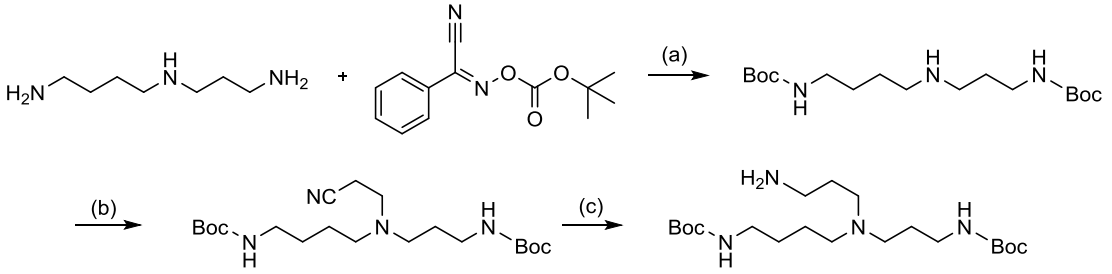

***Scheme 2.4**: Synthesis of branched polyamines. **Reaction conditions**: (a) THF, 0 °C, 4h; (b) acrylonitrile, MeOH, 20 °C, 24 h; (c) Boc_2O, Et_3N, DCM, 20 °C, 24 h; (d) H_2, Raney Ni, NaOH, aq. EtOH, 20 °C, 24 h.*

2.3.4: Polyamine analogues

It has been postulated that the spatial distribution of the charged centre of the cationic metal complexes **111** and **115** the terminal butylamine may enable recognition by the PTS. In order to probe this hypothesis further, a key aim of this work was the design and synthesis of a set of control compounds that would mimic this control complex in size, but with different charge distributions. Complexes derived from triethylene glycol (TEG) monomethyl ether were designed alongside the charge modified complexes **111** – **118**. Whilst the oxygen atoms of the TEG group would not be expected to be protonated at physiological pH, it should have a similar aqueous solubility as the polycationic polyamine complexes, and a useful control compound to test if the polyamine group is an effective vector.

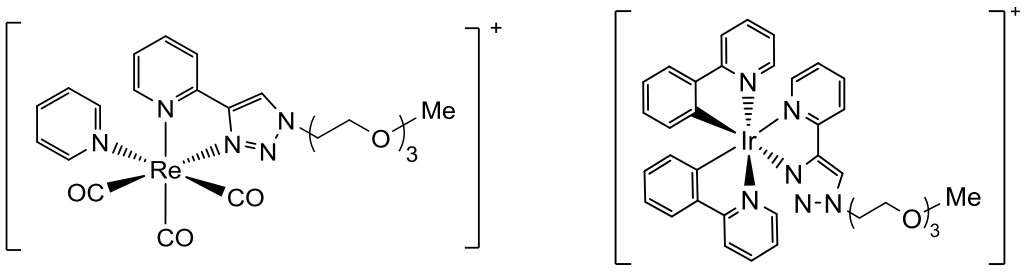

139 **140**

***Figure 2.7**: PEG monomethyl ether complex cations.*

The azide starting material required for the synthesis of the PEG ligand is extremely expensive but is relatively easy to make in two steps from very cheap starting materials. Triethylene glycol monomethyl ether is tosylated (compound **141**) to convert the alcohol to a good leaving group which can subsequently be substituted by sodium azide. Whilst the tosylation step is facile, the work-up can drastically reduce the isolated yield if due care is not given to the quantity of acid added to quench the reaction, and the amount of water used in the washing step. (This compound was synthesised in a 23 % yield by undergraduate student B.Barbi.) On reviewing the literature it was suggested that the conditions used to effect tosylation (see Scheme 2.5) can cause some hydrolysis of the glycol chain and tosyl derivative does not have a good shelf life, and suggested using a mesyl group instead.[238]

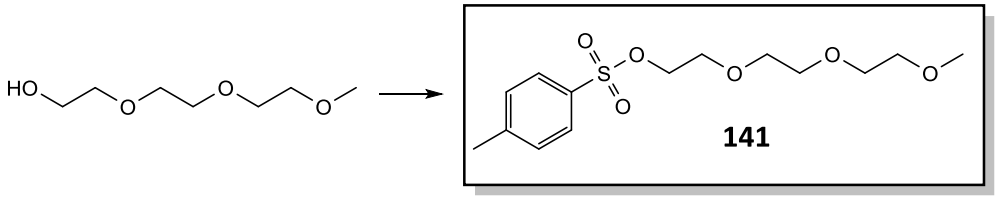

Scheme 2.5*: Tosylation of triethylene glycol monomethyl ether (as carried out by B.Barbi)* ***Reaction conditions****: TsCl, pyridine, 4 °C, 18 h, the neutralised with 12M HCl.*

The cheap and commercially available starting material ethyl 5-bromopentanoate was chosen as the precursor for complexes **113** and **117**. The ester starting material is preferable to the carboxylic acid group as this can coordinate to metals. The ester group can be removed by hydrolysis under mild conditions as a final deprotection step. Unfortunately, diethyl (4-bromobutyl)phosphonate (**142**) the equivalent precursor for the phosphonic acid complexes **114** and **118** was not commercially available however, this starting material could be conveniently prepared using a microwave assisted variant of the Michaelis-Arbuzov reaction.[239] This reaction is commonly used to prepare phosphonates, which are useful starting materials for Horner-Wadsworth Emmons reactions which form stabilised ylides to access E-alkenes.

Villemin *et al.* reported a solvent-free microwave synthesis of **142** by the mono-functionalisation of 1,4-dibromobutane, as shown in scheme 2.6.[239] Heating dibromobutane with triethyl phosphite for 5 minutes at a constant power of 150 Watts, yielded the desired product, **142** in 90 % yield. Over phosphorylation was avoided by

using dibromobutane in a 3-fold excess, (in a similar fashion to the mono Boc protection of Put).

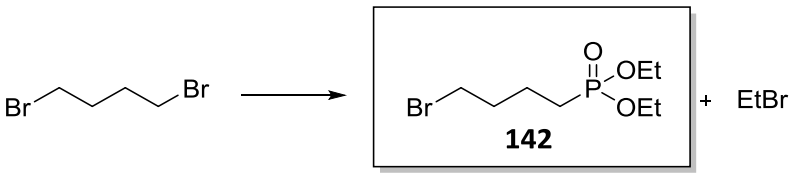

***Scheme 2.6**: Michaelis-Arbuzov reaction to form compound **142**. **Reaction conditions**: (a) P(OEt)$_3$, MW 150W, 2.5 min.*

It was reported that at temperatures exceeding 180˚C, a cyclic by-product, 2-ethoxy-1,2-oxaphosphinane 2-oxide was formed (see Figure 2.8). Initial cautious attempts to prepare compound **142** used a ramped heating method to gradually increase the power to 150 W. To avoid formation of unwanted cyclic by-products the program was set to cut out at a temperature of 125 ˚C, however due to the small volumes used, this occurred after only 1.5 minutes. Analysis of the reaction mixture by ^{31}P- and ^{1}H-NMR showed hardly any conversion of the starting material, with 2 minor products consistent with the reported products of hydrolysis and oxidation of triethyl phosphite, *vide infra*.[240]

Microwave heating at a constant power of 150 W for 5 minutes greatly exceeded 180 ˚C, and although triethyl phosphite was fully consumed, many by-products were produced. Nine resonances were observed in the ^{31}P-NMR spectrum, and whilst the desired product had been produced, it was not the major product formed. Further modifying the microwave method to a lower power (120 W) with a thermal cut-out set to 180 ˚C resulted in an improved conversion to the desired product, but incomplete conversion of the limiting starting material. Scaling up the reaction improved the yield, presumably as the larger reaction volume available to absorb the microwave energy resulted in a longer time before the thermal cut-off was reached. Subsequent purification by flash column chromatography to remove excess dibromobutane resulted in an isolated yield of 65 %. Purification at this step is of vital importance to ensure that the excess dibromobutane is removed from the product, as the next step is azide formation.

Jansa and co-workers explored this reaction further, and identified 2 additional by-products of this reaction, as shown in Figure 2.8.[240] Thermal decomposition of triethyl

phosphite produces the elimination product, diethyl phosphonate, which may also be formed by hydrolysis in the presence of traces water. Triethyl phosphate is derived from oxidation of the starting material and may be eliminated by carrying out the reaction under an inert atmosphere.

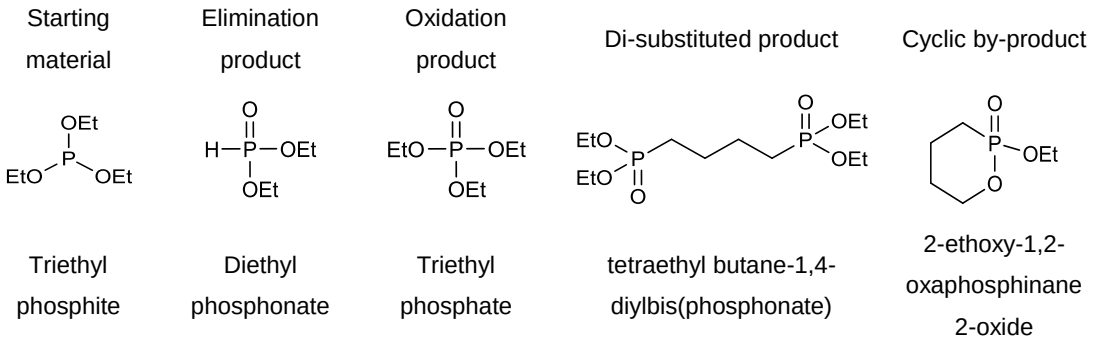

***Figure 2.8**: Major by-products of synthesis of **142**.*

For future use, this reaction could be optimised by several modifications to the current procedure. The easiest modification is to simply further scale up the reaction, which should enable the reaction to be heated for longer. Villemin *et al.* safely scaled this reaction up to 0.1 moles with respect to triethyl phosphite. Additionally, degassing and adopting anhydrous conditions should further eliminate formation of side-products derived from the limiting reagent and achieve yields near the 90 % reported in the literature.

2.4: Alkyne synthesis

2.4.1: Sonogashira coupling

Sonogashira cross-coupling is the palladium catalysed coupling of aryl (or vinyl) halides with terminal acetylenes,[241] and is one of the most widely used carbon-carbon bond forming reactions.[242] Copper(I) is used as a co-catalyst to enhance the reactivity of the acetylene however, this also makes the reaction very sensitive to oxygen. In the presence of oxygen, copper-mediated Glaser-Hay homocoupling of the acetylene can drastically reduce the yields of cross-coupling. Copper-free cross coupling reactions are feasible but require higher temperatures.[243]

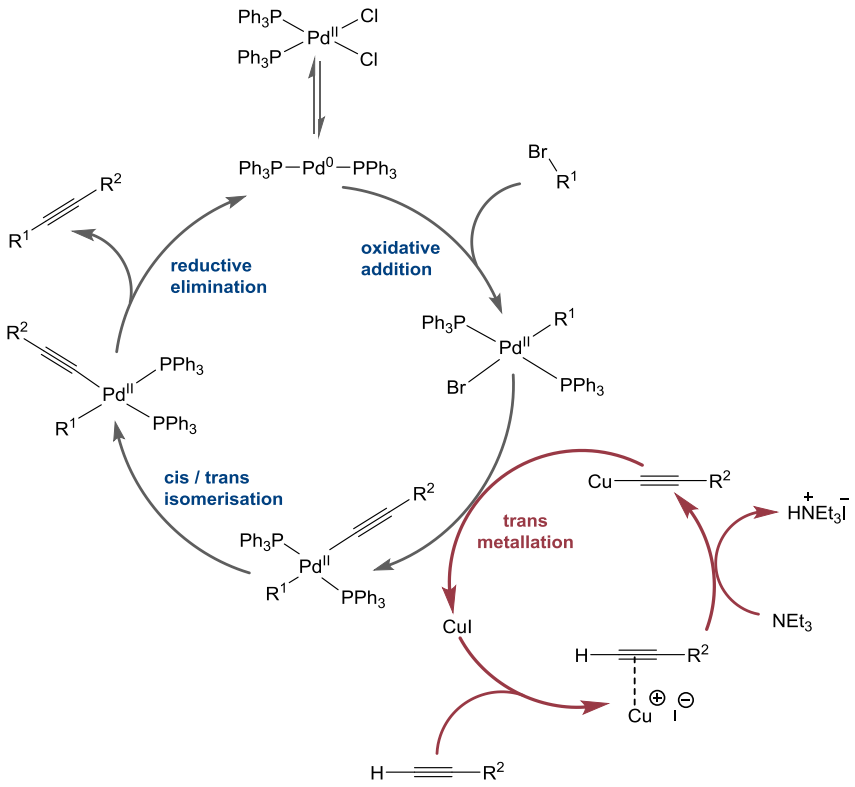

***Figure 2.9**: Catalytic cycle of Sonogashira cross coupling.*

The exact mechanism of the Sonogashira reaction is not entirely understood, however the currently accepted pathway involving two catalytic cycles is shown in figure 2.9. The aryl halide is activated by oxidative addition to the active Pd(0) catalytic species. This step of the reaction is dependent on the breaking of the aryl-halide bond, with aryl iodides being much more reactive than aryl chlorides.[244] Meanwhile, formation of a π-alkyne copper complex promotes deprotonation of the alkyne by the base to form a reactive copper acetylide for the rate-limiting transmetallation step.[245] Following transmetallation, cis/trans isomerisation precedes reductive elimination to liberate the coupled alkyne.

First attempts to synthesise the trimethylsilyl protected alkynes required for the present study followed a procedure reported by Milani *et al.*[246] 2-bromo-5-(trifluoromethyl)pyridine was successfully coupled to trimethylsilyl acetylene using 5 mol% of each of the co-catalysts bis(triphenylphosphine) palladium(II) dichloride and copper iodide in triethylamine after heating at 50 °C for 1 hour using the conditions described in Scheme 2.7. The boiling point of trimethylsilyl acetylene is 53 °C, therefore a large excess of the alkyne was used. This led to significant formation of Glaser coupled

by-products. Despite inefficiencies of the synthetic protocol, yields of around 70 % were routinely achieved using this method.

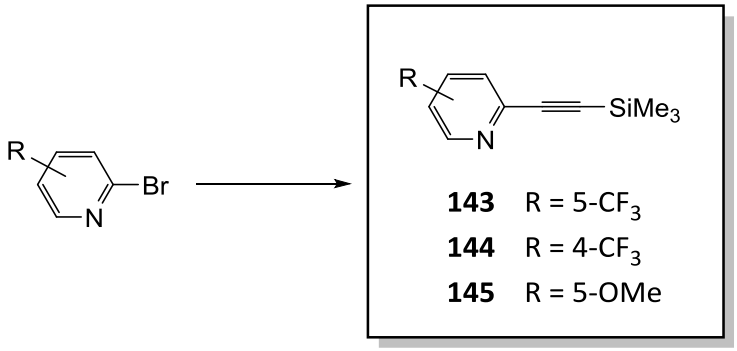

***Scheme 2.7**: Synthesis of 5-CF_3 alkyne. **Reaction conditions**: 1 eq 2-bromo-5-(trifluoromethyl)pyridine, 5 eq TMS acetylene, 5 mol% [$Pd(PPh_3)_2Cl_2$], 5 mol% CuI, in TEA, 50 °C, 1 h under N_2.*

As the 2-bromo-4-(trifluoromethyl)pyridine starting material was significantly more expensive, the method was optimised to reduce the formation of Glasser coupled by-products. Instead of using standard reflux apparatus, the reaction was carried out in a Schlenk flask, and the reaction mixture was thoroughly degassed using a freeze-pump-thaw technique. As a sealed reaction vessel was used, the excess of alkyne was reduced from 5 equivalents to just 1.5. The previous method used triethylamine as a solvent; however, in the optimised conditions, this was reduced to a stoichiometric quantity (with respect to the alkyne) and dry tetrahydrofuran (THF) was used as a solvent. It has been shown that the oxidative addition step proceeds via an S_NAr-like mechanism with aryl bromide and chloride substrates,[247] and thus electron withdrawing substituents *para*- to the halide leaving group facilitates the oxidative addition step by stabilising the charged intermediate shown in Figure 2.10.

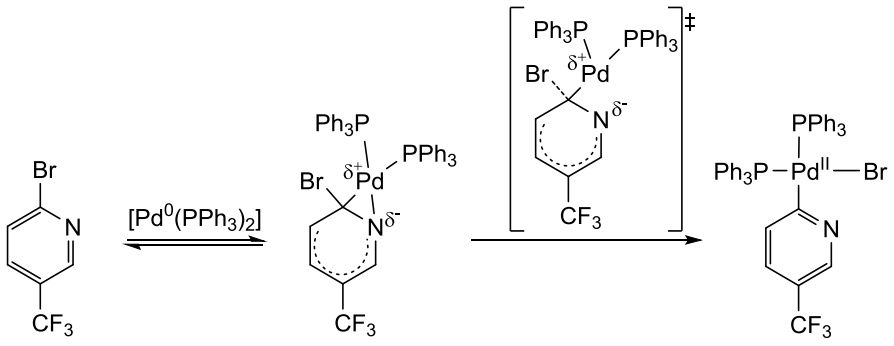

***Figure 2.10**: Proposed S_NAr-like mechanism of oxidative addition of aryl halide (were halide is bromide or chloride).*

This mechanism would support the finding that the 5-OMe alkyne takes longer to form. If the reaction does not go to completion, the starting material and product are extremely hard to separate. However, after heating for 2.5 hours using the optimised conditions alkyne **145** was isolated in a 92 % yield. The 5-OMe alkyne is particularly susceptible to decomposition, forming a brown-coloured product within a few minutes of being isolated and as such must be either used immediately or stored under nitrogen at -20 °C.

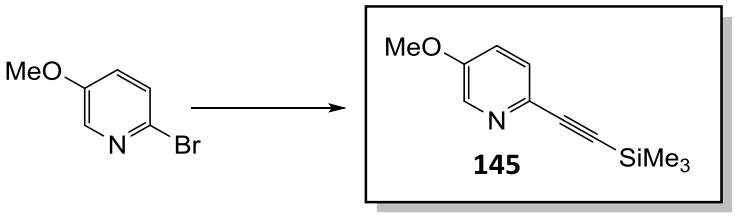

***Scheme 2.8**: Optimised conditions for Sonogashira coupling. **Reaction conditions**: 1 eq 2-bromo-5-(methoxy)pyridine, 1.5 eq TMS acetylene, 1.5 eq TEA, 5 mol% [Pd(PPh$_3$)$_2$Cl$_2$], 5 mol% CuI, in THF, 50 °C, 2 h under N$_2$ (98 % yield).*

2.4.2: Chlorination

Unfortunately slides prepared from cells treated with IrSpm (**123**) and IrPEG (**140**) deteriorated over time due to diffusion of the probes and it was considered unlikely that the probes would be retained in cells following the extensive sample preparation required for electron microscopy. Complexes **146** and **147** was designed with a thiol-reactive chloromethyl group in an attempt to lock the probe onto proteins to enable it to be retained in the cell for analysis by electron microscopy.

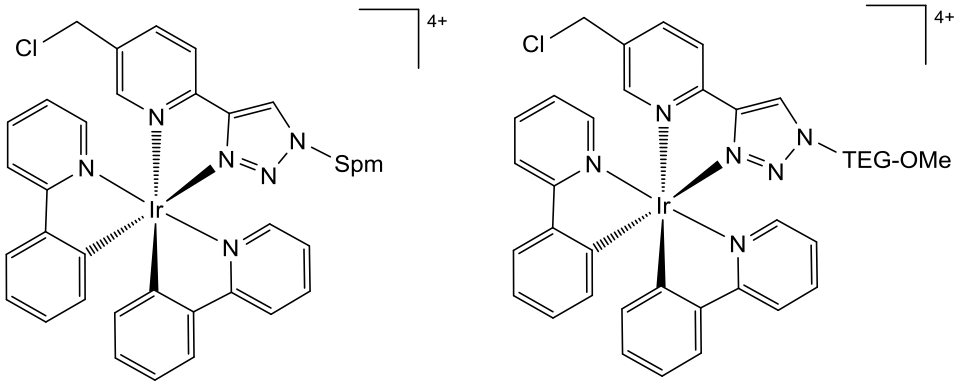

146 **147**

***Figure 2.11**: Chloromethyl iridium complexes **146** and **147**.*

The chloromethyl alkyne **148** was readily accessed by treating (6-((trimethylsilyl)ethynyl)pyridin-3-yl)methanol (prepared by undergraduate student M. Cunningham) with thionyl chloride, as shown in scheme 2.09, and isolated in an 83 % yield.

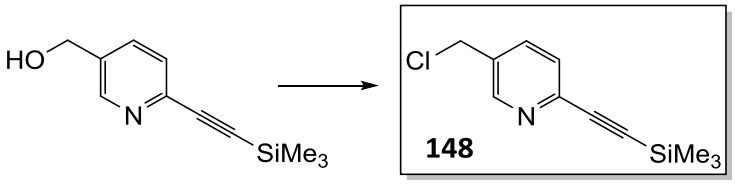

***Scheme 2.9**: Chlorination of (6-((trimethylsilyl)ethynyl)pyridin-3-yl)metanol. **Reaction conditions**: 1 eq (6-((trimethylsilyl)ethynyl)pyridin-3-yl)methanol, 10 eq thionyl chloride, dry DCM, 18 h, 20 °C (83 % yield).*

2.5: Synthesis of 1,2,3-triazole proligands

2,2′-bipyridine (bpy) is a strong chelator and one of the most widely used diimine ligands; however, synthesis of mono-functional bpy derivatives is not straight forward, the multi-step synthetic route is plagued by difficult separations and low overall yields.[248] 4-(2-pyridyl)-1,2,3-triazoles are an attractive alternative due to the ease of formation of monofunctionalised ligands via the CuAAC reaction (copper-catalysed alkyne–azide cycloaddition). This reaction was first reported in 2002 by both the Sharpless and Meldal groups, as a regioselective variant of 1,3-dipolar Huisgen cycloaddition.[249,250] Whereas thermal Huisgen cyclisation gives a mixture of 1,4- and 1,5-disubstituted 1,2,3-triazoles, the copper catalysed variant shows 1,4-regioselectivity. The alternative 1,5- regioisomer may be accessed via ruthenium-catalysed azide-alkyne cycloaddition (RuAAC).[251]

The CuAAC reaction is one of the most widely used click reactions; Sharpless defined a click reaction as one that is efficient, selective, gives high yields and is applicable to a wide range of readily available starting materials.[252] Additionally, it should be tolerant of both oxygen and water, be simple to work up and not require additional purification. 4-(2-pyridyl)-1,2,3-triazole compounds ("pyta" ligands) can be prepared in high yields, using mild reaction conditions requiring minimal purification. The CuAAC reaction is incredibly versatile; 4-(2-pyridyl)-1,2,3-triazoles are conveniently prepared from ethynyl pyridine and any suitable azide.

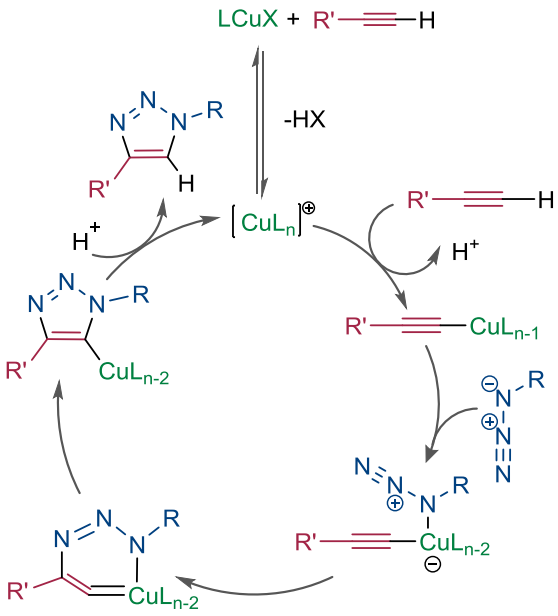

***Figure 2.12**: Early CuAAC mechanism proposed by Sharpless et al.*[250]

The mechanism proposed by Sharpless for CuAAC involved a single catalytic copper species (as shown in Figure 2.12). Upon deprotonation the alkyne sigma coordinates to the Cu(I) catalytic species, the azide ion then coordinates to a vacant site, and the Cu(III) metallocycle intermediate is formed. Transannular ring contraction gives the copper triazolide, which liberates the triazole upon protonation. However, as copper acetylides do not react with benzyl azide unless exogenous copper(II) is added to the reaction mixture, Fokin *et al*. proposed a mechanism involving a dinuclear copper species (shown in Figure 2.13).[253]

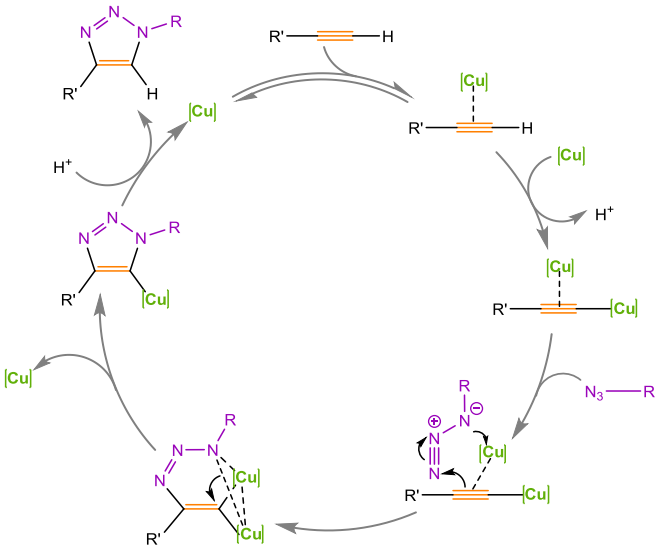

***Figure 2.13**: CuAAC mechanism proposed by Fokin involving a dinuclear copper species.*[253]

Azides are highly energetic molecules and can present an explosion risk. Risk of detonation can be estimated by determining the carbon (and oxygen) to nitrogen ratio as given by equation 2.1. Azides with a ratio less than one should not be isolated.

(No. of C atoms + No. of O atoms) / (No. of N atoms) ***Equation 2.1***

To minimise potential risks, azide formation is often carried out *in situ*. Therefore, azide formation needs to be robust and high yielding with minimal by-products. The azide functionality can be cleanly installed in excellent yield via simple substitution using sodium azide. An alternative approach that is particularly applicable to this work is copper catalysed diazotransfer; both methods are compatible with *in situ* CuAAC reactions. The target ligands are shown in Figure 2.14.

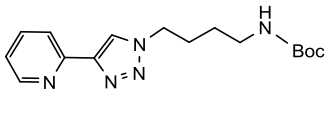

149 BocPut pyta

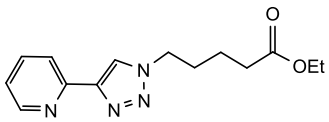

150 COOEt pyta

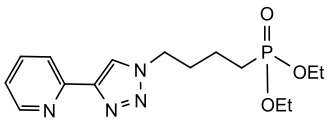

151 $PO(OEt)_2$ pyta

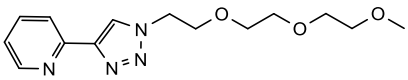

152 PEG pyta

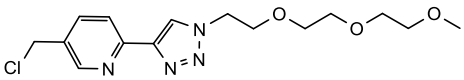

153 5-ClMe PEG pyta

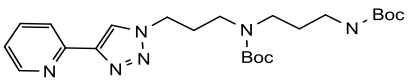

154 APBocPut pyta

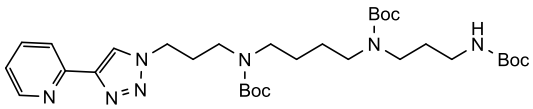

155 BocSpm pyta

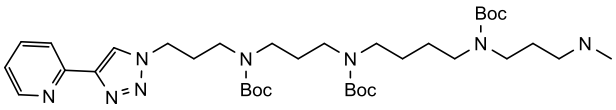

156 APBocSpm pyta

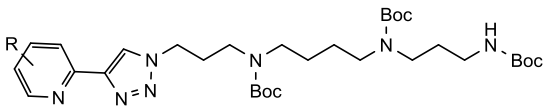

157 5-CF_3 BocSpm pyta
158 4-CF_3 BocSpm pyta
159 5-OMe BocSpm pyta
160 5-ClMe BocSpm pyta

***Figure 2.14**: Target proligands*

2.5.1: Ligand synthesis via substitution of a nucleofuge

The most commonly used route to prepare alkyl azides is displacement of a halide (or other suitable nucleofuge) by azide ion, and this approach was adopted for the synthesis of the non-amine analogues. The phosphonate ligand 151 was prepared smoothly using conventional heating methods. Diethyl (4-azidobutyl)phosphonate was prepared *in situ* by substitution with sodium azide, followed by CuAAC chemistry to generate the pyta ligand, which was isolated in 81% yield, and used without further purification.

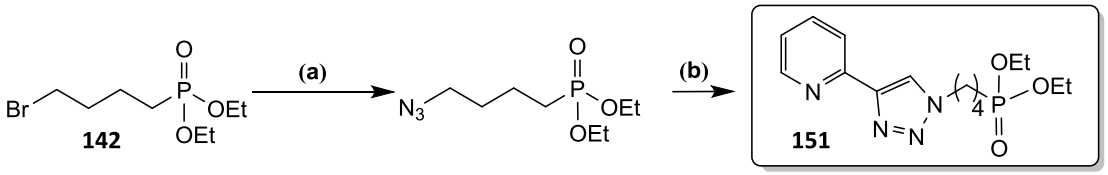

***Scheme 2.10**: synthesis of phosphonate ligand **151. Reaction conditions**: (a) 1.1 eq NaN_3 in THF : H_2O (4:1) 80 °C, N_2, 15 h. (b) 1.1 eq ethynyl pyridine, 0.05 eq $CuSO_4$, 0.1 eq sodium ascorbate, 60 °C*

Ligand 150 was prepared using a modified microwave click reaction, as shown in scheme 2.11.[254] Microwave methods were pursued in an attempt to speed up the synthetic process as the synthesis of azides using conventional heating methods is typically carried out overnight, followed by a 4 hour click reaction.

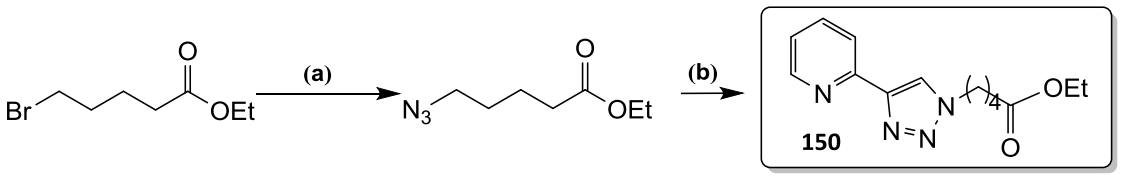

***Scheme 2.11**: Synthesis of ethyl ester ligand **150. Reaction conditions:** (a) NaN_3, ^tBuOH : H_2O (1 : 1), 125 °C, 15 mins µwave. (b) 1.1 eq ethynyl pyridine, 0.05 eq $CuSO_4.5H_2O$, 0.1 eq sodium ascorbate, 125 °C, 30 mins, µwave.*

Ethyl 5-azidopentanoate was prepared from sodium azide and ethyl 5-bromopentanoate heated to 125°C for 15 minutes under microwave irradiation. An aliquot of the reaction mixture was extracted into diethyl ether and evaporated under a steam of nitrogen. (This was deemed safe to isolate partially as the azide was prepared by Khoukhi *et al*. on a 0.3 mol scale, with the isolated azide purified by distillation![255]) Analysis by NMR revealed that the reaction had gone to completion, as all the starting

material had been consumed. The subsequent click reaction was carried out in the microwave for 15 minutes. Analysis of the reaction mixture revealed that a small amount of the azide remained, however after a further 15 minutes of microwave irradiation the reaction had gone to completion, and all traces of the azide had disappeared. Compared to the conventional synthesis the ligand can be prepared in less than 1 hour as opposed to 1 day.

Unfortunately, the yield obtained using microwave synthesis was below 50%. The reaction mixture contained brightly coloured impurities; this is almost certainly due to the formation of erythrulose (a bright orange pigment commonly found in self-tanning products!). In aqueous conditions ascorbic acid is known to decompose; erythrulose is one of the major products of decomposition.[256] CuAAC is catalysed by copper(I) which is generated *in situ* from copper(II) by the reducing agent sodium ascorbate. If the ascorbate is extensively decomposed by the elevated temperature used in microwave synthesis the regioselectivity will be lost as the cycloaddition will occur via the thermal route (Huisgen cycloaddition) giving rise to both 1,4- and 1,5- regioisomers.

Ligands can be prepared using a hybrid method; the initial formation of the azide can be carried out rapidly and cleanly by microwave synthesis and the product used directly in the subsequent click reaction using conventional heating. This hybrid approach enables the ligands to be prepared in under 6 hours as opposed to a whole day, in high yield and without the need for further purification. Going forward, the yield of microwave click reactions could be improved by using a direct source of copper(I) such as copper(I) acetate.

The terminal alcohol group of triethylene glycol was converted into a tosyl group, which being a very good leaving group may be readily displaced by sodium azide. Although click reactions are typically high yielding following a simple extraction to purify the product, extreme care must be taken with PEG compounds due to their high aqueous solubility. Water was kept to a minimum in the reaction mixture and in the subsequent extraction process and more extractions were carried out to maximise the extraction of the pyta from the aqueous washings. As the pyta proligands are themselves fluorescent, the aqueous washing were examined under UV light and organic extractions were carried

out until minimal fluorescence was observed in the aqueous waste, which enabled the PEG ligand to be isolated in an 87 % yield.

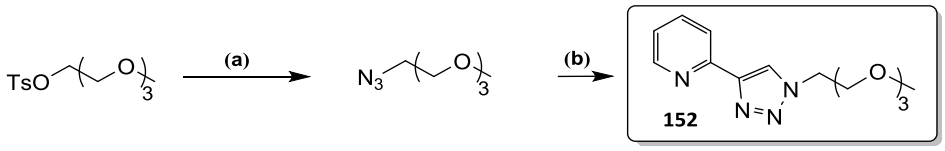

***Scheme 2.12**: Synthesis of momomethyl triethylene glycol pyta ligand (**161**). **Reaction conditions**: (a) 1 eq monomethyl ether triethylene glycol tosylate, 1.1 eq NaN_3 5:1 acetone : water, 60 °C, 18 h. (b) 1 eq ethynyl pyridine, 0.2 eq sodium ascorbate, 0.1 eq $CuSO_4.5H_2O$ 18 h, 20 °C.*

2.3.2: Ligand synthesis via diazo-transfer

The three-step, one-pot diazo-transfer reaction using imidazole-1-sulfonyl azide (ISA) to generate azides from primary amines for use in Click reactions was first proposed by Smith *et al*.[257] as an improvement to the existing method using the unstable reagent triflic azide.[258] The sulfate salt of imidazole sulfonyl azide (ISA) is the diazo-transfer reagent of choice as it can be safely stored for at least a year and is less sensitive to shock than its neutral form or other salts such as the hydrochloride.[259] Diazo-transfer can be catalysed by several metal ions including copper(II); and so is compatible with downstream CuAAC reactions by using sodium ascorbate to reduce the copper(II) catalyst. The reaction is believed to proceed via a metal coordinated tetrazole intermediate and requires basic conditions to enable the amine to coordinate to the copper.[260] The catalytic cycle for the copper catalysed reaction is shown in Figure 2.15.

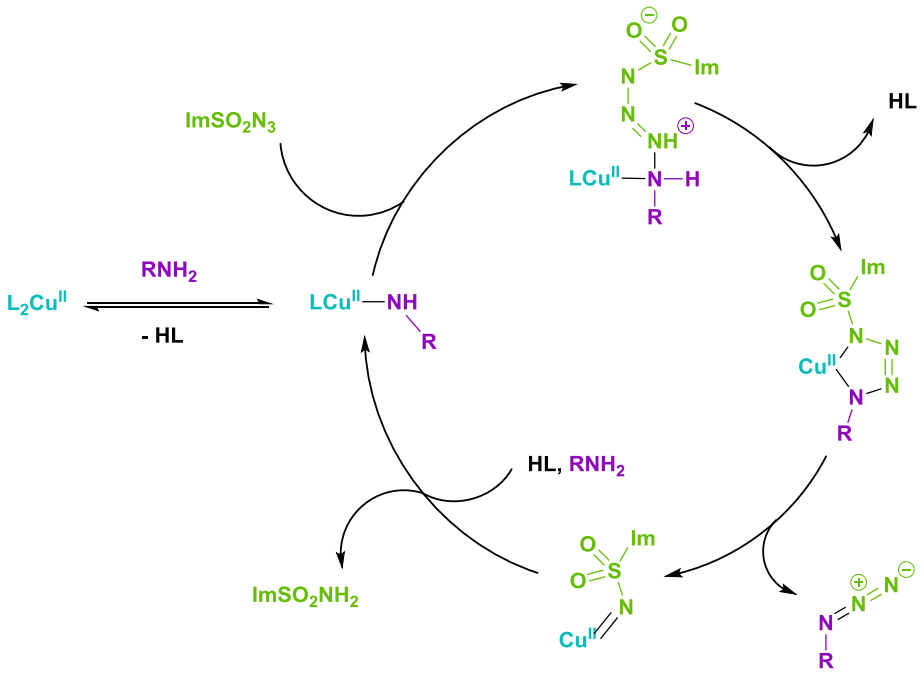

***Figure 2.15**: Proposed mechanism for the copper(II)-catalysed diazotransfer.*[260]

2.3.2.1: Unsubstituted ligands

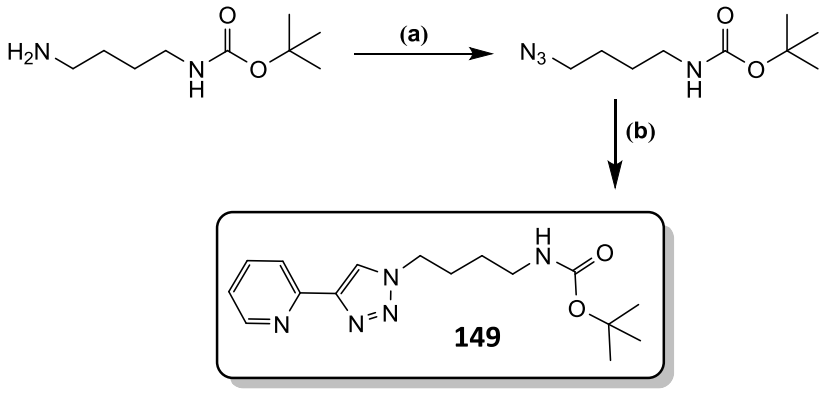

***Scheme 2.13**: Synthesis of putrescine ligand, BocPut pyta (**149**). **Reaction conditions**: (a) 1.1 eq ISA.H_2SO_4, 10 eq $NaHCO_3$, pH > 8, MeOH : H_2O (2 : 1), 4 h, 20 °C. (b) 1.1 eq ethynyl pyridine, 0.05 eq $CuSO_4.5H_2O$, 0.1 eq sodium ascorbate, 16 h, 20 °C, N_2.*

Conversion of the primary amine by diazo-transfer occurs within just a few hours. As the Boc-protected polyamines do not contain a chromophore, the reaction is best monitored using a combination of stains to observe both the disappearance of the primary amine and formation of the azide. The primary amine is revealed using ninhydrin, whilst the azide can be visualised using an on-plate reduction of the azide to give the amine (using triphenyl phosphine) followed by staining with ninhydrin. When

azide formation is complete, sodium ascorbate is added to the reaction mixture to reduce the copper(II) catalyst (as observed by disappearance of the characteristic blue colour) followed by the addition of ethynyl pyridine, as shown in scheme 2.13. As diazo-transfer occurs at room temperature, the second CuAAc step was also carried out at room temperature; this step was found to proceed smoothly overnight with pyta proligands being routinely recovered in yields in excess of 80 % without the need for further purification.

2.3.2.2: Substituted ligands

The substituted ethynyl pyridines are prepared as trimethylsilyl protected alkynes, which need to be deprotected in order for the CuAAC reaction to proceed. With the exception on proligand **161**, t was found that *in situ* deprotection of the alkyne by potassium carbonate added in stoichiometric quantities was compatible with the CuAAC reaction conditions, and occurred within 18 hours at room temperature, without any sacrifices in overall yield compared to the unsubstituted proligands.

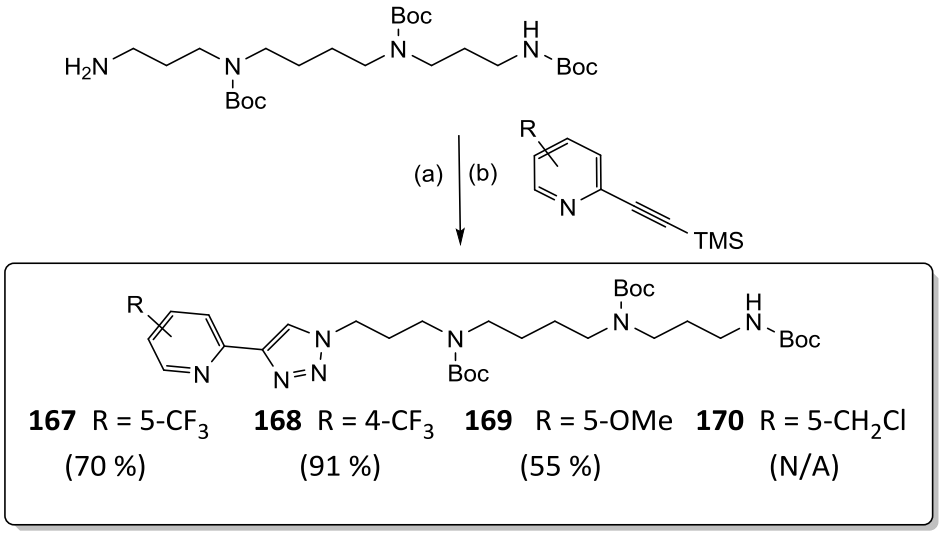

***Scheme 2.14**: Synthesis of substituted spermine ligands. **Reaction conditions**: (a) 1.1 eq ISA.H_2SO_4, 10 eq $NaHCO_3$, pH > 8, MeOH: H_2O (2: 1), 4 h, 20 °C. (b) 1.1 eq substituted pyridine, 1.1 eq K_2CO_3 0.05 eq $CuSO_4.5H_2O$, 0.1 eq sodium ascorbate, 16 h, 20 °C, N_2.*

2.6: Synthesis of MLCs

2.6.1: Rhenium complexes

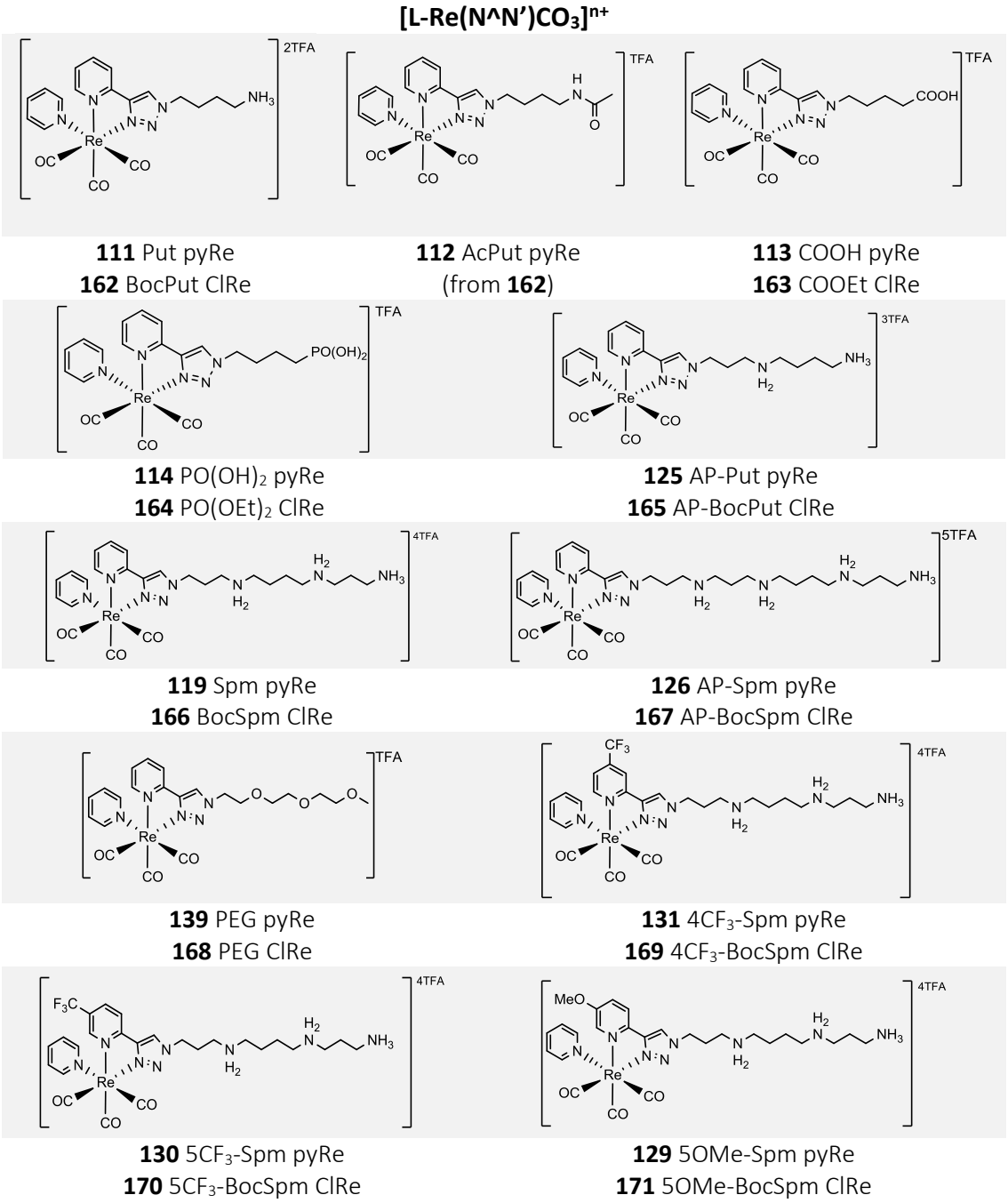

***Figure 2.16**: Structure of cationic rhenium complexes, showing numbers of the synthetic intermediate chlororhenium complexes.*

Microwave assisted ligand substitution reactions proceed smoothly in just a fraction of the time it takes using conventional heating methods and require minimal purification. Complexes of the general formula *fac*-[ReCl(CO)$_3$(N^N')] can be prepared by

heating under reflux in methanol overnight and isolated in yields of around 60 %.[172,248] This can be achieved in almost quantitative yield upon microwave heating at 90 °C for just one hour by the method shown in Scheme 2.15.

Abstraction of the chlorido ligand by silver tetrafluoroborate and subsequent substitution by a neutral pyridine ligand to give cationic rhenium complexes can be accomplished in just three hours heating under microwave irradiation, in high yield and requiring minimal purification. Silver tetrafluoroborate is added to abstract the chloride ligand to leave a vacant coordination site, which is filled by pyridine, and hence a weakly coordinating solvent must be used (such as tetrahydrofuran). As the reaction proceeds, silver chloride precipitates from the reaction mixture which drives the reaction towards completion and is easily removed from the reaction mixture by filtration through Celite; excess pyridine is easily removed by co-evaporation with toluene.

This method has been developed into a telescopic synthesis which has also reduced the overall time needed to synthesise complexes by avoiding the isolation of the intermediate chlororhenium complex. THF is the solvent of choice as it is weakly coordinating and does not compete with pyridine in the final ligand exchange reaction. Previously methanol had been used for the first stage of the reaction; however, this was found to be unsuitable for ligands with ester groups as the high energy used in the microwave led to transesterification. Once the triazole has been coordinated to the rhenium centre, the reactants for the next two steps can be added directly to the reaction vessel without the need for any interim workup. Although the reaction is a multi-step one pot reaction, the final product is still obtained in good yield (≈ 70 %) and purity.

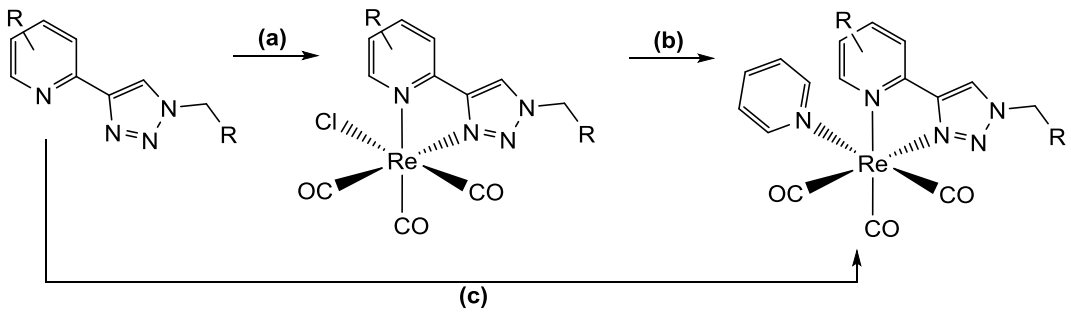

***Scheme 2.15**: Microwave synthesis of chlororhenium pyta complexes. **Reaction conditions**: (a) 1.1 eq $Re(CO)_5Cl$, 1 eq pyta proligand in MeOH, 90 °C, I h, µwave. (b) 2 eq $AgBF_4$, 4 eq pyridine in THF, 90 °C,3 h, µwave. (c) Telescopic 1-pot method: 1.1 eq $Re(CO)_5Cl$, 1 eq pyta proligand in THF, 90 °C, I h, µwave, add 2 eq $AgBF_4$, 4 eq pyridine directly to vessel & return to microwave for 3 h, 90 °C.*

The triazole ligand shows some interesting features in the proton NMR spectra upon complexation to the rhenium centre. As the ligand is de-shielded upon coordination to the metal centre noticeable downfield shifts can be observed for many of the protons; the singlet due to the triazole proton and the proton adjacent to the pyridine nitrogen are shifted down-field by around 0.4 ppm and downfield shifts of around 0.2 ppm were observed for the remainder of the pyridyl moiety. The exception to this is proton 4 which is shifted upfield by approximately 0.3 ppm. In the cationic complex, coordination of pyridine to the metal centre contributes an additional three resonances in the aromatic region and causes the triazole signals to shift further downfield; their order in the spectrum remains unchanged. Pyridine is less affected by its coordination to the metal centre, two of the pyridine signals are hardly shifted at all relative to unbound pyridine, whilst the protons adjacent to the nitrogen atom experience an upfield shift.

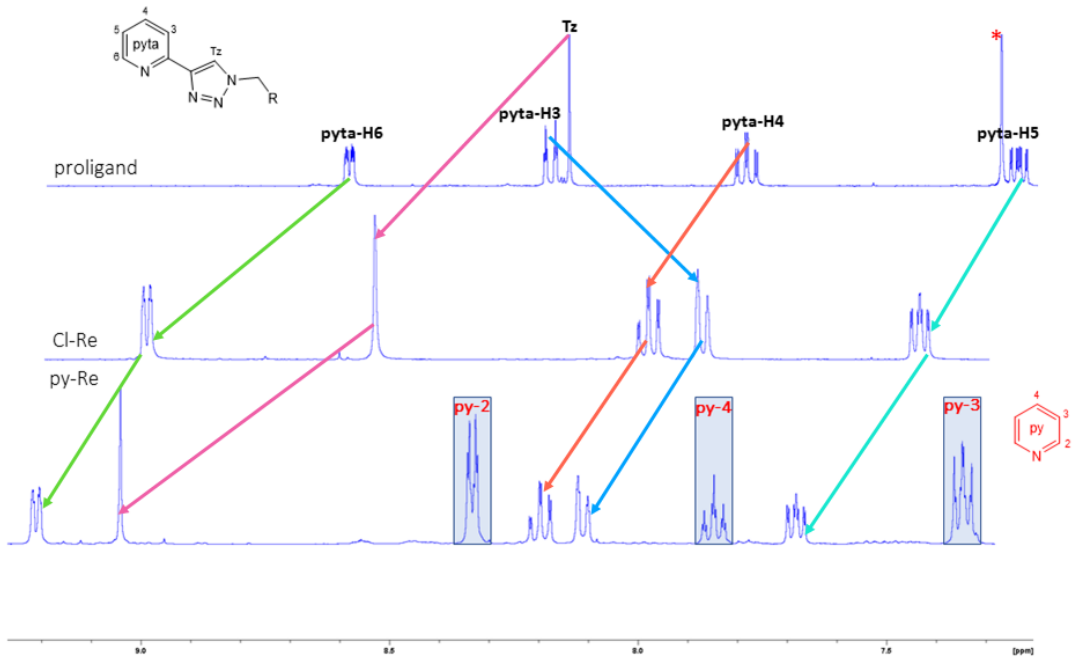

***Figure 2.17**: Changes in aromatic signals upon coordination to rhenium $PO(OEt)_2$ pyta (**151**) and Cl-$Re(CO)_3PO(OEt)_2$ (**164**) in $CDCl_3$, and py-$Re(CO)_3PO(OH)_2$ (**164**) in MeOD, 400 MHz.*

Enantiomers are formed when the ligand coordinates to rhenium, which renders the methylene protons in the chain inequivalent. The methylene protons adjacent to the triazole are equivalent in the proligand; however, upon complexation the protons become diastereotopic giving rise to non-first order splitting effects. This is most

prominent for the methylene group adjacent to the triazole ring. The second order splitting is more complex than a simple AB quartet due to additional adjacent protons. An example is shown in Figure 2.17; the two spectra show the methylene resonance adjacent to the triazole ring for the phosphonate ligand and its chlororhenium complex. The first trace shows the proligand; the methylene resonance is a simple first order triplet. In the second spectrum, the ligand is coordinated to rhenium, and an ABX_2 second order splitting pattern is observed. Highly complex splitting is observed for the alkyl protons associated with the phosphonate ester as ^{31}P also contributes to the observed splitting patterns. The methylene group of the phosphonate ester gives rise to an overlapping ABX_3 system with additional phosphorous coupling.

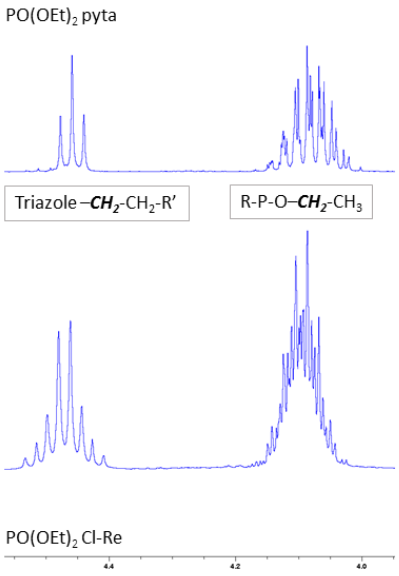

***Figure 2.18**: Non-first order splitting observed in diastereotopic protons.*

Different alkyl substituents attached to the triazole ring have very little effect on the proton NMR or photophysical properties of the ligand as the functional groups are remote from the ring and not conjugated, however substitution on the pyridine ring of the pyridyl triazole has a more significant effect. Pyridyl triazole proton 6 (as shown in figure 2.19) which is adjacent to the pyridyl nitrogen is the most significantly affected by substitution on the ring; being shifted downfield by around 0.3 ppm upon addition of an electron withdrawing CF_3 group and shifted upfield by around 0.3 ppm by an electron donating OMe group. The triazole proton was only modestly shifted upfield by the OMe group, but more substantially shifted downfield by the CF_3; a trend which is also seen

with the remaining resonances associated with the pyta ligand. The CF_3 group is a strongly electron withdrawing group due to the inductive effect of the three fluorine atoms, and whilst the methoxy group is generally considered as an electron donating group due to strong electron donation into the delocalised system via resonance, inductively it is electron withdrawing due to the electronegativity of the oxygen atom, which may explain why the methoxy group has a lesser effect on the electronics compared to the CF_3 group.

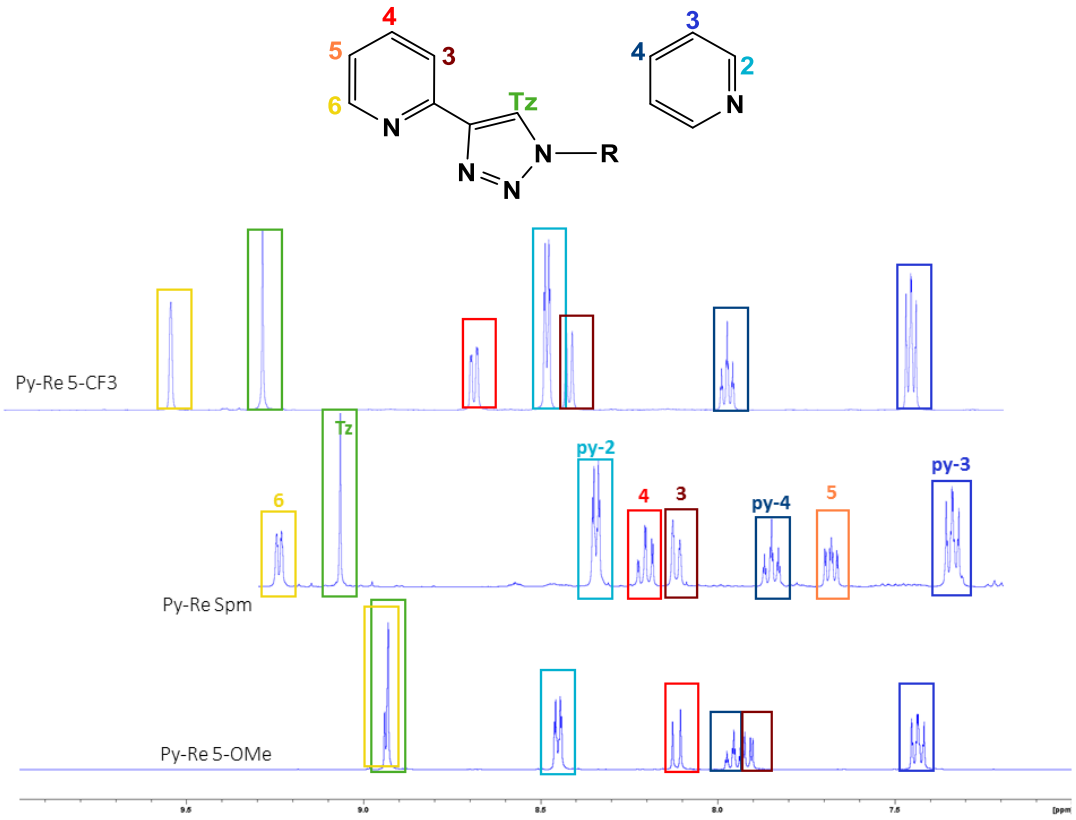

***Figure 2.19**: [1]H NMR of substituted cationic Re complexes, comparing the effect of electron withdrawing versus electron donating substituents.*

Compared to the 4-substituted complex, proton H6 in the 5-CF_3 substituted complex was shifted around 0.2 – 0.3 ppm further downfield relative to the non-substituted complex, as can be seen in figure 2.20. The other pyridyl protons were also shifted downfield by around 0.2 ppm, however H4 in the 5-CF_3 complex was shifted by around 0.4 ppm. There is an interesting difference in the nature of the shift observed for the triazole proton in both complexes. The 5-CF_3 substituent shifts the triazole resonance downfield, whereas it is shifted upfield by the 4-CF_3 substituent. This can be rationalised by considering the relative position of the triazole ring to the trifluoromethyl

group; the 5-CF_3 group is *para*- with respect to the triazole and can therefore be expected to have a more significant effect on the triazole proton compared to the 4-CF_3 which is *para*- with respect to the metal. This trend also extends to the protons borne on the axial pyridine ligand; with the 5-CF_3 protons experiencing a modest downfield shift compared to the 4-CF_3 where the protons are shifted upfield.

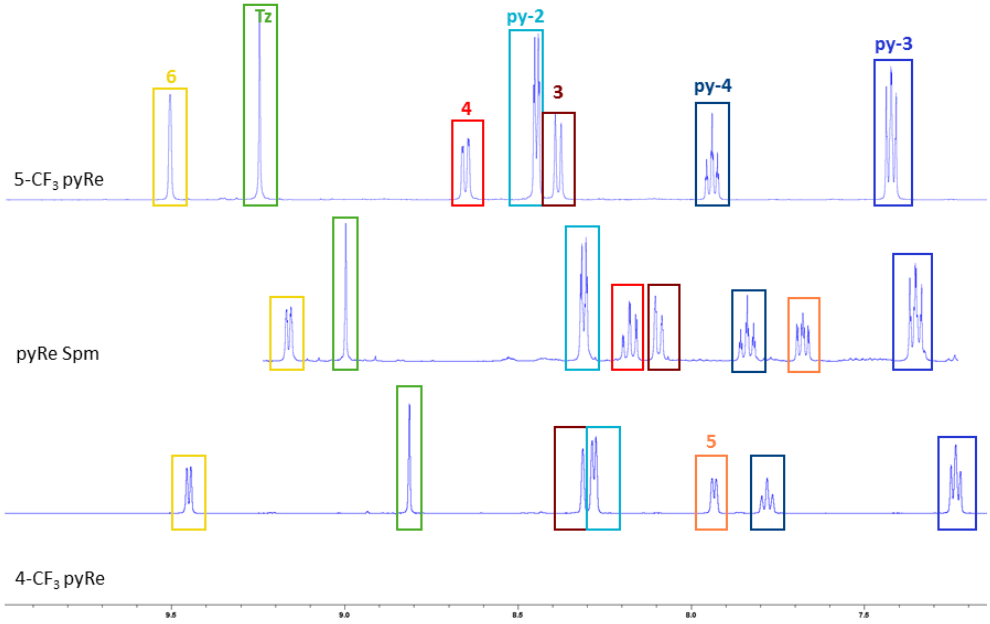

***Figure 2.20**: ^{1}H NMR spectra (400 MHz, in MeOD, 298 K) showing the effect of substituent position.*

2.6.2: Iridium complexes

The synthesis of cationic, heteroleptic iridium(III) complexes was accomplished in two steps; firstly the chloride-bridged dinuclear iridium species [NO] was prepared via a modified Nonoyama reaction, followed by the substitution of the chlorido ligands with an ancillary ligand (as shown in Scheme 2.16).[261,262] The iridium(III) dimers [$(ppy)_2$Ir-μ-Cl]$_2$ and [$(papy)_2$Ir-μ-Cl]$_2$ were prepared by reacting phenyl pyridine or *p*-anisyl pyridine (papy) with $IrCl_3$, in a 1:3 mixture of water/isopropanol at 90 °C, under microwave irradiation giving a product where the cyclometallating ligands are oriented in a *trans*-position with respect to each other.[263] The iridium dimer was then "broken" in a microwave reactor with the appropriate pyta ligand. A range of cyclometallated complexes were prepared using the same, flexible synthetic strategy to give differently charged complexes, complexes with different length polyamine chains and incorporating both C^N substituted and N^N substituted ligands, as shown in the table below. All final

complexes were purified by reverse phase-HPLC (RP-HPLC) and isolated in good to excellent yield.

$[Ir(C^N)_2(N^N')]^{n+}$

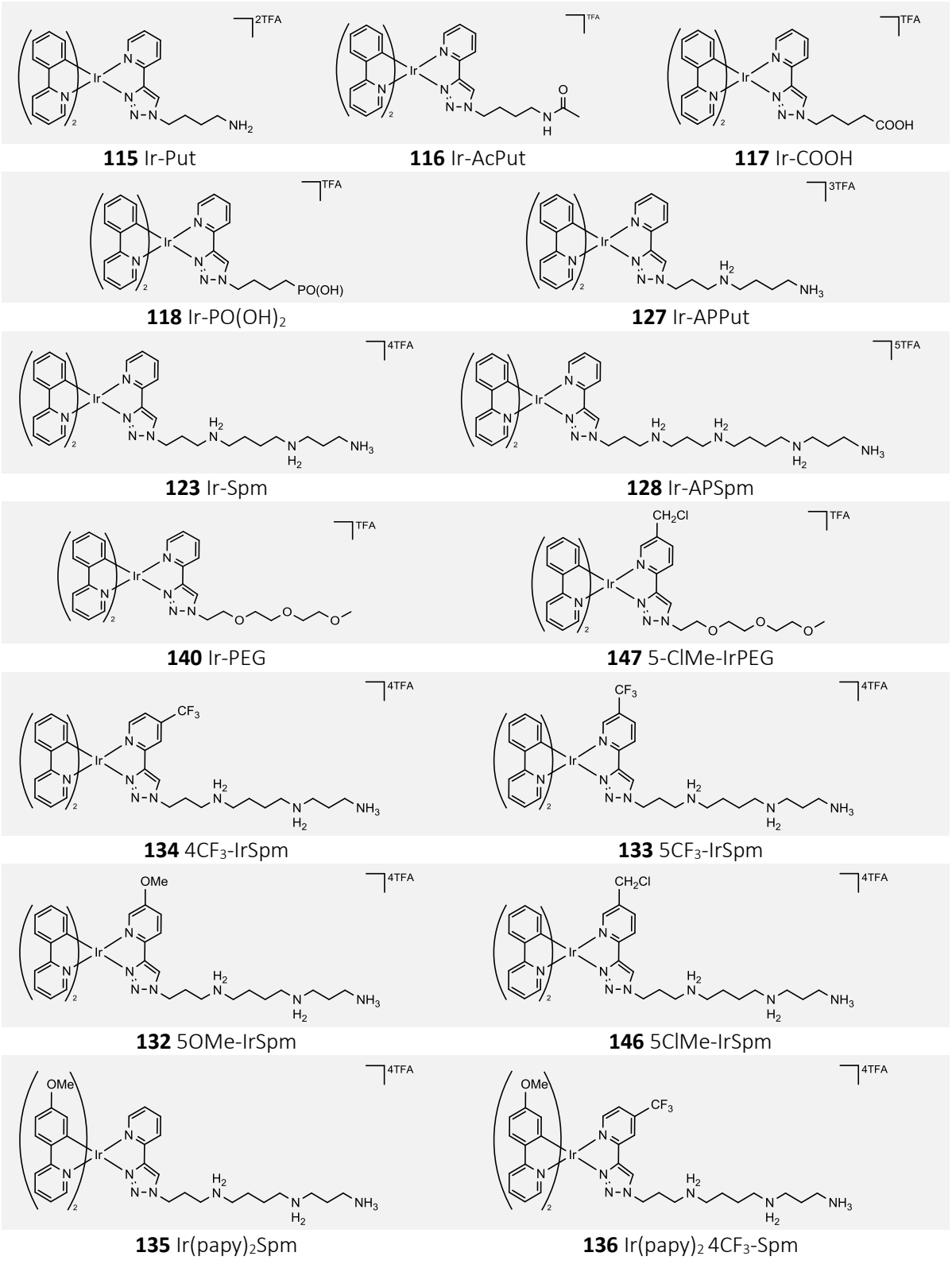

115 Ir-Put **116** Ir-AcPut **117** Ir-COOH

118 Ir-$PO(OH)_2$ **127** Ir-APPut

123 Ir-Spm **128** Ir-APSpm

140 Ir-PEG **147** 5-ClMe-IrPEG

134 4CF_3-IrSpm **133** 5CF_3-IrSpm

132 5OMe-IrSpm **146** 5ClMe-IrSpm

135 Ir$(papy)_2$Spm **136** Ir$(papy)_2$ 4CF_3-Spm

***Figure 2.21**: Iridium complexes made in this study.*

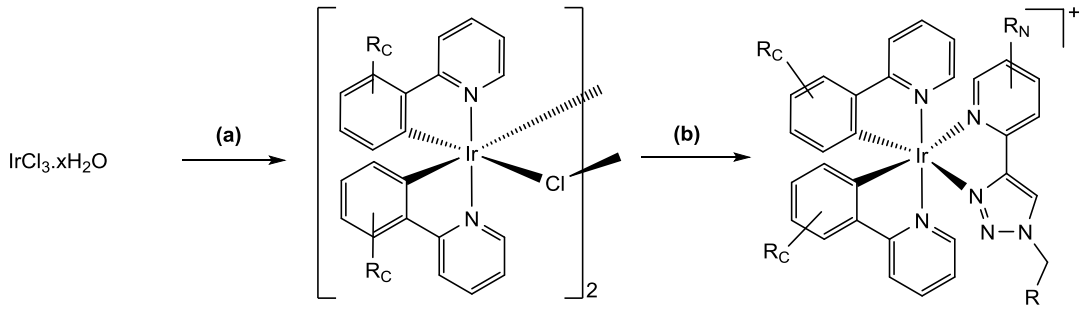

***Scheme 2.16**: Modified Nonoyama dimer synthesis and microwave assisted 'breaking the dimer', where R_C = H, 4-OMe and R_N = H, 5-CF_3, 5-CH_2Cl, 5-OMe, 4-CF_3. **Reaction conditions**: (a) 1 eq $IrCl_3.xH_2O$, 2.2 eq phenyl pyridine, in H_2O: iPrOH (1:3) 90 °C, 1.5 h, µwave. (b) 2 eq pyta ligand, 1 eq $[Ir(ppy)_2Cl]_2$, MeOH, 90 °C, 2 h, µwave.*

Complexes were characterised by high resolution mass spectrometry and 2D NMR experiments. The two most readily identifiable proton resonances occur at the extremes of the aromatic region; the triazole proton is the most downfield signal, whilst that of the proton adjacent to the cyclometallated carbon is the most upfield signal. The aromatic region of NMR spectra is complex as the C^N ligands are inequivalent; however, due to this inequivalence proton correlations for each of the phenyl rings were easily identified from ^{1}H COSY spectra. Assigning the pyridine signals is more difficult due to significant overlap. HMBC experiments were found to be the most useful tools to fully assign spectra, as multiple bond correlations can be used to establish the connectivity between ring systems. Using multiple bond correlations to the cyclometallated carbon, it can be shown which ring system lies trans- to the triazole ring and can also be used to identify which pyridyl ring is associated with each of the phenyl rings of the C^N ligands.

Figure 2.22 shows how the chemical shifts vary with substitution. N^N substitution affects both the N^N' and C^N resonances, whereas C^N substitution only seems to affect the C^N ligand. As would be expected for an electron donating group, 5-OMe N^N' substitution causes the triazole resonance to shift slightly upfield; however, the proton adjacent to the cyclometallated carbon is significantly shifted downfield. This signal is also significantly shifted downfield by the 5-CF_3 substituent, along with the triazole resonance, similar shifts are seen with the 4-CF_3 substituent albeit to a lesser extent. It would appear that the spectral separation of these two resonances can be used as a crude estimation of the effect on the magnitude of the HOMO-LUMO gap, as the bluest emitter shows the smallest energy separation of these two peaks.

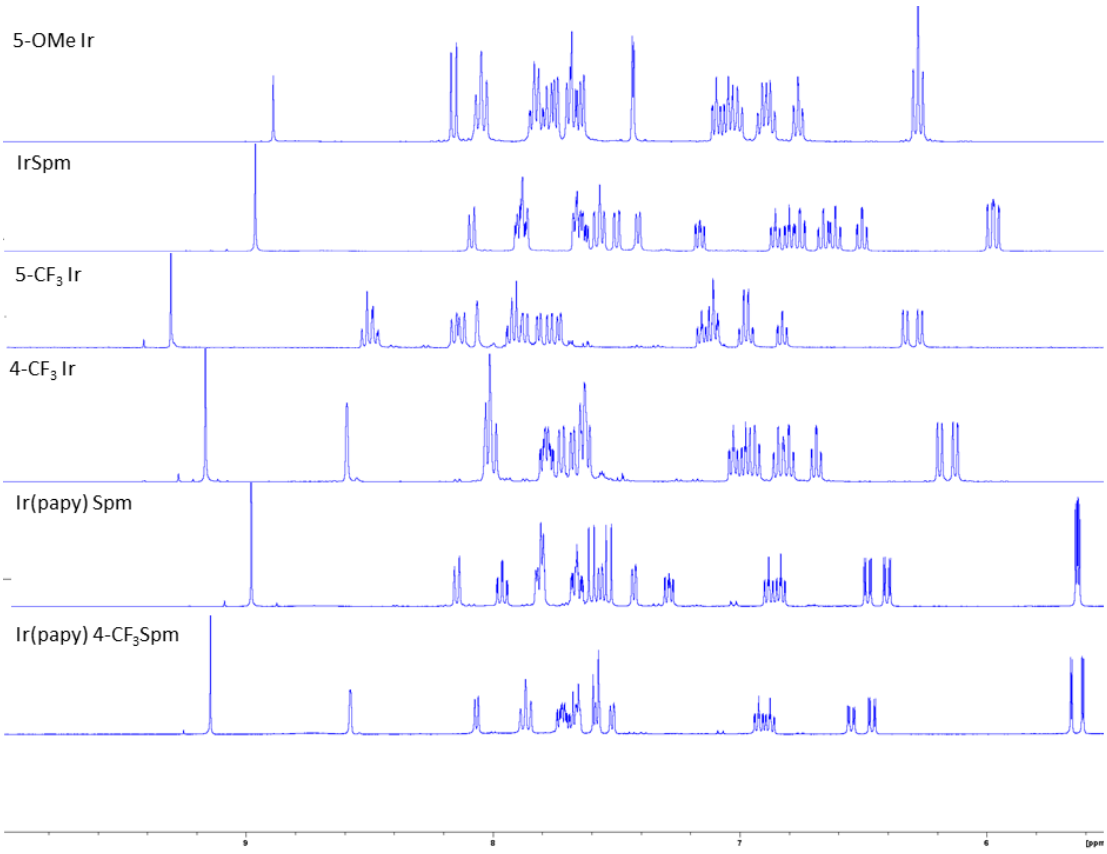

***Figure 2.22**: [1]H NMR spectra of the substituted iridium complexes, 400 MHz, in MeOD at 298 K.*

As expected, OMe substitution at the C^N ligand leads to a significant upfield shift of the adjacent protons, however the N^N' ligand is unaffected, which is also consistent the photophysical data obtained (see Chapter 3).

2.6.3: Platinum complexes

Previous attempts in the Lowe/Cullis group to synthesise a platinum polyamine pyta complex suffered from incredibly low isolated yields (7% over two steps) and thus a more efficient synthesis was required. The synthesis was carried out stepwise to try to understand where loses were occurring. The complex was prepared from *cis*-$[Pt(dmso)_2Cl_2]$, which was heated under reflux in the dark with a stoichiometric quantity of the pyta ligand with in nitromethane. The reaction proceeded in virtually quantitative yield with no traces of unreacted ligand detected after twelve hours, yielding the Boc-protected target complexes in excellent yield.

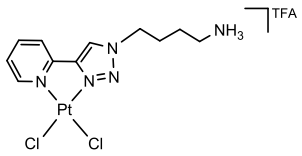

172 $PtCl_2$-Put

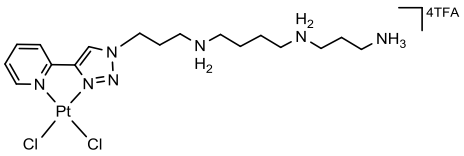

173 $PtCl_2$-Spm

***Figure 2.23**: Platinum complexes designed as cisplatin analogues.*

Boc-protected polyamine MLCs are usually deprotected using TFA immediately prior to purification by reverse phase HPLC, which leaves the metal centre and cationic polyamines as the TFA salt. As these complexes were destined to be used in toxicological evaluation a less toxic counter ion was required, and thus hydrochloric acid was the reagent of choice for the deprotection step. Whilst the removal of the protecting group was efficient, (as evidenced by the complete disappearance of the Boc signal in the ^1H NMR spectrum), the core complex was not unaffected by this process. ^1H NMR of the crude material revealed two distinct sets of resonances corresponding to two different ligand environments. This was resolved by reverting to TFA; deprotection then proceeded smoothly to yield a single product.

HPLC purification of the deprotected complex proved problematic. The complex degraded during purification using the standard conditions; 0.1% TFA in acetonitrile and water, using a gradient elution from 5% to 100 % acetonitrile, with UV detection at 260 nm. Following lyophilisation, the sample had decomposed to form a black residue. During purification the complex is in an acidic water and acetonitrile mixture for around two hours, and thus aquation and/or solvation are highly likely. To circumvent this the complex was purified by flash column chromatography prior to the deprotection step. Following deprotection, strong cation exchange resin was used to furnish the target complex with chloride counterions. The spermine pyta complex was subsequently lyophilised and isolated in an overall yield of around 56 %, which represents a considerable improvement from the previous method.

In an attempt to further streamline the synthesis of the platinum complexes, a direct synthetic route from potassium tetrachloroplatinate was trialled.[264] The pyta ligand was dissolved in acetone, and added to an equimolar aqueous solution of $K_2[PtCl_4]$ and heated to 60 °C overnight. This approach had mixed success; the Put complex

precipitated from the reaction mixture, however some platinum decomposition occurred leaving a black deposit which mixed with the product. Unfortunately, this product was exceptionally insoluble and hence difficult to purify further, and therefore had no advantage over the previous method. This approach was more successful using the spermine ligand as the longer polyamine chain significantly solubilised the product. Although platinum decomposition occurred this could be readily filtered from the soluble product. Due to the issue of platinum decomposition, the reaction did not proceed in as high yields and purity compared to the previous reaction.

2.7: Deprotection and post complexation modifications

2.5.1: Boc deprotection

2.5.1.1: TFA

Boc deprotection of the rhenium complexes was carried out using 4M solution of TFA in dichloromethane. Deprotection usually went to completion after 2 hours giving quantitative conversion. As TFA is volatile it is easily removed from the product by co-evaporation under reduced pressure with dichloromethane. Unfortunately deprotection of the iridium complexes was hampered by tertiary butyl capping, this was minimised by using shorter reaction times of just 30 minutes, which was sufficient to affect complete deprotection, but unfortunately some capping still occurred. This could be minimised by using a peptide cleavage cocktail (95% TFA, 2.5% triisopropyl silane, and 2.5% water) in place of TFA. The presence of water and triisopropyl silane acts as a scavenger to quench tertiary butyl cations, which prevents unwanted alkylation.

2.5.2: Ester hydrolysis

Complexes 124 and 128 were prepared as an ester as this makes the complex more soluble in organic solvents and easier to separate in the interim stages if needed. The ester was smoothly deprotected using a 0.02M sodium hydroxide solution, added to the complex dissolved in methanol, following a published method whereby ester groups were deprotected on a lanthanide complex.[265] Preliminary studies showed that the ester could be cleaved at room temperature without any ligand substitution occurring. The deprotection reaction went to completion overnight.

2.5.3: Phosphodiester cleavage

Trimethylsilyl bromide was chosen as to effect deprotection; however, the reactivity of this reagent was disappointing. Under anhydrous conditions, trimethylsilyl bromide was used to displace the ethyl ester groups from the complex. Subsequent hydrolysis of the silyl groups gave the target complex, but the conversion was disappointing due to a mixture of deprotected, mono-ethyl and unreacted starting material. Following purification by HPLC, partially deprotected material was collected and subjected to a second deprotection, however still a mixture of products was obtained. For future use this could be optimised using the microwave assisted method proposed by Natarajan *et al.* who reported that phosphonate cleavage occurred in 95 % yield when subjected to microwave irradiation at 80 °C in acetonitrile.[266]

2.5.4: Acetylation

N-terminal acetylation of the polyamines occurs *in-vivo* serving to mark polyamines for catabolism or cellular export.[267] This modification was chosen as a charge neutral functionality to incorporate into control complexes **123** and **127**. The desired N-acetylated complexes are readily prepared from the deprotected Put complexes by treatment with 20 % acetic anhydride in DMF overnight at room temperature, as a final step of the synthesis with isolated yields of around 80 % following purification by HPLC. Acetylation of the ligand was carried out with the ligand installed on the rhenium complex, as this avoided the need to synthesise an additional ligand. As the complexes are not damaged by the 4M TFA solution used for removal of the Boc group, it is unlikely that it would be decomposed by the 20 % acetic anhydride solution required for acetylation. Complete acetylation of the complex was achieved overnight at room temperature.

Mass spectrometry data was consistent with a mono-acetylated product, however, did not provide any indication that acetylation had occurred in the desired location. However, the ^{1}H NMR resonance of the methylene group adjacent to the terminal amine showed downfield shift by around 0.2 ppm for the acetylated complex compared to the equivalent signal in the unmodified complex. As an acetyl group would be expected to de-shield the adjacent methylene protons, this downfield shift is consistent with desired modification.

2.6: Summary

Previously established procedures have been optimised to reduce the number of synthetic steps required to synthesise the target polyamine complexes. This has the advantage of reducing the time taken to synthesise target molecules but also leads to a significant increase in overall yields. New synthetic strategies have been developed enabling a far wider range of targeting moieties to be used. This serves to demonstrate the flexibility of the synthetic strategy used, which should enable a wide variety of new targets to be exploited (some further examples of this are elaborated in chapter 6).

Chapter 3 : Tuning Photophysical Properties

3.1: Photophysical properties of MLCs

In general, the highest occupied molecular orbital (HOMO) of luminescent d^6 MLCs has predominately metal d-orbital character, with lower lying d-orbital dominated molecular orbitals. In contrast, the lowest unoccupied molecular orbital (LUMO) has predominantly ligand-based π* character. Upon photoexcitation, an electron is excited from the metal-based HOMO to the ligand-based LUMO. These excited singlet states undergo very rapid intersystem crossing (ISC) on account of the strong spin-orbit coupling (SOC) associated with the metal centre; as such, emission from MLCs tends to be of a phosphorescent nature.

3.1.1: Rhenium(I) tricarbonyl polypyridine complexes

Complexes of the general formula $[Re(N^N)(CO)_3(L)]$ (where N^N = diimine ligands, L = monodentate ligands) show intense spin-allowed intraligand (^{1}IL) absorption bands in the UV region and weak but broad, spin-allowed metal-to-ligand charge-transfer (^{1}MLCT) bands in the visible region. These complexes show intense and relatively long-lived emission in the visible region upon photoexcitation, which is most commonly attributable to a ^{3}MLCT [dπ(Re)->π*(N^N)] excited state, however triplet halide-to-ligand charge-transfer ^{3}XLCT, ^{3}LLCT and mixed emissive states have also been reported.[268] Owing to the charge transfer nature of the emission, these complexes are highly sensitive to solvent polarity with longer lived emission occuring at higher energy in less polar solvents. Tuning the emission colour of rhenium(I) tricarbonyl complexes is relatively straightforward. The HOMO is associated with the metal d orbitals and the LUMO is based on the ligand π* orbitals. Modulating the structure of the diimine ligand significantly alters the photophysical properties of the complex, whilst the axial ligand has a more limited effect.[269]

$[ReCl(CO)_3(bpy)]$ has a maximum emission at 611 nm, a quantum yield of 0.2 % and a lifetime of 29 ns (in acetonitrile).[270] Replacing the chlorido ligand with pyridine causes a blue shift in emission (λ_{em} = 566 nm), which is also accompanied by a large

increase in both the quantum yield (Φ = 5.5 %) and phosphorescent lifetime (232 ns).[270] As a monodentate axial ligand, the 1,2,3-triazole moiety behaves analogously to pyridine,[271] however its effect on photophysical properties is more striking when used as the diimine ligand in place of bpy.

The first use of the pyta ligand in rhenium complexes was reported by Obata *et al.* Compared to the bpy complex, the pyta complex shows a significant blue-shift in emission (λ_{em} = 532 nm) as the LUMO associated with the electron rich pyta ligand is dramatically destabilised compared to bpy. Consequently radiationless decay is supressed and the luminescence lifetime of [ReCl(CO)$_3$(Bn-pyta)] at 77K in methyl-tetrahydrofuran (8.90 μs) is almost three-times longer than that of [ReCl(CO)$_3$(bpy)] (3.17 μs).[172] DFT calculations comparing [ReCl(CO)$_3$(Bn-pyta)] and [ReCl(CO)$_3$(bpy)] showed that the HOMO-1 of both [ReCl(CO)$_3$(Bn-pyta)] and [ReCl(CO)$_3$(bpy)] occur at the same energy and predominantly localize at the Re(I) tricarbonyl core and the Cl atom, whereas the LUMO is essentially the π* orbital of N^N ligand. The lowest energy electronic transition is assigned to the mixed metal–ligand-to-ligand charge transfer (MLLCT) in both complexes.

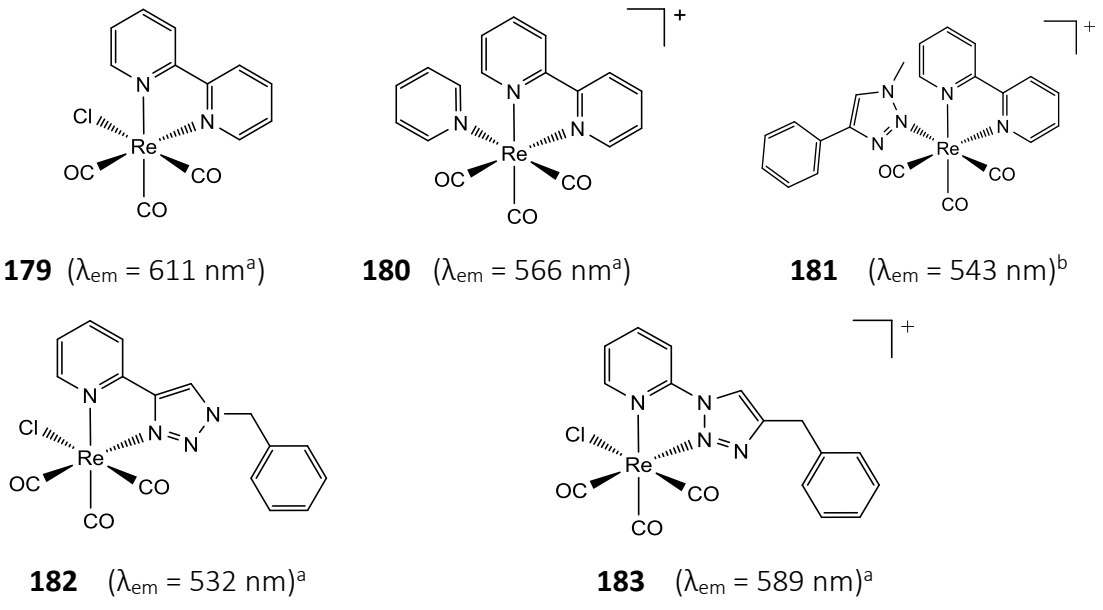

179 (λ_{em} = 611 nm[a]) **180** (λ_{em} = 566 nm[a]) **181** (λ_{em} = 543 nm)[b]

182 (λ_{em} = 532 nm)[a] **183** (λ_{em} = 589 nm)[a]

***Figure 3.1**: Rhenium(I) tricarbonyl triazole complexes, showing emission maxima, ([a] in MeCN, [b] in DCM.)*

Inverse click ligands were designed by Bertrand *et al* in an attempt to circumvent the blue-shift in emission associated with pyridyl triazoles.[173] The inverse click complex **183** is red-shifted (λ_{em} = 589 nm) with respect to the regular triazole ligand (**182**). This

red-shifted absorption is consistent with the poorer electron donating ability of the N2 donor atom of the inverse pyta ligand compared to the N3 donor atom in the regular pyta ligand.[272] Whilst complexes derived from these inverse click ligand tend to have longer emission lifetimes and a greater quantum yield, they are unfortunately much less stable in solution.[272]

3.1.2: Cyclometallated Ir(III) polypyridine complexes

The HOMO of cyclometallated complexes tends to have a greater ligand π character arising owing to a greater contribution from the π system of the cyclometallating aryl rings. As a result, emission from cyclometallated complexes may also have significant intraligand (IL) or ligand to ligand charge transfer (LLCT) character. The photophysics of heteroleptic Ir(III) complexes is further complicated as the introduction of an ancillary ligand not only increases the number of possible electronic transitions to the second set of ligand orbitals from the ancillary ligand, but also causes the Ir(dπ) t_{2g} state to become non-degenerate. The key excited states are illustrated in Figure 3.2.

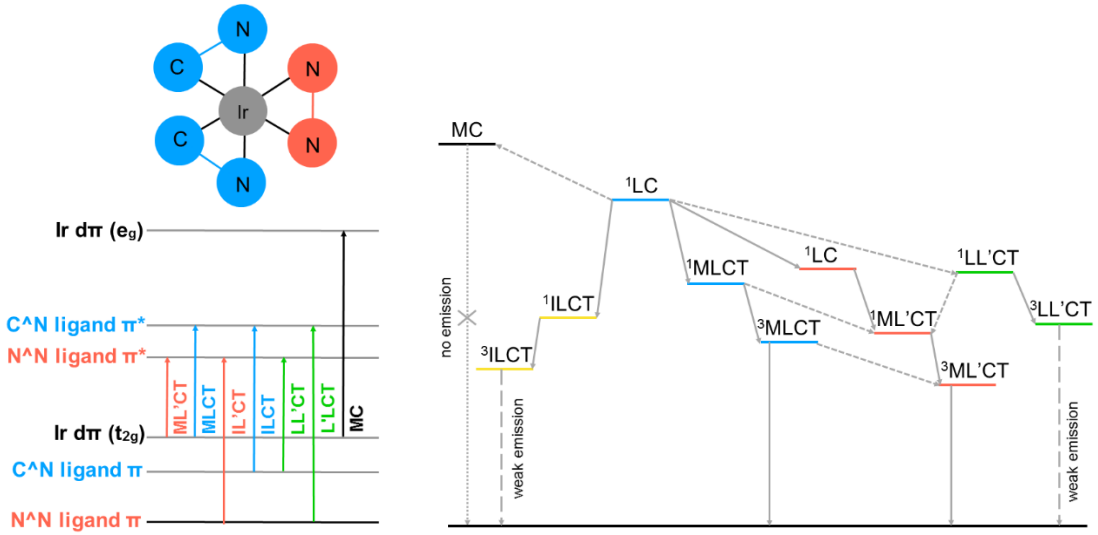

***Figure 3.2**: Excited states of cyclometallated Ir(III) complexes. Metal-centred ligand-field state (MC); ligand-centered state (LC); metal-to-ligand charge-transfer state (MLCT); ligand-to-ligand charge-transfer state (LL'CT); intraligand charge-transfer state (ILCT). Adapted from Nam & You.*[273]

This complexity does however make heteroleptic iridium complexes highly amenable to emission colour tuning. Altering either the extent of conjugation of the ligands or the addition of appropriate electron withdrawing (EWG) or electron donating

groups (EDG) to either the C^N or N^N ligands, provides a means by which to alter the energy levels of the HOMO and LUMO and thus tune the photophysical properties of the MLCs.[142] Reducing the magnitude of the HOMO-LUMO gap by destabilising the HOMO and/or stabilising the LUMO bathochromically (red) shifts emission, conversely, hypsochromically (blue) shifted emission is achieved by stabilising the HOMO and/or destabilising the LUMO, as depicted in Figure 3.3. However, as the emission tends to the ends of the visible spectrum, the quantum yield of emission decreases. Tuning the emission towards the blue destabilises the metal centred and ligand centred states; however, this also depreciates the energetic separation of the two states. Consequently, the metal centred state may be thermally populated resulting in quenching of emission. Towards the red end of the spectrum, the rate of non-radiative decay increases exponentially as the emission energy decreases as a consequence of the energy gap law.[274]

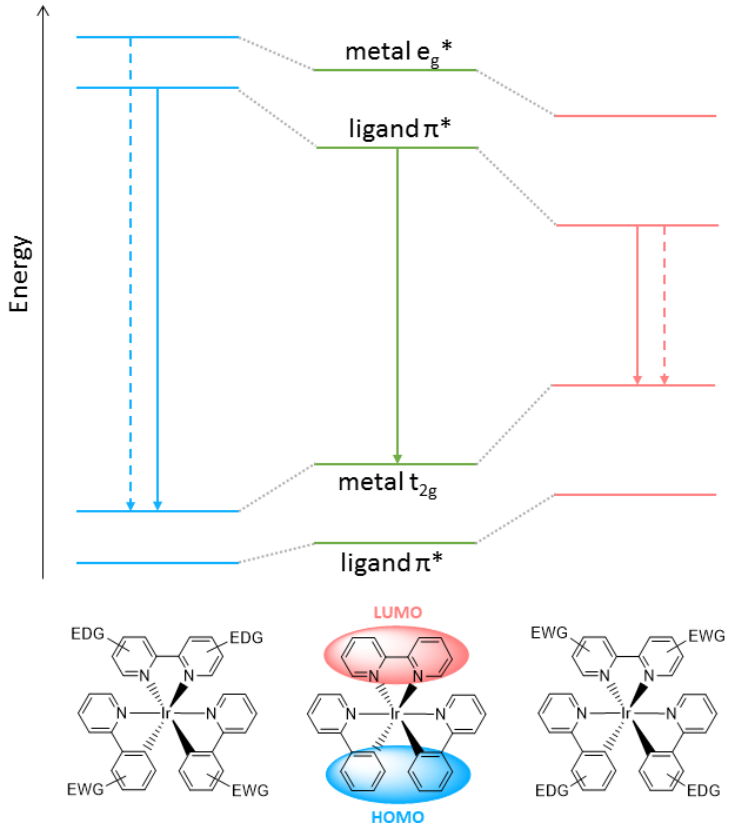

***Figure 3.3**: Colour tuning the emission of [Ir(ppy)$_2$(bpy)] adapted from Zysmann-Coleman et al.*[142]

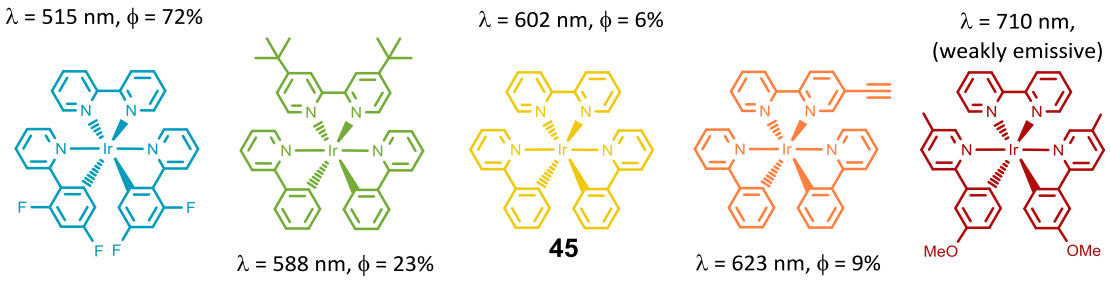

Figure 3.4: *Colour tuned substituted [Ir(ppy)2(bpy)]⁺ complexes.*

One of the most widely studied iridium complexes is $[Ir(ppy)_2(bpy)]^+$ (**45**) it emits orange/yellow light in acetonitrile (λ_{em} = 602 nm) with a quantum yield of 6%. The emission profile of **45** is broad and structureless, characteristic of emission with significant ^{3}MLCT character. Formally, the emission is from a mixed ^{3}MLCT/^{3}LLCT state where the excited electron is associated with the π* of the bpy ligand. Compared to the archetypal complex **45**, iridium complexes with a pyridyl triazole (pyta) ancillary ligand also exhibit significantly blue-shifted emission as the ancillary ligand π* orbital occurs at a higher energy than bpy. Emission from $[Ir(ppy)_2(pyta)]^+$ is vibronically structured, indicating that the lowest emissive triplet state has significant ^{3}LC character. As the π* orbital of the electron rich pyta ligand lies at a higher energy than that of the bpy ligand, the lowest energy transition is from the π* of cyclometallating ligands, and so the emission is of mixed ^{3}MLCT/^{3}ILCT nature.[269]

3.2: Tuning the photophysical properties of Re(I) tricarbonyl and Ir(III) polypyridine complexes.

Despite the ease of conjugation to biological molecules, complexes derived from pyta ligands have blue-shifted emission relative to comparable complexes derived from bpy, which is less desirable for biological imaging. For the Re(I) complexes used in this study, the inclusion of an axial pyridine ligand to enhance kinetic stability causes a further blue shift in the emission. Re(I) tricarbonyl pyta complexes do not emit very efficiently when excited at 405 nm, the wavelength used for confocal microscopy (Figure 3.6). In contrast to its rhenium counterpart, the excitation maximum of the Ir(III) pyta complex coincides with the optimal wavelength used in confocal microscopy. Whilst the iridium pyta complex appears to have useful photophysical properties for use as cellular probes,

it would be particularly useful to tune the both the excitation maximum of Re(I) pyta complexes towards the red to enhance the performance of these probes. It was proposed that incorporation of electron withdrawing groups onto the pyridine ring would stabilise the ligand-based LUMO to red-shift the both emission and absorption.

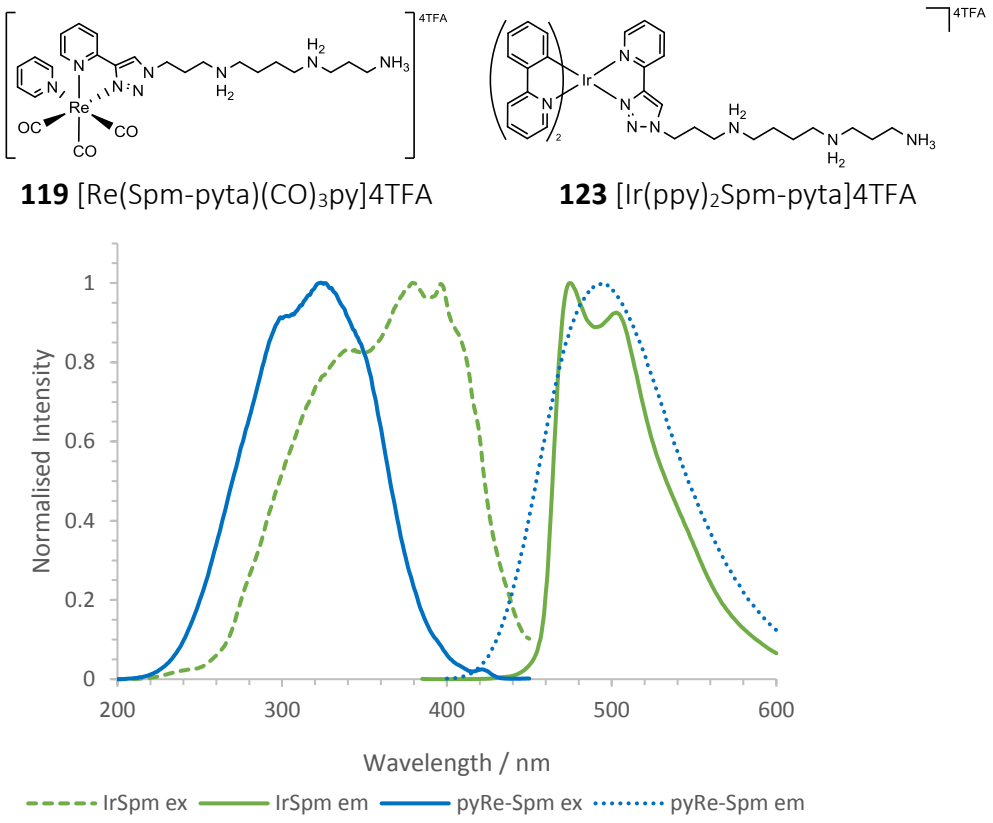

***Figure 3.5**: Normalised excitation and emission profiles of **119** [Re(Spm-pyta)(CO)$_3$py]$^+$ (Φ = 0.005, τ = 157 ns) and **123** [Ir(ppy)$_2$(Spm-pyta)]$^+$ (Φ = 0.209, τ = 404 ns), measured in aerated water (0.1 mM).*

3.2.1: Tuning the N^N ligand

The initial focus was to optimise the absorption of rhenium complexes at 405 nm. Efforts by others to tune the photophysical properties of rhenium pyta complexes have mainly involved increasing the extent of conjugation of the diimine ligand,[173] varying the N1-substituent on the triazole ring,[275] modifying the axial ligand or using the inverse click ligand.[272] Very few reports detail direct modifications of the pyridyl ring by the incorporation of electron donating and/or withdrawing groups, although this strategy has been more widely adopted with cyclometallated iridium complexes. The substituted complexes used in this study are shown in figures 3.6 and 3.7. As discussed in chapter 2, substituted ethynyl pyridines are readily accessible via Sonogashira coupling.

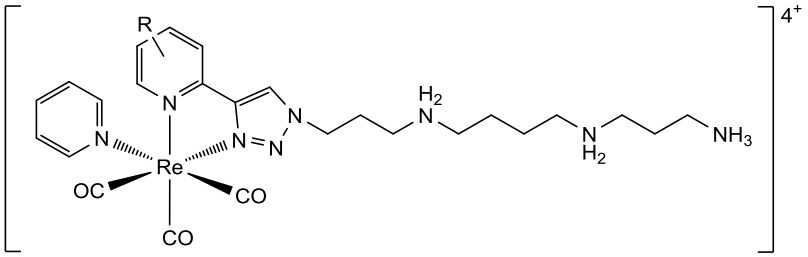

119 (R = H) **129** (R = 5-OMe) **130** (R = 5-CF_3) **131** (R = 4-CF_3)

***Figure 3.6**: Substituted $[Re(CO)_3(py)(pyta)]^+$ complex cations.*

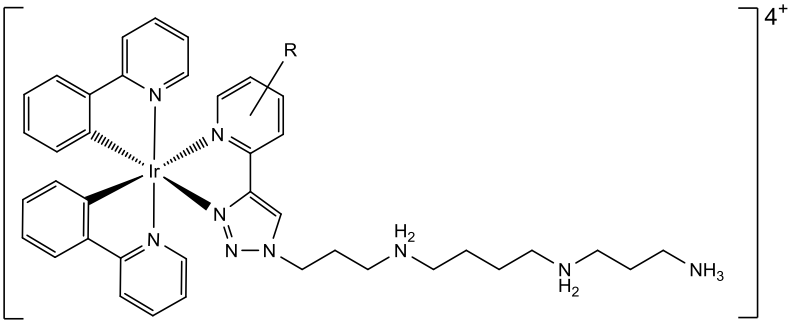

123 (R = H) **132** (R = 5-OMe) **133** (R = 5-CF_3) **134** (R = 4-CF_3)

***Figure 3.7**: Substituted $[Ir(ppy)_2(pyta)]^+$ complex cations.*

3.2.1.1: Absorption

The electronic absorption spectra for the rhenium pyta tricarbonyl complexes are shown in Figure 3.8. The absorption band around 240 nm with ε values in the range 5000 - 29000 $M^{-1}\,cm^{-1}$ arises as a result of spin-allowed π-π* (^{1}LC) transitions of the triazole ligand, which overlaps with weaker absorption from the pyridyl ligand. The weaker band around 330 nm is attributed to the dπ-π* ^{1}MLCT transition and has an extinction coefficient of around 4000 $M^{-1}\,cm^{-1}$. The extinction coefficients for these transitions are shown in table 3.1. UV data is in agreement with Obata's first reports of Re pyta complexes,[172] and similar compounds reported by Donnelly and Crowley.[275,276]

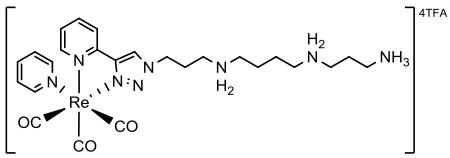

119 pyRe-Spm

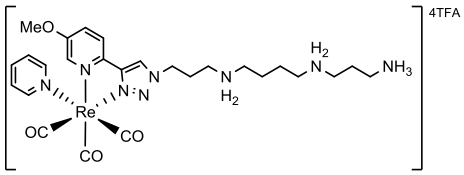

129 5OMe-Spm pyRe

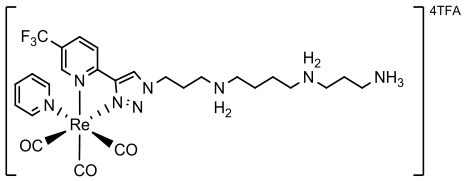

130 5CF_3-Spm pyRe

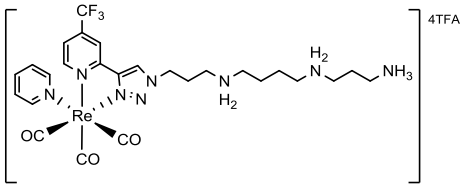

131 4CF_3-Spm pyRe

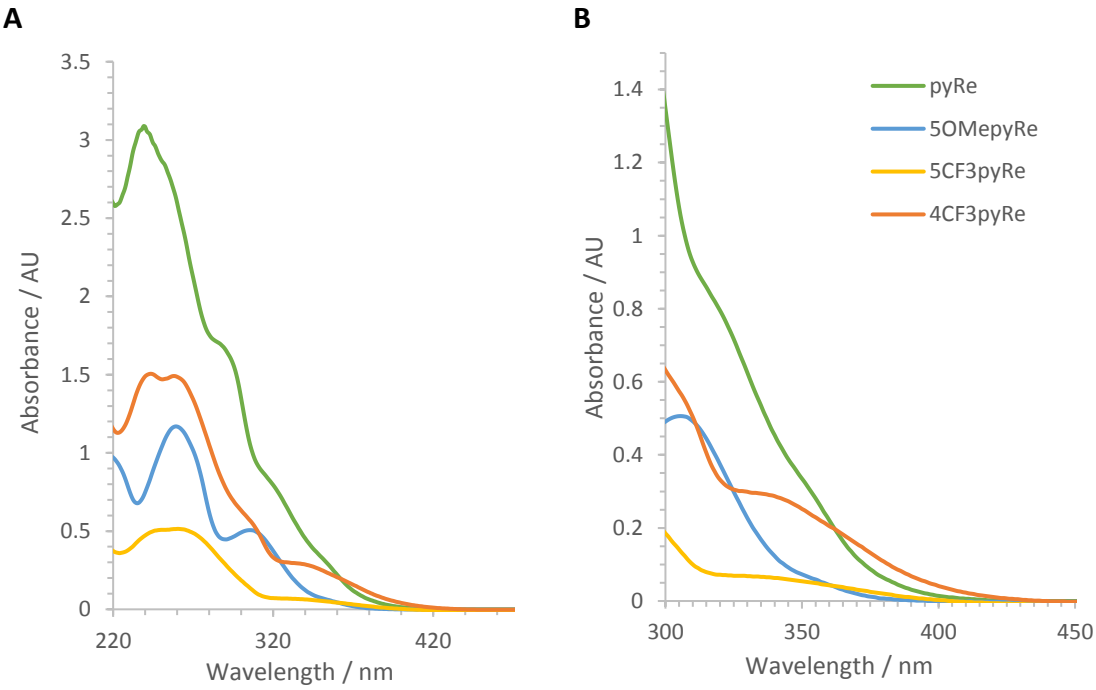

***Figure 3.8**: Electronic absorption spectra for Re(I) complexes measured in aerated water, at ambient temperature. A) Electronic absorption spectrum, showing intense ligand π π* transitions and the weak spin allowed MLCT band. B) Expanded spectrum showing weak MLCT transition.*

	λ_{max} (nm)	$\varepsilon_{\pi\text{-}\pi^*}$ ($M^{-1}cm^{-1}$)	λ_{max} (nm)	ε_{MLCT} ($M^{-1}cm^{-1}$)
5-OMe (129)	258	12640	307	5606
pyReSpm (119)	280	28935	327	6739
5-CF_3 (130)	242	4836	321	1044
4-CF_3 (131)	238	15049	331	3596

***Table 3.1**: Extinction coefficients for ligand centred and MLCT transitions in py-Re(CO)$_3$pyta complexes.*

The electronic absorption spectra of the iridium pyta complexes are shown in Figure 3.9 and show typical features of this class of compound, similar to complexes reported by Donnelly and De Cola.[277–279] The intense high energy band around 250 nm arises from spin-allowed ligand based π-π* ligand centred (^{1}LC) transitions of the cyclometallating (C^N) ppy and ancillary (N^N) pyta ligands with ε values in the range 40 000 – 50 000 M^{-1} cm^{-1}. Bands in the low energy region (360 to 420 nm) arise as a result of spin-allowed mixed CT transitions, the extinction coefficient (ε) for this absorption is approximately 4000 M^{-1} cm^{-1}. The very weak band found around 460 nm is attributed to spin forbidden mixed CT transitions. Compared to the unsubstituted complex (**119**) the substituted complexes seem to have a more intense high energy band, this effect is largest for the for the OMe complex (**129**), this is likely due to additional contribution from the lone pair of the methoxy to the conjugated system of the triazole ligand. The methoxy complex and the unsubstituted complexes have more prominent features around 379 nm and 465 nm compared to the CF_3 substituted complexes.

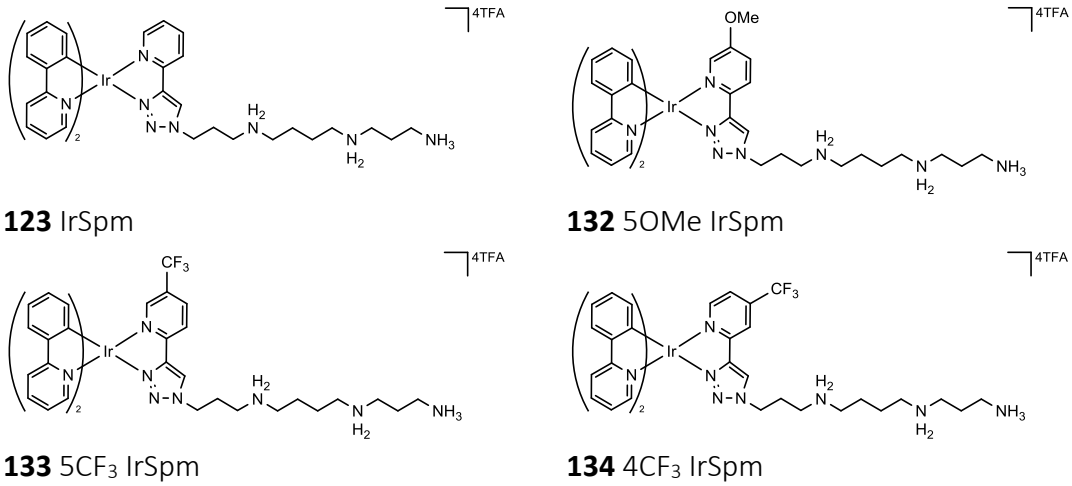

123 IrSpm

132 5OMe IrSpm

133 5CF_3 IrSpm

134 4CF_3 IrSpm

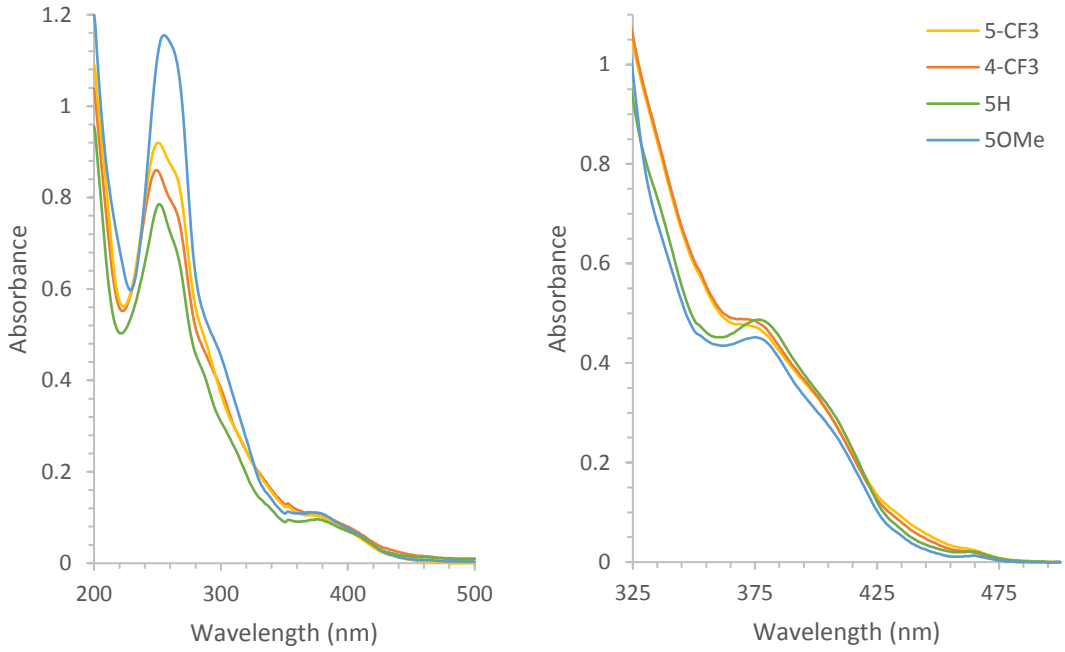

***Figure 3.9**: Absorption spectra of N^N substituted Ir complexes, measured in aerated water. (Left) Full range electronic absorption spectrum, showing intense ligand π π* transitions and the weak spin allowed MLCT band. (Right) 100 µM solutions showing the spin allowed MLCT band and weak spin forbidden transitions.*

	λ_{max} (nm)	$\varepsilon_{\pi\text{-}\pi^*}$ ($M^{-1}cm^{-1}$)	λ_{max} (nm)	ε_{MLCT} ($M^{-1}cm^{-1}$)
5-OMeIr (132)	258	53061	379	4362
IrSpm (123)	252	45937	381	4713
5-CF_3Ir (133)	251	44141	379	5000
4-CF_3Ir (134)	249	43293	374	4948

***Table 3.3.2**: Extinction coefficients for ligand centred and MLCT transitions in Ir(III) C^N substituted complexes.*

3.2.1.2: Emission

As expected, decorating the pyridyl ring of the pyta ligand with an electron withdrawing group red shifted both the emission and the excitation of the Re(I) complexes (as a result of stabilising the LUMO) whereas adding an electron donating group caused a hypsochromic shift (by destabilising the LUMO). This caused a visible difference in the colour of the emission in aqueous solution; the unsubstituted complex shows a blue-green emission, whereas the CF_3 substituted complex showed a yellow emission and the methoxy substituted complex was cyan-coloured, as shown in Figure 3.10.

R	λ_{ex} / nm	λ_{em} / nm
OMe (**129**)	311	477
H (**119**)	326	496
5-CF_3 (**130**)	343	536
4-CF_3 (**131**)	354	545

***Figure 3.10**: Emission colours of rhenium complexes, in aqueous solution, viewed under 360 nm illumination; complex **130** (5-CF_3) **119** (unsubstituted) and **129** (5-OMe)*

Introducing an electron withdrawing substituent at the pyridyl ring increased the structured appearance of the excitation spectra of the Re(I) complexes as shown in figure 3.11, however the emission remained broad and featureless reflecting the ^{3}MLCT nature of the transition. The methoxy group (129) afforded a modest blue shift of around 15 nm for the excitation and 19 nm for the emission. The 5-CF_3 group (130) red-shifted the excitation maximum by 17 nm, but had a more profound effect on the emission, causing a 40 nm bathochromic shift. The 4-CF_3 group (131) gave rise to the largest shifts, increasing the excitation and emission maxima by 28 nm and 49 nm respectively. Despite a significant red shift from the introduction of a single CF_3 group, (most notably when installed *para*- with respect to the rhenium-nitrogen bond) the intensity of emission when excited at 405 nm, is still rather low, although significantly higher than that of the unsubstituted complex 119. Unfortunately, there was only a small enhancement in the absorption at 405 nm.

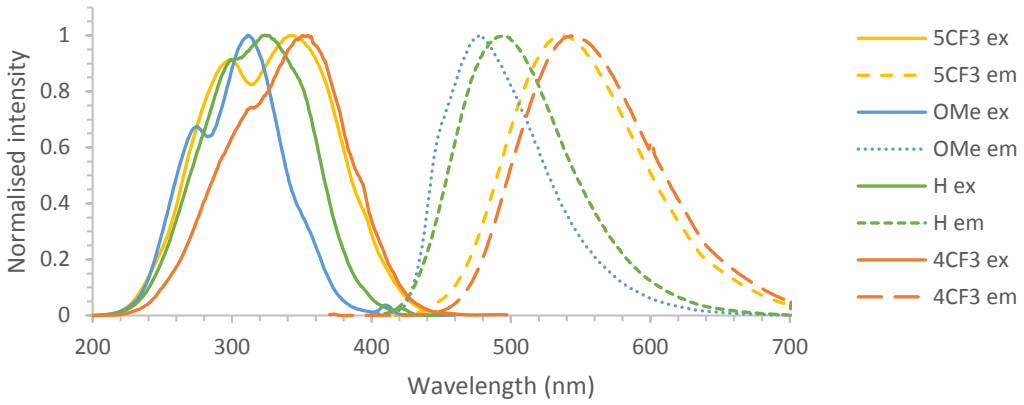

***Figure 3.11**: Excitation and emission profiles of Re(I) complexes **119**, and **129** - **131** in aerated water (0.1 mM) at ambient temperature. λ_{ex} = 330 nm.*

Although the excitation properties of the iridium pyta complex are satisfactory for use in confocal microscopy substituted iridium complexes were made in an attempt to tune the emission to the red. Broadly speaking, alterations of the diimine ligand had very little effect on the excitation, as can be seen in figure 3.12. However, subtle differences can be found in the fine structure of the excitation spectra. There are two distinct features of the excitation spectrum, the second of which is more structured. The non-substituted complex (**123**) has two maxima at 313 nm and 392 nm that are roughly equal. The OMe substituted complex (**132**) has a significantly smaller higher energy component compared to **123**, whist the CF_3 substituted complexes **133** and **134** have a more prominent high energy feature. This higher energy feature occurs at a similar wavelength to the excitation of the rhenium complexes and appears to reflect the extent of ^{3}MLCT character to the emission of the Ir(III) complexes.

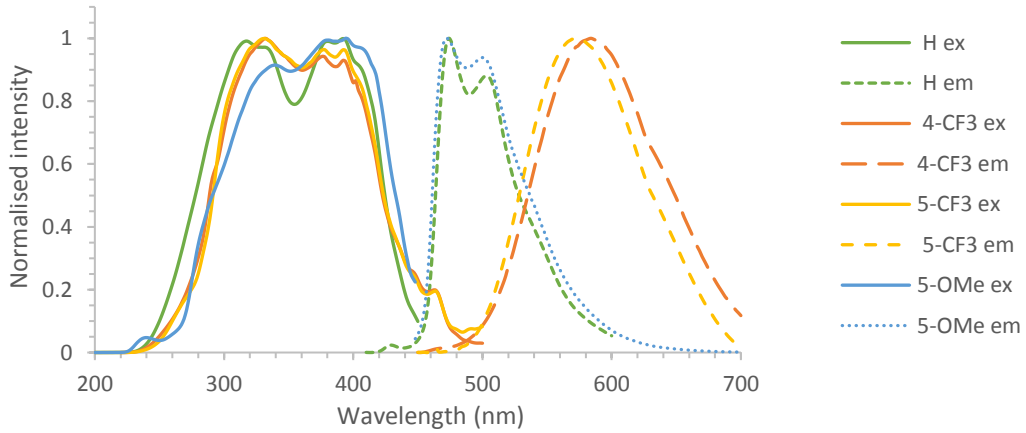

***Figure 3.12**: Excitation and emission profiles of N^N substituted Ir complexes **123**, and **132** - **134** in aerated water (0.1 mM) at ambient temperature, compared to unsubstituted complex 150.*

Structured emission bands arise as a result of the excited state coupling to the vibronic states of the ligand. Complexes **123** and **132** exhibit bright blue-green emission with an intense band at 475 nm, an almost equally intense vibronic progression at 510 nm and a shoulder at approximately 545 nm. The general appearance of the spectra and the emission wavelengths observed are very similar to the related complexes $[Ir(dfppy)_2(pyta)]^+$ and $[Ir(ppy)_2(pyta)]^+$ previously reported by De Cola and co-workers and Elliot *et al.*[278–281] The similar intensity of the two vibronic features is a strong indication that the transition is largely localised on the cyclometallating ligand. The electron donating OMe group did not cause any significant shift in emission although a slight enhancement in the intensity of the second vibronic feature at 510 nm implies a reduced contribution of MLCT character compared to the non-substituted complex.[282] Given that the excited state is of ^{3}MLCT/^{3}ILCT character further destabilisation of the diimine π* orbital caused by the EDG is unlikely to elicit any further changes in emission as the excited electron is associated with the cyclometallating ligand π* orbital and not the diimine ligand. The vibronically structured emission profiles of complexes **123** and **132** overlap significantly with the emission of the equivalent rhenium complexes **119** and **129**.

In contrast, the inclusion of an electron withdrawing group on the pyridyl ring of the pyta ligand significantly shifted the emission over 100 nm towards the red. Emission from the CF_3 substituted complexes (**133** & **134**) is broad and structureless, implying a greater contribution from the ^{3}MLCT excited state. It is likely that the stabilising effect of electron withdrawing CF_3 group is sufficient to reduce the energy of the diimine π* orbital below that of the cyclometallating ligand π* orbital. As a result, the lowest energy transition will be associated with the diimine ligand, giving rise to an excited state with ^{3}MLCT/^{3}LLCT character. Given that the emission from these complexes is dominated by the N^N ligand, it stands to reason that these complexes should be more affected by structural alterations of the diimine ligand. These complexes showing emission of ^{3}MLCT/^{3}LLCT nature have a more orange colour, as can be seen in figure 3.13. The key photophysical properties are summarised in table 3.3.

R	λ_{ex} / nm	λ_{em} / nm
OMe (**132**)	(342) 380, 394	472
H (**123**)	313, (380) 392	474
5-CF_3 (**133**)	331, (378, 392)	572
4-CF_3 (**134**)	332, (376, 392)	584

***Figure 3.13**: Emission colours of iridium complexes, complex **132** (5-OMe), **123** (unsubstituted) and **133** (5-CF_3) and **134** (4CF_3) in aqueous solution viewed under 360 nm illumination.*

Complex	$\varepsilon_{\pi-\pi^*}$ ($M^{-1}cm^{-1}$)	ε_{MLCT} ($M^{-1}cm^{-1}$)	λ_{ex} (nm)	λ_{em} (nm)	Φ	τ (ns)
119	12640	5606	326	496	0.0054	157.3
129	28935	6739	311	477	0.0052	78.3
130	4836	1044	343	536	0.0068	408.1
131	15049	3596	354	545	0.0099	605.0
123	45937	4313	392	474	0.209	404.0
132	53061	4713	394	472	0.225	404 (96 %) 17 (4 %)
133	44141	5000	331	572	0.012	420 (94 %) 45 (6 %)
134	43293	4948	332	584	0.005	340 (89 %) 17 (11 %)

***Table 3.3.3:** Summary of key photophysical data for substituted pyta Re and Ir complexes, measured in aerated water.*

3.2.2: Tuning C^N ligand

Incorporating the pyta ligand into the Ir(III) coordination sphere as opposed to bpy gives rise to emission with ^{3}MLCT/^{3}ILCT character with both the HOMO and the LUMO being associated with the cyclometallating (C^N) ligand. It is therefore likely that modifying the C^N ligand may prove to be a more effective approach to tune the photophysical properties of these complexes. To investigate this further, an electron donating methoxy group was installed at the 4-position of the phenyl ring of the C^N ligand as shown in figure 3.14.

3.2.2.1: Absorption

The electronic absorption spectra for the substituted C^N complexes **135** and **136** compared to the N^N substituted complexes (**123** and **134**) are shown in Figure 3.15. Complexes containing the methoxy-substituted phenylpyridine ligand (papy), show an

additional high energy band centred around 270 nm. This may arise due to increased conjugation within the phenylpyridine ligand from the lone pair of electrons from the methoxy substituent enhancing C^N ligand based π→π* transitions. In the ppy complexes the weak CT band shows two features; a prominent feature centred around 375 nm with a shoulder around 400 nm, corresponding to spin allowed and spin forbidden MLCT transitions. This first feature occurs with a higher intensity in the papy complexes, and weak shoulder associated with spin forbidden ^{3}MLCT transitions appears to be absent. The weak spin forbidden transition associated with the unsubstituted N^N ligand is noticeably weaker in the papy complex (135) compared to the ppy complex 123.

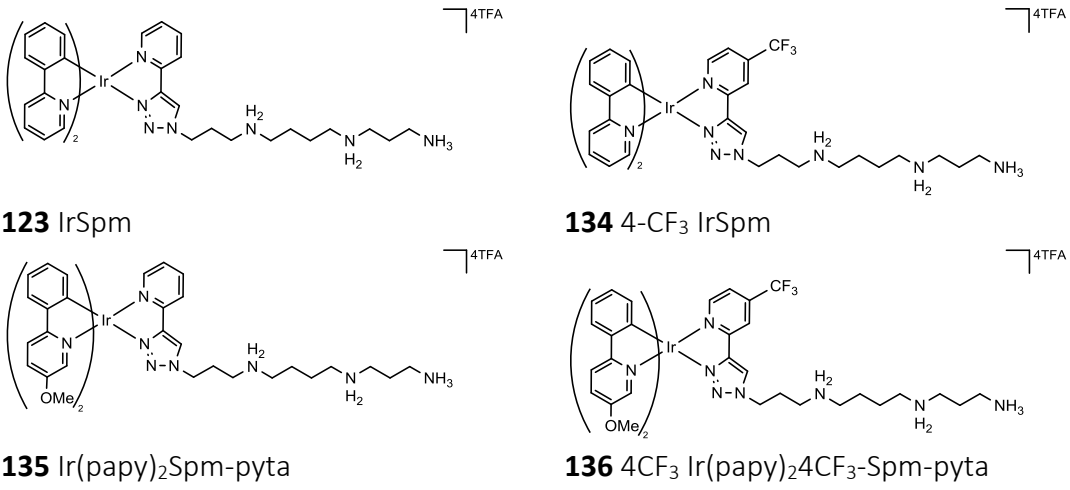

123 IrSpm

134 4-CF_3 IrSpm

135 Ir(papy)$_2$Spm-pyta

136 4CF_3 Ir(papy)$_2$4CF_3-Spm-pyta

***Figure 3.14**: Substituted C^N Ir(III) complexes.*

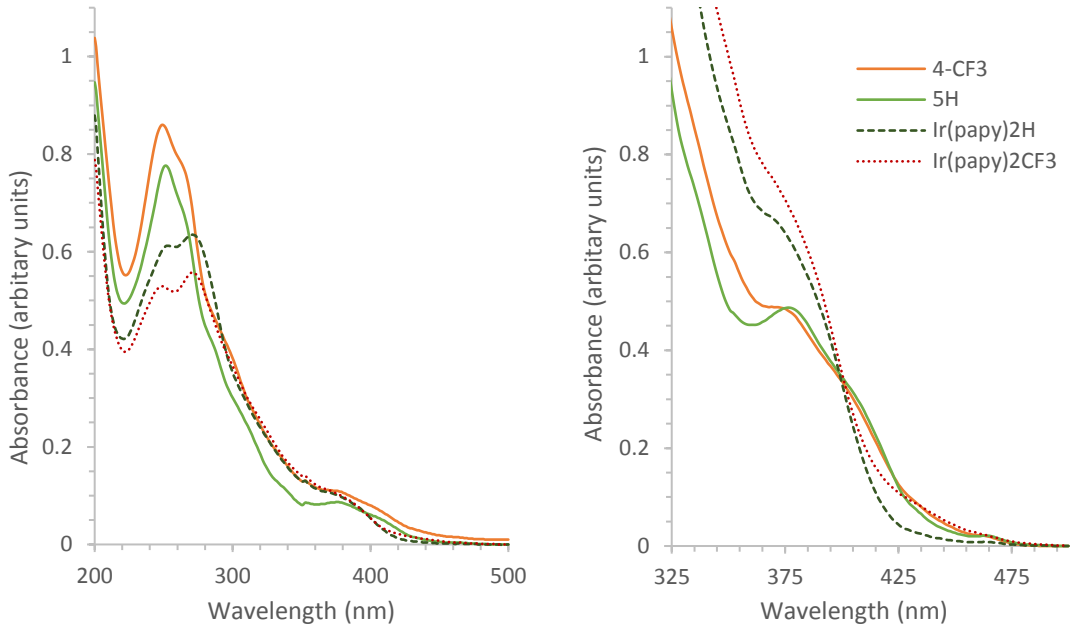

***Figure 3.15**: Absorption spectra of C^N substituted Ir complexes (0.1mM), measured in aerated water. Electronic absorption spectrum, showing intense ligand π π* transitions and the weak spin allowed CT band (left) and expansion showing the spin allowed CT band and weak spin forbidden transitions (right).*

	λ_{max} (nm)	$\varepsilon_{\pi-\pi^*}$ ($M^{-1}cm^{-1}$)	λ_{max} (nm)	$\varepsilon_{d\pi-\pi^*}$ ($M^{-1}cm^{-1}$)
IrSpm	252	45937	381	4713
$Ir(papy)_2H$	274	43203	379	6826
$4\text{-}CF_3Ir$	249	43293	374	4948
$Ir(papy)_2\,4\text{-}CF_3$	271	39749	374	7056

***Table 3.3.4:** Extinction coefficients for ligand centred and MLCT transitions in Ir(III) substituted C^N complexes.*

3.2.2.2: Emission

As the HOMO has been found to be based on the metal and the phenyl rings of the cyclometallating ligand in most iridium pyta complexes, it would be expected that attempts to tune the emission of these complexes via modifications of the C^N ligand would be a judicious choice. To this end phenylpyridine ligands bearing an electron withdrawing methoxy group on the phenyl ring were used with the belief that they would destabilise the HOMO and red-shift emission.

Complex **135** exhibits green, vibronically structured emission similar to that of **123**, with maxima at 475 nm and 510 nm, and a discrete shoulder around 545 nm, pointing to emission is of mixed ^{3}ILCT/^{3}MLCT nature. Compared to complex **123**, the

intensity of the band at 475 nm is much larger than the lower energy band at 510 nm and implies a greater contribution from an MLCT excited state. The emission profile of **135** is narrower than that of **123**, with a less prominent shoulder at 545 nm, which mirrors the effects seen on the excitation spectrum.

The orange emitting papy complex **136** also shows very little change in the emission and excitation profiles compared to **134**. Emission shows a large broad feature consistent with emission of MLCT nature; however, intraligand emission is also evident as a shoulder on the leading flank of the emission profile. The excitation profile of complex **136** is not red-shifted, but narrower compared to the analogous ppy complex.

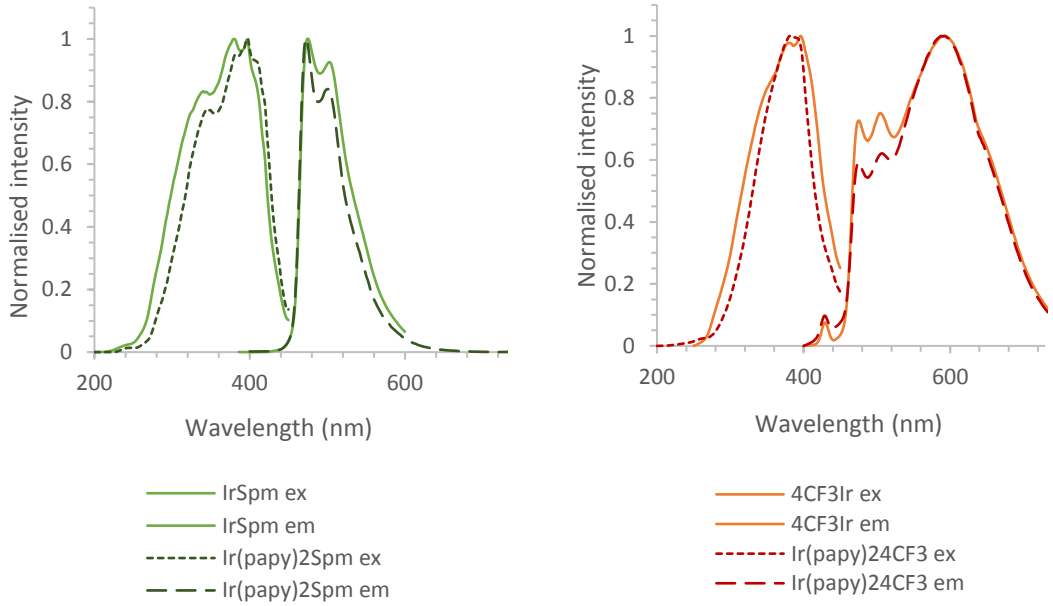

Figure 3.16**: (Left) excitation (λ_{em} 474 nm) and emission (λ_{ex} 379 nm) spectra of complexes **123** and **134** in water, (right) excitation (λ_{em} 594 nm) and emission (λ_{ex} 379 nm) spectra of complexes **135** and **136.

R	λ_{ex} / nm	λ_{em} / nm
IrSpm (**123**)	392	474
Ir(papy)$_2$ H (**135**)	398	474
Ir 4-CF$_3$ (**134**)	394	584
Ir(papy)$_2$ 4CF$_3$ (**136**)	386	584

***Figure 3.17**: Colour of emission of C^N substituted Ir(III) complexes green emitting complexes **123** and **135** and orange emitting complexes **134** and **136**.*

From the results obtained in this study, the effect on emission of the methoxy group at the 4-position of the phenyl ring of the C^N ligand is negligible. This finding was also born out in a study by Zysmann-Coleman *et al.*[141] Davies *et al* demonstrated that 3-OMe substituted phenyl pyrazole complexes (where the OMe group is *para*- to the Ir-N bond) show significantly red-shifted emission,[140] however Zysmann-Coleman *et al* reported that whilst 3-OMe phenyl pyridine complexes showed significantly red-shifted emission, they are only weakly luminescent with short emission lifetimes.[141] Key photophysical data is summarised in table 3.5.

Complex	$\varepsilon_{\pi\text{-}\pi^*}$ ($M^{-1}cm^{-1}$)	ε_{MLCT} ($M^{-1}cm^{-1}$)	λ_{ex} (nm)	λ_{em} (nm)	Φ	τ (ns)
123	45937	4313	392	474	0.209	404.0
134	43293	4948	332	584	0.005	340 (89 %) 17 (11 %)
135	43203	6826	398	474	0.105	0.467 (92 %) 0.028 (8 %)
136	39749	7056	386	584	0.004	0.284 (91 %) 0.016 (9 %)

Table 3.5: *Summary of key photophysical data for C^N substituted Ir complexes, measured in aerated water.*

3.4: Quantum Yields

The quantum yield (Φ) represents the number of photons emitted relative to the number of photons absorbed and is proportional to the emission lifetime. Φ may be derived from the decay rates as shown in equation 3, where Γ is the emissive rate constant and k_{nr} is the non-radiative decay constant. Φ is essentially a measure of the the brightness of the emission; if non-radiative decay processes are minimal, the quantum yield may be close to unity.

$$\Phi = \Gamma / (\Gamma + k_{nr}) \qquad \textit{Equation 3.1}$$

Quantum yield is commonly measured experimentally by comparison with a standard of known quantum yield with a similar emission profile and wavelength range under identical experimental conditions. A range of solutions of the test substance and the standard are prepared to have the same absorption at a specific wavelength, with

the absorption of these solutions not exceeding 0.1 to avoid self-quenching. It can be assumed that solutions with the same absorption at the same wavelength in the same solvent are emitting the same number of photons, and therefore the quantum yield can be determined graphically from the ratio of the gradients of the graph of absorbance against integrated emission intensities of the standard and test solutions, according to equation 3.2 where Φ_{ref} is the quantum yield of the reference sample and m_x and m_{ref} are the gradients of the graph of absorbance against integrated emission intensities of the sample (x) and reference (ref).[283,284]

$$\Phi_x = \Phi_{ref} (m_x / m_{ref}) \qquad \textit{Equation 3.2}$$

The quantum yields of the luminescent MLCs are commonly measured relative to $[Ru(bpy)_3]^{2+}$ however as $[Ru(bpy)_3]^{2+}$ is virtually non-emissive in the range of rhenium's emission, quinine sulfate was the standard of choice for rhenium complexes.[285] The quantum yield of the rhenium complexes are shown below in table 3.5. The quantum yield of all the complexes are rather low (below 1%) however, the 4-CF_3 complex (**131**) is twice as bright as the unsubstituted complex **119** and would be the complex of choice for cellular imaging using rhenium pyta complexes.

Re Complex	λ_{em} (nm)	Φ
Quinine sulfate	450	0.5490
5-OMe (**129**)	477	0.0052
H (**119**)	496	0.0054
5-CF_3 (**130**)	536	0.0068
4-CF_3 (**131**)	545	0.0099

***Table 3.5**: Quantum yield values of py-$ReCO_3$(pyta) complexes, measured in aerated water, at ambient temperature.*

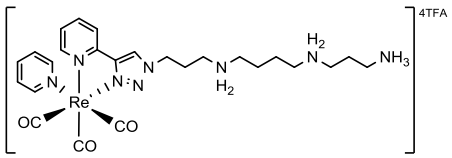

119 pyRe-Spm

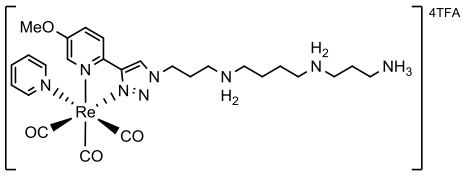

129 5OMe-Spm pyRe

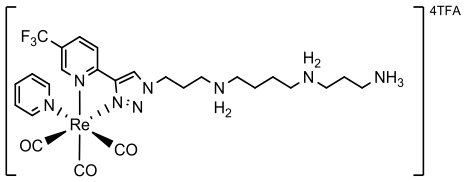

130 5CF_3-Spm pyRe

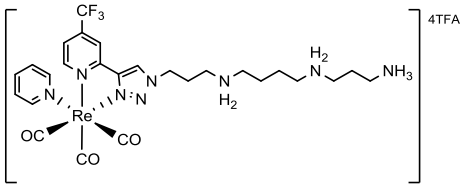

131 4CF_3-Spm pyRe

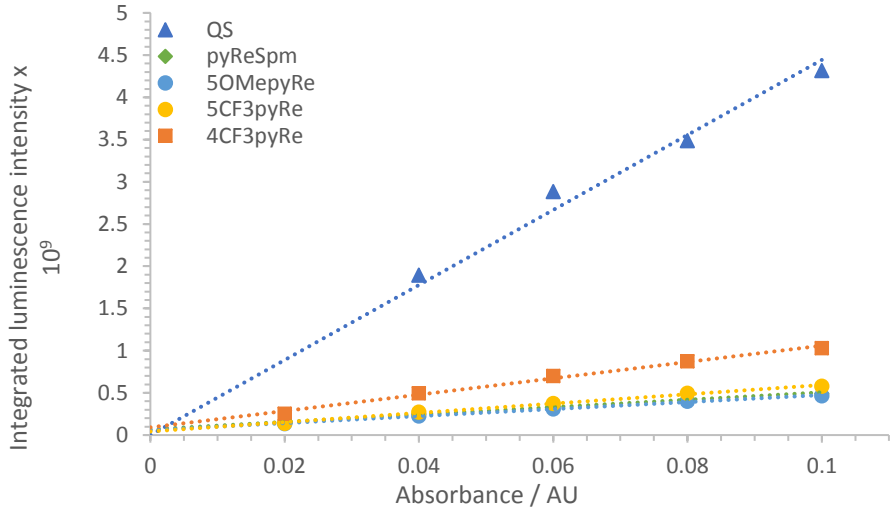

Figure 3.18: *Integrated fluorescence intensity-absorbance plot of Re complexes showing linear fit.*

The quantum yield values of the iridium complexes studied reflect the nature of the excited states of the complexes. The non-substituted complex **123** and the OMe substituted pyta complex **129** showed relatively high quantum yields of 0.209 and 0.225 respectively, compared to the significantly lower values of 0.012 and 0.005 for the 5-CF_3 and the 4-CF_3 complexes respectively. The complexes with MLCT/ILCT character have significantly higher quantum yields than the complexes with MLCT/LLCT character. This could be argued as being a consequence of the energy gap law; the complexes with MLCT/LLCT nature are more likely to undergo non-radiative decay as the energy gap between the excited and ground states is smaller.

Complex	λ_{em} (nm)	Φ
5-OMeIr (132)	472	0.225
IrSpm (119)	474	0.209
5-CF_3Ir (133)	572	0.012
4-CF_3Ir (134)	584	0.005
Ir(papy)$_2$H (135)	474	0.105
Ir(papy)$_2$ 4-CF_3 (136)	584	0.004

***Table 3.6**: Quantum yield values for cationic Ir(III) complexes in aerated water.*

However, this argument does not hold true for the C^N substituted complex. 135 has green emission that is vibronically coupled indicating an emissive state with a high degree of ILCT character. The intensity of the second vibronic progression at 510 nm is significantly smaller than the first, which implies a greater degree of MLCT character contributing to the emissive state. Consistent with this, this complex has a quantum yield of 0.105, which is significantly greater than that of the CF_3 substituted complexes, but around half of that of the non-substituted counterpart. The bi-functionalised complex 136 has the smallest quantum yield of 0.0035. Broadly speaking the quantum yield of the C^N substituted complexes are about half of the analogue complex without C^N substitution and this cannot be explained by the energy gap law. Zysman-Coleman has previously noted the weak luminescence of OMe substituted phenyl pyridine complexes, and has proposed that this is a consequence of electron donation into the Ir-C bond which leads to rapid non radiative decay of the excited state.[141]

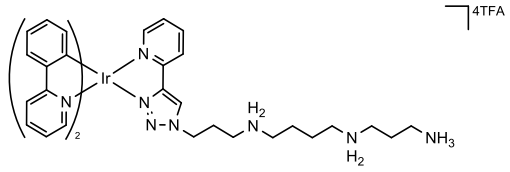

123 IrSpm

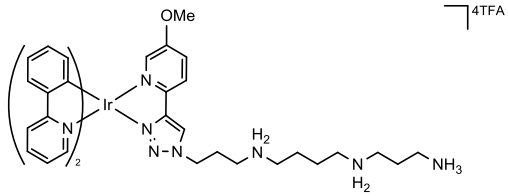

132 5OMe IrSpm

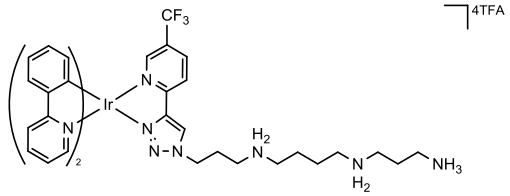

133 $5CF_3$ IrSpm

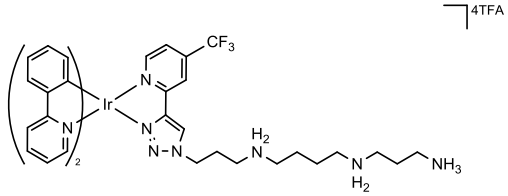

134 $4CF_3$ IrSpm

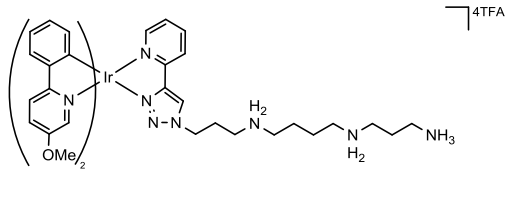

135 $Ir(papy)_2Spm$-pyta

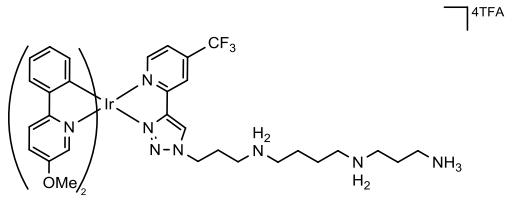

136 $4CF_3$ $Ir(papy)_24CF_3$-Spm-pyta

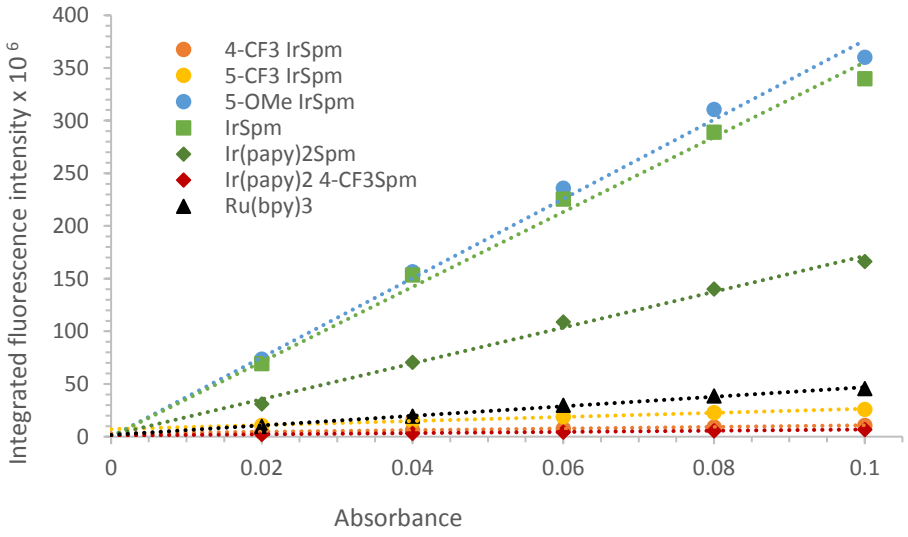

***Figure 3.19**: Integrated fluorescence intensity-absorbance plots used to determine Φ, showing linear fit.*

3.5: Emission lifetime

Radiative decay of the excited state is a random (stochastic) process, which can be described by its emission lifetime (τ). This is defined as the average time spent in the excited state before relaxation to the ground state occurs. The luminescent decay as a function of time is given by equation 5, where I_t is the intensity at time t, I_0 is the intensity at time = 0.

$$I_t = I_0 \, e^{(-t/\tau)} \qquad \textit{Equation 3.3}$$

For a simple single exponential decay process, τ is the reciprocal of the sum of the rates of the radiative and non-radiative decay processes, as given by equation 6, where Γ is the rate of radiative decay and k_{nr} is the rate of the non-radiative decay process.

$$\tau = 1 / (\Gamma + k_{nr}) \qquad \textit{Equation 3.4:}$$

Time-correlated single photon counting (TCSPC) is a widely used experimental method for determining fluorescence lifetime. The sample is excited using pulsed light with a short pulse width relative to the decay time of the fluorophore. The number of emitted photons after each pulse is recorded over time, and lifetime is calculated from the slope of the decay curve, according to equation 3.4. Fluorescence lifetimes can also be determined using frequency domain measurements. Sinusoidally modulated excitation light causes emission to occur at the same frequency, but is phase delayed with respect to the excitation light. If this phase shift is measured it can be used to determine the fluorescence lifetime.[136]

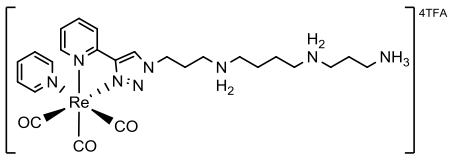

119 pyRe-Spm

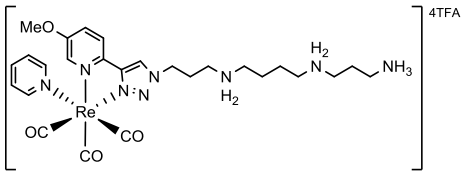

129 5OMe-Spm pyRe

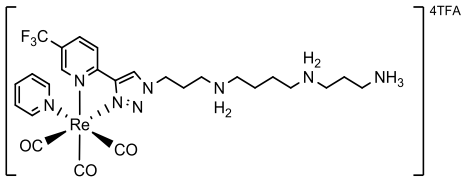

130 5CF_3-Spm pyRe

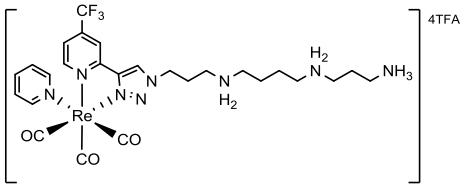

131 4CF_3-Spm pyRe

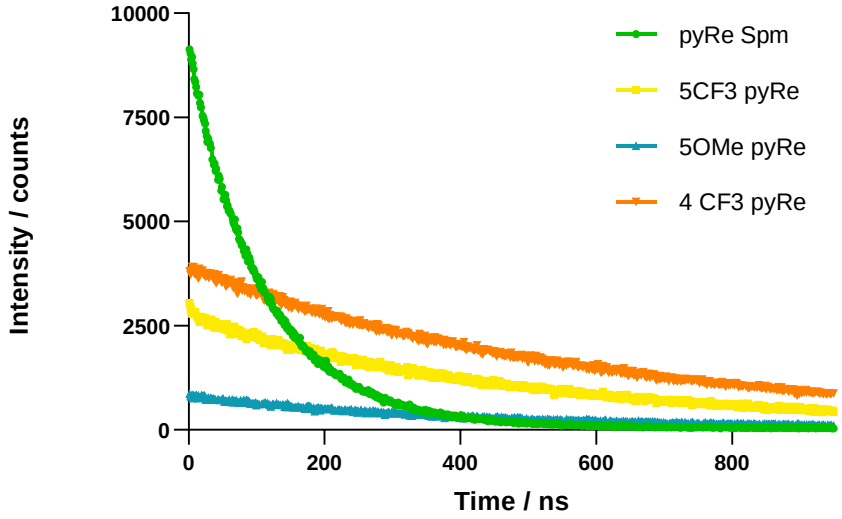

***Figure 3.20**:TCSPC exponential luminescence decay plots, (GraphPad Prism 8.0.0), measured in water, 20 μM, λ_{ex} 330 nm, λ_{em} 510 nm.*

Re Complex	λ_{em} (nm)	τ (ns)
5-OMe (129)	477	78.3
H (119)	496	157.3
5-CF_3 (130)	536	408.1
4-CF_3 (131)	545	605.0

***Table 3.3.7:** Excited state lifetimes of py-Re(I)CO_3(pyta) complexes. Measured in aerated water.*

Emission from the Re complexes fits a simple mono-exponential decay. The emission lifetime of complex **129** with the OMe group was roughly half of that of the unsubstituted complex **119**. It is likely that destabilisation of the LUMO by the EDG leads to quenching of the ^{3}MLCT excited state. As the d-d excited state is energetically close to

the ^{3}MLCT excited state, thermal population of the non-emissive metal-centred excited state quenches the emission. In contrast, the CF_3 substituted complexes (**130** and **131**) showed a dramatic increase in emission lifetime, with complex **130** (with the EWG lying *para*- with respect to the triazole ring) showing a two-fold increase and complex **131** (with the EWG lying *para*- with respect to the Re metal centre), showing a three-fold increase in emission lifetime with respect to the unsubstituted complex **119**.

The emission lifetimes of the iridium complexes follows the opposite trend and reflects the nature of the excited states. Complexes showing greatest ILCT character have the longest lifetimes, and those with greater MLCT character having shorter emission lifetimes. The non-substituted complex **123** fits a single exponential decay profile (R^2 = 0.9971) with an emission lifetime of 404 ns in aerated water. Both the lifetime and the quantum yield of the non-substituted complex agree well with literature values for complexes **184** and **185** (Figure 3.22) reported by De Cola et al. Both complexes have a similar quantum yield to complex **123** and both exhibit mono-exponential decay. Although the reported lifetimes are slightly higher, this is most likely due to the fact that measurements were carried out in deaerated dichloromethane rather than aerated water.

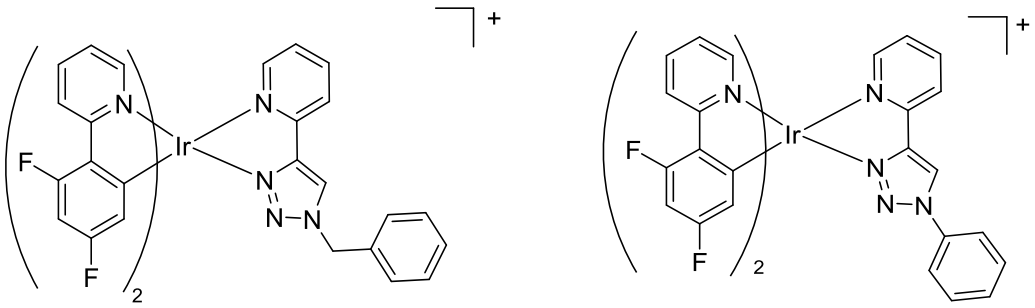

184

λ_{em} = 452, 483 nm

Φ = 0.22

τ = 0.63 µs

185

λ_{em} = 453, 483 nm

Φ = 0.17

τ = 0.72 µs

***Figure 3.21**: Similar triazole complexes reported by De Cola et al.[278] Emission, quantum yield and lifetimes measured in deaerated dichloromethane.*

Both of the N^N substituted complexes are best fitted to a bi-exponential decay comprising of a fast component and a slow component (data shown in figure 3.22 and

table 3.8). Complex **132** has a very similar overall lifetime to complex **123**; with a 96 % contribution from the longer-lived component, whereas complex **133** shows 94 % contribution from the short-lived species. The lifetime of complex **134** (data shown in figure 3.23 and table 3.8) is shorter still, showing a very similar lifetime to complex **136** (*vide infra*).

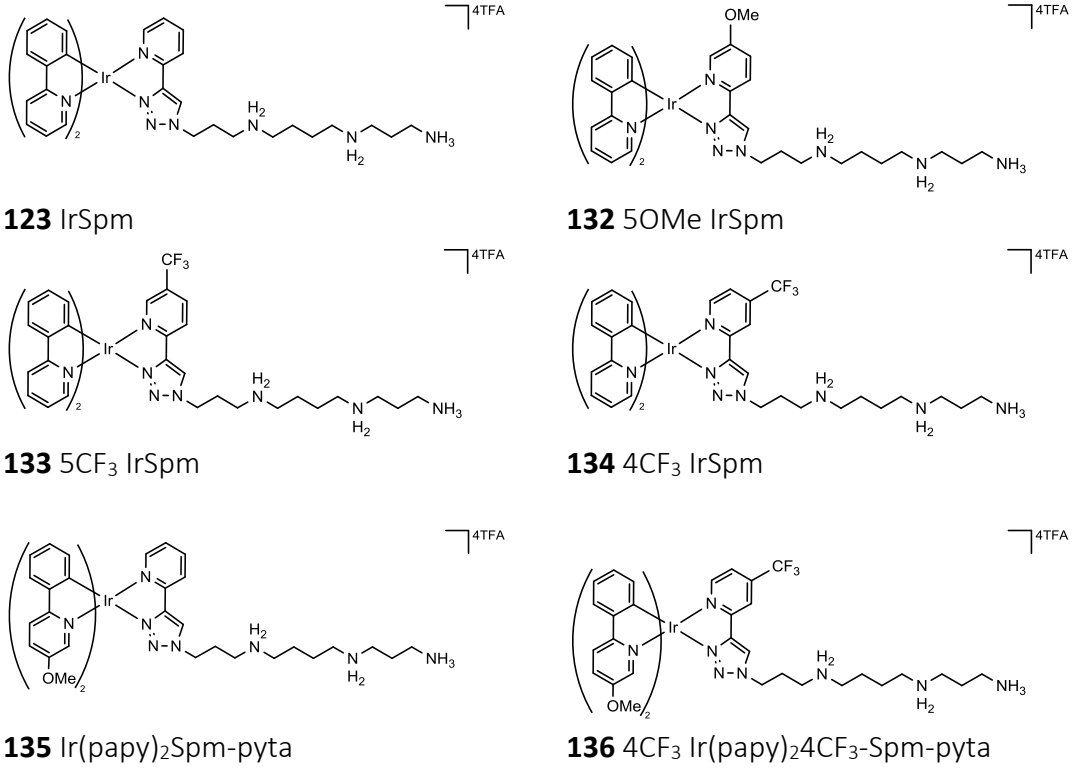

123 IrSpm

132 5OMe IrSpm

133 5CF_3 IrSpm

134 4CF_3 IrSpm

135 Ir(papy)$_2$Spm-pyta

136 4CF_3 Ir(papy)$_2$4CF_3-Spm-pyta

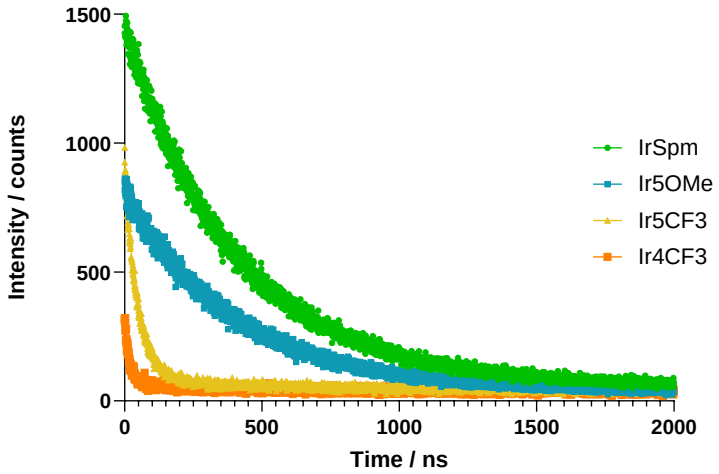

***Figure 3.22**: TCSPC exponential luminescence decay plots N^N substituted Ir complexes, (GraphPad Prism 8.0.0), measured in water, 20 µM, λ_{ex} 374 nm, λ_{em} 543 nm.*

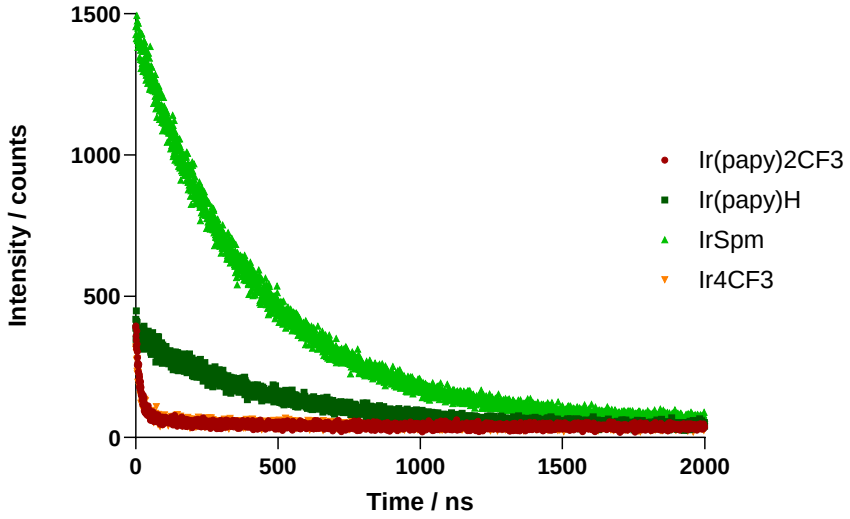

***Figure 3.23**:TCSPC exponential luminescence decay plots C^N substituted complexes, (GraphPad Prism 8.0.0), measured in water, 20 μM, λ_{ex} 374 nm, λ_{em} 543 nm*

Complex	λ_{em} (nm)	τ (μs)
5-OMeIr (129)	472	0.404 (96 %) 0.017 (4 %)
IrSpm	474	0.404
5-CF_3Ir	572	0.420 (94 %) 0.045 (6 %)
4-CF_3Ir	584	0.340 (89 %) 0.017 (11 %)
Ir(papy)$_2$H	474	0.467 (92 %) 0.028 (8 %)
Ir(papy)$_2$ 4-CF_3	584	0.284 (91 %) 0.016 (9 %)

***Table 3.3.8**: Excited state lifetimes of Ir(III) complexes. Measured in aerated water.*

3.6: Oxygen sensitivity

There is a large difference in emission wavelengths of the two phosphorescence bands. In addition to the differences in quantum yield and lifetimes, the two different bands show very different oxygen sensitivities, as shown in Figure 3.25 showing the emission spectra of the iridium complexes in aerated and degassed water. The high energy (HE) and low energy (LE) phosphorescence bands have been assigned to ^{3}IL and ^{3}MLCT excited states respectively. In aerated solutions the HE emission is significantly quenched leading to the predominance of a broad LE band for complexes with a greater MLCT character, such as the CF_3 substituted complexes. The 5-CF_3 complex is the least sensitive to oxygen, with its emission profile unchanged upon degassing.

The 4-CF_3 complexes show signs of dual emission as the relative intensities of the two bands varies with oxygen concentration. The HE emission is very susceptible to quenching by oxygen, whilst the LE emission is oxygen insensitive. As a result, the emission spectra of the MLCT complexes can vary slightly showing variable contributions from the HE band depending on the amount of oxygen present in the solution. Complex **136** shows interesting dual emission, which may be of use as a probe for hypoxia. There is a ratiometric response which could act as a "turn on" effect under hypoxic conditions, but more promising is the potential for use in lifetime imaging as there is a large difference in phosphorescence lifetime between the lifetime of the HE band and that of the LE band.

As the HE band is most affected by quenching by oxygen, it stands to reason that the complexes with the highest degree of ILCT nature should be the most sensitive to oxygen. **123** and **135** both show around a 2.5-fold enhancement in intensity when degassed, and **132** shows a 1.5-fold enhancement; however, the most significant change in intensity is (unexpectedly) seen with **134** and **136** which shows an 8-fold enhancement upon degassing.

132

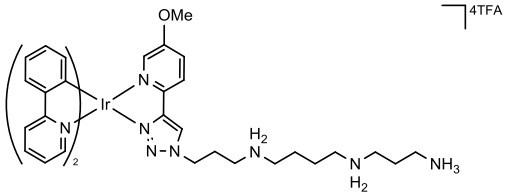

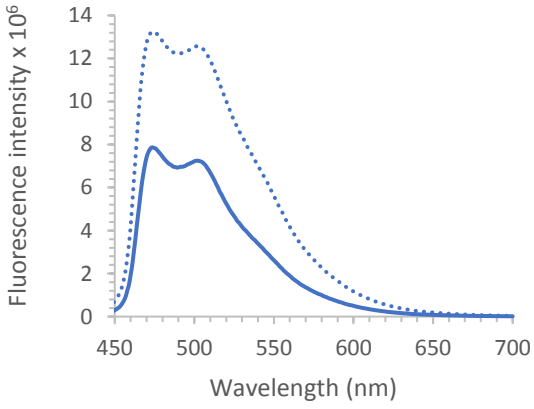

123

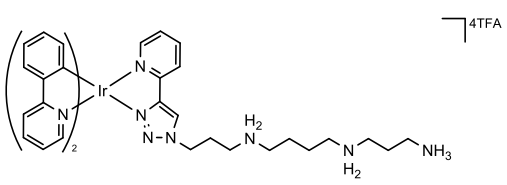

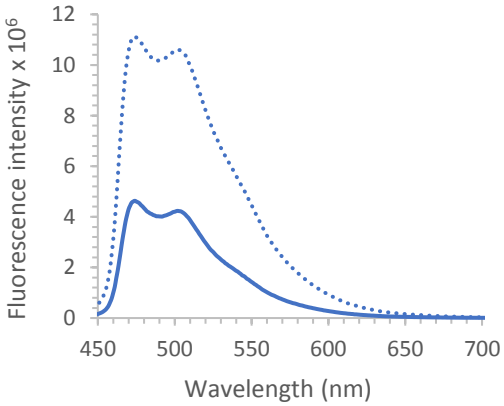

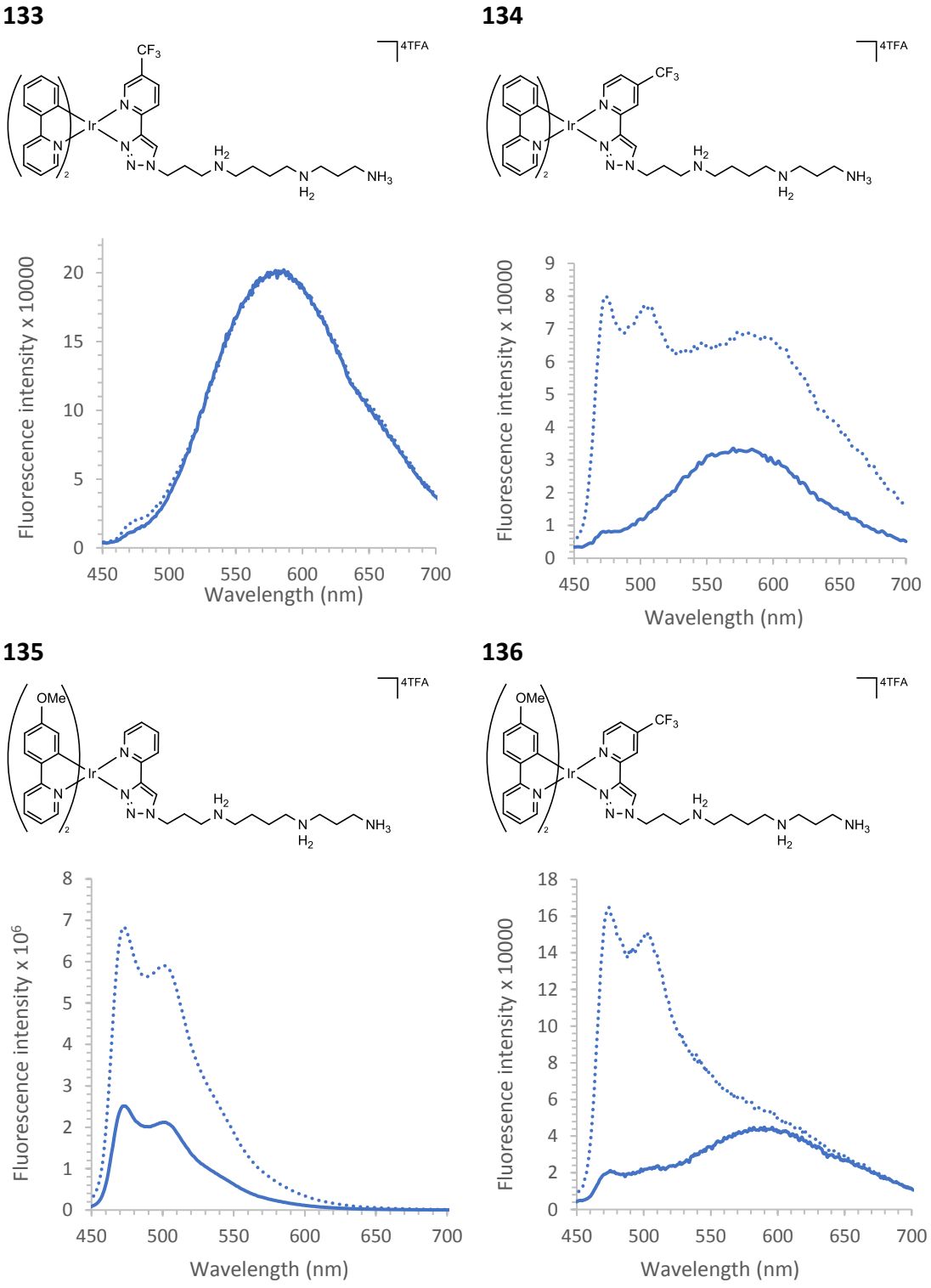

***Figure 3.24**: Emission of iridium complexes in aerated (solid line) and degassed (dotted line) aqueous solution, at ambient temperature.*

3.7: Solvatochroism

Although quantum yields in dichloromethane were not determined, luminescence was perceptibly brighter compared to aqueous solutions, even in aerated

solutions. Formation of the ^{3}MLCT excited state occurs with a large change in dipole moment which is most effectively stabilised in polar solvents. As a result, triplet excited states with high CT character have smaller quantum yields and shorter emission lifetimes in polar solvents as solvation leads to rapid decay of the excited state. In non-polar solvents the ^{3}MLCT state is destabilised and hence emission is hypsochromically shifted. Of all the complexes evaluated in this study, 5-CF_3 IrSpm shows emission with the greatest degree of MLCT nature in aqueous solution, it has a short emission lifetime and a low quantum yield. In dichloromethane the emission is blue shifted by approximately 10 nm.

The emission of complexes exhibiting a high degree of ^{3}ILCT character was not shifted upon changing to the non-polar solvent, and the emission profile retained its vibronic coupling. However, a reduced intensity of vibronic sidebands with respect to the origin band points towards an enhanced contribution from the ^{3}MLCT excited state in non-polar solutions. Complexes showing dual emission in aqueous solutions showed a switch to broad emission of MLCT character in non-polar solvent. If the energy gap between the ^{3}MLCT and ^{3}LC states is sufficiently small, the destabilisation of the ^{3}MLCT state could be sufficient to change in the nature of emission.[286]

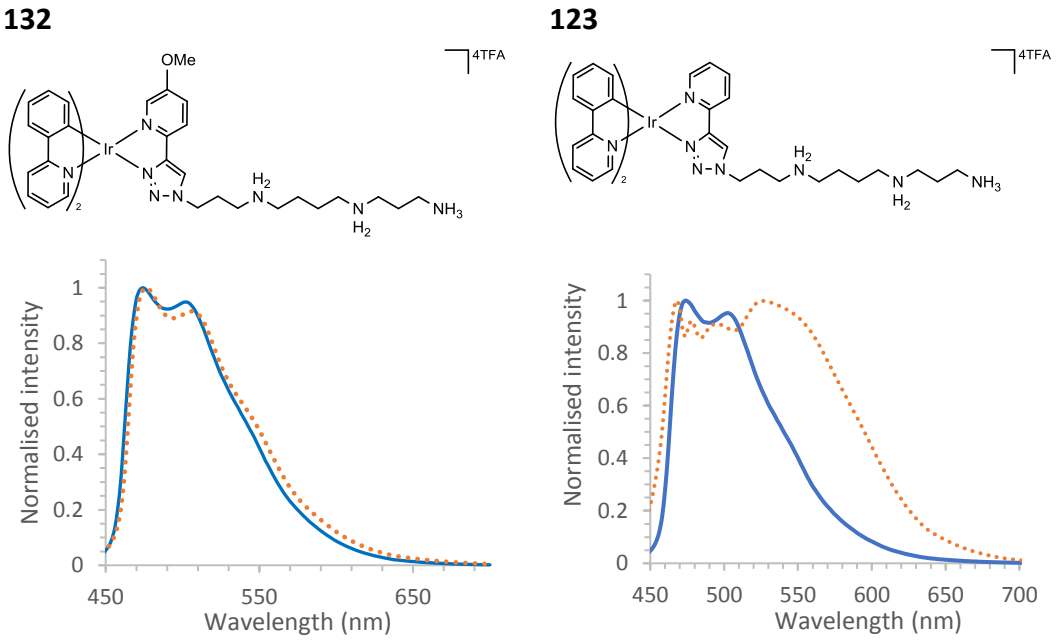

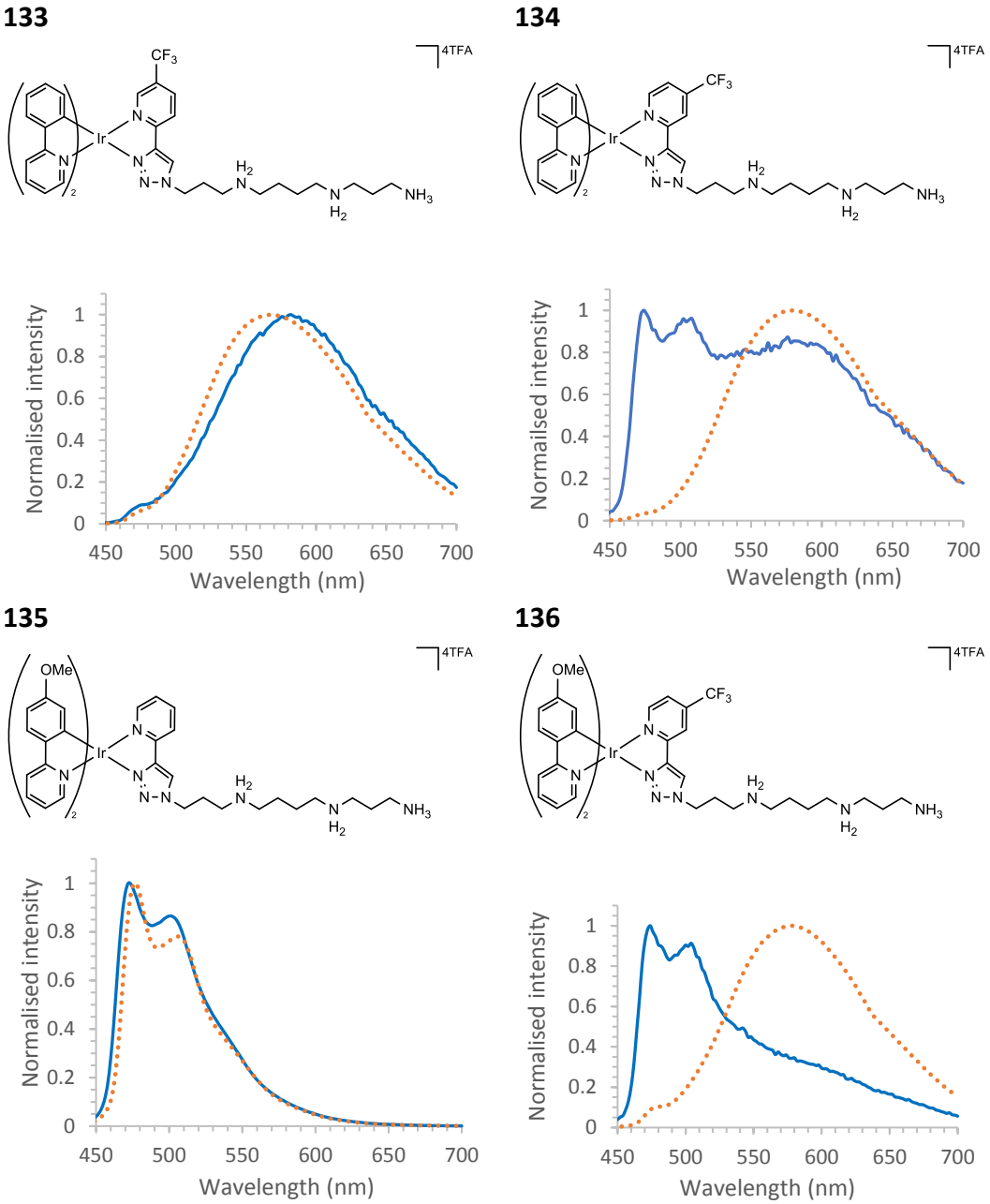

***Figure 3.25**: Emission of Ir complexes in degassed aqueous (solid line) and dichloromethane (dotted line) solutions.*

3.8: Summary

The complexes investigated in this study show interesting emission properties that vary between two extremes. At one end of the spectrum, is the high energy, blue-green coloured, vibronically coupled emission that is highly sensitive to oxygen, with long emission lifetime and high quantum yields arising from the emission from mixed

MLCT/ILCT excited states. The lower energy orange emission originating from mixed MLCT/LLCT excited states is broad and structureless with short emission lifetimes, low quantum yields and is insensitive to oxygen. The high energy (HE) emission is mainly associated with the cyclometallating ligands, whilst the lower energy (LE) emission emanates from the diimine ligand.

A strong electron withdrawing CF_3 group is sufficient to overcome the blue-shift bestowed by the pyridyl triazole ligand and restores its role as the chromophoric ligand. This is confirmed by comparing emission from the 4-CF_3 substituted pyta complex **134** with the C^N substituted complex **136**. If the cyclometallating ligand was the chromophoric ligand, substitution at the C^N ligand would be expected to change the nature of the emission; however, the position of emission maximum, the quantum yield and the emission lifetime remain unchanged.

The role of the cyclometallating ligand as the chromophoric species in the complexes with MLCT/ILCT nature emission is confirmed by comparing the emission properties of the unsubstituted pyta complex with the C^N substituted complex, and the 5-OMe N^N substituted complex. The simplest approach is to consider the effect of introducing the OMe substituent onto the N^N ligand. The nature of the emission is not changed a great deal; shifts in emission are minimal, there is very little change in the shape of the vibronic structured emission bands, and the quantum yield and lifetimes are very similar, which when taken together imply that the diimine is not the chromophoric ligand.

This is further substantiated by considering the emission of the C^N substituted complex compared to the unsubstituted phenyl pyridine analogue. At a first glance, the emission does not seem to change a great deal as the emission profile retains the vibronic structure and both emission and excitation maxima are hardly shifted; however, the subtle changes in intensities of the vibronic progressions is evidence of a shift towards MLCT character. This supported by the change in magnitude of the quantum yield, which for the C^N substituted complex is just half of that of the unsubstituted complex and insinuates a higher degree of MLCT character. The emission lifetime data best fits a two-phase exponential decay which assigns 8 % of the emission to a rapidly decaying species.

As the unsubstituted iridium complexes have a propensity to be quenched by oxygen it would suggest that these complexes would be very effective singlet oxygen generators for photodynamic therapy (particularly using two-photon excitation). The emission tail into the red is also enhanced under hypoxic conditions and a red shift in emission is observed in non-polar solvents. These dual emission properties warrant further investigation to determine if they can be functionally exploited in cellular imaging.

Chapter 4 : Biological imaging.

Antonie van Leeuwenhoek is widely renowned as the father of microbiology. He made some of the first observations of cells using the lenses he developed for microscopy, which could resolve structures of around 1 micron (μm) in size. Around the same time Robert Hooke developed the compound microscope. The modern microscope has changed very little from this original instrument however, substantial improvements in optics has improved resolution to around 200 nm; however, despite further technological advances, image resolution remains limited by the diffraction of visible light, to around half the wavelength of the light used.[287]

Heimstädt constructed the first fluorescence microscope in 1911 which was superseded by Ellinger and Hirt's epifluorescence microscope in 1929. Epifluorescence images often appear blurry as the image is constructed from both in focus and out of focus light. The light detected from a single point source can be described by its point spread function (PSF). The PSF is essentially the light intensity distribution observed at the detector as a result of the diffraction of light transmitted through the objective.

Minsky proposed the concept of confocal microscopy in 1957 to address the issue of image blurring,[288] but they were not commercially available until 1987.[289] Instead of using wide field illumination a small point is illuminated and the sample is sequentially scanned. The key feature is the confocal aperture; this restricts out of focus light reaching the detector and improves the signal to noise ratio giving more defined images. Only the light originating from the focal plane reaches the detector; this creates optical sections. By collecting images at different depths throughout the specimen, individual images can be recombined to construct three-dimensional images of entire cells.[290] Confocal microscopy is now widely adopted, and new techniques within the field have enabled the resolution limit to be gradually whittled away. New techniques can acquire images with resolution approaching that of electron microscopy.

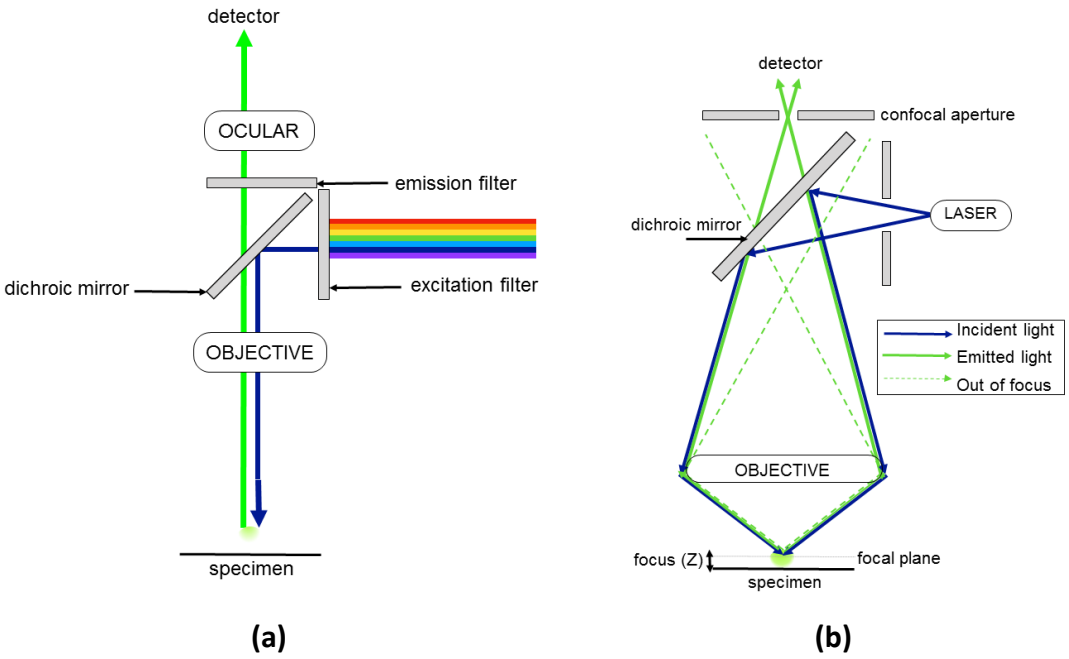

***Figure 4.1**: Schematic diagrams of (a) epifluorescence microscope and (b) confocal microscope.*

4.1.1: Two-photon microscopy

The concept of two-photon excitation (2PE) was first proposed by Göppert-Mayer in 1931; she proposed that two photons with half the energy required for a transition could induce the same quantum event as a single photon if absorbed simultaneously.[291]

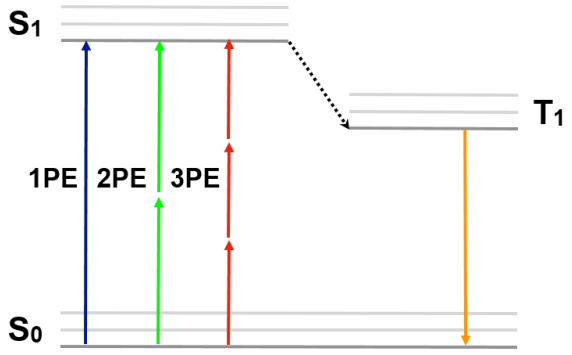

***Figure 4.2**: Jablonski diagram illustrating multi-photon excitation*

The statistical probability of two photons arriving at a single point simultaneously is very low, and hence very high powered, fast pulsed lasers are required to effect 2PE.[292] Photon density is only sufficiently high to excite the fluorophore at the focal plane, and so image quality is not adversely affected by out of focus light. Two-photon microscopy

is becoming more widely used for biological imaging as two-photon microscopy uses light with double the wavelength, which is less damaging to live cells, shows improved tissue penetration and causes less photobleaching of fluorophores.

4.1.2: Fluorescence lifetime imaging (FLIM)

Fluorescence lifetime imaging (FLIM), and phosphorescence lifetime imaging (PLIM) are compatible with both confocal and two-photon microscopies. Images are generated by either generating a pixel-by-pixel lifetime map or by measuring the change in intensity of each pixel over short timeframe. As fluorescence and phosphorescence lifetimes are particularly sensitive to the local environment, luminophores can be used as sensors to identify changes in the cellular environment.[293] Changes in emission lifetime can be caused by the presence of quenchers such as chloride ions or oxygen, binding to biomolecules, changes in pH and changes in viscosity.

4.1.3: Correlative light-electron microscopy (CLEM)

Ruska was awarded a share of the Nobel Prize for Physics in 1986, for his fundamental work in electron optics and designing the first electron microscope. Electron microscopy (EM) can achieve much higher resolution than light microscopy as the De Broglie wavelength of electrons is significantly smaller than visible light.[294] Modern instruments can resolve fine detail to a resolution of a few Angstroms, however specimens must be fixed, stained, dehydrated, embedded in resin, and sliced into thin sections prior to imaging. Despite its unparalleled resolving power, EM is of little use to view dynamic processes in living cells. Fluorescence microscopy observes labelled molecules or organelles of interest, however, as much of the cell remains unlabelled, its localisation context is somewhat lacking. Correlative light-electron microscopy (CLEM) combines the strengths of these two modalities to provide nanometre resolution using molecule or organelle specific labelling to pinpoint regions of interest.[295] The use of MLCs in this application is of great interest due to their high electron density. Cells treated with mitochondria targeting iridium complexes showed significantly enhanced contrast in TEM images.[296]

4.1.4: Super resolution microscopy

Super resolution microscopy (SRM) is one of the most recent advances in microscopy, for which its inventors, Betzig, Hell and Moerner were awarded the Nobel prize for Chemistry in 2014.[297] Super resolution techniques can surpass the diffraction limit to achieve nanometre resolution. The first step towards this goal was the discovery of stimulated emission depletion (STED) of fluorescence.[298] In this technique, the effective area illuminated by the excitation light is reduced by using a second doughnut-shaped beam of light focussed around the periphery of the excitation beam. The STED beam is time delayed and red-shifted relative to the excitation beam and selectively deactivates excited fluorophores in its path as illustrated in figure 4.3.

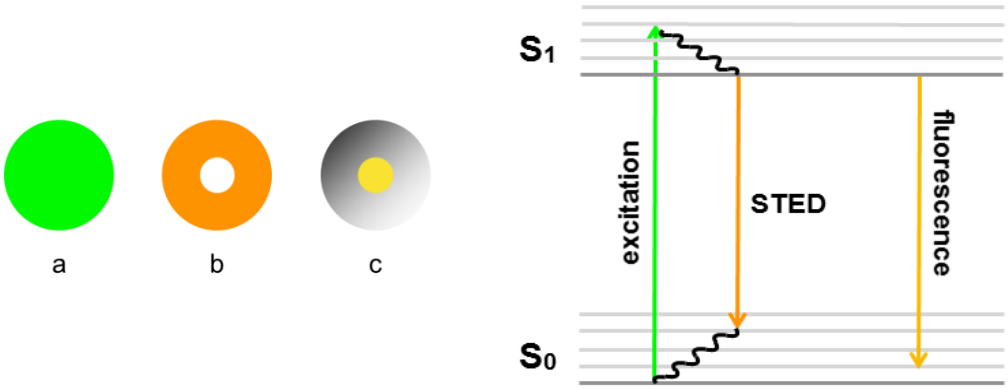

***Figure 4.3**: The STED principle; the sample is illuminated with green excitation light a, followed by a time delayed doughnut-shaped STED beam, b to give super resolution emission c.*

The high-intensity STED beam that is used to induce stimulated emission has an energy that is an exact match for the energy difference between the ground and excited state of the fluorophore. When the STED beam photons interact with the fluorophore in its excited state, it is stimulated to relax to the ground state through stimulated emission before fluorescence can occur, as shown in figure 4.3. As a result, the effective point spread function is reduced increasing resolution beyond the diffraction limit. Resolution up to 20 nm is possible with this technique; however, unlike electron microscopy, SRM methods are fully compatible with live cell imaging.[299]

A single fluorophore can only be resolved as its point spread function, (approximately 200 nm laterally, and 500 nm axially). If two or more fluorophores lie within a few hundred nanometers of one another they cannot be resolved. The

probability of detecting simultaneously emitting particles from a single point can be significantly reduced if a low number of fluorophores are present at a given time; this is the basis of super resolution techniques. The two major single molecule techniques are photoactivated localisation microscopy (PALM)[300] and stochastic optical reconstruction microscopy (STORM).[301] Controlled fluorophore photoblinking is used to ensure low numbers of fluorophores are activated.[302] Photoblinking is a transient deactivation of luminescence, whereby the fluorophore is temporarily sequestered in a dark state.[303]

4.2: Luminescent probes

Fluorescent probes are available with emission wavelengths spanning the entire visible spectrum from the ultraviolet (UV) region to the near infrared (NIR) and have literally "illuminated biological processes."[304] Fluorescent scaffolds can be modified to alter emission wavelengths and influence cellular localisation. For example, the planar aromatic molecule 4',6-diamidino-2-phenylindole, (DAPI) (**186**) is a DNA-intercalator widely used to stain the nucleus, whereas MitroTracker deep red FM (**187**), based on Cy5 (**55**) has a thiol-reactive chloromethyl group to lock onto mitochondrial membrane proteins. Molecular probes are also available with reactive moieties to enable them to be conjugated to molecules of interest such as the thiol reactive maleimides and the amine reactive isothiocyanates. As fluorescence microscopy is a non-destructive technique, molecular probes can be used to observe cellular processes in real time.

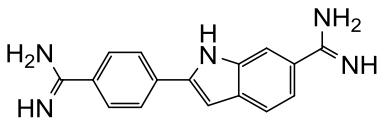

186

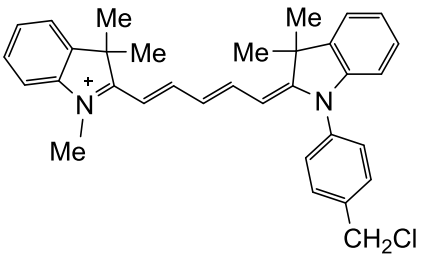

187

***Figure 4.4**: Chemical structures of some commonly used fluorescent probes the DNA intercalating nuclear stain DAPI, (**186**) and the Cy5 based mitochondrial labelling dye MitoTracker deep red FM (**187**).*

Organic fluorophores are highly absorptive with very large molar extinction coefficients however, they are sensitive to light, and often readily photobleached. Whilst this makes their practical manipulation somewhat awkward it also precludes their use

for extended periods of time with high intensity lasers required for fluorescence microscopy. Some of the more traditional fluorescent probes such as **186**, bleach extremely rapidly. [305] Several newly developed techniques make use of photobleaching to observe dynamic processes in cells such as fluorescence recovery after photobleaching (FRAP),[306] fluorescence localisation after photobleaching (FLAP),[307] and fluorescence loss in photobleaching (FLIP).[308] Despite the fact that phosphorescent MLCs are generally exceptionally photostable, their use is still not mainstream.

Organic fluorophores are also blighted by self-quenching upon accumulation.[136] As MLCs have large Stokes shifts they are less prone to self-quenching however, their emission is often quenched by oxygen. The lifetime of the ^{3}MLCT excited state is particularly sensitive to its environment and so the emission lifetime changes based depending upon the local environment in the cell. This sensitivity of MLCs to their surroundings can be exploited for phosphorescence lifetime imaging (PLIM). The oxygen-sensitive nature of the emission of MLCs has been widely exploited to probe hypoxia. Despite their shortcomings, organic fluorophores are still widely used for fluorescence imaging, but MLC based probes are gaining popularity.

4.2.1: PTS targeting molecular probes

Imaging biomarkers are powerful tools that can be used to follow disease progression, detect therapeutic response and to select appropriate patient groups for novel therapies. It is now common practise to design probes for prognostic biomarkers that can be used to predict therapeutic efficacy of new drug candidates so that chemotherapy regimens can be tailored to individual patients. Targeted fluorescent probes may be used for image-guided surgery but are most routinely used for *in vitro* diagnostic tests. Guminski *et al*. designed several fluorescent spermine conjugates alongside the polyamine targeted drug F14512 to stratify suitable candidates with PTS-active cancers, as shown in Figure 4.5.[93,167,309] The most effective probe, N^1-(7-nitrobenzoxadiazole) methylspermine (**188**), was found to be a faithful reporter of PTS status. Interestingly, not all probes showed PTS-specific uptake. Rhodamine and fluorescein-based probes (typified by compound **189**) were not internalised and the BODIPY conjugate (**190**) was not PTS specific. The probes with bulky, charged

fluorophores appeared to lack uptake and/or specificity which may be of importance for the molecules studied herein.

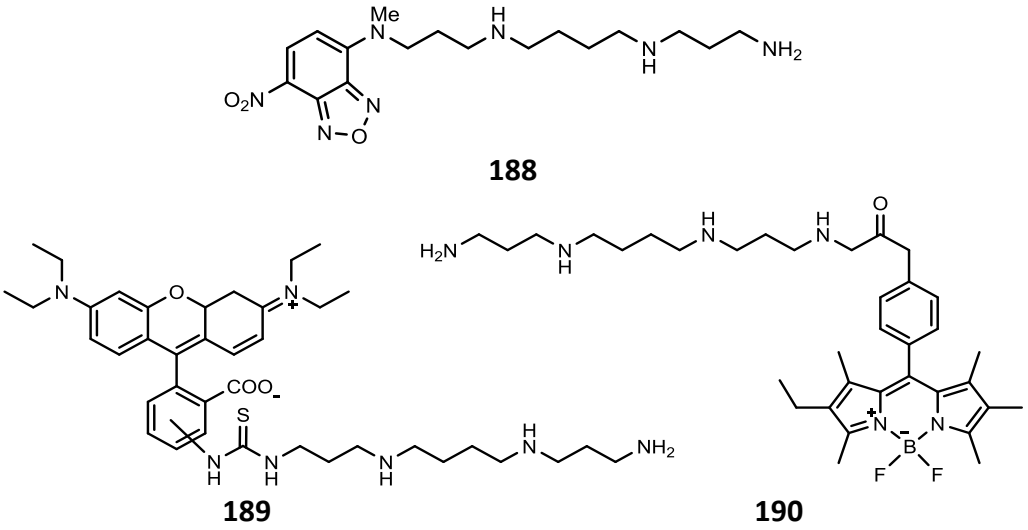

188 **189** **190**

Figure 4.5*: Structures of polyamine conjugates designed to probe PTS status of cells N1-(7-nitrobenzoxadiazole) methylspermine (**188**) rhodamine spermine conjugate (**189**) and BODIPY spermine conjugate (**190**).*

4.3: Confocal method development

4.3.1: Live cells

The A549 cell line was used for preliminary imaging experiments as it is known to have an active PTS and data is available from analogous studies using organic fluorophores.[58,59] Spd uptake in A549 cells has been characterized by Cullis *et al*. using ^{14}C labelled Spd. The maximal uptake (V_{max}) was found to be 17 pmol/min/10^5 cells with a K_M of 0.5 μM. From measuring the radioactivity incorporated into the cells at saturation, the concentration of Spd accumulated was estimated at 1.9 mM. N^1-N-methyl anthranilic acid (MANT) conjugate (**191**) shown in Figure 4.6 was found to be a potent inhibitor of Spd uptake, with a K_i of 0.11 μM, implying a very high affinity for the polyamine transporter.

Preliminary studies to confirm uptake were carried out using A549 cells incubated for 10 minutes at 37 °C, 5% CO_2 with solutions of MLCs dissolved in PBS (**123** at 30 μM, **119** at 100 μM) prior to observation using CSLM. Cells were incubated at 37 °C during imaging without CO_2. Transportation of the cells to the microscope took around 15 minutes. Cells did not survive well under these conditions and died during imaging. Cells treated with 100 μM **119** did not show any significant luminescence. This has also been

reported by others; due to the low absorption at 405 nm and low quantum yields of complexes of this nature, doses of up to 1 mg/mL have been used in order to detect luminescence in cells.[170] As this concentration had been shown to be toxic in cells (see Chapter 5) efforts were focused on iridium complexes.

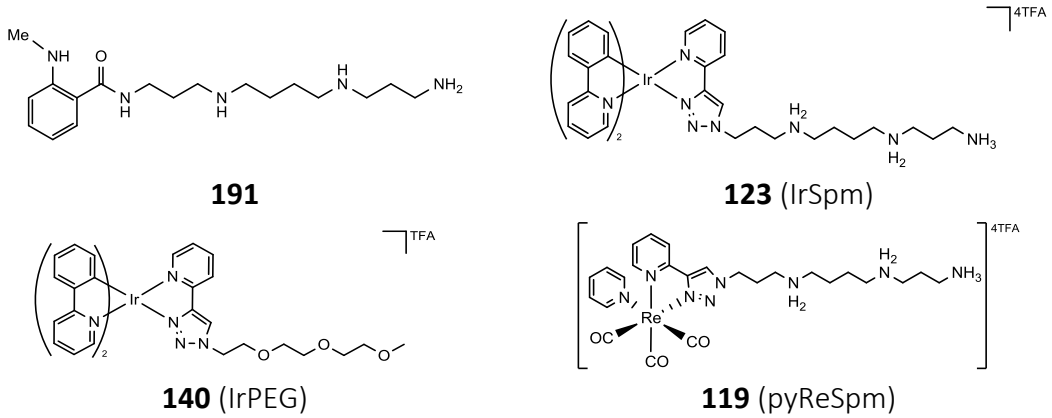

***Figure 4.6**: The fluorescent N1-Spermine MANT probe (**191**) and luminescent MLCs used to probe polyamine uptake in this study **123**, **140** and **119**.*

Cells incubated with the iridium complex 123 showed significant perinuclear accumulation of the dye and intensely stained nucleoli, as shown in Figure 4.7. Cells were rounded and visibly shrinking, showing signs of severe stress. The intense staining observed is most likely to have occurred due to the loss of integrity of the plasma and nuclear membranes leading to dye loading. Cells incubated with the control complex 140 appeared to be undergoing apoptotic cell death with significant blebbing of the cell membrane.

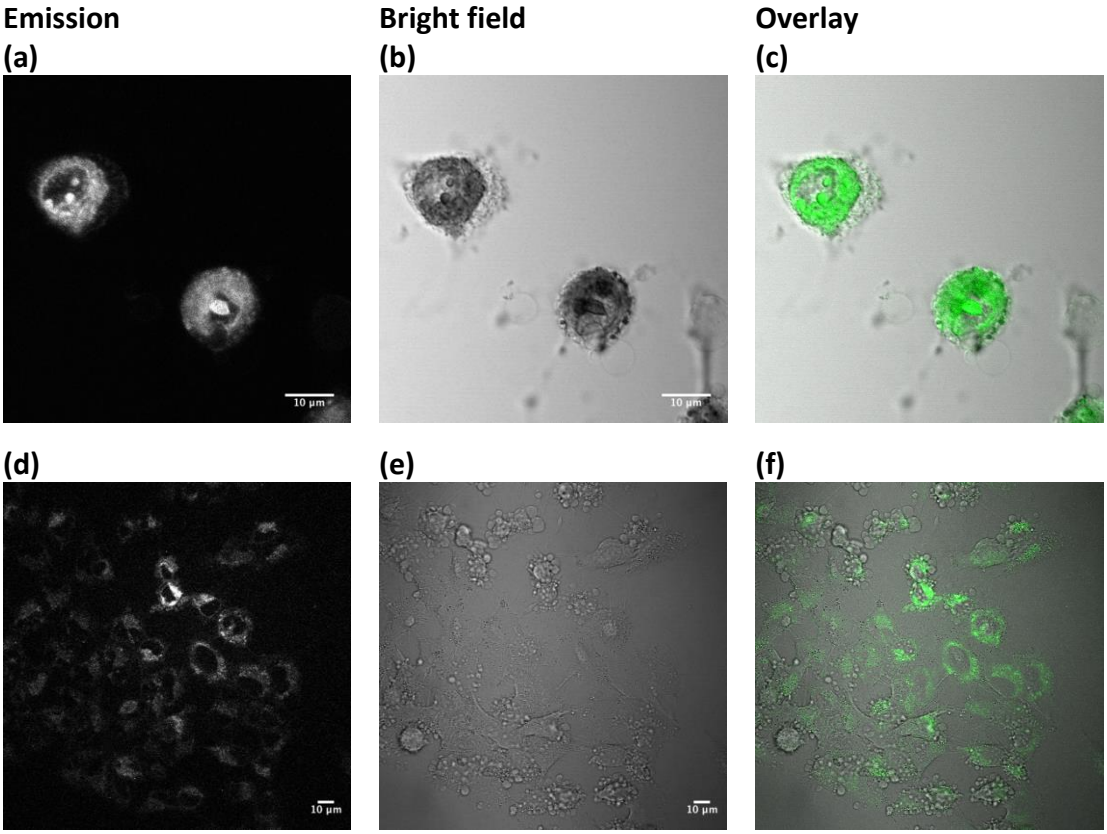

***Figure 4.7**:Live A549 cells incubated with **123** (a), (b), (c) and **140** (d), (e), (f) (30 µM in PBS) and imaged by CLSM, λ_{ex} 405 nm, using a 430/25 emission filter.*

The experiment was repeated substituting PBS for phenol-red free RPMI 1640 medium supplemented with 10 % foetal calf serum (FCS) and shown in Figure 4.8. This significantly improved cell survival, although cells were still rounded, and showing signs of stress. Cells incubated with **123** showed some nucleolar staining, but this was less intense than previously observed. Cytoplasmic staining was also more discrete, with clear structures visible, the cell membrane and nuclear envelope also showed some faint staining. Similar localisation was observed with complex **140**, although staining of the nucleoli was much weaker.

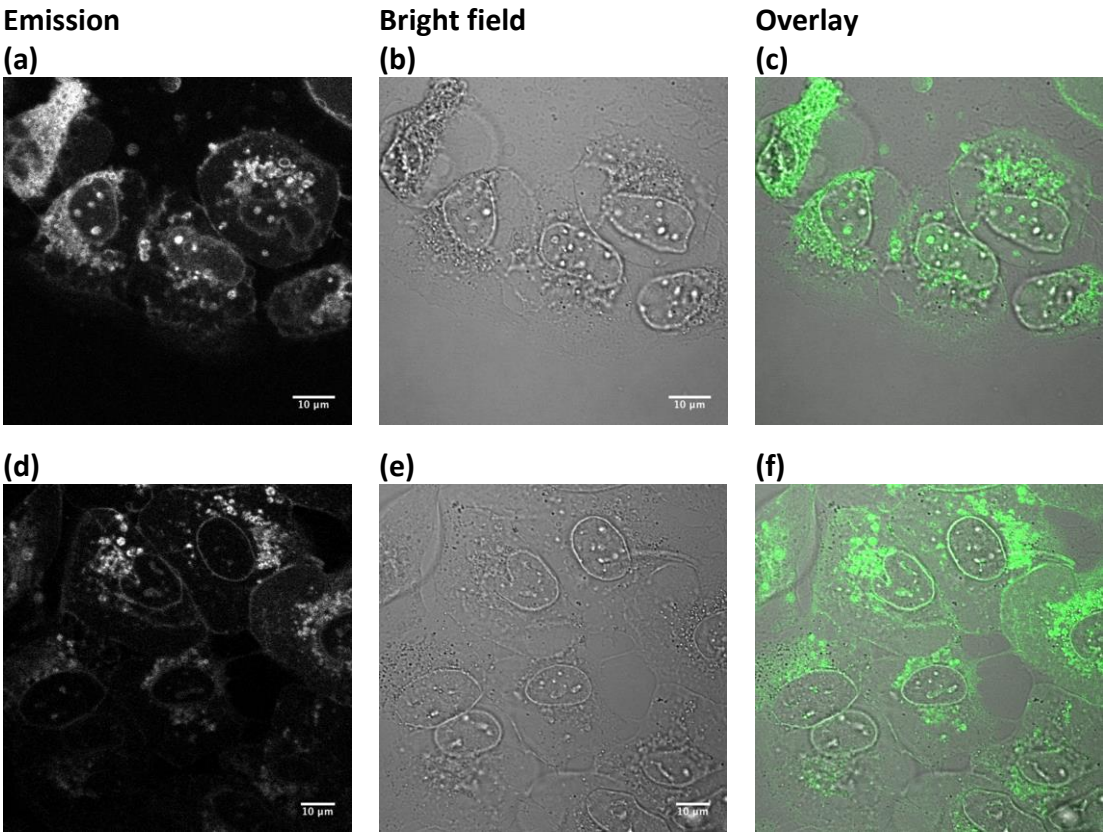

***Figure 4.8**: Live A549 cells incubated with **123** (a), (b), (c) and **140** (d), (e), (f) 30 µM in RPMI medium and imaged by CSLM, λ_{ex} 405 nm, using a 430/25 emission filter.*

Best results were obtained when cells were incubated at 37°C with 5% CO_2 for 30 minutes prior to imaging to allow cells to recover from transit. Incubation with CO_2 is critical as RPMI 1640 contains a sodium bicarbonate buffer; a minimum of 5% CO_2 is required to maintain physiological pH. Under these conditions, cells had good attachment to the slide and healthy morphology. Nuclear staining was no longer observed, with labelling confined to discrete structures in the perinuclear region, as shown in Figure 4.9 (a) to (c).

In viable cells the inherent phototoxicity of the complexes became apparent. In the process of recording time-lapsed images of cells, the cellular structures containing the iridium complexes degraded and the cell was visibly damaged, as can be seen in figure 4.9 (d) to (f). Upon irradiation, luminescence became much more diffuse, and cells could be seen to shrink. Even using the lowest possible laser power resulted in significant cell damage. Whilst this is of potential benefit for use as a photosensitiser for photodynamic therapy, it makes the task of examining cellular uptake extremely difficult in live cells, and future studies were carried out using fixed cells.

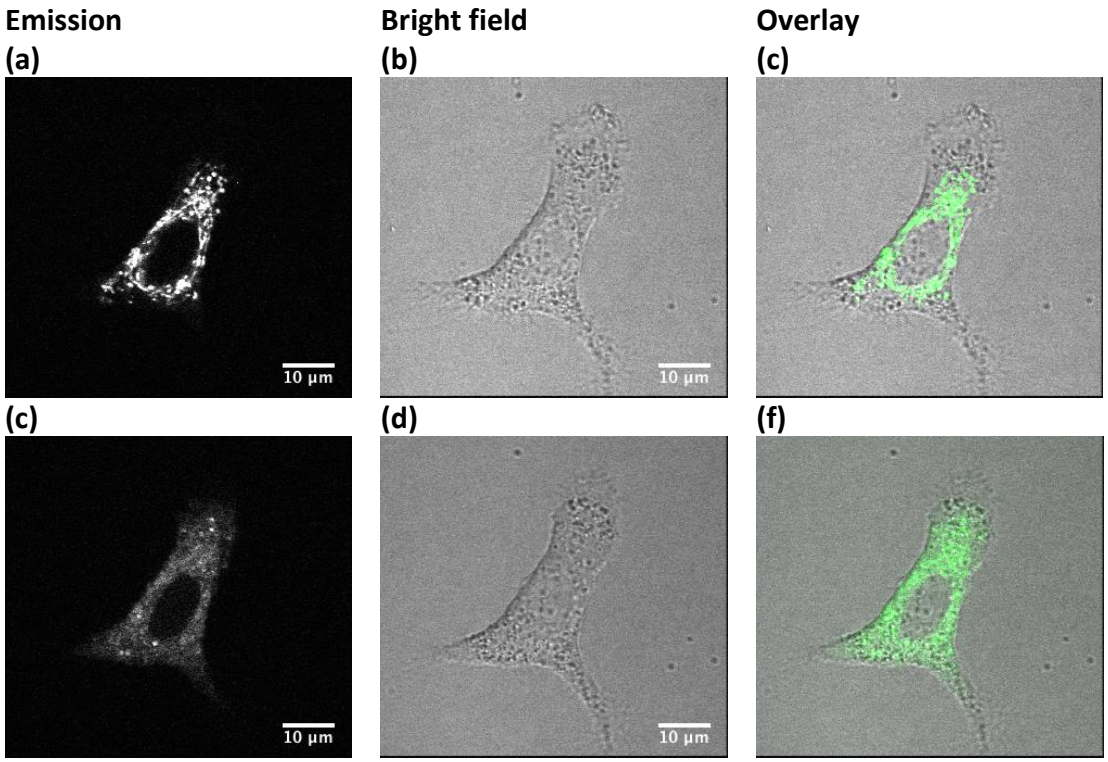

***Figure 4.9**: Live A549 cells incubated with 30 µM **140** (a), (b), (c) at t = 0 and (d), (e), (f) t = 5 min and imaged by CSLM, λ_{ex} 405 nm, using a 430/25 emission filter.*

4.3.2: Fixed cells

Cells can be fixed by using organic solvents such as methanol or acetone, or cross-linking aldehydes such as formaldehyde or glutaraldehyde. Organic solvents dehydrate cells, which can lead to significant shrinkage. As one of the most powerful features of CSLM is the ability to image optical sections through the cell, these fixatives are not recommended. Cross-linking aldehydes are the reagents of choice for fixing cells for CSLM as they better preserve the three-dimensional architecture of cells.

In this study A549 cells were grown on coverslips coated with poly-D-lysine, treated with MLCs, then fixed by incubating with a 4% solution of formaldehyde in PBS for 15 minutes at room temperature. Coverslips were mounted onto slides using Prolong diamond antifade mountant. This reagent contains glycerol and sets with a refractive index close to that of glass. This is important to ensure a uniform optical path as the refraction that occurs at an interface between glass and air can significantly reduce optical resolution. (This is also why oil immersion lenses are used at high magnification.)

Images of live cells appear sharper and more clearly defined compared to images of fixed cells, both in the fluorescence channel and the brightfield images. This is clearly visible in Figure 4.10.

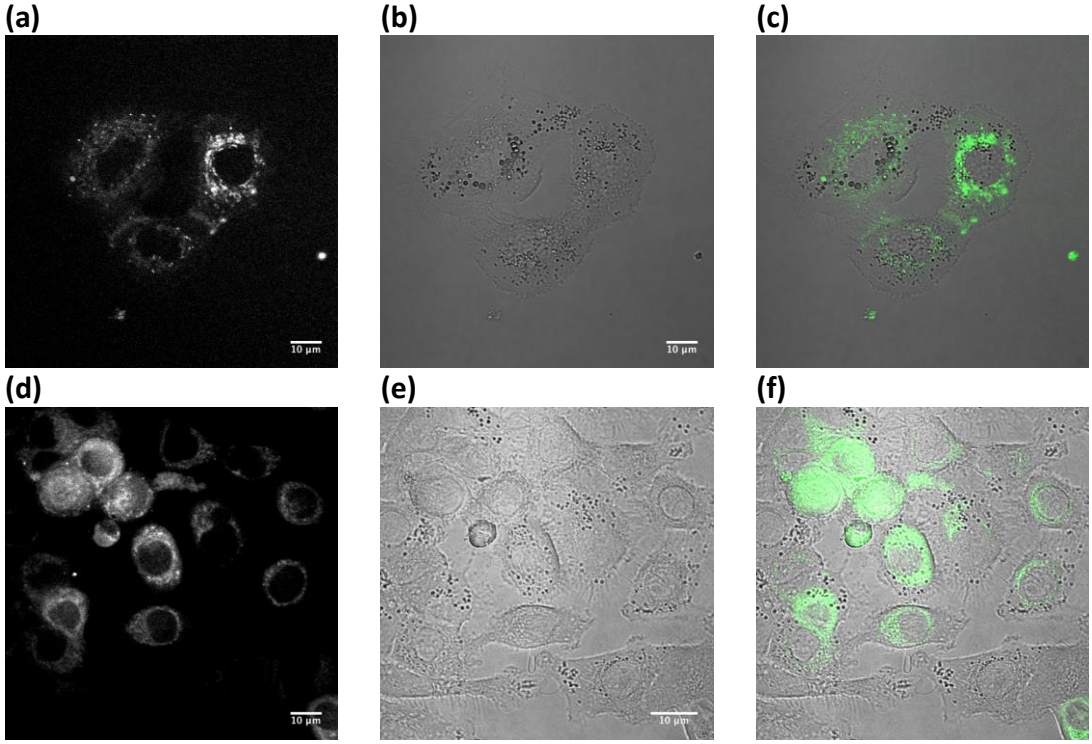

***Figure 4.10**: cells treated with 30 µM IrL3.1, (a) – (c) live cells in RPMI medium, (d) – (f) fixed, mounted cells. Imaged by CSLM, λ_{ex} 405 nm, using a 430/25 emission filter.*

Images (a) – (c) were obtained from live cells incubated with **123** for one hour compared to images (d) – (f) of cells incubated with **123** for one hour prior to being fixed with formaldehyde. When fixed slides were imaged immediately post fixation, the luminescent signals were sharp and well defined; however, upon standing the luminescent staining became gradually more diffuse, even when slides were stored in the freezer. Membrane staining was seen in live cells but not in fixed cells, this has also been observed by Lo.[310] Association of these complexes with the membrane could indicate its association with glypican, consistent with its known method of uptake. Slides prepared more than 48 hours before imaging showed weaker, more diffuse emission with substantial background luminescence, rendering slides of little use beyond this timepoint. The more diffuse appearance of fixed slides compared to those obtained with live cells must be taken into consideration when interpreting images.

4.4: Time course studies.

Cells were incubated with 123 over a period of 48 hours to determine the best treatment regime for imaging and to gain some insight as to the fate of the compound in the cell. Uptake of the probe was found to be rapid; weak, diffuse luminescence was observable after just 10 minutes in fixed cells. After 20 minutes the probe had accumulated sufficiently to begin to highlight some cellular structures, whereas after 40 minutes the probe could clearly be seen to be accumulating in discrete organelles. At both 40 minutes and 1 hour the organelles containing the probe were distributed throughout the cell, whereas at 2 hours the organelles containing the probe were more concentrated in the perinuclear region. After incubation for 2 hours, individual structures were more clearly resolved. Diffuse cytoplasmic and nuclear staining could also be seen, although it is unclear if this occurred as a result of the fixation and mounting procedure or due to passive diffusion of the probe into the cell. From these images taken at early timepoints it is apparent that cells need to be incubated with the probe for a minimum of 1 hour to yield any meaningful data at this concentration.

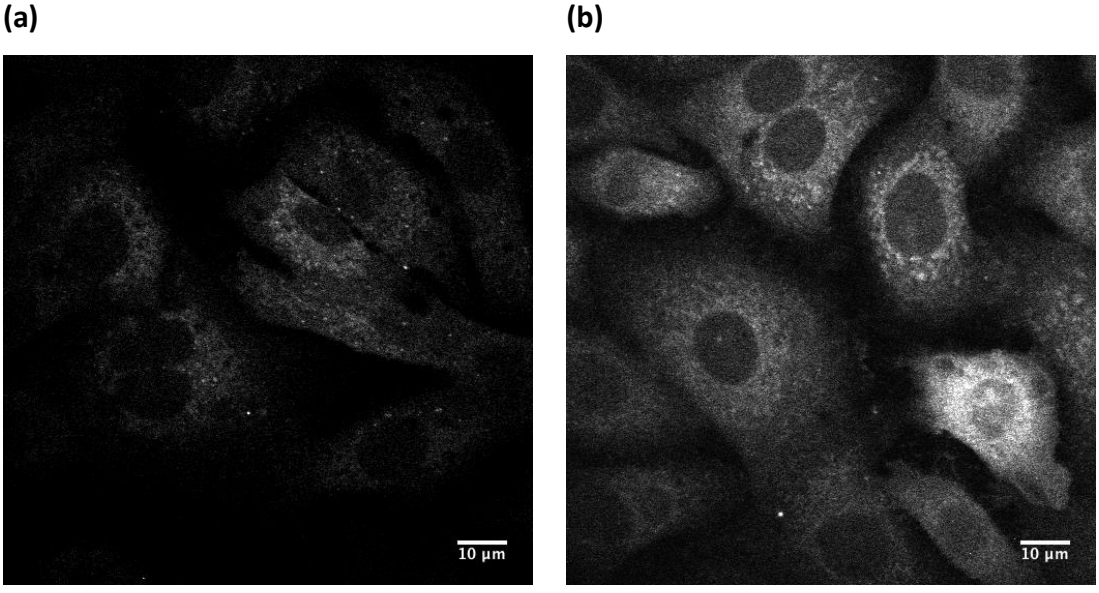

***Figure 4.11**: Accumulation of **123** in cells (a) 20 minutes (b) 40 minutes. Imaged by CSLM, λ_{ex} 405 nm, using a 430/25 emission filter.*

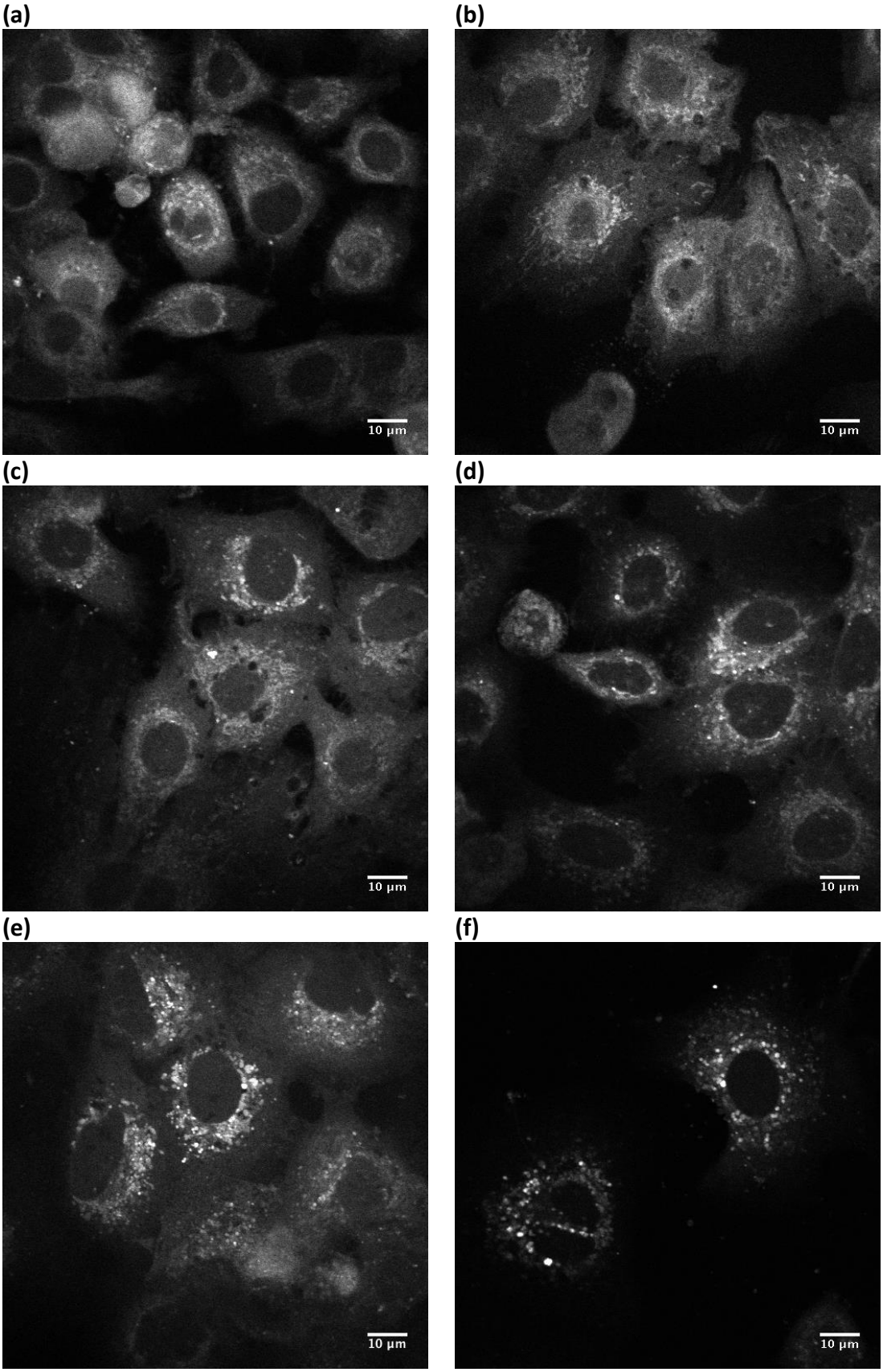

***Figure 4.12**: Accumulation of **123** in cells (a) 1 h (b) 2 h (c) 8 h (d) 24 h (e) 36 h and (f) 48 h. Imaged by CSLM, λ_{ex} 405 nm, using a 430/25 emission filter.*

Uptake of **123** was consistent with previous studies of Spd uptake in this cell line.[58] Spd uptake was seen to increase steadily between 1 and 2 hours, and then plateau. Uptake of **123** also increased steadily in the first 2 hours, but after 8 hours localisation and phosphorescent intensity had changed little from that observed at 2 hours (Figure 4.12c). After 36 hours localisation appeared to change with the probe appearing in circular, densely stained vesicles in the perinuclear region Figure 4.12e. At 48 hours the punctate luminescent organelles had reduced in number and were more widely spread throughout the cytoplasm Figure 4.12f. This may indicate that the complex is being exported out of the cell. At 24 hours (Figure 4.12d) localisation appeared to be intermediate between these two extremes; as such cells were incubated with complexes for 18 hours in further studies.

4.5: Probing the mechanism of uptake.

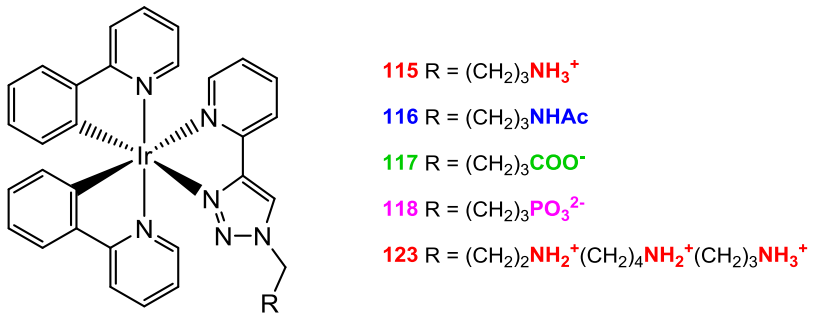

***Figure 4.13**: Control complexes designed to probe polyamine transport.*

Previous studies had shown that both complexes **119** and **123** were internalised by A549 cells.[96] Whilst uptake of the spermine-derived complex **123** was expected, it was not anticipated that complex **119** would be internalised. Being derived from the diamine Put and possessing only a single ionisable amine group, it was considered to be a poor substrate for the PTS. What was not taken into consideration was that fact that the iridium complex is cationic, and whist the charge separation exceeds the optimal four-carbon spacing, it may still have some affinity for the PTS. Compounds with a charge separation corresponding of up to seven methylene units can still be recognised as a substrate for the PTS.[56]

Given that uptake by the PTS is highly charge-dependent, a series of ligands were designed to give differently charged analogues of Put which should be more effective controls with respect to polyamine transport. The charge-modified complexes are shown in Figure 4.13. Polyamine transport is known to be rapid, and widely reported to occur via caveolin-dependent endocytosis (see Section 1.1.3) as such, polyamine vectored iridium complexes would be expected to localise endosomes upon uptake via the PTS.

Lipophilic cationic iridium complexes are widely reported to localise in mitochondria, however, examples can be found that localise within lysosomes, the nucleus, the endoplasmic reticulum (ER) and microtubules.[311,312] Generally, highly lipophilic complexes tend to accumulate in membranous structures such as the Golgi apparatus or the ER, complexes with weakly basic groups localise in acidic compartments such as lysosomes and endosomes and complexes with large planar π-systems (such as dppz ligands) localise in the nucleus as they can intercalate with DNA. Whilst localisation data for these complexes is abundant, studies into their mechanisms of uptake are less common; where uptake has been defined it tends to be attributed to either endocytosis or passive diffusion.

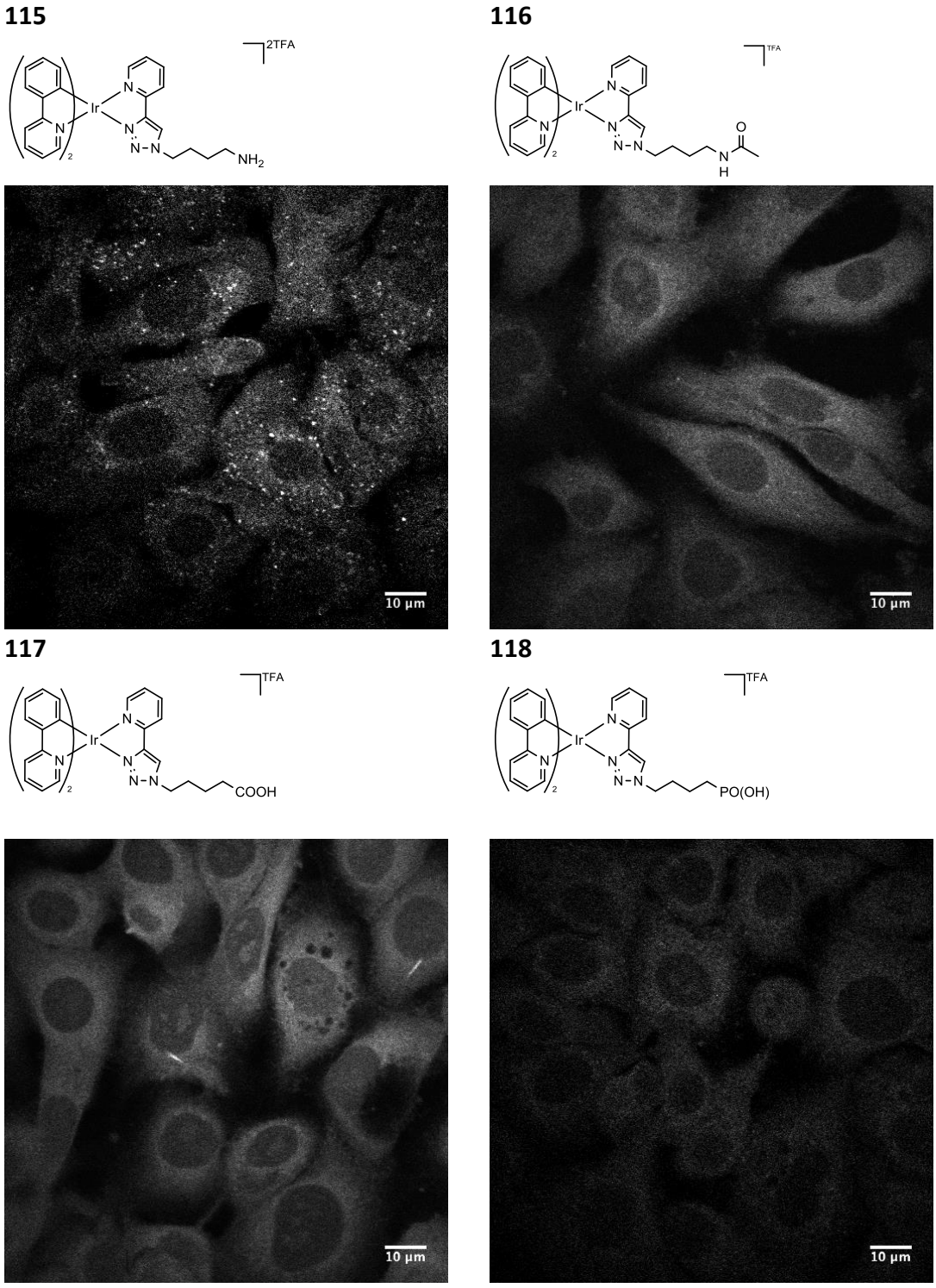

***Figure 4.14**:Fixed A549 cells incubated with 25 µM Ir complexes for 4 h. Imaged by CSLM, λ_{ex} 405 nm, using a 430/25 emission filter.*

Uptake of **115** after 4 hours shows the complex to be predominantly localised in small, intensely stained vesicles scattered throughout the cytoplasm (Figure 4.14). There is also some feint, diffuse cytoplasmic staining. In comparison, **123** is extensively localised

in discrete organelles in the perinuclear region after just 2 hours. Uptake of Spm and Spd by the PTS has been shown to be around ten-fold greater than that of Put, and that would also appear to be true of these iridium complexes. The uptake of **115** after 4 hours (with respect to the intensity of the emission seen) is reminiscent of the uptake of **123** after just 20-40 minutes. The markedly slower rate of uptake of **115** compared to that of **123** could be argued to be consistent with uptake mediated by the PTS; as **115** is likely to be a poor substrate for the PTS it is likely to have a slower rate of uptake as a result of its poor affinity for the transporter.

However, this could also be argued to be consistent with the uptake of other previously reported iridium complexes. Lipophilic cationic iridium complexes can gain entry to cells by passive diffusion and diffuse cytoplasmic staining is often indicative of this. Lo *et al* reported that uptake of a similar complex (**192,** Figure 4.15) occurred by both active and passive transport. Upon incubation with the iridium complex at 4˚C the intense staining at specific foci was abolished, however, the diffuse cytoplasmic staining was unaffected.[313] It is highly likely that **115** also gains entry to the cell by more than one route.

Neutral tris-cyclometallated complexes **193** and **194** with weakly basic nitrogen atoms have also been shown to enter the cell by endocytosis and localise in endosomes/lysosomes.[314,315] In particular the morpholine appended complex **193** may be a useful probe for observing the dynamics of endocytosis as is has been shown to be retained in acidic vesicles for up to 4 days. Commercially available probes such as the LysoSensor (**195**) and LysoTracker (**196**) dyes also contain weakly basic amine groups to confer selective localisation to acidic compartments, and are available in a range of emission colours, as shown in Figure 4.15.

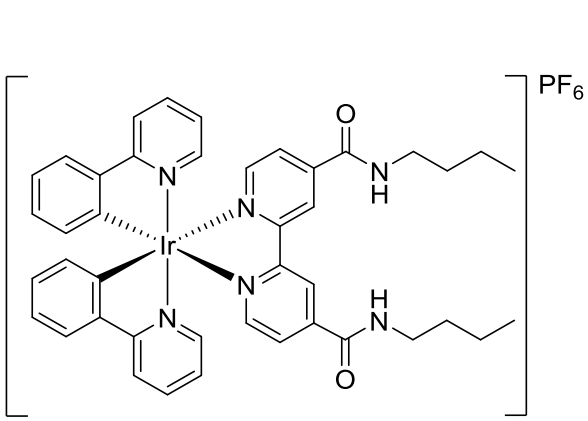

192

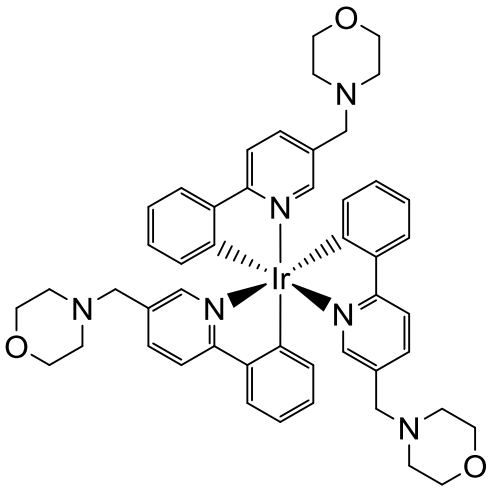

193

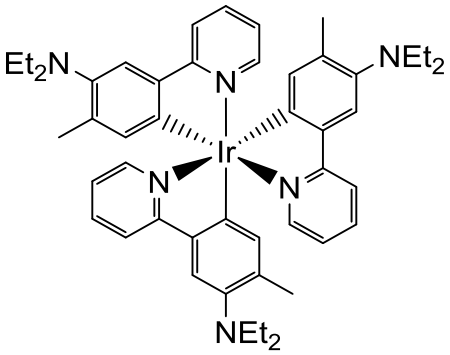

194

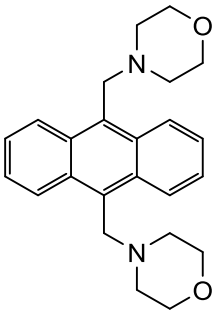

195

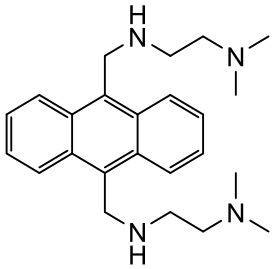

196

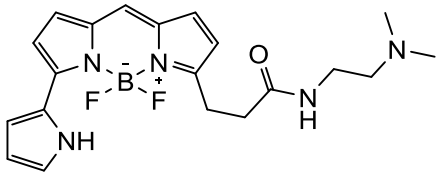

197

***Figure 4.15**: endosomal localising probes complex **192** with both active and passive uptake, morpholine-appended complex **193**, diethylamine appended complex **194**, LysoSensor blue **195**, LysoTracker blue **196** and lysotracker deep red **197**.*

Control complex 116 has an acetyl group at the end of the polyamine chain which neutralises the only remaining cationic amine group of the Put vector; as such is not expected to be a substrate for the PTS, but it is expected to be cell-permeant owing to its cationic, lipophilic nature (as reported for similar iridium complexes). 116 localises differently to 115; showing diffuse cytoplasmic staining characteristic of uptake by

passive diffusion (Figure 4.14). Complex **116** was sequestered in vesicles and excluded from the nucleus, however **117** showed weak, diffuse staining in the nucleus, with some cells showing accumulation of the probe in the nucleoli. Complex **117** is a net neutral complex with a terminal carboxylate group to counteract the cationic nature of the iridium complex. The charged centres are spatially resolved so **117** could potentially interact with either anion or cation binding molecules. As seen previously for complex **116**, **117** showed diffuse accumulation in the cytoplasm. Weak, diffuse luminescence was also seen in the nucleus with most cells exhibiting feint nucleolar staining (c).

Two similar complexes were studied by Wang *et al.*[316] The butyl ester complex **198** was found to accumulate rapidly and have potent cytotoxicity in A549 cells and cisplatin resistant A549R cells, with IC_{50} values of 1.7 and 2.1 μM respectively. The hydrolysis product, **199** was found to be essentially non-toxic. Complex **198** showed a very similar pattern of localisation as **117** with diffuse cytoplasmic staining and intense nucleolar staining. This complex was shown to be actively transported into the cell as incubation at 4 °C significantly reduced its uptake. This was shown to occur via a non-endocytotic pathway as treatment with chloroquine (an inhibitor of endocytosis) did not inhibit uptake of complex **198**. The probe showed significant colocalisation with MitoTracker™ and was found to induce significant depolarisation of the mitochondrial membrane. Incubation with a 4 μM solution of compound **198** for 6 hours resulted in 90% of mitochondria being damaged (assed by JC-1 staining).

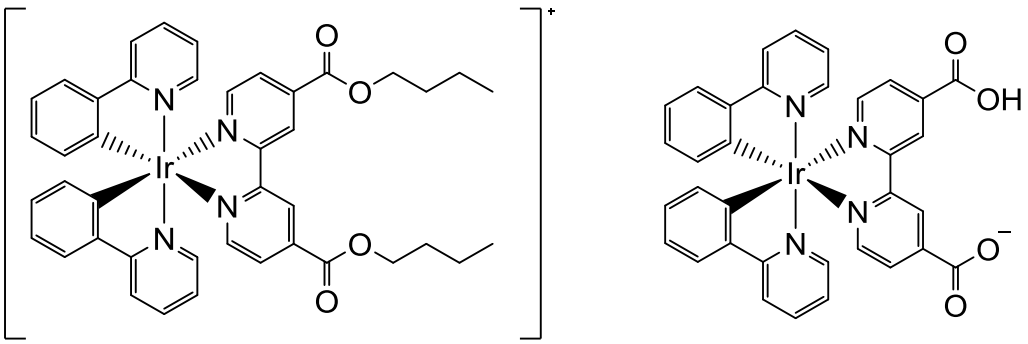

198 **199**

***Figure 4.16**: Ester-Modified Cyclometallated Iridium(III) Complex and its hydrolysis product.*

The final analogue in this series, **118**, was designed to have a phosphonate group to render the complex anionic. As the cell membrane is negatively charged, it was

expected that this complex would be largely excluded from the cell. This was in fact the case, with only very feint luminescent detected. This study shows that the polyamine derived complexes localise differently and appear to have a different uptake mechanism compared to the control complexes. Whilst some tentative parallels can be drawn between uptake of the complexes and polyamines, this by no means demonstrates PTS dependent uptake and remains somewhat speculative evidence at this point.

4.6: Studies with polyamine transport deficient cell lines

In order to obtain more compelling evidence that these polyamine complexes are transported by the PTS, uptake was investigated in a range of polyamine transport deficient cell lines. The CHO-MG cell line is a particularly useful tool for the study of the PTS.[317] Chinese hamster ovary cells (CHO) were treated with MGBG (**18**) and resistant strains were isolated. Compound **18** is both a potent inhibitor of polyamine biosynthesis and a substrate for the PTS. Resistance occurs due to a reduction in the activity of the PTS. CHO-MG cells transfected with a cationic amino acid transporter remained unable to transport polyamines; however, the precise nature of this deficiency has not been genetically identified. Evidence seems to suggest that polyamine transport into the cell is not affected, but the deficiency arises either as a result of defective endosomal release,[318] or upregulated efflux.[81]

The two other cell lines used were isolated by Casero *et al*. Human non-small cell lung carcinoma cells (NCI H157) were treated with the polyamine analogue BESpm (**23**) and the resistant strain was isolated. The resistant cell line was shown to be insensitive to the polyamine biosynthesis inhibitor **18** and inhibition of proliferation with DMFO could not be reversed by exogenous polyamines. Taken together this points to a deactivated PTS.[319] An analogous polyamine transport deficient mutant cell line was derived from A549 cells. The A549 cell line is also a non-small cell lung cancer derived from an adenocarcinoma from alveolar epithelium.

4.6.1: CHO-MG cell line

Cells were incubated at 37 °C with 5 % CO_2 in with RPMI medium with 10 % FCS containing **123** at a concentration of 25 μM for 18 hours. Cells were then co-stained with either MitoTracker deep red or LysoTracker then fixed and mounted. It should be noted that the mutant cell line is not entirely deficient in polyamine transport but shows reduced activity relative to the parent cell line. Cullis *et al.* studied uptake in this deficient cell line using Spm-MANT (**18**).[58] In the PTS competent parent cell line, the fluorescence intensity observed as a result of uptake of **18** increased rapidly in the first 5 hours of treatment and began to plateau around 10 hours with maximal uptake achieved at around 24 hours. Uptake was considerably slower in the mutant cell line. However, after 24 hours **18** had accumulated to around half the maximal concentration observed in the parent cell line.

Consistent with the previously mentioned studies by Cullis *et al*, **123** accumulated in the CHO-MG cells with the complex localising in punctate organelles distributed throughout the cytoplasm. On examining co-localisation of **123** with MitoTracker (MTR), it can be seen that almost all the luminescence arising from **123** colocalises with the cellular structures that are the most intensely strained by MTR. Whilst there was a clear colocalisation with the MitoTracker probe, colocalization of **123** with LysoTracker was minimal. This could be argued to be supportive of uptake of **123** being mediated by the PTS. As polyamine transport is widely acknowledged to occur as a result of caveolar endocytosis, it would be anticipated that **123** would accumulate in acidic vesicles and hence co-localise with LysoTracker (LTR) if its uptake is mediated by the PTS.

Cells do not appear to be homogenous in their uptake of **123**. This could imply that cells are beginning to lose their resistance. There are sub-populations of cells that show little uptake of **123**; these cells seem to show diffuse cytoplasmic staining, which could imply that more than one mechanism of transport is responsible for cellular accumulation of **123.** Whilst these results show some useful results, without a comparison with the unmodified cell line, it is difficult to draw conclusions.

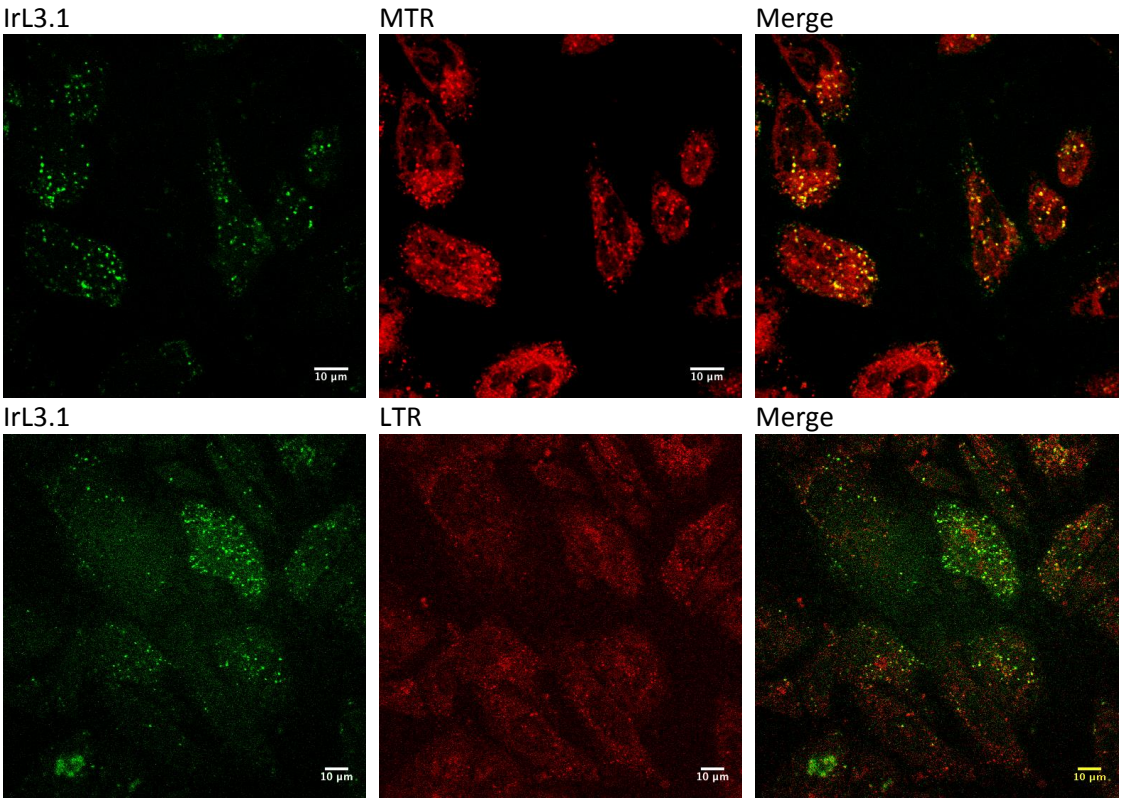

***Figure 4.17**: Fixed CHO-MG cells incubated at 37 °C with 5 % CO2 in with RPMI medium with 10 % FCS containing IrL3.1 at a concentration of 25 µM for 18 h, fixed with formaldehyde and imaged by CSLM, λ_{ex} 405 nm using a 430/25 emission filter.*

4.6.2: H157/H157R cells

Cells were treated as described above, and imaged by CSLM, some representative images are shown in Figure 4.18. Imaging revealed that uptake of **123** in the wild type H157 cell line was low, being confined to discrete vesicle-like structures, which did not localise with MitoTracker. Colocalisation with LysoTracker was inconclusive due to poor uptake of the LysoTracker probe. Uptake of **123** in the resistant cell line was negligible. Whilst a difference between uptake in the resistant and non-resistant cell lines is perceptible, given the level of uptake seen in the PTS deficient CHO-MG cell line, these results are not overly convincing of the role the PTS may play in uptake of this complex. Quantitative analysis by ICP-MS may give more convincing results.

The culture conditions used in this work were as used by the researchers reporting the isolation of this cell line, however, these cell lines did not grow well, especially the PTS deficient cell line. This is consistent with previous research.[319] Casero

et al. reported growth curves for the polyamine transport deficient cell line in both the presence and absence of BESpm; cells grew equally under both conditions, doubling after 72 hours, however, this level of growth was not sustained with the cell population remaining static beyond this timepoint. The resistant cell line was harvested from its parent cell line after treatment with a toxic dose of BESpm for 96 hours (10 µM). A dose of just 1 µM of BESpm was reported to be toxic to the parent cell line within 96 hours. It is likely that this cell line is particularly sensitive to polyamine analogues and hence may not be the most useful cell line to study in this respect, however the toxicity in these cell lines warrants further investigation.

Interestingly, uptake of the polyethylene glycol (PEG) analogue, **140** appeared to be more efficient than that of **123** in both the parent and the polyamine transport deficient cell lines, albeit still at a low level. There also seemed to be little difference in uptake between the resistant and wild type cells, which taken together with the previous results does lend support to the hypothesis that the polyamine complex **123** gains access to the cell via the PTS.

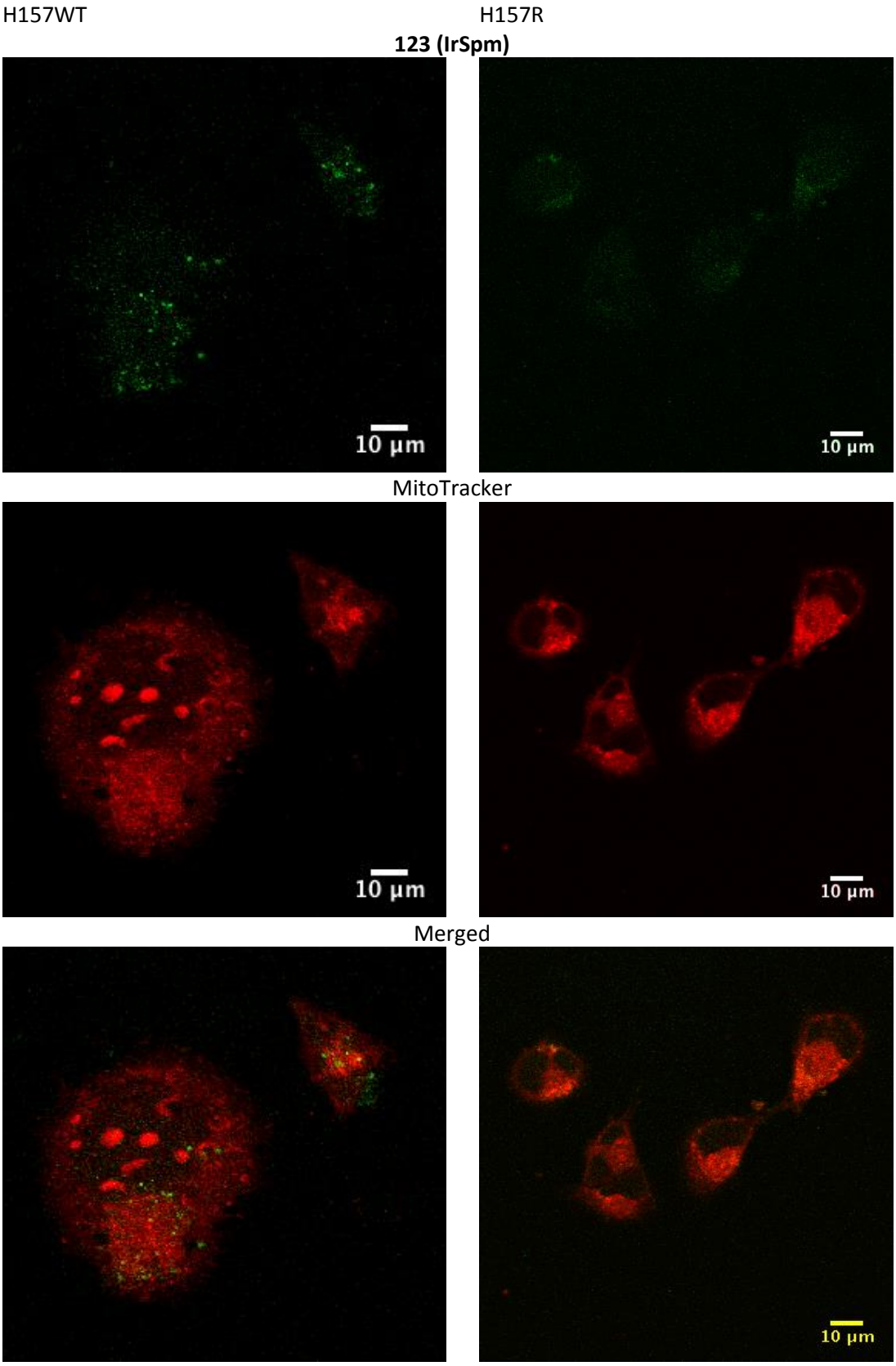

***Figure 4.18**: Fixed H157 cells incubated at 37 °C with 5 % CO_2 in with RPMI medium with 10 % FCS containing IrL3.1 at a concentration of 25 µM for 18 h, fixed with 4% formaldehyde and imaged by CSLM, λ_{ex} 405 nm using a 430/25 emission filter.*

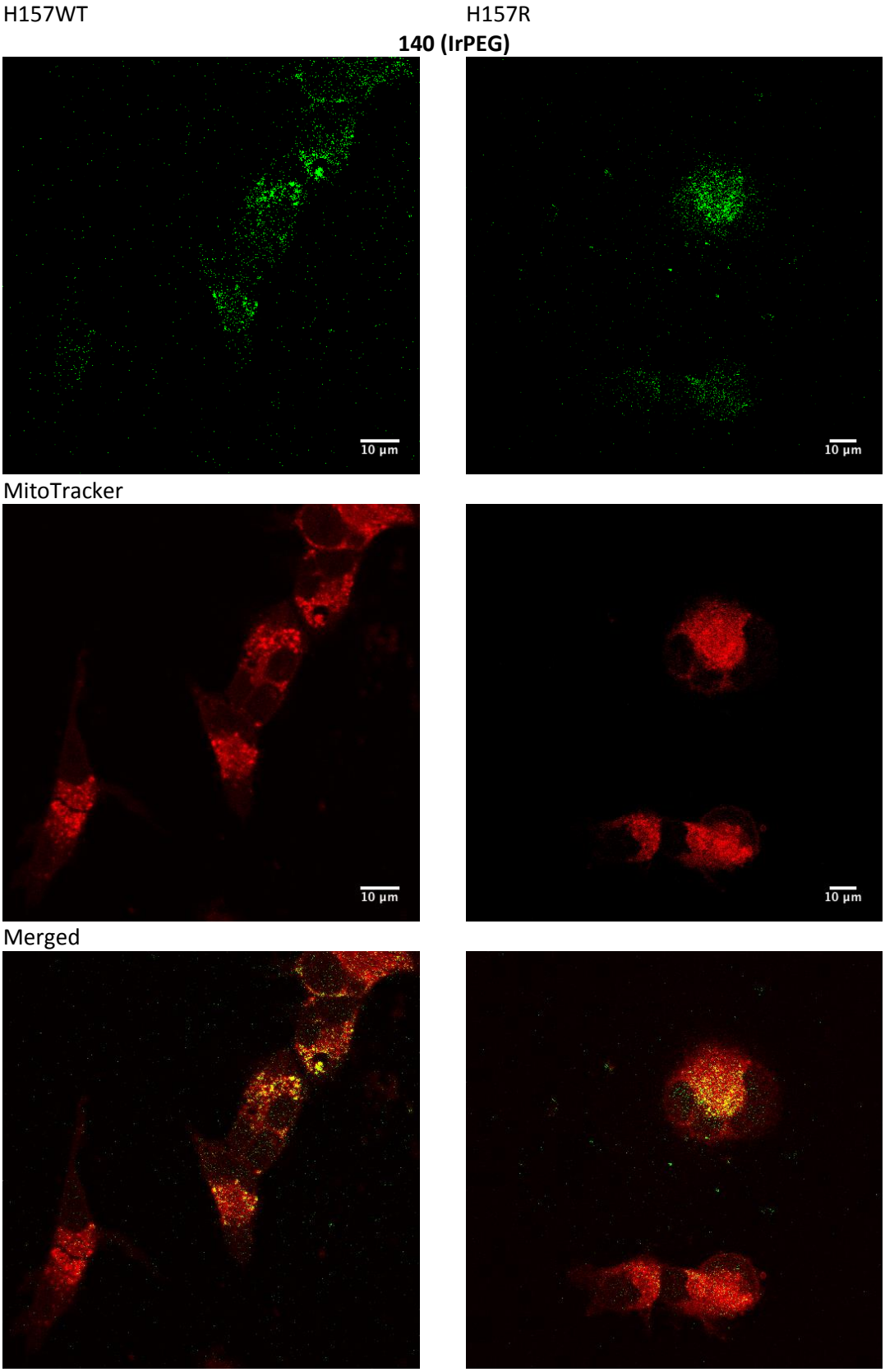

***Figure 4.19**: H157 cells incubated at 37 °C, 5 % CO_2 in with RPMI medium with 10 % FCS containing IrL5.1 at a concentration of 25 µM for 18 h, fixed with 4% formaldehyde and imaged by CSLM, λ_{ex} 405 nm using a 430/25 emission filter.*

4.6.3: A549/A549R cells

The lungs have a particularly active PTS, with alveolar epithelium showing one of the highest levels of polyamine uptake.[56] A549 adenocarcinoma cells are derived from alveolar epithelium that have been extensively used in studies of the PTS. A549 cells have been shown to carry a *KRAS* mutation,[320] known for its ability to upregulate polyamine transport.[42] Evidence for Polyamine transport as the major route of uptake for complex **123** is most compelling in these cell lines as there is significant uptake in the parent cell line which is substantially reduced in the resistant cell line. Studies carried out with A549 cells and the PTS deficient A549R cell lines are highly suggestive of uptake via endocytosis as accumulation of **123** appears in vesicle-like structures that are distributed throughout the cytoplasm. Luminescence from **123** does not colocalise with MitoTracker and is excluded from the nucleus. Uptake in the PTS deficient cell line was significantly reduced, although not entirely absent, as seen in the other cell lines.

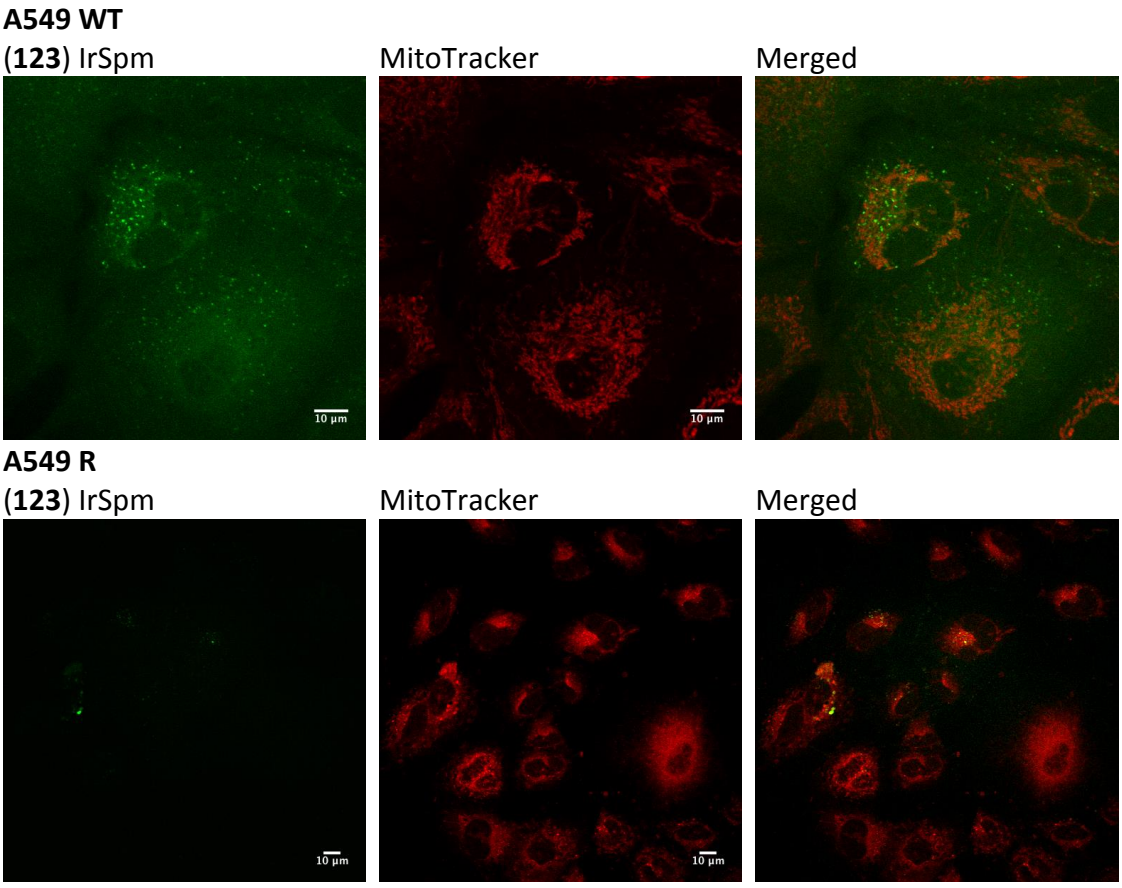

***Figure 4.20**: Uptake of IrL3.1 in wild type A549 cells and PTS deficient A549R cells. incubated at 37 °C with 5 % CO_2 in with RPMI medium with 10 % FCS with **123** (25 µM) for 18 h, counterstained with MitoTracker deep red, fixed with 4% formaldehyde and imaged by CSLM, λ_{ex} 405 nm using a 430/25 emission filter.*

4.7: Summary

Comparing uptake of polyamine complexes **115** and **123** with control complexes **116**, **117** and **118** shows clear differences in localisation and uptake. As anticipated, the anionic complex **118** was almost entirely excluded from the cell, whereas complexes **116** and **117** showed diffuse cytoplasmic staining. Polyamine complexes **115** and **123** were localised in discrete structures that resemble endosomes which is broadly consistent with uptake by endocytosis as expected if uptake is mediated by the PTS. Given that many iridium complexes have also shown to be internalised by endocytosis, this evidence is insufficient on its own to implicate the PTS in the transport of these complexes.

Complex **115** meets the requirements to be recognised as a substrate for the PTS but falls short of many of the optimum parameters for uptake and would be expected to be a poor substrate of the PTS. This was certainly seen on comparison of uptake of complexes **115** and **123** at early timepoints. Uptake of **115** after 4 h was approximately comparable with that seen for complex **123** between 20 and 40 minutes; which is broadly in line with the comparative uptake of Put relative to Spd.

Uptake of **123** in the CHO-MG cell line draws some interesting parallels with uptake of polyamine conjugates previously studied in this cell line. In the absence of comparable data from PTS competent CHO cells, this is somewhat subjective nevertheless, uptake is broadly consistent with that of previously documented polyamine conjugates. Uptake of **123** in the PTS deficient non-small cell lung cancer H157 cell line is much lower than that observed in the PTS competent cells, but this could be argued to be a result of the impaired growth of the deficient cell line. However, given that uptake of the polyethylene conjugate **140** localises similarly in both the PTS competent and deficient cells, this data is highly suggestive of uptake mediated by the PTS. A549 cells with a competent PTS show significant accumulation of the probe in structures that resemble endosomes, and a distinct lack of uptake in cells with a compromised PTS. Taken together, the data obtained from these experiments is entirely consistent with uptake of polyamine complexes mediated by the PTS.

Chapter 5 : Toxicity

5:1: Viability assays

The MTT assay is a quantitative colorimetric assay widely used to measure cell viability.[321] (3-(4,5-dimethylthiazol-2-yl)-2,5-diphenyl tetrazolium bromide (MTT) is an almost colourless substrate that is reduced to give the dark blue product (*E,Z)*-5-(4,5-dimethylthiazol-2-yl)-2,5-diphenylformazan (formazan) when incubated with metabolically active cells. The tetrazolium ring is cleaved in mitochondria by dehydrogenase enzymes (as shown in figure 5.1) and hence only produced by living cells. As the formazan product is only partially soluble in cell medium it must be solubilised by the addition of an organic solvent (typically DMSO) prior to colorimetric analysis.

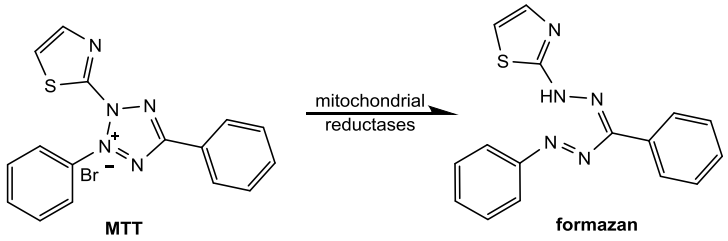

Figure 5.1*: Formation of the deep blue formazan product for the colorimetric MTT cell viability assay.*

Although cheap to perform, the MTT assay is relatively insensitive with a detection limit of around 25 000 viable cells/well. The formazan product may also be formed by non-specific reduction by antioxidants and is rapidly degraded, which can lead to problems with reproducibility. The ATP luciferase-luciferin assay has been shown to be more reproducible and can detect the ATP produced from as little as 20 cells.[322] The amount of ATP is directly linked to the number of cells, and as ATP degrades rapidly after cell death it is a good marker of viability.[323]

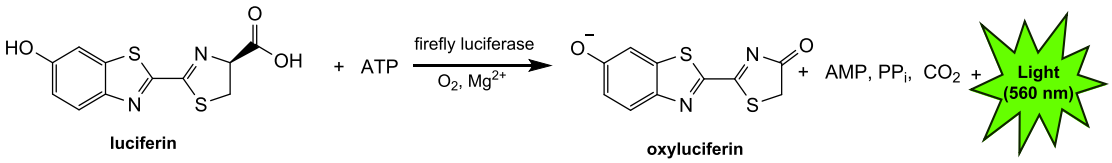

Figure 5.2*: Luciferin-Luciferase reaction used in ATP quantitation of cell viability.*

5.2: Platinum resistance and polyamines

Cisplatin enters cells via multiple pathways where it activates and silences many different genes, perturbing almost every mechanism supporting cell survival. Resistance to cisplatin is usually characterised by reduced accumulation of cisplatin due to activated efflux, impaired influx, increased detoxification and increased DNA damage repair.[324] Cisplatin, being a charge-neutral complex accumulates via passive diffusion, however, the copper transporter CTR1 is also thought to be an important mode of uptake that is significantly down-regulated in cisplatin-resistant ovarian cancer.[325,326]

Platinum drugs also perturb polyamine pathways. The catabolic enzyme SSAT is up-regulated and the two critical biosynthesis enzymes ODC and SAMDC are down-regulated, leading to polyamine depletion which stifles growth. Therefore, cells that have acquired resistance to cisplatin should be expected to show good uptake of polyamine conjugates.[327] [$PtCl_2$Spm] (**173**) was designed to overcome cisplatin resistance by aiding its accumulation in cells enhancing its toxicity via additional DNA targeting and binding. As the platinum centre is charge-neutral, [$PtCl_2$Put] (**172**) should act as a true control for the polyamine-vectored complexes. The luminescent rhenium complexes **119** and **166** were also evaluated alongside the platinum compounds as potential theranostics.

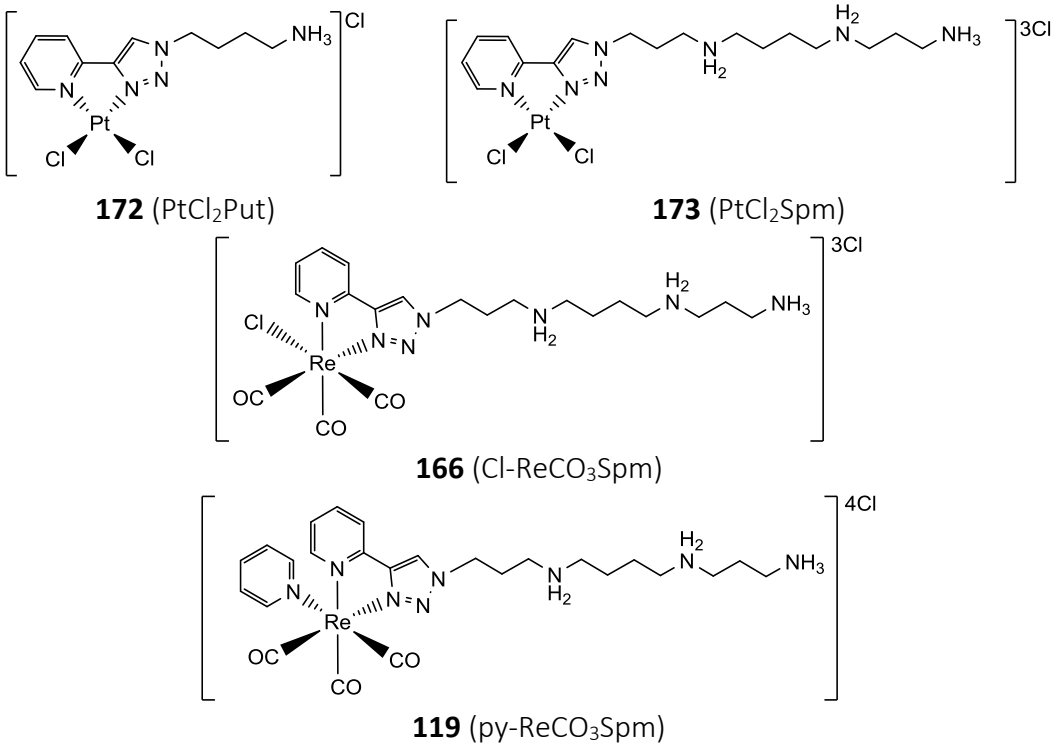

***Figure 5.3**: Polyamine platinum drugs **172** and **173**, and rhenium theranostics **166** and **119**.*

5.3: Results in A2780 ovarian adenocarcinoma cells

Compounds were incubated with A2780 cisplatin sensitive and A2780-cis cisplatin resistant cells for 72 hours and the CellTitre-Glo® (Promega)assay kit was used to quantify ATP as a measurement of cell viability; the dose response curves are shown in figure 5.4, and IC_{50} values are shown in Figure 5.5. The control compound **172** was not toxic in the cisplatin sensitive cell line but showed a slight increase in efficacy in the cisplatin resistant cell line, although with an IC_{50} value of over 100 µM it lacks cytotoxic activity. **173** displayed limited potency in the cisplatin sensitive cell line but was found to be around 4-fold more potent in the cisplatin resistant cell line, with an IC_{50} of 26.2 µM.

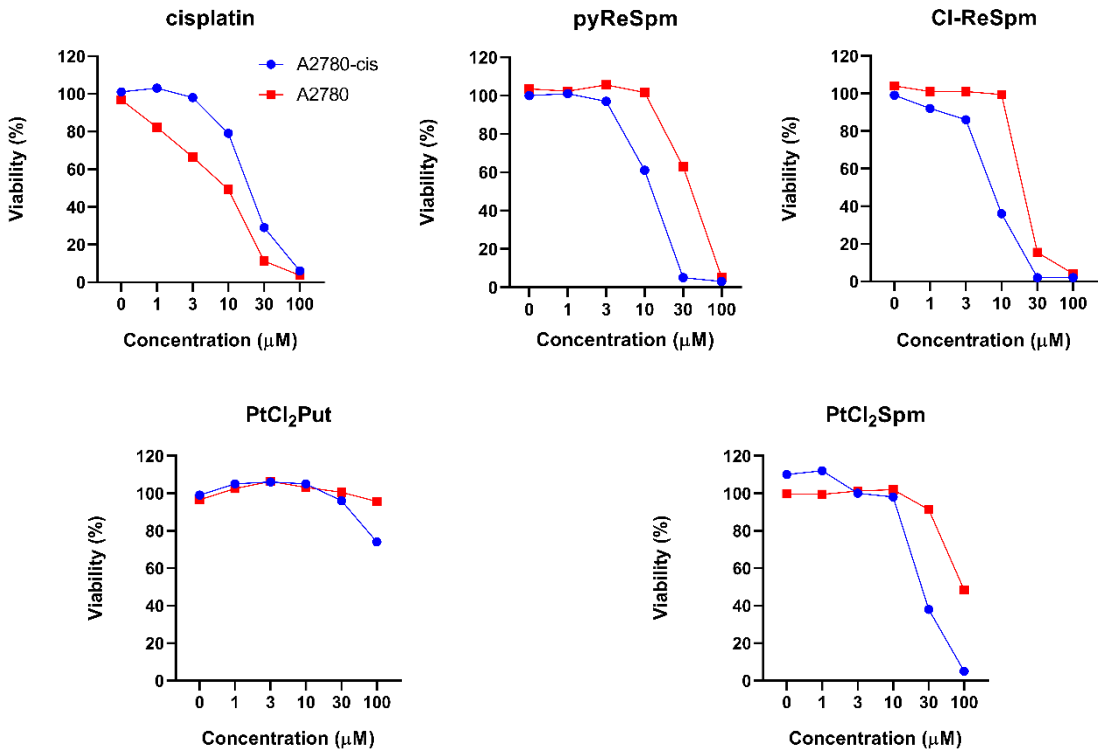

***Figure 5.4**: Dose response curves for A2780 and A2780-cis cells treated with complexes for 72 h.*

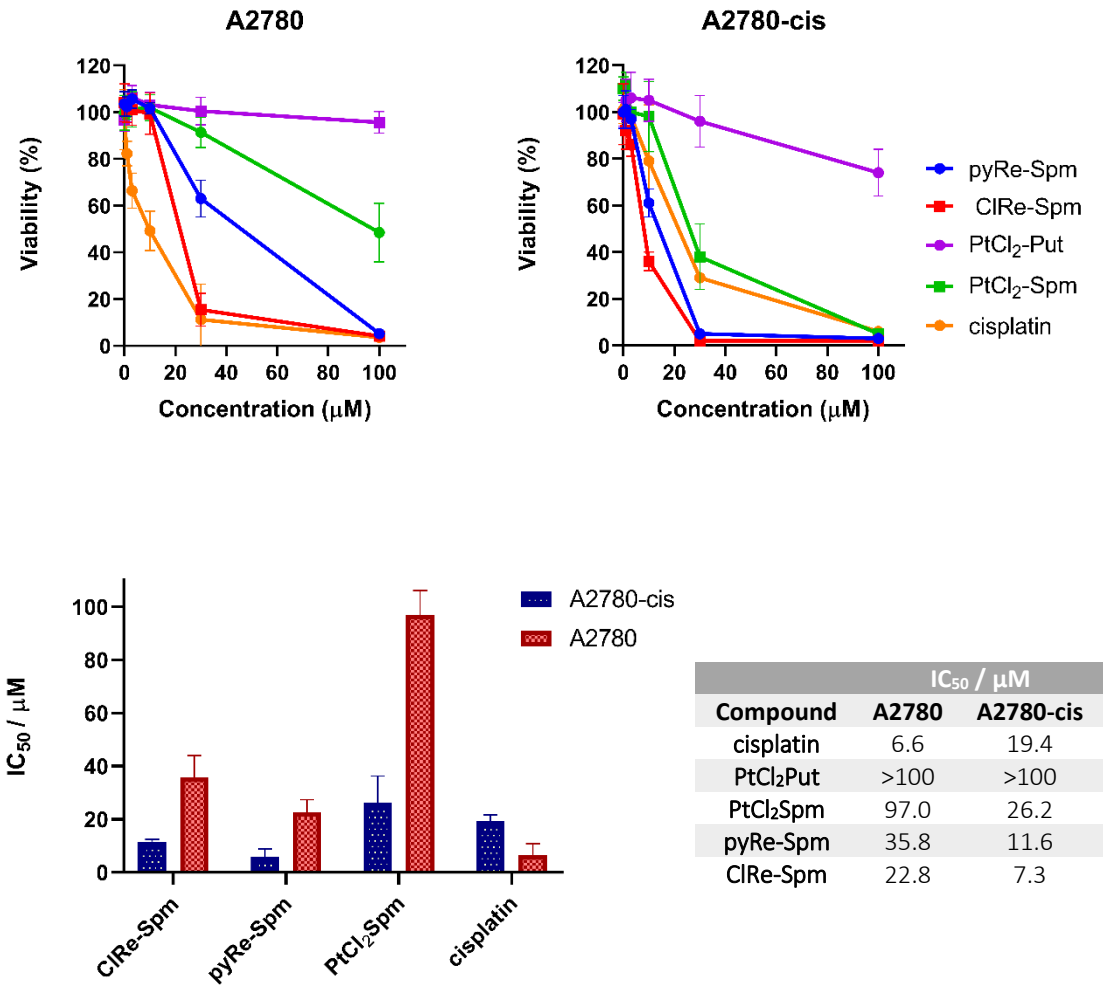

Compound	IC$_{50}$ / μM A2780	IC$_{50}$ / μM A2780-cis
cisplatin	6.6	19.4
$PtCl_2$Put	>100	>100
$PtCl_2$Spm	97.0	26.2
pyRe-Spm	35.8	11.6
ClRe-Spm	22.8	7.3

***Figure 5.5**: IC$_{50}$ data values after incubation with complexes after 72 h.*

The rhenium compounds **119** and **166** showed the most promising cytotoxic activity with Cl-ReCO$_3$Spm, **166** showing a similar potency to cisplatin in A2780 cells and a low IC$_{50}$ value of 7.3 μM in the resistant cell line. The axial pyridine ligand was incorporated to minimise ligand exchange and limit toxicity for use as a cellular probe however, py-ReCO$_3$Spm has a similar IC$_{50}$ value to Cl-ReCO$_3$Spm. Ligand exchange *in vitro* cannot be discounted as a range of rhenium(I) tricarbonyl aqua complexes (compounds **200** – **202** shown in figure 5.5) reported by Wilson *et al.* have similar IC$_{50}$ values (in HeLa cells) to the rhenium complexes reported in this study.[328] The IC$_{50}$ values obtained in this study are also consistent with that reported for a similar fructose-vectored compound **203** (in MCF-7 breast cancer cells) reported by Lo *et al.* and shown in figure 5.5.[329] This fructose vectored complex also demonstrated sub-micromolar toxicity in the light.

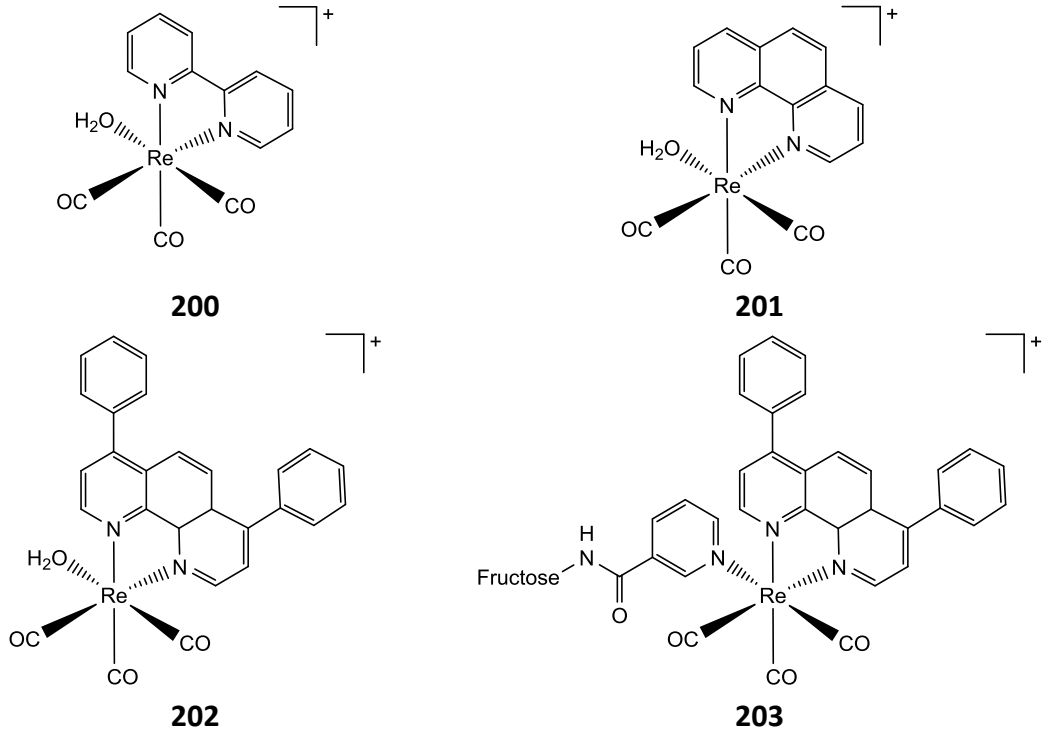

***Figure 5.6**: Cytotoxic rhenium polypyridyl complexes **200**, IC_{50} 15 µM, **201** IC_{50} 9.7 µM, **202**, IC_{50} 15 µM;[328] and fructose vectored **203** IC_{50} 9.6 µM.*[330]

From the data obtained from these preliminary studies, utilising the PTS as a vector to overcome cisplatin resistance appears to be a valid strategy; all three spermine-derived complexes show at least a 3-fold enhancement in toxicity in the resistant cell line. Interestingly, the aqua complexes reported by Wilson and co-workers did not show any selectivity for cisplatin sensitive cells over the cisplatin resistant cells, implying an important targeting role for the polyamine moiety. This warrants further investigation to determine if this this occurs as a result of enhanced accumulation or is due to a fundamental difference in toxic response between the two cell lines.

Although the platinum complexes lacked efficacy, the low IC_{50} values of these prototype rhenium complexes show great promise for use as theranostics. They may also show phototoxicity, either acting as a photoCORM and/or as a sensitiser for PDT.

Chapter 6 : Discussion

6.1: Conclusions

6.1.1: Synthesis

Polyamine synthesis has been optimised to reduce the number of synthetic steps and improve overall yields from around 30 % to 50 %. Polyamines were incorporated into chelating pyridyl triazole ligands using click chemistry and subsequently coordinated to rhenium, iridium and platinum metal centres, in a series of clean and high-yielding reactions. The synthesis of platinum pyta complexes was also optimised increasing the overall isolated yield from 7 % to 50 % over 3 steps. Sonogashira coupling was successfully employed to generate substituted alkynyl pyridines which were used with the existing synthetic methodology to prepare a series of ligands designed to modulate the photophysical properties of the luminescent iridium and rhenium complexes.

6.1.2: Tuning emission

The emission of cationic rhenium tricarbonyl compounds was successfully tuned towards the red by the addition of an electron withdrawing CF_3 group onto the pyridine ring of the pyta ligand. Notably, the emission lifetime of the 4-CF_3 complex was significantly increased from 157 ns to 605 ns, although quantum yields of all complexes remained very low (below 1%). In contrast, the iridium pyta complexes have bright, long lived emission with the excitation maximum close to 405 nm, making them ideal candidates for fluorescence microscopy. Unfortunately, efforts to red shift the emission of these complexes were detrimental to the photophysical properties as stabilising the N^N based LUMO significantly enhanced the MLCT character of the emission drastically reducing the quantum yield and the emission lifetimes. Modulating emission by using substituted C^N ligands has generated 2 complexes that may have future potential as dual emission probes, warranting further investigation.

6.1.3: Cellular uptake

Uptake of the complexes was found to be highly charge dependant; the net anionic complex 129 was almost entirely excluded from the cell, with complexes 127 and 128 showing diffuse cellular localisation. Polyamine complexes showed increased uptake with increased cationic charge, consistent with uptake via the PTS. Both IrSpm and IrPut

showed significant cellular uptake in A549 cells, accumulating in discrete, punctate structures within the cytoplasm, however uptake of IrSpm in polyamine transport deficient A549 cell was negligible. The uptake of IrSpm in CHO-MG cells is consistent with that observed by others using organic fluorophore conjugates, showing that the iridium complexes are good reporters of polyamine transport. Co-localisation experiments using Mitotracker™ showed that the iridium complexes localised in the mitochondria and indicates some degree of mitochondrial damage.

6.1.4: Toxicity

Overall results from preliminary studies would support the notion that polyamines are a viable option for the delivery of chemotherapeutic drugs to PTS active cancers. The cisplatin resistant cell line (A2780-cis) was at least three times more sensitive to the polyamine drugs compared to the cisplatin sensitive cell line (A2780) consistent with cisplatin mediated polyamine depletion in the resistant cell line. The chlororhenium complex was found to be the most toxic with an IC_{50} of just 7.3 µM in the cisplatin resistant cell line. The pyridylrhenium complex was slightly less potent with an IC_{50} value of 11.6 µM. As the rhenium complexes are luminescent, they show great promise as a targeted, single-molecule theranostic. These constructs can be used *in vitro* to assess polyamine transport status, and directly assess pharmacological response, however the luminescent intensity of these complexes requires some enhancement to be of clinical relevance. The platinum complexes showed disappointing toxicity, this could be due to the complex binding to serum proteins in the cell medium due to the highly cationic nature of the polyamine vector.

6.1.5: Evaluation of progress

The work presented in this thesis would support the use of the polyamine transport system as a means of targeting metallodrugs to PTS-active cells. Although $PtCl_2$Spm was found to be virtually non-toxic in the cisplatin sensitive A2780 cells, it showed a 4-fold enhancement in activity in cisplatin resistant A2780-cis cells, implying that polyamines could play an important role in cisplatin resistant cancers. The rhenium metallodrugs proved to be potent cytotoxic agents showing a significant enhancement in toxicity in the cisplatin resistant cell line. Efforts to tune the photophysical properties of the rhenium complexes using electron withdrawing CF_3 groups has proved partially

successful; incorporation of the 4-CF_3 group has significantly enhanced absorption at 405 nm and doubled the quantum yield compared to the non-substituted complex, however, it remains very low (around 1 %).

The toxicity of the iridium complexes has not been quantified, however it is tolerated well in cells at a concentration of 33 μM, so likely to have minimal toxicity. Although these complexes show minimal dark toxicity, they display potent phototoxicity and given the oxygen-sensitivity of emission, are likely to make good photosensitisers for PDT. Efforts to bathochromically shift emission of the iridium complexes by incorporating electron withdrawing groups resulted in a dramatic reduction in both luminescence quantum yield and phosphorescence lifetime, however the incorporation of an electron donating methoxy group increases luminescent intensity and emission lifetime.

6.2: Future Directions

6.2.1: Tuning Emission

6.2.1.1: Re

The cationic rhenium pyta complexes presented in this work are not good luminescent probes for cellular imaging due to their low quantum yield and dose-limiting toxicity. Extending the conjugation is an alternative strategy commonly employed to tune emission towards the red, however Policar *et al*. found that the 1,2,3-quinolyltriazole complex has a rather low quantum yield. Although the inverse click complexes have a greater quantum yield, they have been found to be somewhat unstable. Future endeavours should consider using alternative N^N ligands and developing the methodology to mono-functionalise them.

1,2,4-pyridyltriazoles could be a useful alternative N^N ligand that is also amenable to mono-conjugation of the polyamine moiety; the proposed synthesis is shown below in figure 7.1. Picolinonitrile is reacted with hydrazine, then reacted with an acyl chloride functionalised polyamine. Unlike the 1,2,3-pyridyltriazoles, the 1,2,4-pyridyl triazoles are deprotonated upon coordination giving rise to a neutral metal centre. This could be useful to further investigate charge distribution and cellular uptake. Rhenium and iridium complexes bearing 1,2,4-triazole N^N ligands have been reported boasting

high quantum yields.[331,332] Extending conjugation using quinoline 2-carbonitrile as the starting material may also shift the emission towards the red.

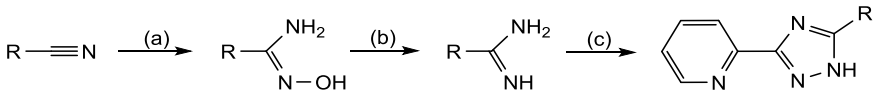

***Figure 6.1**: Proposed synthesis of 1,2,4-pyridyl triazole ligands, where R represents the polyamine chain.*
***Reaction conditions**: (a) H_2NNH_2 in EtOH. (b) RCOCl, Na_2CO_3, DMMA, ethylene glycol, 200 °C.*[332]

6.2.1.2: Ir

Tuning the emission of the iridium complex via modification of the C^N ligand warrants further investigation. The 3-OMe-ppy C^N ligand may prove to be more effective at shifting emission to the red; as the substituent lies *para*-to the metal. The synthesis of this complex is not as straightforward as there are two possible sites for cyclometallation (as shown in figure 7.2) and by-products could prove difficult to separate; however, the desired product would be expected to be the predominate on steric grounds. Davies *et al*. reported the formation of multiple products when using microwave irradiation to prepare the dimer,[262] however Zysmann-Coleman reported only a single product using the classical Nonoyama synthesis;[141] in this instance conventional heating at a lower temperature may facilitate the formation of the desired product. A more powerful electron donating group such as NMe_2 may prove to be more effective at tuning the photophysical properties and is also more likely give a single product owing to the increased steric bulk of the NMe_2 substituent.

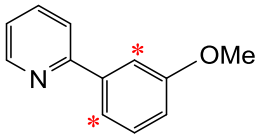

***Figure 6.2**: 3-substituted phenyl pyridine C^N ligand, highlighting possible sites of cyclometallation.*

Extending the conjugation of the C^N ligand has been shown to be an effective approach to red-shift emission, so replacing 2-phenylpyridine with 2-phenylquinoline or 2-napthylpyridine would by an interesting lead to follow. Incorporating additional nitrogen atoms in the pyridine ring can also bathochromically shift emission, whilst the benzo[g]quinoxaline ligands (shown in figure 7.3) with an both extended ring system and

additional nitrogen atoms in the pyridine ring give rise to complexes exhibiting near IR emission.[333]

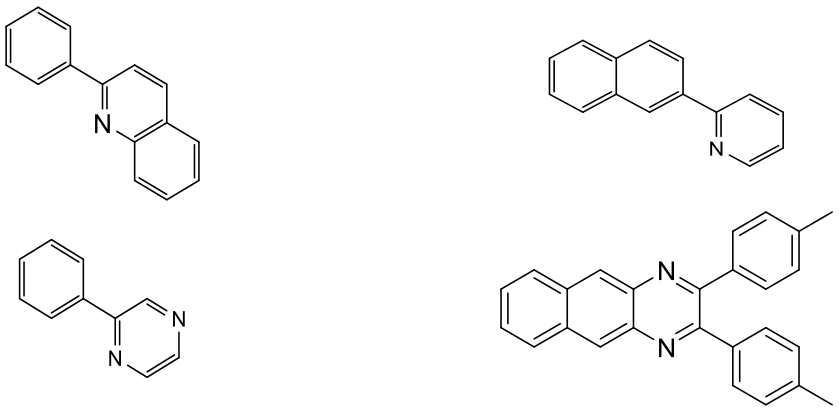

Figure 6.3: *Alternative C^N ligands with extended conjugation to shift emission towards the red, and/or increasing pyridyl ring electronegativity to shift emission to the red.*

6.2.2: Hypoxia probes

Complexes of this nature often show significant changes in emission lifetime in response to oxygen concentration and make excellent probes for PLIM. An iridium luminophore is therefore very well suited to this application. The benzothienylpyridine iridium complex BPTDM1 (**204**) with a cationic pendant group was designed by Tobita and coworkers as an *in vivo* oxygen sensor.[334]

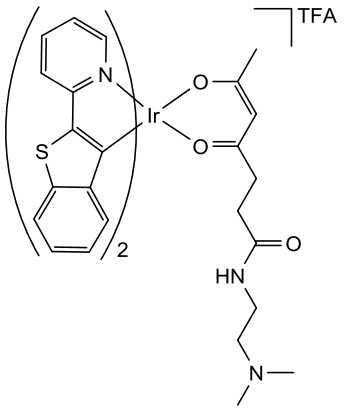

204

Figure 6.4*: Hypoxia imaging probe BTPDM1, (**204**).*[335]

Uptake of the complex was facilitated by the cationic dimethylamino group and found to localise in the lysosomes. The complex has a has a quantum yield of 29 % and an emission lifetime of around 100 ns in aerated solution, but this increased dramatically to 5 µs in degassed solutions. Nangaku *et al*. subsequently used complex **204** to visualise

intravital oxygen gradients at the surface of the kidney *in vivo*, to a depth of up to 10 µM using confocal microscopy.[335] Following administration of the probe by tail vein injection, sufficient concentrations of complex had accumulated in the kidney to allow the lifetime of phosphorescent decay to be measured. As the complexes studied in this work have a similar quantum yield and emission lifetime in aerated solution, there is huge potential for their future use as probes for PLIM.

An interesting approach would be to use a polyamine chain appended to the acetylacetonato ligand used by Tobita *et al*. as an alternative to the pyridine triazole ancillary ligand (proposed retrosynthesis shown in figure 7.3). The iridium complex **204** with 2-(2-pyridyl)benzothiophene (btp) as the cyclometallating ligand has a high quantum yield (especially under hypoxic conditions) and an emission maximum of around 600 nm. Complex **204** is synthesised from the chloride bridged dimer which was subsequently broken using succinylacetone, and finally the amine was coupled onto the terminal acid group.[334] This approach should also be feasible with Boc-protected amines.

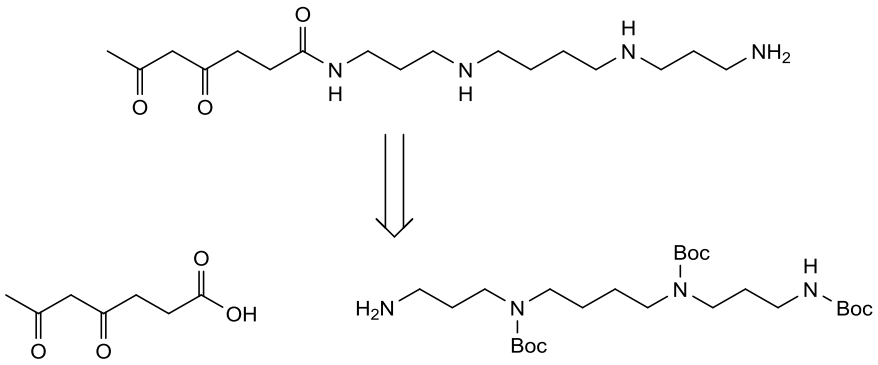

Figure 6.5: *Polyamine appended aetylacetone (acac) ligand.*

6.2.3 Iridium labelled peptides

The iridium pyta complexes used in this study were shown to be well tolerated in cells and have good photophysical properties for use in confocal microscopy. As these iridium complexes are highly photostable, they are excellent candidates for cellular imaging over extended periods of time, and so a complex that can be used to label peptides and other biomolecules is highly desirable. Previous work in the Lowe/Cullis group has established methods to attach polyamines to a carboxylic acid functionalised ligand using peptide coupling. This methodology has been optimised to be used with the

metal complexes used in this study and found to be fully compatible with solid phase peptide synthesis, enabling peptides to be labelled on-resin.

A short peptide (GGK) was synthesised using standard Fmoc solid phase peptide synthesis (SPPS) on rink amide resin. The N-terminal Fmoc protecting group was removed and the peptide labelled with an NHS ester of complex the carboxylic acid complex **174**. An activated ester was pre-formed by reacting the iridium complex with N-hydroxysuccinamide (NHS) and diisopropylcarbodiimide (DIC) for 2 hours, and the reaction mixture transferred directly to the peptide on resin to couple the active ester to the N-terminus of the peptide. The peptide-complex was then cleaved from the resin using 95 % TFA. Purification by HPLC gave the iridium functionalised tripeptide, as confirmed by high resolution mass spectrometry. The reaction scheme is shown in figure 6.6. This has huge potential not only for labelling peptides at the N-terminus, but also for the site specific labelling of lysine residues. By using an orthogonal methyltrityl protecting group for the ε-amine of the lysine, the sidechain can be selectively deprotected to enable the sidechain to be labelled with the iridium probe prior to cleavage of the peptide from the resin. This labelling strategy has the potential to be applied widely to targeting peptides (including monoclonal antibodies) and presents an exciting future application for theranostic iridium complexes.

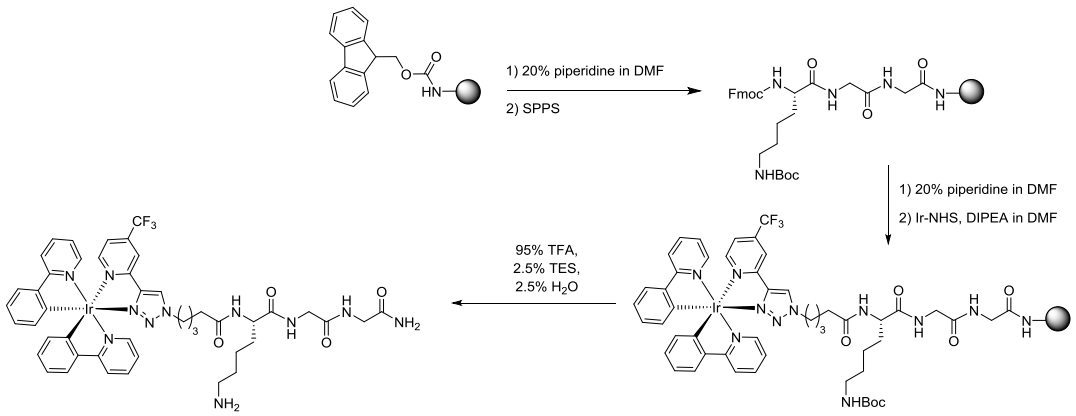

***Figure 6.6**: Solid phase synthesis of iridium-labelled tripeptide.*

6.2.4: Probes for EM/CLEM

One of the major issues encountered during cellular imaging was the lack of dye fixing. The complexes used are highly water-soluble and significant diffusion occurred in

fixed cells stored (in the freezer) over the course of a 72-hour time-course study. Formaldehyde is a weaker fixative than glutaraldehyde, and the cross linking can be reversible. Switching to glutaraldehyde as a fixative may improve the stability of fixed slides. This is particularly important if these probes are to be used in electron microscopy. Fixed cells undergo a series of dehydrations in organic solvents prior to being embedded in resin, for this to be successful the dye must not be washed out of the cells.

The chloromethyl complexes 146 and 147 were designed to overcome diffusion of the probes. The sulfhydryl reactive chloromethyl group has been widely exploited to lock luminophores onto protein molecules to enhance cellular retention. The PEG complex was successfully isolated in moderate yield in 2 synthetic steps under mild conditions and is an interesting prospect for future use as a probe for CLEM, however synthesis of the polyamine complex was less successful.

Optimisation of the synthesis of the chloromethyl polyamine complex is important as this probe that may help to solve some of the un-answered questions regarding the precise nature of polyamine transport. Formation of the chloromethyl polyamine ligand occurred in low yield presumably due to the competing reaction of the chloromethyl group with the amine moiety. There are several alternative approaches towards this synthesis; the azide could be pre-formed and isolated prior to the click reaction, or the chloromethylation step could be carried out at the end of the synthesis, prior to deprotection as the hydrogen chloride liberated by the S_N2 displacement reaction many also lead to partial deprotection the polyamine. Dry HCl in dioxane would be the reagent of choice for the final deprotection.

6.2.5: Phototoxicity PDT & PACT

An interesting study by Murata and co-workers parallels the findings of this work, showing that the introduction of electron withdrawing or electron releasing groups exerts a profound level of control over the excited state lifetime.[336] The photophysical properties of s series of N^N substituted $[Ir(btp)_2(bpy)]PF_6$ complexes were investigated; the phosphorescence lifetimes of complexes bearing electron-donating OMe groups were found to be significantly longer than those bearing electron-withdrawing CF_3 groups, which did not exhibit detectable phosphorescence at room temperature. This was attributed to the effect on the ligand field strength; the increased σ-donating ability

of the ancillary ligand bearing an electron donating group destabilizes a short-lived, non-emissive ^{3}MC state and increases the energy separation between the ^{3}MC state and emissive ^{3}LC state based on the btp ligand. The electron withdrawing group does not destabilise the ^{3}MC state as effectively due to its decreased σ-donating ability, leading to significant non-radiative decay of the excited state.

Although the emission maximum of these btp complexes is around 600 nm, the emission spectrum shows significant vibronic coupling, consistent with an excited state with significant intraligand character, and hence phosphorescent lifetimes and quantum yields are high. The complexes with the longest-lived excited states were found to be potent photosensitisers. The btp ligand would be useful to develop iridium complexes for PDT using the OMe-pyta ligands presented in this work. This complex is also likely to be an excellent hypoxia probe for PLIM, bearing similarity to the complexes used by Tobita[337] and Nangaku.[335]

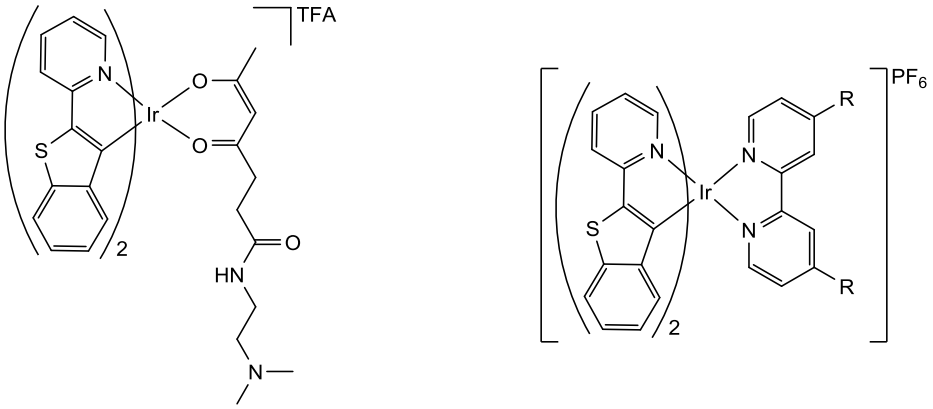

204 **205**

***Figure 6.7**: Ir-btp complexes investigated by Murata, and proposed Ir-btp complex for use as a photosensitiser for PDT and/or measuring hypoxia using PLIM.*

6.2.6: Pt(IV) polyamine

One of the most promising avenues for the development of new platinum drugs is the construction of multi-threat Pt(IV) complexes, taking advantage of the additional 2 coordination sites available in Pt(IV) complexes. As one of the downfalls of previously used polyamine vectored drugs has been excessive off target toxicity incorporation a polyamine vector at one of the labile axial sites it an attractive proposition. In addition to the targeting polyamine moiety that has been demonstrated as a useful vector for platinum-resistant cells, the second labile ligand included is the polyamine biosynthesis

inhibitor DMFO as this enzyme is purportedly downregulated by platinum drugs, its inhibition is likely to lead to cell cycle arrest. This construct would be equally applicable to the PDKi dichloroacetate, the HDACi inhibitors SAHA and valproate. The polyamine could be attached to a suitable linker such as adipic acid using standard peptide coupling methods.

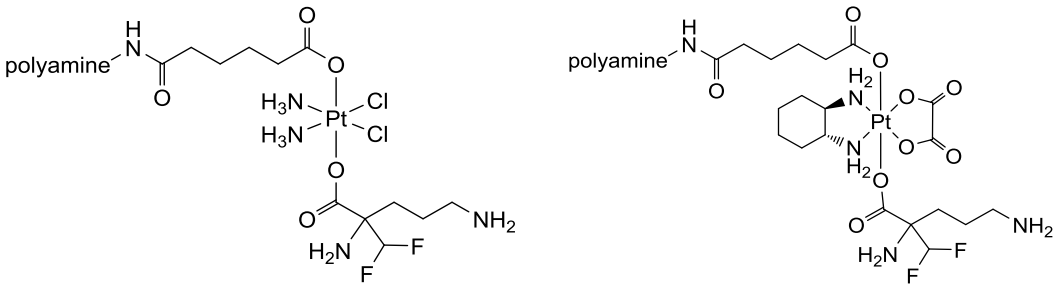

206 **207**

***Figure 6.8**: Polyamine vectored Pt(IV) drugs*

6.2.7: Summary

Many interesting new avenues of research have been proposed; of particular interest are the iridium benzothiophene complexes. Previous researchers have used similar complexes for oxygen sensing in cells and in living animals to good effect, and similar complexes show promise as photosensitisers for PDT. Iridium complexes derived from the benzothiophene ligand show oxygen sensitive, intense, long-lived ^{3}LC emission that is significantly red-shifted, and would be the modification of choice to continue efforts to modulate the emission properties of the iridium complexes. These complexes may be clinically applicable to probing ischemic reperfusion injury arising from myocardial infarctions or stroke.

As the rhenium complexes showed promising cytotoxicity, it would be of interest to investigate this further in other cancer cell lines and compare the result with non-cancer cell lines, to determine if the polyamine vector can differentiate between cancerous and healthy cells. It would also be useful to further enhance the photophysical properties of the complexes so that they can be used as theranostics to report on polyamine transport status of the cell lines used. Complexes using other more highly conjugated diimine ligands have shown a similar level of toxicity, and so it would be prudent to investigate alternative ligands that can be readily functionalised without compromising the photophysical properties. It would also be prudent to determine if

toxicity is linked to the polyamine by including a polyamine free compound such as the PEG complex. Understanding the extent of cellular accumulation is critical to understanding the toxic effects in cells, and so quantification of uptake by ICP-MS is of vital importance in future studies.

The Pt(IV) complexes proposed are an exciting prospect as the multi-threat approach is currently generating lead compounds that exhibit nanomolar IC_{50} values. The key to the success in this approach is identifying drugs that can act synergistically with compatible doses. The synthetic methodology presented in this thesis is highly versatile and can be readily adapted to a wide range of metal centres and/or alternative targeting functionalities. This approach is particularly amenable to developing personalised, theranostic constructs for the future generation of metallalodrugs.

Chapter 7 : Experimental

7.1: General Considerations

All reagents and solvents were obtained commercially and used without further purification with the exception of tetrahydrofuran and acetonitrile which were dried using a PureSolv solvent drying system from Innovative Technologies. Imidazole 1-sulfonyl azide hydrogensulfate was prepared by SG Phillips according to literature methods.[338] MeO-PEG-OTs, was prepared by Bea Barbi, (6-((trimethylsilyl)ethynyl)pyridin-3-yl)methanol was prepared by Matt Travers, [4-CF_3-IrCOOH]PF_6 was prepared by Abi Herbert and 2-(4-OMe-phenyl)-2-pyridine was prepared by Natasha Bullman (undergraduate MChem students).

Analytical TLCs were run on aluminium-backed silica or neutral alumina plates with a fluorescence indicator at 254 nm, preparative flash column chromatography was performed with silica gel 60 (230-400 mesh) or neutral activated Brockmann I grade alumina (150 mesh).

Analytical and preparative HPLC was performed on a ThermoFisher Ultimate3000 system with Chromeleon software on a Phenomenex Luna® 5 µm C18 100 Å, LC Column (250 x 21.2 mm) using the following method: (solvent A = 0.1% TFA in H2O, solvent B = 0.1%TFA in MeCN) 5% B for 5 min, 5-100% B over 30 min, 100% B for 5 min, 100-10% B for 5 min, 10% B for 5 min at 10 ml/min.

NMR spectra were recorded on Bruker AV500, AV400, DRX400 or DPX300 MHz spectrometers at 298 K unless otherwise specified. Chemical shifts are quoted in ppm relative to tetramethylsilane (TMS). All coupling constants are quoted in Hz and were calculated from spectra directly using ACD labs. Mass spectra were recorded on a Micromass Quatro LC spectrometer (electrospray), high resolution mass spectrometry was performed on a Waters Acquity XEVO Q ToF and are measured in m/z.

Electronic absorption spectra were recorded on a Shimadzu UV 180 spectrometer using a 10 × 10 mm quartz cuvette with 2 nm slit width and are recorded in nm, numbers in

brackets represent the extinction coefficient, ε, given in M^{-1} cm^{-1}. Luminescence data was recorded using a Jobin Yvon Horiba FluoroMax-P spectrometer in a 10 × 10 mm quartz cuvette. Excitation and emission maxima are limited in accuracy to the monochromator slit width of 3 nm and are recorded in nm. Excited state lifetimes were measured using a Jobin Yvon Horiba FluoroLog spectrometer in a 10 × 10 mm quartz cuvette. Decay data was fitted to a mono- or bi- exponential decay using GraphPad Prism7.

Azide Handling:

A blast shield was always used when synthesising azides.

[(Number of C atoms + Number of O atoms)/Number N atoms]

If the ratio is less than 3, these low molecular weight organic azides should not be stored in pure form, avoid isolating if possible. If the ratio is less than 1, the azide must not be isolated.

To treat metal azide waste: Dilute to give no more than 5 wt % of azide. Treat with 150 wt % of $NaNO_2$ with respect to azide. Cool to 0 °C and add 20% sulfuric acid dropwsise until the azide spot test is negative – dilute a couple of drops of azide waste with 1 mL of 1 M HCl add 1 drop of 1 M $FeCl_3$. Bright red precipitate indicates the presence of azide ion.

To treat organic azide waste: Reducing to the amine by dissolving the azide in a 5 wt % solution in 6 M HCl and add excess granular tin and stirring at room temperature for 1 h.

7.2: Ligand precursors

***tert*-butyl (4-aminobutyl)carbamate (137)**[75]

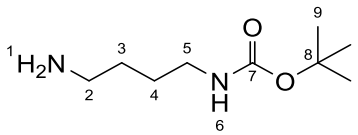

Di-*tert*-butyl dicarbonate (18.34 g, 84 mmol) was dissolved in 1,4-dioxane (50 mL) and added dropwise over 2 h via an addition funnel to a rapidly stirring solution of 1,4-diaminobutane (**1**) (22.21 g, 0.25 mol) in 1,4-dioxane (50 mL) under dry nitrogen at 0 ^{o}C. After addition was complete, the ice bath was removed and left to stir overnight. Solvent was removed *in vacuo* and residues dissolved in water (100 mL). Insoluble bis-substituted by-product was removed by filtration. The filtrate was extracted with dichloromethane (5 x 200 mL), dried over anhydrous sodium sulfate and the solvent removed under reduced pressure to afford colourless oil (11.92 g, 75%) which was used without further purification. NMR δ_H (400 MHz, $CDCl_3$, Me_4Si, 298K) 4.69 (s br, 1H, 6-N*H*Boc), 3.17-2.03 (m, 2H, 5-CH_2), 2.68 (t, *J* = 6, 2H, 2-CH_2), 1.55-1.42 (m, 4H, 3-CH_2, 4-CH_2), 1.41 (s, 9H, (9-(CH_3)$_3$), 1.13 (s br, 2H, 1-NH_2); NMR δ_C (125 MHz, $CDCl_3$, Me_4Si, 298K) 156.0 (7-C), 78.9 (8-C), 41.8 (5-C), 40.39 (2-C), 30.8 (4-C), 28.5 (9-C), 27.5(3-C); MS (ES+) 189 $[M+H]^+$, 133 $[(M-^tBu)+2H]^+$, 89 $[(M- Boc)+2H]^+$; HRMS (ES^+) $C_9H_{21}N_2O_2$ $[M+H]^+$requires 189.1603 found 189.1601.

***tert*-butyl (4-((2-cyanoethyl)amino)butyl)carbamate "ACN-BocPut" (208)**

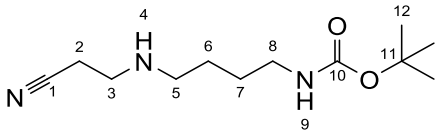

Compound **137** (1.0064 g, 5.34 mmol) was dissolved in MeOH (20 mL) and stirred at room temperature. Acrylonitrile (290.5 mg, 5.47 mmol) in MeOH (10 mL) was added dropwise, then left to stir overnight. Solvent was removed in vacuo to give the title compound as a pale-yellow oil, (1.3021 g, 89 %) used without further purification. NMR δ_H (400 MHz, $CDCl_3$, Me_4Si, 298K) 4.83 (s br, 1H, 9-N*H*Boc), 3.13 (m, 2H, 8-CH_2), 2.92 (br t, *J* = 6.7, 2H, 3-CH_2), 2.66 (br t, *J* = 6.7, 2H, 5-CH_2) 2.53 (t, *J* = 6.7, 2H, 1-CH_2) 1.55-1.50 (m, 4H, 6-CH_2,

7-C*H*$_2$), 1.41 (s, 9H, (12-(CH_3)$_3$), 1.25 (s br, H, 4-N*H*); NMR δ_C (101 MHz, CDCl3, Me4Si, 298K) 156.1 (10-C), 118.5 (1-CN), 79.0 (11-C), 48.7 (5-C), 45.0 (3-C), 40.4 (8-C), 28.4 (12-C), 27.7 (7-C), 27.2 (6-C) 18.6 (2-C); MS (ES$^+$) 264 [M+H]$^+$; HRMS (ES+) $C_{12}H_{23}N_3O_2Na$ [M+Na]$^+$ requires 264.1688 found 264.1690.

tert-butyl (4-((_tert_-butoxycarbonyl)amino)butyl)(2-cyanoethyl)carbamate "ACN-Boc$_2$Put" (209)

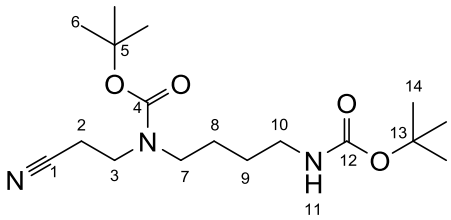

Compound 208 (0.9770 g, 3.7 mmol) was dissolved in dry DCM (20 mL). Boc$_2$O (821.6 mg, 3.8 mmol) in dry DCM (20 mL) was added dropwise under a nitrogen atmosphere at room temperature and left to stir overnight. The reaction was quenched with water and the product extracted with DCM (3 x 30 mL). Combined organic extracts were washed with brine, dried over Na_2SO_4 and concentrated in vacuo prior to purification by flash column chromatography eluting with 10 % MeOH in DCM. Solvent was evaporated *in vacuo* to give the title compound as pale-yellow oil (1.3179 g, 81 %). NMR δ_H (500 MHz, $CDCl_3$, Me_4Si, 294K) 4.69 (s br, 1H, 11-N*H*Boc), 3.46 (t, *J* = 6.7, 2H, 3-CH_2), 3.28 (t, *J* = 7.3, 2H, 2-CH_2), 3.14 (m, 2H, 10-C*H*$_2$), 2.59 (br s, 2H, 7- C*H*$_2$), 1.63-1.51 (m, 4H, 8-C*H*$_2$, 9-C*H*$_2$), 1.47 (s, 9H, (14-(CH_3)$_3$), 1.44 (s, 9H, (6-(CH_3)$_3$); NMR δ_C (126 MHz, $CDCl_3$, Me_4Si, 295K) 155.3 (12-C), 154.7 (4-C), 117.9 (1-CN), 80.6 (13-C), 79.1 (5-C), 48.2 (7-C), 43.8 (3-C), 40.1 (10-C), 28.6 (14-C), 28.3 (6-C), 27.4 (9-C), 26.0 (8-C) 17.5 (2-C); MS (ES$^+$) 364 [M+Na]$^+$; HRMS (ES+) [M+Na]$^+$ $C_{17}H_{31}N_3O_4Na$ requires 364.2212 found 364.2210.

***tert*-butyl (3-aminopropyl)(4-((*tert*-butoxycarbonyl)amino)butyl)carbamate "AP-Boc$_2$Put" (210)**

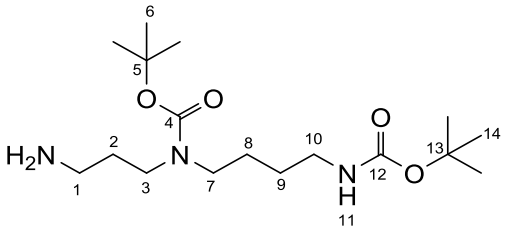

Compound 209 (0.8267 g, 2.27 mmol) was dissolved in 1 M NaOH in 5 % aqueous ethanol (100 mL). A teaspoon of Raney Nickel was added and hydrogenated at 50 psi for 24 h. Raney nickel was filtered through Celite and washed with ethanol. The filtrate was concentrated in vacuo and redissolved in DCM. The organic layer was washed with saturated $NaHCO_3$, dried over Na_2SO_4 then concentrated *in vacuo* to give the title compound as a colourless oil (0.7189 g, 86 %). NMR δ_H (400 MHz, $CDCl_3$, Me_4Si, 320K) 4.62 (s br, 1H, 11-N*H*Boc), 3.24 (m, 2H, 3-CH_2), 3.15-3.01 (m, 4H, 1- CH_2, 2-CH_2), 2.68 (m, 7-CH_2), 1.55-1.42 (m, 4H, 8-CH_2, 9-CH_2), 1.38 (s, 9H, (14-$(CH_3)_3$), 1.38 (s, 9H, (6-$(CH_3)_3$); NMR δ_C (101 MHz, $CDCl_3$, Me_4Si, 320K) 156.0 (12-C), 155.7 (4-C), 79.3(13-C), 79.1, (5-C), 46.6 (1-C), 44.4 (3-C), 40.4 (10-C), 39.5 (7-C), 32.2 (2-C), 28.6 (15-C), 28.4 (7-C), 27.5 (9-C), 25.7 (8-C); MS (ES^+) 368 $[M+Na]^+$; HRMS (ES+) $[M+Na]^+$ $C_{17}H_{35}N_3O_4Na$ requires 368.2525 found 368.2525.

***tert*-butyl (3-aminopropyl)(4-((*tert*-butoxycarbonyl)(3-((*tert*-butoxycarbonyl)amino)propyl)amino)butyl)carbamate "BocSpm" (138)**

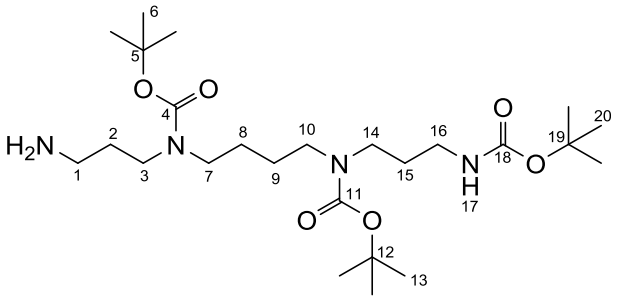

Spermine (**3**), (1.03 g: 5.1 mmol) was dissolved in 25% MeOH/DCM (200 mL) and stirred with anhydrous Na_2SO_4 (5.72 g: 40.3 mmol) at 0° C. 2-hydroxybenzaldehyde (0.64 g: 5.2 mmol) in 25% MeOH/DCM (50 mL) was added dropwise over 2 h, then left to stir overnight at room temperature. The reaction mixture was cooled to 0 °C, and di-*tert*-butyl dicarbonate (3.32 g, 15.6 mmol) dissolved in dry DCM (50) mL was slowly added. The reaction was stirred overnight at room temperature. Methoxyamine (1.60 g, 18.7 mmol) and Na_2CO_3 (2.0 g, 18.7 mmol) were added to the reaction mixture the stirred for 2 h. The solvents were removed under reduced pressure, dissolved in DCM (50 mL) and washed with 10 % Na_2CO_3 solution. The organic layer was separated, filtered, and concentrated. The crude mixture was purified by column chromatography using 1% NH_4OH, 5% MeOH in dichloromethane, to give a colourless, sticky oil, (1.44 g, 56 %). NMR δ_H (500 MHz, CD_3OD, 323K) 3.38 (br s, 1H, 4-NHBoc), 3.29 (t, *J* = 6.8, 2H, 16-CH_2), 3.27-3.21 (m, 6H, 14-CH_2, 10-CH_2, 7-CH_2), 3.06 (t, *J* = 6.8, 2H, 3-CH_2), 2.65 (t, *J* = 6.8, 2H, 3-CH_2), 1.76 - 1.66 (m, 4H, 2-CH_2, 15-CH_2), 1.60 - 1.51 (m, 4H, 8-CH_2, 9-CH_2), 1.48 (s, 18H, (13-$(CH_3)_3$, 6-$(CH_3)_3$); NMR δ_C (125 MHz, CD_3OD, 323K) 158.4 (18-C), 157.6 (11-C), 157.5 (4-C), 81.0, 80.9, 80.1 (5-, 12- and 19-C), 48.0 (10- and 7-C), 48.5(14- and 16-C) 39.9 (1-C), 39.1 (16-C), 32.5 (15-C), 29.9 (1-C), 28.9 (6-, 13- and 20-C), 26.9 (2-C); MS (ES^+) 503 $[M+H]^+$; HRMS (ES^+) $[M+H]^+$ $C_{25}H_{51}N_4O_6$ requires 503.3809 found 503.3803.

tert-butyl (4-((tert-butoxycarbonyl)(3-((tert-butoxycarbonyl)amino)propyl)amino)butyl)(3-((2-cyanoethyl)amino)propyl)carbamate "ACN-BocSpm" (211)

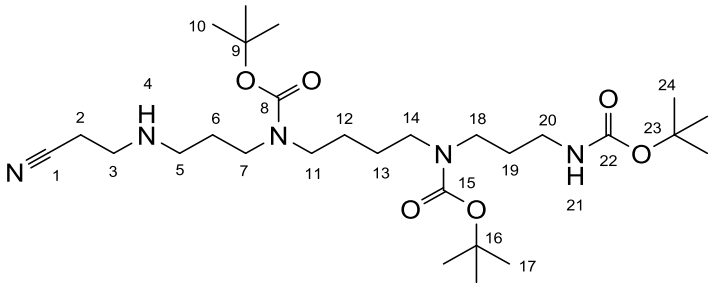

Compound 138 (0.3804 g, 0.757 mmol) was dissolved in MeOH (5 mL) and stirred at room temperature. Acrylonitrile (40.2 mg, 0.757 mmol) in MeOH (5 mL) was added dropwise, then left to stir overnight. Solvent was removed in vacuo to give the title compound as a pale yellow oil, (286.2 mg, 52 %) after purification by flash column chromatography (10 % MeOH in DCM). NMR δ_H (500 MHz, $CDCl_3$, Me_4Si, 323K) 5.24 (s br, 1H, 21-N*H*), 4.94 (s br, 1H, 4-N*H*), 3.24 (m, 4H, 18- and 20-CH_2), 3.17 (m, 4H, 11- and 14-CH_2), 3.14 - 3.06 (m, 2H, 7-CH_2), 2.91 (t, 2H, *J* = 6.6, 3-CH_2), 2.63 (t, 2H, *J* = 6.8, 5-CH_2), 2.51 - 2.46 (t, 2H, *J* = 6.6, 2-CH_2), 1.70 - 1.66 (m, 4H, 6- and 19-CH_2), 1.53 - 1.47 (m, 4H, 12-CH_2, 13-CH_2), 1.47 - 1.42 (m, 27H, 10- 17- and 24-CH_3); NMR δ_C (125 MHz, $CDCl_3$, Me_4Si, 323K) 156.0, 155.6 (8-, 15- and 22-C), 118.5 (1-CN), 78.9, 79.3, 78.9 (9-, 16- and 23-C), 46.8 (5-C), 46.6 (7-C), 46.3 (11-C), 45.2 (3-C), 44.7 (14-C), 44.2 (18-C), 37.8 (20-C), 28.5 (6-, 19-C), 28.4 (10-, 17- and 24-C), 25.8 (12- and 13-C), 18.7 (2-C); MS (ES^+) 557 $[M+H]^+$; HRMS (ES^+) $[M+H]^+$ $C_{28}H_{54}N_5O_6$ requires 556.4074 found 556.4050.

tert-butyl (3-((tert-butoxycarbonyl)(2-cyanoethyl)amino)propyl)(4-((tert-butoxycarbonyl)(3-((tert-butoxycarbonyl)amino)propyl)amino)butyl)carbamate "ACN-Boc$_4$Spm" (212)

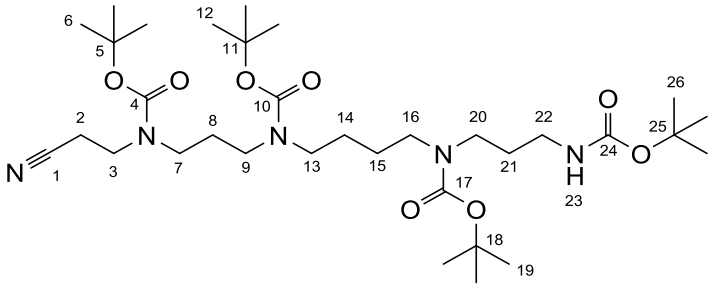

Compound **211** (136.7 mg, 0.25 mmol) was dissolved in dry DCM (2 mL). Boc_2O (80.5 mg, 0.37 mmol) in dry DCM was added dropwise under a nitrogen atmosphere at room temperature and left to stir overnight. The reaction was quenched with water and the product extracted with DCM (3 x 10 mL). Combined organic extracts were washed with brine, dried over Na_2SO_4 and concentrated in vacuo prior to purification by flash column chromatography eluting with 10 % MeOH in DCM. Solvent was evaporated *in vacuo* to give the title compound as a sticky gum (129.7 mg, 79 %). NMR δ_H (500 MHz, $CDCl_3$, Me_4Si, 323K) 5.19 (s br, 1H, 23-N*H*Boc), 3.47 (t, *J* = 6.7, 2H, 3-CH_2), 3.30-3.21 (m, 4H, 20- and 9-CH_2), 3.20-3.13 (m, 6H, 13-, 16- and 20-CH_2), 3.12 - 3.05 (m, 2H, 3-CH_2), 2.60 (br m, 2H, 2- CH_2), 1.82 – 1.73 (m, 2H, 21-CH_2), 1.70 – 1.62 (m, 2H, 8-CH_2), 1.51 – 1.48 (m, 4H, 14- and 15- CH_2), 1.47 – 1.43 (m, 36H, 6-, 12-, 19- and 26-CH_3,); NMR δ_C (125 MHz, $CDCl_3$, Me_4Si, 323K) 156.1, 155.8, 155.5, 155.0, (4-, 10-, 17- and 24-C), 118.0 (1-CN), 80.6, 79.6, 79.5, 79.0, (5-, 11-, 18- and 25-C), 47.1 (13-C and 16-C), 46.9 (21-C) 44.9 (20-C) 44.3 (3-C), 44.0 (9-C), 37.9 (7-C), 28.8 (8-C), 28.5 (6-, 12-, 19- and 26-C), 25.7 (14- and 15-C), 17.3 (2-C); MS (ES+) 557 $[M+H]^+$; HRMS (ES^+) $[M+H]^+$ $C_{33}H_{62}N_5O_8$ requires 656.4598 found 656.4631.

tert-butyl (3-((3-aminopropyl)(tert-butoxycarbonyl)amino)propyl)(4-((tert-butoxycarbonyl)(3-((tert-butoxycarbonyl)amino)propyl)amino)butyl)carbamate "AP-Boc$_4$Spm" (213)

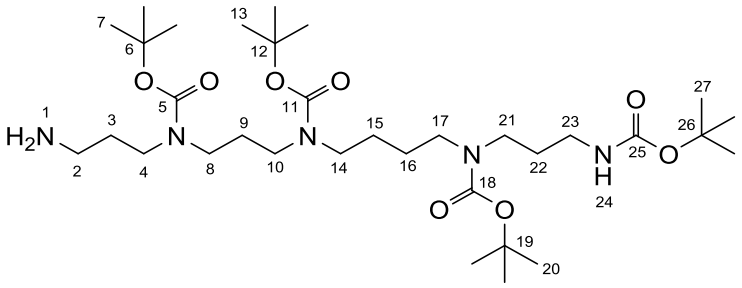

Compound 212 (117.3 mg, 0.18 mmol) was dissolved in 1 M NaOH in 5 % aqueous ethanol (100 mL). A teaspoon of Raney Nickel was added and hydrogenated at 50 psi for 24 h. Raney nickel was filtered through Celite and washed with ethanol. The filtrate was concentrated in vacuo and dissolved in DCM. The organic layer was washed with saturated $NaHCO_3$, dried over Na_2SO_4 then concentrated *in vacuo* to give the title compound as a colourless oil (102.7 mg, 86 %). NMR δ_H (500 MHz, $CDCl_3$, Me_4Si, 323K) 5.10 (s br, 1H, 24-N*H*Boc), 3.22-3.14 (m, 4H, 8- and 23-CH_2), 3.13-3.05 (m, 8H, 10-, 14-, 17- and 21-CH_2), 3.02 (m, 2H, 4-CH_2), 2.65 (br s, 2H, 1- N*H*2), 1.72 – 1.64 (m, 2H, 22-CH_2), 1.63 - 1.54 (m, 4H, 9- and 3-CH_2), 1.46 – 1.40 (m, 4H, 15- and 16- CH_2), 1.40 - 1.33 (m, 36H, 7-, 13-, 20- and 27-CH_3,); NMR δ_C (125 MHz, $CDCl_3$, Me_4Si, 323K) 155.9, 155.7, 155.5, 155.4, (5-, 11-, 18- and 25-C), 79.4, 79.3, 79.2, 78.9, (6-, 12-, 19- and 26-C), 46.8 (14-C and 17-C), 44.9 (21-C) 44.8 (10-C) 44.4 (4- and 8-C), 44.1 (23-C), 39.3 (2-C), 37.9 (22-C), 32.4 (9-C), 28.5 (6-, 12-, 19- and 26-C), 27.7 (3-C), 25.8 (15-and 16-C); MS (ES+) 661 $[M+H]^+$; HRMS (ES^+) $[M+H]^+$ $C_{33}H_{66}N_5O_8$ requires 660.4911 found 660.4943.

Diethyl (4-bromobutyl)phosphonate (142)[239]

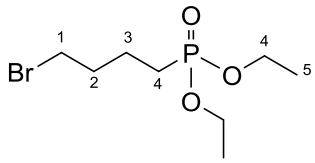

Dibromobutane (0.432 g, 2.00 mmol) and triethyl phosphite (0.107 g, 0.67 mmol) were heated to 180 ^{o}C in a microwave reactor, for 2.5 minutes. The reaction mixture was cooled then purified by flash column chromatography, using 10:1 petroleum ether : ethyl acetate, to yield the title compound as a colourless oil (0.359 g, 65%) δ_H (400 MHz; $CDCl_3$; Me_4Si, 298K) 4.09 (m, 4H, 5-CH_2), 3.40 (td, 2H, J = 6.7, $^2J_{HP}$ = 1.8, 4-CH_2), 1.94 (m, 2H, 1-CH_2), 1.75 (m, 4H, 3-CH2, 2-CH_2); δ_P (100 MHz; $CDCl_3$; Me_4Si, 298K) 31.5; δ_C (100 MHz; $CDCl_3$; Me_4Si, 298K) 61.7 (4-C), 32.7 (1-C), 25.4 (4-C) , 24.0 (2-C), 21.1 (3-C), 16.3 (5-C). MS (ES^+) 274 $[M+H]^+$.

7.3: Alkynes

5-(trifluoromethyl)-2-((trimethylsilyl)ethynyl)pyridine (143)

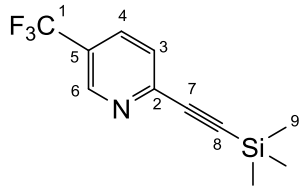

2-bromo-5-(trifluoromethyl)pyridine (0.5066 g, 2.24 mmol), bis(triphenylphosphine) palladium(II) dichloride (0.0765 g, 0.11 mmol) and copper iodide (0.0236 g, 0.12 mmol) were added to a round bottomed flask under a positive pressure of nitrogen. The flask was sealed with a septum then purged with nitrogen. Triethylamine (15 mL) and ethynyltrimethylsilane (1.56 mL, 11 mmol) were then added via the septum. The reaction was stirred under nitrogen for 1 h at 50 °C, then cooled to room temperature. Diethyl ether (20mL) was added to the reaction mixture, filtered through Celite then washed with saturated aqueous ammonium chloride (3 x 25mL). The organic extract was dried over sodium sulfate and concentrated *in vacuo*. The residue was purified by filtration through a short silica plug; by-products were removed with 9:1 hexane: ethyl acetate, and the product eluted with 100% ethyl acetate and concentrated in vacuo to give the title compound as an off-white solid, (396.4 mg, 73 %). NMR δ_H (400 MHz, $CDCl_3$, $SiMe_4$, 298K) 8.57 (s br, 1H, 6-CH), 7.72 (d, 1H, *J*=8.2, 4-C*H*), 7.41 (1H, d, *J* =8.2Hz, 3-C*H*), 0.28 (9H, s, 9-(CH_3)$_3$); NMR δ_C (100 MHz, $CDCl_3$, $SiMe_4$, 298K) 146.9 (q, $^3J_{CF}$ = 4.8, 6-C), 146.8 (2-C), 133.7 (m, 4-C), 126.9 (3-C), 125.8 (q, $^2J_{CF}$ = 33.6, 5-C), 123.1 (q, $^1J_{CF}$ = 271.6, 1-C), 102.8 (7-C), 98.5 (8-C), -0.30 (9-C); δ_F (376 MHz, $CDCl_3$, $SiMe_4$) -62.5 (1-CF_3); *m/z* (ES+) 244 $[M+H]^+$; HRMS (ES+) $C_{11}H_{13}NF_3Si$ requires 244.0769 found 244.0774.

4-(trifluoromethyl)-2-((trimethylsilyl)ethynyl)pyridine (144)

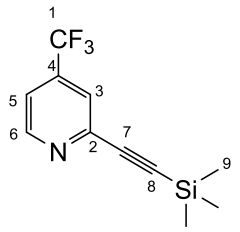

2-chloro-4-(trifluoromethyl)pyridine (181.8 mg, 1.0 mmol), bis(triphenylphosphine) palladium(II) dichloride (44.4 mg, 0.07 mmol) triphenylphosphine (33.0 mg, 0.14 mmol) and copper iodide (20.7 mg, 0.14 mmol) were added to a Schlenk flask under a positive pressure of nitrogen. The flask was sealed with a septum then purged with nitrogen. Dry THF (6 mL) triethylamine (1.5 mL) and ethynyltrimethylsilane (156 µL, 11 mmol) were then added via the septum. The reaction was stirred under nitrogen overnight at 55 °C, then cooled to room temperature. Diethyl ether (20mL) was added to the reaction mixture, filtered through Celite, and washed with saturated NH_4Cl solution (3 x 25mL). The organic extract was dried over $MgSO_4$ and concentrated *in vacuo*. The residue was purified by filtration through a short silica plug; by-products were removed with 9:1 hexane: ethyl acetate, and the product eluted with 100% ethyl acetate and concentrated in vacuo to give the title compound as a pale brown oil, (230.6 mg, 95 %). NMR δ_H (400 MHz, $CDCl_3$, $SiMe_4$, 298K) 8.66 (d br, *J* = 4.8, 1H, 6-C*H*), 7.48 (m, 1H, 3-C*H*), 7.25 (1H, dd, ^3J = 5.2, ^4J = 1.0, 5-C*H*), 0.10 (9H, s, 9-(CH_3)$_3$); NMR δ_C (100 MHz, $CDCl_3$, $SiMe_4$, 298K) 149.9 (6-C), 144.8 (2-C), 124.2 (m, 3-C), 123.4 (4-C), 121.5 (5-C), 118.9 (1-C), 102.8 (7-C), 98.5 (8-C), -0.20 (9-C); δ_F (376 MHz, $CDCl_3$, $SiMe_4$) -65.0 (1-CF_3); *m/z* (ES+) 244 $[M+H]^+$; HRMS (ES+) $C_{11}H_{13}NF_3Si$ requires 244.0769 found 244.0774.

5-methoxy-2-((trimethylsilyl)-ethynyl)pyridine (145)

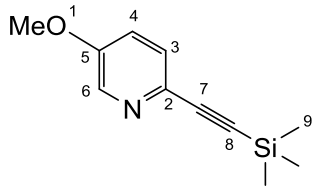

A Schlenk tube was purged with nitrogen then 2-bromo-5-methoxypyridine (358.4 mg, 1.76 mmol), bis(triphenylphosphine) palladium(II) dichloride (61.9 mg, 0.09 mmol), triphenylphosphine (74.8 mg, 0.35 mmol) and copper iodide (90.3 mg, 0.35 mmol) were added under a positive pressure of nitrogen. Tetrahydrofuran (4mL), triethylamine (360 µL, 2.60 mmol) and ethynyltrimethylsilane (375 µL, 2.63 mmol) were added to the tube, then flash frozen in liquid nitrogen and degassed (three freeze-pump-thaw cycles). The reaction mixture was stirred under nitrogen overnight. The crude reaction mixture was filtered through celite. Diethyl ether (15mL) was added to the reaction mixture which was then washed with saturated aqueous ammonium chloride (3 x 10mL). The organic layer was dried over magnesium sulfate, filtered and concentrated *in vacuo*. The product was purified by passing through a short silica plug; impurities were eluted with 9:1 hexane: ethyl acetate and the product eluted with ethyl acetate. Solvent was removed in vacuo to yield an off white solid (366.6 mg, 94 %) NMR δ_H (400 MHz, $CDCl_3$ $SiMe_4$) 8.25 (1H, dd, *J*=3.0, 0.6Hz, 6-C*H*), 7.40 (1H, dd, *J*=8.3, 0,6Hz, 3-C*H*), 7.12 (1H, dd, *J*=8.3, 3.0Hz, 4-C*H*); 3.86 (3H, s, 1-CH_3), 0.25 (9H, s, 5-(CH_3)$_3$); NMR δ_C (100 MHz, $CDCl_3$, $SiMe_4$) 155.2 (2-C), 138.1 (6-C), 132.0 (5-C), 128.1 (4-C), 124.3 (3-C), 103.7 (7-C), 92.9 (8-C), 55.9 (1-C), -0.17 (9-C); *m/z* (ES+) 206 $[M+H]^+$; HRMS (ES+) $C_{11}H_{16}NOSi$ requires 206.1005 found 206.1001.

5-(chloromethyl)-2-((trimethylsilyl)ethynyl)pyridine (145)

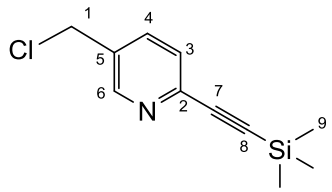

(6-((trimethylsilyl)ethynyl)pyridin-3-yl)methanol (204.2 mg, 1 mmol) was dissolved in dry DCM (10 mL) to which thionyl chloride (2 mL, 27 mmol) was added dropwise at 0 °C, then left to stir overnight. The reaction was quenched with 2M aqueous Na_2CO_3, then extracted with DCM (3 x 20 mL). The organic extracts were dried over magnesium sulfate, and solvent removed under reduced pressure to give the title compound as a waxy brown solid, (198.8 mg, 89 %) NMR δ_H (500 MHz, $CDCl_3$, Me_4Si, 298K) 8.57 (s, 1H, 6-C*H*), 7.70 (dd, 1H, ^3J = 7.9, ^4J =2.2, 4-C*H*), 7.46 (d, 1H, *J* = 7.9,3-C*H*), 4.58 (s, 2*H*, 1-CH_2), 0.32 - 0.24 (s, 9H, 9-CH_3); NMR δ_C (125 MHz, $CDCl_3$, Me_4Si, 298K) 150.0 (6-C), 143.3 (2-C) 136.6 (4-C), 132.6 (5-C) 127.4 (3-C), 103.5 (7-C). 96.2 (8-C), 43.1 (1-C), 0.3 (9-C); MS (ES^+) 224 $[M+H]^+$; HRMS (ES^+) $C_{11}H_{15}N^{28}Si^{35}Cl$ requires 224.0662 found 224.0670.

7.4: Proligands

Ethyl 5-(4-(pyridin-2-yl)-1H-1,2,3-triazol-1-yl)pentanoate "COOEt pyta" (150)

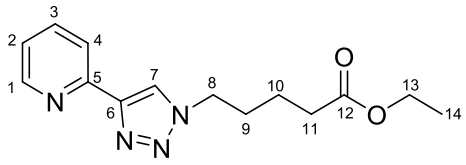

Ethyl 5-bromopentanoate (0.209 mg, 1.07 mmol) was dissolved in water: *tert*-butanol 1:1 (4 mL) and sodium azide (79 mg, 1.2 mmol) was added. The solution was degassed with nitrogen and heated in a microwave reactor to 125 ^{o}C for 15 minutes. $CuSO_4.5H_2O$ (15 mg, 60 µmol) and sodium ascorbate (24 mg, 120 µmol) were added followed by ethynyl pyridine (104 µL, 1.03 mmol) and heated in the microwave reactor for a further 30 minutes at 125 ^{o}C. Saturated ethylenediaminetetraacetic acid solution (adjusted to pH 10 with ammonium hydroxide) was added, and the mixture stirred at room temperature for 15 minutes. The reaction mixture was extracted with ethyl acetate (3 x 10 mL) and the organic layer separated and washed with water (10 mL) then saturated sodium chloride solution (10 mL). The organic layer was dried over anhydrous magnesium sulfate and was evaporated to dryness to afford the title compound as a straw-coloured oil (109 mg, 40%). NMR δ_H (400 MHz, $CDCl_3$, Me_4Si) 8.57 (ddd, 1H, ^3J = 4.7, ^4J = 1.6, ^5J = 0.9, 1-C*H*), 8.16 (app dt, 1H, ^3J = 8.1, ^4J =0.8, 4-C*H*), 8.15 (s, 1H, 7-C*H*), 7.76 (m, 1H, 3-C*H*), 7.21 (ddd, 1H, ^3J = 7.4, 4.8, ^4J = 1.2, 2-C*H*), 4.4 (t, 2H, 8-C*H*), 4.06 (q, 2H, *J* = 5.6, 13-CH_2), 2.30 (t, 2H, *J* = 7.3, 11-CH_2), 2.01 – 1.94 (m, 2H, 9-CH_2), 1.67 – 1.61 (m, 2H, 10-CH_2), 1.18 (t, 3H, *J* = 7.1, 14-CH_3); NMR δ_C (100 MHz, $CDCl_3$, Me_4Si) 172.9 (12-C) 150.1 (1-C), 149.4 (3-C), 148.2 (5- C), 137.0 (1-C), 122.8 (6-C), 121.9 (3-C), 120.3 (2-C), 122.1 (7-C), 120.3 (4-C), 60.6 (13-C), 50.2 (8-C), 33.6 (11-C), 29.7 (9-C), 21.9 (10-C), 14.4 (14-C); MS (ES+) $[M+Na]^+$ 297, $[M+H]^+$ 275; HRMS (ES+) $C_{14}H_{19}N_4O_2$ $[M+H]^+$ requires 275.1508 found 275.1518.

Diethyl (4-(4-(pyridin-2-yl)-1H-1,2,3-triazol-1-yl)butyl)phosphonate "PO(OEt)$_2$ pyta" (151)

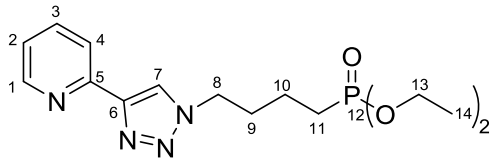

Phosphonate (**155**) (199 mg, 0.73 mmol) and NaN_3 (52 mg, 0.80 mmol) were dissolved in a 4:1 mixture of THF: water, (10 mL), and stirred at 80 ^oC overnight, under a nitrogen atmosphere. $CuSO_4.5H_2O$ (9 mg, 36 µmol) sodium ascorbate (15 mg, 76 µmol) and ethynyl pyridine (81 µL, 79 mmol) were added which was stirred for 4 h at 60 ^oC for 4 h. Saturated EDTA solution (adjusted to pH 10 with ammonium hydroxide) was added, and the mixture stirred for 15 minutes. The reaction mixture was extracted with ethyl acetate (3 x 30 mL) and the organic layer separated and washed with water (20 mL) and saturated sodium chloride solution (20 mL). The organic layer was dried over anhydrous magnesium sulfate and evaporated to dryness to afford the title compound as a yellow oil (185 mg, 93%). NMR δ_H (400 MHz, $CDCl_3$, Me_4Si) 8.5 (ddd, 1H, ^3J = 4.9, ^4J = 1.7, ^5J = 0.9, 1-C*H*), 8.15 (m, 1H, 4-C*H*), 8.13 (s, 1H, 7-C*H*), 7.78 (app td, 1H, ^3J = 7.8, ^4J = 1.7, 3-C*H*), 7.23 (ddd, 1H, ^3J = 7.6, 3.8, ^4J = 1.1, 2-C*H*), 4.44 (t, 2H, J = 7.1, 8-CH_2), 4.14 – 4.02 (m, 2H, 11-CH_2), 2.08 (app quin, 2H, J = 7.5, 11-CH_2), 1.83 – 1.63 (m, 2H, 9-CH_2, 10-CH_2), 1.42 (s, 9H, 15-CH_3); NMR δ_P (162 MHz, $CDCl_3$, Me_4Si) 30.79; NMR δ_C (100 MHz, $CDCl_3$, Me_4Si) 150.1 (13-C), 149.4 (5-C), 148.5 (5- C), 149.6 (1-C), 148.6 (6-C), 137.0 (3-C), 122.8 (2-C), 121.8 (7-C), 120.3 (4-C), 50.8 (8-C), 49.8 (13-C), 30.8 (11-C), 29.7 (2-C), 25.6 (9-C) 19.7 (10-C) 16.5 (14-C); MS (ES$^+$) 361 $[M+Na]^+$ 361 $[M+H]^+$ 339; HRMS (ES$^+$) $C_{15}H_{24}N_4O_3P$ $[M+H]^+$ requires 339.1586 found 339.1599.

2-(1-(2-(2-(2-methoxyethoxy)ethoxy)ethyl)-1H-1,2,3-triazol-4-yl)pyridine "PEG pyta" (152)

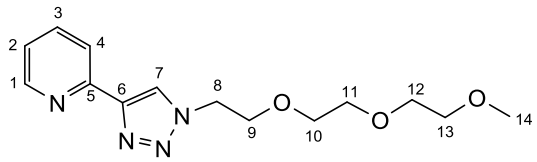

2-(2-(2-methoxyethoxy)ethoxy)ethyl 4-methylbenzenesulfonate "PEG-OTs" (**141**) (611.3 mg, 1.92 mmol) and NaN_3 (137.3 mg, 2.11 mmol) were dissolved in a 5:1 mixture of acetone: water, (10 mL), and stirred at 80 ^{o}C overnight, under a nitrogen atmosphere. $CuSO_4.5H_2O$ (42.9 mg, 0.19 mmol), sodium ascorbate (80.6 mg, 0.38mmol) and ethynyl pyridine (198.1 mg, 1.92 mmol) were added which was stirred for 4 h at 60 ^{o}C for 4 h. Saturated EDTA solution (6 mL) (adjusted to pH 10 with ammonium hydroxide) was added, and the mixture stirred for 15 minutes. The reaction mixture was extracted with DCM (3 x 50 mL) then with ethyl acetate (3 x 50 mL) and the organic layer separated and washed with water (20 mL) and saturated sodium chloride solution (20 mL). The organic layer was dried over anhydrous magnesium sulfate and evaporated to dryness to afford the title compound as a yellow oil (489.3 mg, 87 %). NMR δ_H (400 MHz, $CDCl_3$, Me_4Si, 298K) 8.58 (d, 1H *J* = 4.2, 1-C*H*), 8.33 (s, 1H, 7-C*H*), 8.16 (d, 1H, *J* = 7.9, 4-C*H*), 7.77 (dt, 1H, ^3J = 7.7, ^3J = 1.8, 3-C*H*), 7.22 (ddd, ^3J = 7.5, ^4J =4.9, ^5J =1.9, 2-CH_2), 4.62 (t, 2H, *J* = 5.1, 8-CH_2), 3.93 (t, *J* = 5.2 Hz, 2H, 9-CH_2), 3.66 - 3.62 (m, 2H, 12-CH_2), 3.62 - 3.57 (m, 4H, 10- and 11- CH_2), 3.54 - 3.51 (m, 2H, 13- CH_2), 3.36 (s, 3H, 14-CH_3); NMR δ_C (100 MHz, $CDCl_3$, Me_4Si) 150.4 (1-C), 149.3 (5-C), 148.2 (6-C), 136.9 (3-C), 123.2 (7-C), 122.7 (2-C), 120.2 (4-C), 71.8 (13-C), 70.6, 70.5, 70.4 (10-, 11- and 12-C) 69.4 (9-C), 58.9 (14-C), 50.1 (8-C). MS (ES^+) 293 $[M+H]^+$; HRMS (ES+) $C_{14}H_{21}N_4O_3$ $[M+H]^+$ requires 293.1614 found 293.1616.

General Method A for one pot diazo-transfer CuAAC (unsubstituted ligands)

Boc-protected amine (0.5 mmol) was dissolved in MeOH (4 mL) and H_2O (2 mL). Sodium hydrogen carbonate (168 mg, 2.5 mmol) and $CuSO_4.5H_2O$ (14 mg, 55 µmol) were added followed by $ISA.H_2SO_4$ (0.55 mmol). The reaction was stirred at room temperature for 4 h while keeping the pH above 8 with $NaHCO_3$. Sodium ascorbate (22 mg, 110 µmol) and ethynyl pyridine (50 µL, 0.5 mmol) were added and the mixture stirred overnight at room temperature. Saturated EDTA solution (adjusted to pH 10 with ammonium hydroxide) was added to the mixture and stirred for 15 minutes. The reaction mixture was extracted with EtOAc (3 x 30 mL). Combined organic layers were washed with water (20 mL) then brine (20 mL). The organic layer was dried over anhydrous Na_2SO_4 and was evaporated to dryness.

tert-butyl (4-(4-(pyridin-2-yl)-1H-1,2,3-triazol-1-yl)butyl)carbamate, "BocPut pyta" (149)

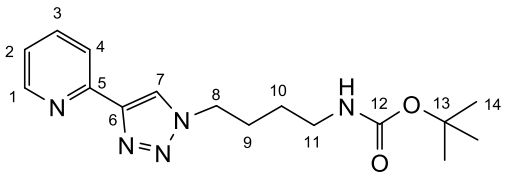

Compound (137) (0.207 g, 1.10 mmol) was reacted with $NaHCO_3$ (0.307 g, 3.65 mmol) and $CuSO_4$ solution (1.28 M (aq), 50 µL, 64 µmol) and $ISA.H_2SO_4$ (0.313 g, 1.15 mmol) according to general method A, followed by sodium ascorbate (22 mg, 110 µmol) and ethynylpyridine (50 µL, 0.5 mmol) to give the title compound as a white solid, m.p. = 54–55 ^oC, (0.250 g, 79%). NMR δ_H (400 MHz, $CDCl_3$, Me_4Si) 8.56 (ddd, 1H, ^3J = 4.8, ^4J = 1.8, ^5J = 1.1, 1-C*H*), 8.15 (ddd, 1H, ^3J = 7.8, ^4_J =1.2, ^5J = 0.9, 4-C*H*), 8.12 (s, 1H, 7-C*H*), 7.76 (ddd, 1H, ^3J = 7.7, 7.8, ^4J = 1.8, 3-C*H*), 7.22 (ddd, 1H, ^{3}J = 7.6, 4.9, ^4J = 1.2, 2-CH), 4.60 (s br, 1H, 12-N*H*), 4.44 (t, 2H, *J* = 7.1, 8-CH_2), 3.19 – 3.12 (m, 2H, 11-CH_2), 2.02 – 1.97 (m, 2H, 9-CH_2), 1.57 – 1.50 (m, 2H, 10-CH_2), 1.42 (s, 9H, 15-CH_3); NMR δ_C (100 MHz, $CDCl_3$, Me_4Si) 156.0 (13-C), 150.3 (5-C), 149.4 (1-C), 148.5 (6-C), 137.0 (3-C), 122.9 (2-C), 121.9 (7-C), 120.2 (4-C), 79.3 (14-C), 50.0 (8-C), 39.7 (11-C), 28.4 (15-C), 27.5 (9-C), 27.1 (10-C); MS (ES^+) 340 $[M+Na]^+$; HRMS (ES^+) $C_{16}H_{24}N_5O_2$ $[M+H]^+$ requires 318.1930 found 318.1937.

tert-butyl (4-((tert-butoxycarbonyl)amino)butyl)(3-(4-(pyridin-2-yl)-1H-1,2,3-triazol-1-yl)propyl)carbamate "BocAPPut pyta" (154)

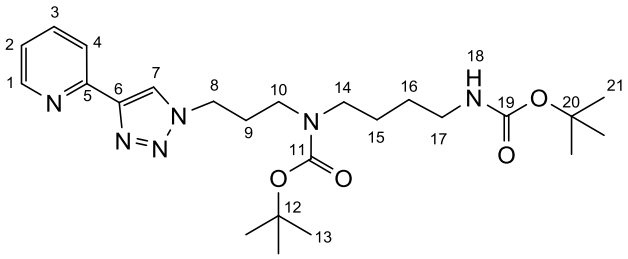

Amine (**210**) (345.5 mg, 0.96 mmol), was reacted with ISA.H_2SO_4 (270.1 mg, 1.0 mmol), $CuSO_4.5H_2O$ (32.5 mg, 0.13 mmol), and $NaHCO_3$ (869.9 mg, 10.4 mmol) as described in general method A, followed by sodium ascorbate (40 mg, 0.2 mmol) and ethynylpyridine (101 µL, 1.0 mmol) to give the title compound as a sticky gum, which was purified by flash column chromatography using 10 % MeOH in DCM, (367.2 mg, 74 %). NMR δ_H (400 MHz, $CDCl_3$, Me_4Si, 320K) 8.59 (ddd, 1H, ^3J = 4.8, ^4J = 1.8, ^5J = 0.8, 1-C*H*), 8.17 (m, 2H, 4- and 7-C*H*), 7.78 (ddd, 1H, ^3J = 7.7, 7.8, ^4J = 1.8, 3-C*H*), 7.23 (ddd, 1H, ^3J = 7.5, 4.9, ^4J = 1.2, 2-C*H*), 4. 85 (s br, 1H, 18-N*H*), 4.44 (m, 2H, 8-CH_2), 3.36 – 3.26 (m, 2H, 10-CH_2), 3.26 – 3.17 (m, 2H, 14-CH_2), 3.17 – 3.06 (m, 2H, 17-CH_2), 2.22 (s, 9H, 9-CH_3) 1.52 – 1.43 (m, 4H, 16- and 15-CH_2) 1.46 (s, 9H, 13-CH_3) 1.45 (s, 9H, 21-CH_3); NMR δ_C (100 MHz, $CDCl_3$, Me_4Si, 320K) 156.0 (19-C), 155.6 (11-C), 150.4 (5-C), 149.4 (1-C), 148.5 (6-C), 136.7 (3-C), 122.7 (2-C), 122.0 (7-C), 120.2 (4-C), 79.8 (12-C), 79.1 (20-C), 48.2 (8-C), 47.1 (14-C), 44.4 (10-C), 40.3 (17-C), 29.4 (9-C), 28.5, 28.4 (13- and 21-C), 27.4 (16-C) 25.7 (15-C); MS (ES^+) 497 $[M+Na]^+$; HRMS (ES^+) $C_{24}H_{39}N_6O_4$ $[M+H]^+$ requires 497.2852 found 497.2852.

tert-butyl (4-((tert-butoxycarbonyl)(3-((tert-butoxycarbonyl)amino)propyl)amino)butyl)(3-(4-(pyridin-2-yl)-1H-1,2,3-triazol-1-yl)propyl)carbamate "BocSpm pyta" (155)

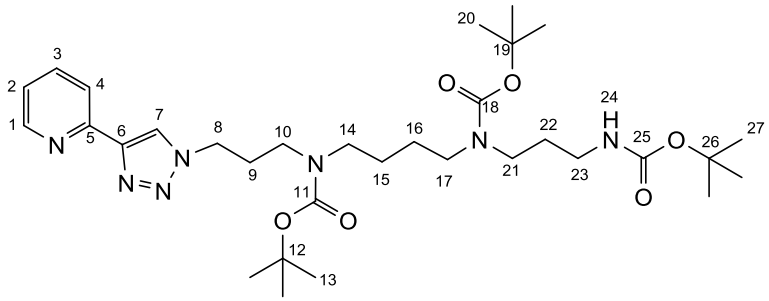

Amine (**138**) (262.9 mg, 0.52 mmol), was reacted with ISA.H_2SO_4 (147.1 mg, 0.54 mmol), $CuSO_4.5H_2O$ (148.0 mg, 0.55 mmol), and $NaHCO_3$ (850.1 mg, 10.1 mmol) as described in general method A, followed by sodium ascorbate (19.6 mg, 0.1 mmol) and ethynylpyridine (51.5 mg, 0.5 mmol) to give the title compound as a sticky gum (188.6 mg, 57 %). NMR δ_H (500 MHz, $CDCl_3$, CD_3OD, 323K) 8.63 (m br, 1H, 1-C*H*), 8.44 (s, 1H, 7-C*H*), (ddd, 1H, ^3J = 7.8, ^4_J =1.2, ^5J = 0.9, 4-C*H*), 8.09 (d, 1H, ^3J = 7.8, 4-C*H*), 7.91 (dt, 1H, ^{3}J = 7.7, ^4J = 1.6, 3-C*H*), 7.37 (m, 1H, 2-C*H*) 5.19 – 5.07 (m br, 1H, 24-N*H*), 4.53 (t, 2H, *J* = 6.9, 8-CH_2), 3.32 – 3.23 (m, 2H, 10-CH_2), 3.22 – 3.12 (m, 6H, 21-, 17- and 14-CH_2), 3.05 (t, 2H, *J* = 6.7, 23-CH_2), 2.33 – 2.11 (m, 2H, 9-CH_2), 1.79 – 1.60 (m, 2H, 22-CH_2), 1.57 – 1.46 (m, 4H, 15, 16-CH_2), 1.47 (s, 18H, 13- and 20-CH_3)1.42 (s, 9H,27-CH_3); NMR δ_C (100 MHz, CD_3OD, 323K) 158.4, 157.4 (11, 18, 25-C), 151.1 (5-C), 150.5 (1-C), 148.8 (6-C), 138.8 (3-C), 127.7 (2-C), 124.5 (7-C), 121.5 (4-C), 81.2, 80.9, 80.0 (12-, 18- and 26-C), 48.2 (8-C), 47.8 (14-C), 46.1 (17-C), 45.8 (10-C) 44.6 (21-C), 38.9 (23-C), 30.4 (9-C), 30.3 (22-C), 30.2 (13, 20, 27-C), 28.8 (15, 16-C), 26.6 (15, 16-C); MS (ES^+) 633 $[M+Na]^+$; HRMS (ES+) $C_{32}H_{54}N_7O_6$ $[M+H]^+$ requires 632.4136 found 632.4150.

tert-butyl (4-((tert-butoxycarbonyl)(3-((tert-butoxycarbonyl)(3-(4-(pyridin-2-yl)-1H-1,2,3-triazol-1-yl)propyl)amino)propyl)amino)butyl)(3-((tert-butoxycarbonyl)amino)propyl)carbamate "BocAPSpm pyta" (156)

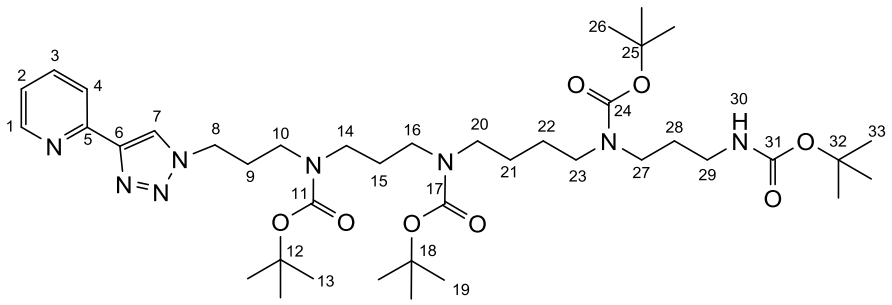

Amine (**213**) (373.4 mg, 0.62 mmol), was reacted with ISA.H_2SO_4 (168.8 mg, 0.62 mmol), $CuSO_4.5H_2O$ (15.5 mg, 0.06 mmol), and $NaHCO_3$ (522.9 mg, xx mmol) as described in general method A, followed by sodium ascorbate (24.7 mg, 0.12 mmol) and ethynylpyridine (65.5 µL, 0.62 mmol), then purified by flash column chromatography using 3 % MeOH in DCM, to give the title compound as a sticky gum (397.8 mg, 81 %). NMR δ_H (400 MHz, $CDCl_3$, Me_4Si, 320K) 8.49 (ddd, 1H, ^3J = 5.0, ^4J = 1.8, ^3J = 0.9, 1-C*H*), 8.11 (br s, 1H, 7-C*H*), 8.08 (td, ^3J = 7.9, ^4J =1.1, 4-C*H*), 7.69 (dt, ^3J = 7.7, ^4J = 1.8, 3-C*H*), 7.14 (ddd, ^3J = 7.5, ^4J = 1.2, ^5J = 1.2, 2-C*H*), 5.22 (s br, 1H, 30-N*H*), 4.36 (t, 2H, *J* = 7.1, 8-CH_2), 3.27 – 3.20 (m, 2H, 10-CH_2), 3.16 (t, 2H *, J* = 6.6, 14-CH_2), 3.14 - 3.04 (m, 8H, 16, 20, 23, 27-CH_2), 3.04 – 2.99 (m, 2H, 29-CH_2), 2.14 (quin, 2H, *J* = 7.0, 9-CH_2), 1.70 - 1.62 (m, 2H*, 2*9-CH_2), 1.62 - 1.54 (m, 15-CH_2), 1.43 - 1.39 (m, 4H, 20, 21-CH_2), 1.38 – 1.36 (m, 36, 13, 19, 26, 33-CH_3); NMR δ_C (100 MHz, $CDCl_3$, Me_4Si, 320K) 156.0, 155.4 (11, 17, 24, 31), 150.4 (5-C), 149.4 (1-C), 148.5 (6-C), 136.7 (3-C), 122.7 (2-C), 122.1 (7-C), 120.2 (4-C), 79. 9, 79.5, 79.3, 77.2, (12, 18, 25, 32-C) 48.2 (8-C), 46.8 (14-C), 46.7 (16-C), 46.7 (10-C), 45.3 (14-C), 44.8 (23-C), 44.5 (20-C), 44.1 (27-C), 29.3 (29-C), 28.5 (13, 19, 26, 33-C) 25.9 (9, 28-C), 25.8 (15, 21, 22-C); MS (ES^+) 789 $[M+Na]^+$; HRMS (ES^+) $C_{40}H_{69}N_8O_8$ $[M+H]^+$ requires 789.5238 found 789.5237.

General Method B for one pot diazo-transfer CuAAC (substituted ligands)

The azide is formed as described in general method A; briefly Boc-protected amine (0.5 mmol) in MeOH (4 mL) and H_2O (2 mL) was reacted with $NaHCO_3$ (168 mg, 2.5 mmol), $CuSO_4.5H_2O$ (14 mg, 55 µmol) and $ISA.H_2SO_4$ (0.55 mmol). The reaction was stirred at room temperature for 4 h at a pH above 8. Sodium ascorbate (22 mg, 110 µmol), substituted alkyne, (0.5 mmol) and K_2CO_3 (0.5 mmol) were added and the mixture stirred overnight at room temperature. The reaction was worked up as described in general method A, to give the substituted proligand.

tert-butyl (4-((tert-butoxycarbonyl)(3-((tert-butoxycarbonyl)amino)propyl)amino)butyl)(3-(4-(5-(trifluoromethyl)pyridin-2-yl)-1H-1,2,3-triazol-1-yl)propyl)carbamate "5CF_3 BocSpm pyta" (157)

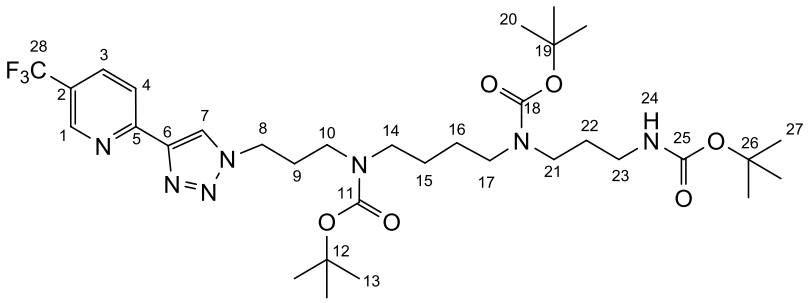

Amine (**138**) (142.6 mg, 0.28 mmol), was reacted with $NaHCO_3$ (168 mg, 2.5 mmol), $CuSO_4.5H_2O$ (15.2 mg, 0.06) and $ISA.H_2SO_4$ (84.6 mg, 0.29 mmol) as described in general method B. Addition of sodium ascorbate (11.3 mg mg, 0.06 mmol), alkyne (**153**), (0.5 mmol) and K_2CO_3 (43.2 mg, 0.31 mmol) gave the title compound as a sticky gum which gave (137.4 mg, 70 %). NMR δ_H (400 MHz, $CDCl_3$, Me_4Si, 298K) 8.72 (m, 1H, 1-C*H*), 8.26 - 8.08 (m, 2H, 7, 4-C*H*), 7.90 (dd, 1H, ^3J = 8.4, ^4J = 2.2, 3-C*H*), 5.12 (s br, 1H, 24-N*H*), 4.42 – 4.25 (m, 2H, 8-CH_2), 3.31 -2.88 (m, 10H, 10, 14, 17, 21, 23-CH_2), 2.21 – 2.03 (m, 2H, 9-CH_2), 1.59 – 1.46 (m, 2H, 23-CH_2), 1.43 – 1.35 (m, 4H, 15, 16-CH_2), 1. 34 - 1.25 (m, 27H, 13, 20, 27-CH_3); NMR δ_C (100 MHz, $CDCl_3$, Me_4Si, 298K) 157.7, 157.4, (11, 18, 25-C), 153.5 (1-C), 146.5 (6-C), 134.1 (3-C), 134.0 (2-C), 123.4 (7-C), 119.6 (4-C), 79.9, 79.7 (12-, 18- and 26-C), 48.3 (8-C), 47.8 (14-C), 46.1 (17-C), 45.8 (10-C) 44.2 (21-C), 38.9 (23-C), 30.4 (9-C), 30.3 (22-C), 29.3 (13, 20, 27-C), 28.4 (15, 16-C), 25.9, 25.8 (15, 16-C); MS (ES^+) 701 $[M+H]^+$; HRMS (ES^+) $C_{33}H_{53}N_7O_6F_3$ $[M+H]^+$ requires 700.4009 found 700.4039.

tert-butyl (4-((tert-butoxycarbonyl)(3-((tert-butoxycarbonyl)amino)propyl)amino)butyl)(3-(4-(4-(trifluoromethyl)pyridin-2-yl)-1H-1,2,3-triazol-1-yl)propyl)carbamate "4-CF_3 BocSpm pyta" (158)

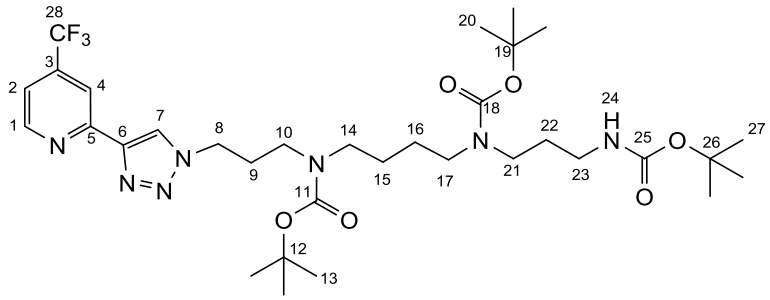

Amine (**138**) (149.5 mg, 0.30 mmol), was reacted with $NaHCO_3$ (1252 mg, 1.5 mmol), $CuSO_4$.5H2O (7.5 mg, 0.03 mmol) and ISA.H_2SO_4 (95.0 mg, 0.3 mmol) as described in general method B. Addition of Sodium ascorbate (11.7 mg, 0.12 mmol), alkyne (**154**), (72.3 mg, 0.3 mmol) and K_2CO_3 (41.5 mg, 0.5 mmol) gave the title compound as a sticky gum (190.2 mg, 91 %). NMR δ_H (500 MHz, $CDCl_3$, Me_4Si, 323K) 8.75 (d, 1H, *J* = 5.1, 1-C*H*), 8.41 (s, 1H, 7-C*H*), 8.23 (s br, 4-C*H*), 7.42 (dd, 1H, ^3J = 5.0, ^4J = 1.0, 2-C*H*), 5.06 (s br, 1H, 24-N*H*), 4.45 (t, 2H, *J* = 7.1, 8-CH_2), 3.30 (t, 2H, *J* = 6.9, 10-CH_2), 3.26 – 3.13 (m, 6H, 21-, 17- and 14-CH_2), 3.09 – 3.03 (m, 2H, 23-CH_2), 2.22 (t, 2H, *J* = 7.0, 9-CH_2), 1.66 (t br, 2H, *J* = 6.6, 22-CH_2), 1.51 -1.48 (m, 4H, 15, 16-CH_2), 1.47 (m, 18H, 13- and 20-CH_3)1.44 (s, 9H,27-CH_3); NMR δ_C (125 MHz, CDCl3, Me_4Si, 323K) 156.0, 155.6 (11, 18, 25-C), 153.6 (5-C), 150.3 (1-C), 146.5 (6-C), 135.7 (3-C), 125.3 (2-C), 123.2 (7-C), 119.6 (4-C), 79.9, 79.6, 77.8 (12-, 18- and 26-C), 48.3 (8-C), 46.9 (14-C), 46.7 (17-C), 44.4 (10-C) 44.2 (21-C), 37.8 (23-C), 29.3 (9-C), 29.1 (22-C), 28.4 (13, 20, 27-C), 27.5 (15, 16-C), 25.8 (15, 16-C); MS (ES+) 701 [M+H]+; HRMS (ES+) $C_{33}H_{53}N_7O_6F_3$ [M+H]+ requires 700.4009 found 700.4007.

tert-butyl (4-((tert-butoxycarbonyl)(3-((tert-butoxycarbonyl)amino)propyl)amino)butyl)(3-(4-(5-methoxypyridin-2-yl)-1H-1,2,3-triazol-1-yl)propyl)carbamate "5OMe BocSpm pyta" (159)

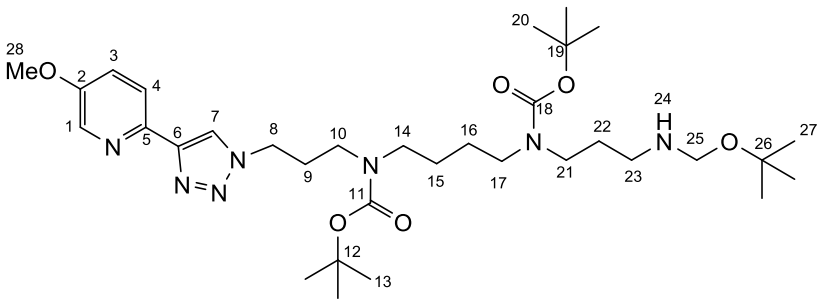

Amine (**138**) (266.5 mg, 0.49 mmol), was reacted with $NaHCO_3$ (455.5 mg, 4.87 mmol), $CuSO_4.5H_2O$ (14.2 mg, 55 µmol) and $ISA.H_2SO_4$ (150.0 mg, 0.49 mmol) as described in general method B. Addition of sodium ascorbate (25.0 mg, 110 µmol), alkyne (**155**), (0.5 mmol) and K_2CO_3 (0.5 mmol) gave the title compound as a sticky gum (177.4 mg, 55 %) after purification by flash column chromatography (10 % MeOH in DCM). NMR δ_H (400 MHz, $CDCl_3$, Me_4Si, 323K) 8.28 (dd, 1H, ^3J = 3.0, ^4J = 0.6, 1-C*H*), 8.10 (d, 1H, *J* = 8.8, 4-C*H*), 8.08 (s br, 1H, 7-C*H*), 7.30 (dd, 1H, ^3J = 8.7, ^4J = 3.0, 3-C*H*), 5.13 (m br, 1H, 24-N*H*), 4.42 (t, 2H, *J* = 7.1, 8-CH_2), 3.32 – 3.23 (m, 2H, 10-CH_2), 3.22 – 3.12 (m, 6H, 21-, 17- and 14-CH_2), 3.09 – 3.03 (m, 2H, 23-C*H*2), 2.19 (t br, 2H, *J* = 7.0, 9-CH_2), 1.70 – 1.57 (m, 2H, 22-CH_2), 1.44 (br s, 4H, 15, 16-CH_2), 1.43 (s, 18H, 13- and 20-CH_3)1.42 (s, 9H, 27-CH_3); NMR δ_C (100 MHz, CD_3OD, 323K) 156.1, 155.4 (11, 18, 25-C), 155.2 (1-C), 152.8 (5-C), 150.5 (6-C), 137.2 (3-C), 121.0 (2-C), 120.7 (7-C), 103.0 (4-C), 79.9, 78.2, 77.2 (12-, 18- and 26-C), 55.7 (28-C) 48.2 (8-C), 47.3 (14-C), 46.8 (17-C), 44.2 (10-C) 43.9 (21-C), 37.2 (23-C), 29.4 (9-C), 29.3 (22-C), 28.5, 28.4, 28.3 (13, 20, 27-C), 28.3 (15, 16-C), 25.7 (15, 16-C); MS (ES+) 684 $[M+Na]^+$; HRMS (ES+) $C_{33}H_{55}N_7O_7$ [M+Na]+ requires 684.4061 found 684.4058.

5-(chloromethyl)-2-(1-(2-(2-(2-methoxyethoxy)ethoxy)ethyl)-1H-1,2,3-triazol-4-yl)pyridine ClMePEG pyta" (153)

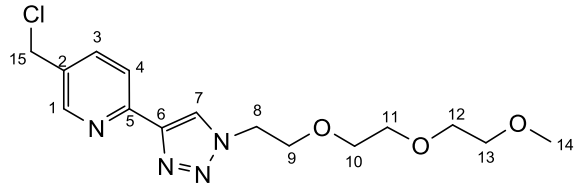

2-(2-(2-methoxyethoxy)ethoxy)ethyl 4-methylbenzenesulfonate "PEG-OTs" (**141**) (64.8, 0.205 mmol) and NaN_3 (14.1 mg, 0.21 mmol) were dissolved in a 4:1 mixture of THF: water, (10 mL), and stirred at 80 ^oC overnight, under a nitrogen atmosphere. $CuSO_4.5H_2O$ (5.3 mg, 0.02 mmol), sodium ascorbate (8.7 mg, 0.04mmol) K_2CO_3 (28.4 mg, 0.21 mmol), and 5-(chloromethyl)-2-((trimethylsilyl)ethynyl)pyridine (**148**) (45.9 mg, 0.21 mmol) were added which was stirred for 4 h at 60 ^oC for 4 h. Saturated EDTA solution (adjusted to pH 10 with ammonium hydroxide) was added, and the mixture stirred for 15 minutes. The reaction mixture was extracted with ethyl acetate (3 x 30 mL) and the organic layer separated and washed with water (20 mL) and saturated sodium chloride solution (20 mL). The organic layer was dried over anhydrous magnesium sulfate and evaporated to dryness to afford the title compound as a dark yellow oil (62.8 mg, 90 %). NMR δ_H (400 MHz, $CDCl_3$, Me_4Si, 298K) 8.60 (m, 1H, 1-C*H*), 8.33 (s, 1H, 7-C*H*), 8.16 (d br, 1H, *J* = 8.1, 4-C*H*), 7.81 (dd, 1H, ^3J = 9.1, ^3J = 2.0,3-C*H*), 4.65 – 4.58 (m, 4H, 15- and 8-CH_2), 3.93 (t, *J* = 5.0, 2H, 9-CH_2), 3.66 - 3.58 (m, 6H, 10-, 11- and 12-CH_2), 3.62 - 3.57 (m, 2H, 13- CH_2), 3.36 (s, 3H, 14-CH_3); NMR δ_C (100 MHz, $CDCl_3$, Me_4Si) 150.4 (1-C), 149.3 (5-C), 147.8 (6-C), 137.1 (3-C), 132.1 (7-C), 123.5 (2-C), 120.1 (4-C), 71.9 (13-C), 70.7, 70.6, 70.5 (10-, 11- and 12-C) 69.4 (9-C), 59.0 (14-C), 50.5 (8-C), 43.2 (15-C*H*2) MS (ES^+) 293 $[M+H]^+$.

7.5: Neutral Rhenium Complexes

General Method C for microwave synthesis of chlororhenium complexes

Ligand (0.1 mmol) was dissolved in THF (4 mL). $Re(CO)_5Cl$ (38.0 mg, 0.105 mmol) was added and the mixture was heated to 90 °C in a microwave reactor for 1 h. The mixture was filtered through Celite then the solvent was removed under reduced pressure to give the title compound as a yellow solid.

[Re(BocPut-pyta)$(CO)_3$Cl] (162)

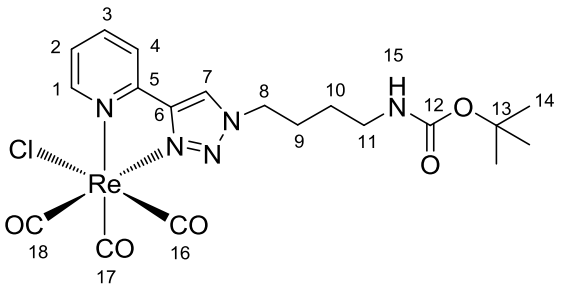

Proligand **149** (32.7 mg, 0.103 mmol) and $Re(CO)_5Cl$ (38.0 mg, 0.105 mmol) were reacted according to general method C giving the title compound as a yellow solid (59.0 mg, 89 %). NMR δ_H (400 MHz, $CDCl_3$, Me_4Si, 298 K) 8.96 (d, 1H, *J* = 5.4, 1-C*H*), 8.54 (s, 1H, 7-C*H*), 7.96 (ddd, ^3J = 7.9, 7.8, ^4J = 1.1, 1H, 3-C*H*), 7.86 (d, 1H, ^3J = 7.9, 4-C*H*), 7.42 (ddd, 1H, ^3J = 7.2, 5.5, ^4J = 1.1, 2-CH), 4.80 (s br, 1H, 12-N*H*), 4.54 – 4.42 (m , 2H, 8-CH_2), 3.21-3.10 (m, 2H, 14- CH_2), 2.03-1.92 (m, 2H, 9-CH_2), 1.61-1.49 (m, 2H, 10-CH_2), 1.45 (s, 9H, 15-CH_3); NMR δ_C (100 MHz, $CDCl_3$, Me_4Si) 156.3 (12-C), 153.2 (1-C), 149.2 (5-C), 148.7 (6-C), 139.5 (3-C), 125.8 (2-C), 124.0 (7-C), 122.1 (4-C), 79.4 (13-C), 51.5 (8-C), 39.1 (11-C), 28.5 (15-C), 27.0 (9-C), 26.8 (10-C), 25.5 (14-C); IR (solid state): ν_{CO} (cm^{-1}) 2015, 1892; HRMS (ES^+) $C_{27}H_{38}N_6O_7{}^{187}Re^+$[M-Cl]$^+$ requires 588.1257 found 588.1257.

[Re(COOEt-pyta)(CO)$_3$Cl] (163)

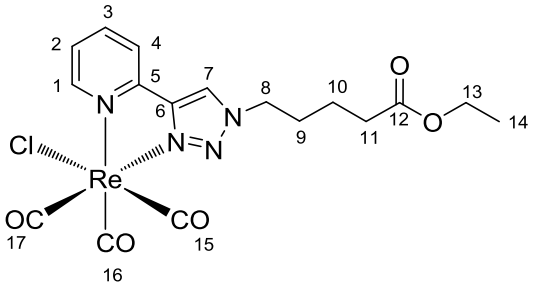

Proligand **150** (28.6 mg, 0.104 mmol) and $Re(CO)_5Cl$ (38.7 mg, 0.107 mmol) were reacted according to general method C. The complex was purified by flash column chromatography on silica, eluting yellow fractions with 10 % methanol in ethyl acetate to give the title compound as a yellow solid (39.7 mg, 68 %). NMR δ_H (400 MHz, $CDCl_3$, Me_4Si, 298 K) 8.96 (d, 1H, *J* = 5.4, 1-C*H*), 8.54 (s, 1H, 7-C*H*), 7.96 (ddd, ^3J = 7.9, 7.8, ^4J = 1.1, 1H, 3-C*H*), 7.86 (ad, 1H, *J* = 7.9, 4-C*H*), 7.42 (ddd, ^3J = 7.2, 5.5, ^4J = 1.1, 1H, 2-C*H*), 4.80 (s br, 1H, 12-N*H*), 4.58 – 4.46 (m , 2H, 8-CH_2), 3.21-3.10 (m, 2H, 14-CH_2), 2.03-1.92 (m, 2H, 9- CH_2), 1.61-1.49 (m, 2H, 10- CH_2), 1.45 (s, 9H, 15-CH_3); NMR δ_C (100 MHz, $CDCl_3$, Me_4Si, 298 K) 156.3 (13-C), 153.2 (1-C), 149.2 (5-C), 148.7 (6-C), 139.5 (3-C), 125.8 (2-C), 124.0 (7-C), 122.1 (4-C), 79.4 (13-C), 51.5 (8-C), 39.1 (11-C), 28.5 (15-C), 27.0 (9-C), 26.8 (10-C), 25.5 (14-C); IR (solid state): ν_{CO} (cm^{-1}) 2020, 1925; MS (ES+) 545 [M-Cl]+; HRMS (ES+) $C_{17}H_{21}N_5O_5{}^{187}Re$+[M-Cl]+ requires 545.0835 found 545.0835.

[Re(PO(OEt)$_2$-pyta)(CO)$_3$Cl] (164)

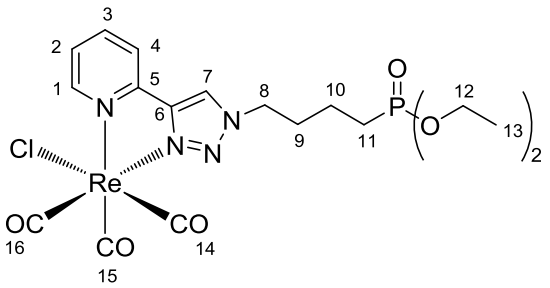

Proligand **151** (38.5 mg, 0.11 mmol) and $Re(CO)_5Cl$ (38.2 mg, 0.106 mmol) were reacted according to general method C. Solvent was evaporated *in vacuo* to give the title compound as a yellow solid (43.4 mg, 81 %). NMR δH (400 MHz, $CDCl_3$, Me_4Si, 298 K) 8.98 (ddd, 1H, ^3J = 5.5, ^4J = 1.4, ^5J = 0.8, 1-C*H*), 8.51 (s, 1H, 7-C*H*), 7.97 (td, 1H, ^3J = 8.0, ^4J

= 1.3, 3-C*H*), 7.86 (d, 1H, *J* = 7.7, 4-C*H*), 7.42 (ddd, 1H, ^{3}J = 7.5, 3.4, ^{4}J = 1.4, 2-CH), 4.80 (s br, 1H, 12-N*H*), 4.58 – 4.41 (m , 2H, 8-CH_2), 4.16 – 4.00 (m, 4H, 12- CH_2), 2.12-2.05 (m, 2H, 9- CH_2), 1.86 - 1.74 (m, 2H, 10- CH_2), 1.74 – 1.61 (m, 9H, 15- CH_3), 1.31 (td, ^{3}J = 7.1, $^{3}J_{31P,1H}$ = 3.5); NMR δ_P (162 MHz, $CDCl_3$, Me_4Si) 30.8; NMR δ_C (100 MHz, $CDCl_3$, Me_4Si) 197.2, 195.7, 188.9 (14, 15, 16-C), 153.0 (1-C), 149.1 (5-C), 148.7 (6-C), 139.5 (3-C), 125.9 (2-C), 124.0 (7-C), 122.3 (4-C), 61.8(12-C) 51.5 (8-C), 30.1 (11-C), 25.1 (9-C), 23.7 (10-C), 16.4 (13-C); MS (ES+) 667 $[M + Na]^+$ 609 $[M-Cl]^+$; HRMS (ES+) $C_{18}H_{23}N_4O_6P^{187}Re$ $[M-Cl]^+$ requires 609.0917 found 609.0913.

[Re(APBocPut-pyta)(CO)$_3$Cl] (165)

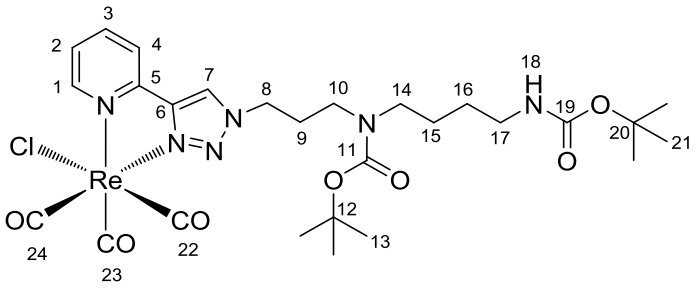

Proligand **154** (28.6 mg, 0.104 mmol) and $Re(CO)_5Cl$ (38.7 mg, 0.107 mmol) were reacted according to general method C, which after evaporation gave the title compound as a yellow solid (39.7 mg, 68 %). NMR δ_H (400 MHz, $CDCl_3$, Me_4Si, 320K) 8.91 (m, 1H, 1-C*H*), 8.63 (s br, 1H, 7-C*H*), 7.78 (dt, 1H, ^{3}J = 8.1, ^{4}J = 1.9, 3-C*H*) 7.34 (ddd, ^{3}J = 7.5, ^{4}J 5.8, ^{5}J = 1.3, 1H, 2-CH), 4.39 (m , 2H, 8-CH_2), 3.27-3.18 (m, 2H, 14-CH_2), 3.13 (m, 1H, 17-CH_2) 2.19-2.08 (m, 2H, 9-C*H*2), 1.61-1.49 (m, 2H, 15-CH_2), 1.45 (s, 9H, 16-CH_3), 1.40 (s, 9H, 13-CH_3), 1.36 (s, H, 21-C*H*3); NMR δ_C (100 MHz, $CDCl_3$, Me_4Si, 320K) 197.2, (22-C) 195.5 (23-C), 189.1, (24-C) 156.1 (11- and 19-C), 153.2 (1-C), 149.5 (5-C), 148.6 (6-C), 139.1 (3-C), 125.7 (2-C), 124.1 (7-C), 122.0 (4-C), 80.2 (9-C),79.2 (13-C), 53.3 (8-C), 39.1 (11-C), 28.6 (13- and 21-C), 27.0 (16-C), 26.8 (10-C), 25.5 (14-C); MS (ES+) 545 [M-Cl]+; HRMS (ES+) $C_{29}H_{41}{}^{35}N_7O_7{}^{187}Re^+[M+H]^+$ requires 786.2625 found 786.2627.

[Re(BocSpm-pyta)(CO)$_3$Cl] (166)

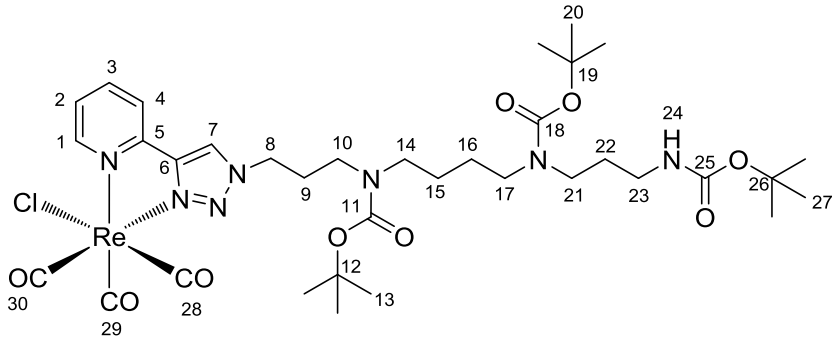

Proligand **138** (188.6 mg, 0.30 mmol) and $Re(CO)_5Cl$ (108.1 mg, 0.30 mmol) were reacted according to general method C, then evaporated under reduced pressure to give the title compound as a yellow solid (284.8 mg, 98 %). NMR δ_H (500 MHz, CD_3OD, Me_4Si, 323K) 8.96 (app dd, 1H, ^3J = 5.6, ^4J = 0.8, 1-C*H*), 8.94 (s, 1H, 7-C*H*), 8.18 (ddd, ^3J = 7.9, 7.8, ^4J = 1.7, 1H, 3-C*H*), 8.13(ddd, 1H, ^3J = 7.9, ^4J = 1.7, ^5J = 0.9, 4-C*H*), 7.58 (ddd, 1H, ^{3}J = 7.2, ^3J = 5.5, ^4J = 1.1, 2-C*H*), 4.66 -4.63 (m, 2H, 8-CH_2), 3.42-3.34 (m, 2H, 10-CH_2), 3.32 – 3.09 (m, 6*H* , 14-, 17-and 21-CH_2) 3.05 (t, 2H, *J* = 6.8. 23-CH_2), 2.38 – 2.28 (m, 2H, 9-CH_2), 1.75-1.67 (m, 2H, 22-CH_2), 1.56 – 1.52 (m, 4H, 15- and 16-CH_2), 1.48 (s, 9H, 13-CH_3) 1.46 (s, 9H, 20-CH_3) 1.45 (s, 9H, 27-CH_3); NMR δ_C (125 MHz, CD_3OD, Me_4Si, 323K) 198.43 (30-C), 196.94 (29-C), 190.25 (28-C), 158.4 (11-18- and 25-C), 154.3 (1-C), 151.0 (5-C), 141.3 (6-C), 139.5 (3-C), 125.8 (2-C), 124.0 (7-C), 122.1 (4-C), 79.4 (12, 19 and 26-C), 51.5 (8-C), 49.8 (14-C), 48.1 (17-C), 46.0 (24-C), 45.5 (10-C), 39.1 (23-C), 29.7 (9 and 22-C), 28.7 (13, 20, 27-C), 27.0 (9-C), 25.5 (15 and 16-C); IR (solid state): ν_{CO} (cm^{-1}) 2021, 1888; MS (ES+) 901 [M+Na]+; HRMS (ES+) $C_{35}H_{53}{}^{35}ClN_7O_9Na^{187}Re^+$ [M+Na]+ requires 960.3066 found 960.3049.

[Re(APBocSpm-pyta)(CO)$_3$Cl] (167)

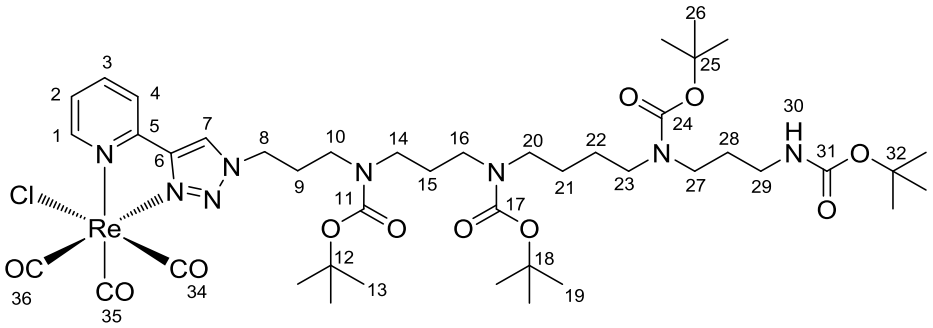

Proligand **156** (152.8 mg, 0.19 mmol) and $Re(CO)_5Cl$ (75.6 mg, 0.21 mmol) were reacted according to general method C. The solvent was evaporated *in vacuo* to give the title compound as a yellow solid (167.1 mg, 84 %). NMR δ_H (400 MHz, $CDCl_3$, Me_4Si, 320K) 8.93 (dd, 1H, ^3J = 5.5, ^4J = 1.5, ^5J = 0.9, 1-C*H*), 8.60 (s, 1H, 7-C*H*), 7.90 (ddd, ^3J = 7.9, 7.8, ^4J = 1.5, 1H, 3-C*H*), 7.85 – 7.69 (m, 1H, 4-C*H*), 7.34 (ddd, 1H, ^3J = 7.6, ^3J = 5.6, ^4J = 1.3, 2-C*H*), 4.58 – 4.33 (m, 2H, 8-CH_2), 3.32 - 3.20 (m, 2H, 10-CH_2), 3.20 – 3.06 (m, 10H, 14-, 16-, 20-, 23- and 27-CH_2) 3.06 – 2.98 (m, 2H, 29-CH_2), 2.27 – 2.10 (m, 2H, 9-CH_2), 1.75-1.67 (m, 2H, 15-CH_2), 1.59 (s, 2H, 28-CH_2), 1.44 – 1.42 (m, 4H, 21- and 22-CH_2) 1.41 - 137 (m, 36H, 13-, 19-, 26 and 33-CH_3); NMR δ_C (100 MHz, $CDCl_3$, Me_4Si, 320K) 197.2 (30-C), 197.1 (29-C), 195.5 (28-C), 156.0 (11, 17, 24 and 31-C), 155.5 (1-C), 153.3 (5-C), 149,5 (6-C), 124.1(7-C), 121.9 (4-C), 81.0, 80.3, 79.6, 79.4, (12, 18, 25 and 31-C), 53.3 (8-C), 49.9 (10-C), 47.0 (14-C), 46.9 (16-C), (20-C), 45.5 (23-C) 44.9 (27-C), 44.3 (29-C), 30.3 (9-C), 29.0 (15-C), 28.9 (28-C) 28.5 (13-, 19-, 26- and 33-C), 26.9 (21 and 22); MS (ES+) 1095 [M+H]+; HRMS (ES+) $C_{43}H_{68}N_8O_{11}{}^{185}Re^+$ $[M\text{-}Cl]^+$ requires 1057.4537 found 1057.4548.

[Re(PEG-pyta)(CO)$_3$Cl] (168)

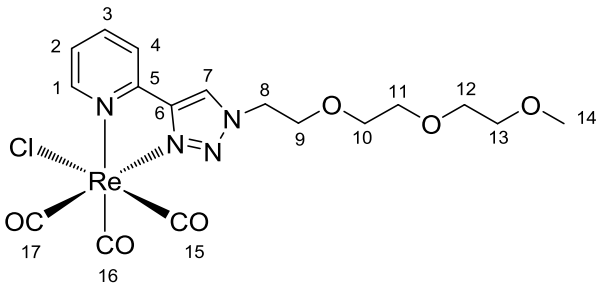

Proligand **152** (57.0 mg, 0.20 mmol) and $Re(CO)_5Cl$ (73.8 mg, 0.20 mmol) were reacted according to general method C, then evaporated under reduced pressure to give the title compound as a yellow solid (96.6 mg, 81 %). NMR δ_H (500 MHz, CD_3OD, 298K) 8.90 (m 1H, 1-C*H*), 8.86 (s, 1H, 7-C*H*), 8.09 - 8.03 (m, 1H, 3-C*H*), 7.49 - 7.42 (m, 1H, 2-C*H*), 4.70 – 4.66 (m, 2H, 8-CH_2), 3.89 (t, *J* = 4.8, 2H, 9-CH_2), 3.58 – 3.56 (m, 2*H* , 10-CH_2) 3.54 – 3.50 (m, 4H, 11 and 12-CH_2), 3.49 – 3.46 (13-CH_2), 3.19 (m, 3H, 14-CH_3); NMR δ_C (125 MHz, CD_3OD, 298K) 198.5 (17-C), 197.1 (16-C), 190.3 (15-C), 154.3 (1-C), 151.02 (5-C), 150.08 (6-C), 141.38 (3-C), 127.22 (2-C), 127.12 (7-C), 123.61 (4-C), 73.0 (8-C), 71.4 (10 and 11-C), 71.3 (9-C), 69.6 (12-C), 59.1 (13-C), 53.3 (14-C); IR (solid state): ν_{CO} (cm^{-1}) 2015, 1892; MS (ES+) 563 $[M\text{-}Cl]^+$; HRMS (ES+) $C_{17}H_{20}N_4O_6{}^{187}Re^+$ $[M\text{-}Cl]^+$ requires 563.0940 found 563. 0941.

[Re(4CF$_3$-pyta)(CO)$_3$Cl] (169)

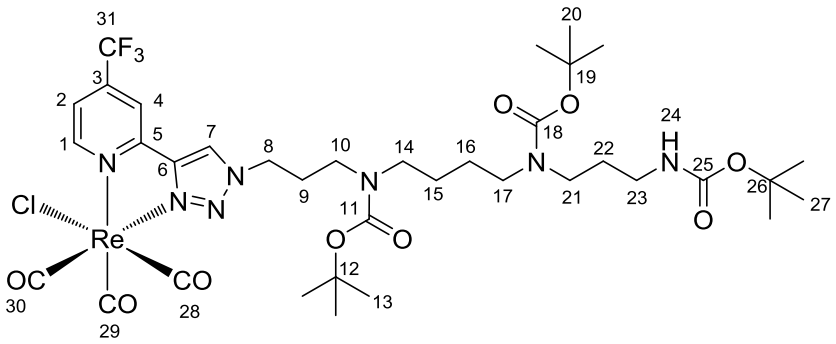

Proligand **158** (58.1 mg, 0.0.083 mmol) and $Re(CO)_5Cl$ (31.4 mg, 0.0.086 mmol) were reacted according to general method C. The mixture was filtered through Celite then reduced to dryness to give the title compound as a yellow solid (72.6 mg, 87 %). NMR δ_H (500 MHz, CD_3OD, 323K) 9.19 (d br, 1H, *J* = 5.8, 1-C*H*), 8.78 (s, 1H, 7-C*H*), 8.09 (dd, ^3J = 8.4, ^4J = 1.9, 1H, 4-C*H*), 7.93 (d, 1H, *J* = 8.2, 2-C*H*), 4.59 – 4.48 (m, 2H, 8-CH_2), 3.28-2.86 (m, 10H, 10-, 14-, 17-, 21- and 23-CH_2), 2.17 – 2.09 (m, 2H, 9-CH_2), 1.60-1.52 (m, 2H, 22-CH_2), 1.50 – 1.39 (m, 4H, 15 and 16-C), 1.36 – 1.32 (m, 36H, 13-, 20- and 27-CH_3); NMR δ_C (125 MHz, CD_3OD, Me_4Si, 323K) 198.6 (30-C), 196.4 (29-C), 188.4 (28-C), 178.2 (1-C), 156.4 (5-C), 154.4 (11-18- and 25-C), 143.2 (1-C), 140.9 (q, $^2J_{CF}$ = 38.6, 3-C), 141.3 (6-C), 139.5 (3-C), 122.8 (2-C), 118.1 (31-C), 122.1 (4-C), 79.3 (12, 19 and 26-C), 51.5 (8-C), 47.2 (14-C), 48.1 (17-C), 46.0 (24-C), 45.5 (10-C), 39.1 (23-C), 29.7 (9-C), 28.5 (13, 20, 27-C), 27.9 (22-C), 25.9 (15 and 16-C); IR (solid state): ν_{CO} (cm^{-1}) 2042, 1945; MS (ES+) 1006 [M+H]+; HRMS (ES+) $C_{36}H_{52}N_7O_9F_3{}^{187}Re^+$ [M-Cl]+ requires 970.3336 found 970.3353.

[Re(5CF$_3$-pyta)(CO)$_3$Cl] (170)

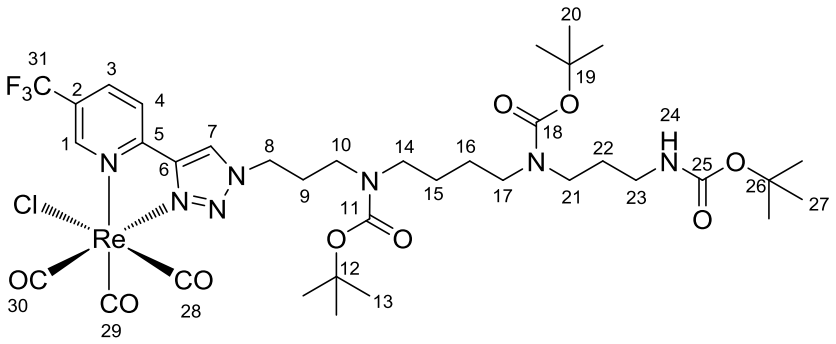

Proligand **157** (102.7 mg, 0.147 mmol) and $Re(CO)_5Cl$ (53.0 mg, 0.147 mmol) were reacted according to general method C. The complex was purified by flash column chromatography on silica, eluting yellow fractions with 10 % methanol in ethyl acetate to give the title compound as a yellow solid (145.8 mg, 98 %). NMR δ_H (400 MHz, $CDCl_3$, Me_4Si) 9.08 (m , H, 1-CH), 8.78 (s, 1H, 7-CH), 8.09 (dd, ^3J = 8.4, ^4J = 1.9, 1H, 3-CH), 7.93 (d, 1H, *J* = 8.2, 4-C*H*), 4.59 - 4.50(m , 2H, 8-CH_2), 3.28 - 2.86 (m, 2H, 14-CH2), 2.21 - 2.01 (m, 2H, 9-CH2), 1.60 - 1.52 (m, 2H, 10-CH2), 1.45 – 1.38 (m, 4H 15 and 16 CH3), 1.36 (s, 9H), 1.34 (s, 9H), 1.32 (s, 9H); NMR δ_F (376 MHz, $CDCl_3$, Me_4Si) -62.4; NMR δ_C (100 MHz, $CDCl_3$, Me_4Si) 196.5, 194.9, 188.3, (11, 18 and 26-C), 157.3 (13-C), 152.7 (1-C), 149.8 (5-C), 147.5 (6-C), 136.5 (3-C), 128.7 (2-C), 125.6 (7-C), 121.9 (4-C), 79.7 (12, 19 and 26-C), 51.5 (8-C), 47.31(14-C), 46.57(17-C), 43.95(21-C), 43.37(10-C), 39.1 (23-C), 28.5 (13, 20, and 27-C), 27.0 (9-C), 26.8 (22-C), 25.5 (15 and 16-C); IR (solid state): ν_{CO} (cm^{-1}) 2024, 1893; MS (ES+) 1028 $[M+Na]^+$; HRMS (ES+) $C_{36}H_{52}N_7O_9F_3{}^{185}Re^+$ $[M-Cl]^+$requires 968.3308 found 968.339.

[Re(5OMe-pyta)(CO)$_3$Cl] (171)

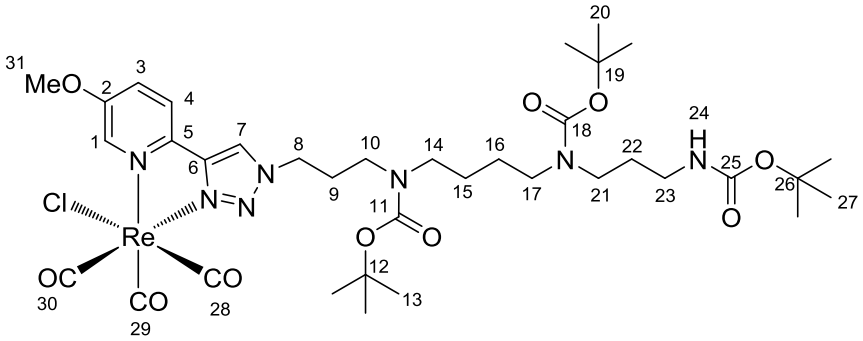

Proligand **159** (73.2 mg, 0.11 mmol) and $Re(CO)_5Cl$ (40.0 mg, 0.11 mmol) were reacted according to general method C. The complex was purified by flash column chromatography on silica, eluting yellow fractions with 10 % methanol in ethyl acetate to give the title compound as a yellow solid (48.4 mg, 51 %). NMR δ_H (400 MHz, $CDCl_3$, Me_4Si, 323K) 8.71 – 8.59 (m, 1H 1-C*H*), 8.54 (s, 1H, 7-C*H*), 7.81 (d, 1H, *J* = 8.8, 3-C*H*), 7.42 (dd, ^3J = 8.9, ^4J = 2.7, 1H, 2-C*H*), 4.56 – 4.37 (m , 2H, 8-CH_2), 3.41 – 3.26 (m, 2H, 10-C*H*2), 3.27 – 3.13 (m, 6H, 14, 17, 21-CH_2), 3.13 – 3.03 (m, 2H, 23-CH_2), 2.29-2.14 (m, 2H, 9-CH_2), 1.71-1.62 (m, 2H, 22-CH_2), 1.54 -1.48 (m, 4H, 15 and 16-CH_2) 1.48 – 1.41 (m, 27H, 13, 20 and 27-CH_3); NMR δ_C (100 MHz, $CDCl_3$, Me_4Si) 197.34, 195.68, 189.21, (28, 29 and 30-C), 157.02 (11, 18, 25-C), 148.7 (1-C), 141.9 (5-C), 140.8 (6-C), 130.3 (3-C), 127.1 (2-C), 123,7 (7-C), 122.9 (4-C), 79.9 (11, 19 and 26-C), 60.3 (31-C), 56.5 (8-C), 49.7 (10-C), 47.6 (14-C), 46.7 (17-C), 44.6 (21-C). 44.3 (9-C), 37.6 (23-C), 28.5 (13, 20 and 27-C), 27.0 (9-C), 26.8 (22-C), 28.5 (13, 20 and 27-C), 26.0 (15 and 16-C); IR (solid state): ν_{CO} (cm^{-1}) 2029, 1929; MS (ES+) 930 $[M\text{-}Cl]^+$; HRMS (ES+) $C_{36}H_{55}N_7O_{10}{}^{185}Re^+$ $[M\text{-}Cl]^+$ requires 930.3540 found 930.3556.

7.6: Cationic Rhenium Complexes

General Method D for microwave synthesis of pyridyl rhenium complexes

[Re(pyta)$(CO)_3$Cl] (0.05 mmol), $AgBF_4$ (0.10 mmol) and pyridine dissolved in 4 mL dry THF and heated to 90 °C for 3 h in a microwave reactor, after which the reaction mixture was cooled, filtered through Celite, evaporated to dryness. Complexes were deprotected, concentrated and re-dissolved in water. Solutions were filtered through a nylon membrane prior purification by RP-HPLC.

[Re(Put-pyta)$(CO)_3$py]2TFA (111)

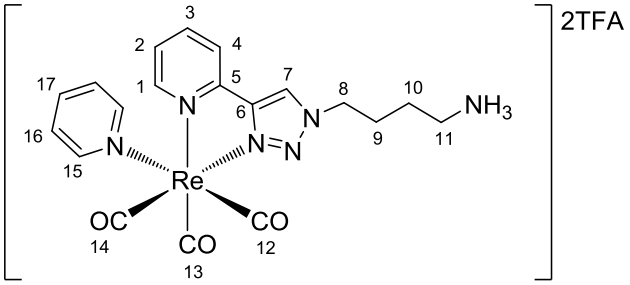

$Re(CO)_5Cl$ (36.6 mg, 0.101 mmol) and proligand **149** (32 mg, 0.101 mmol) were dissolved in THF (4 mL) and heated in a microwave reactor at 90 °C for 1 h. $AgBF_4$ (27.9 mg, 0.143 mmol) and pyridine (16.1 µL, 0.200 mmol) were then added and the reaction vessel returned to the microwave reactor at 90 °C for 3 hr. After cooling, the reaction mixture was filtered through Celite and the solvent removed to give a yellow solid which was dissolved in 4M TFA in dichloromethane and stirred for 2 h at room temperature. The volatiles were removed, the crude solid was dissolved in water and filtered through a nylon membrane prior to purification by RP-HPLC method A, t_R = 20.83 mins, (36.4 mg, 73 %). NMR δ_H (400 MHz, CD_3OD, 323K) 9.30 (ddd, 1H, ^3J = 5.6, ^4J = 1.4, ^5J = 0.8 1-C*H*), 9.04 (s, 1H, 7-C*H*), 8.40 (m, 2H, 17- C*H*), 8.28 (ddd, ^3J = 8.6, 7.9, ^4J = 1.7, 3-C*H*), 8.20 (app dt, 1H, ^3J = 7.7, ^4J = 1.0, 2-C*H*), 7.93 (m, 2H, 19-CH), 7.76 (ddd, 1H, ^3J = 6.9, ^4J = 5.5, ^5J = 1.1, 4-C*H*), 7.46 (m, 2H, 18-C*H*), 4.71 (t, 2H, J = 7.2, 8-CH_2), 3.05 (t, 2H, J = 7.0, 11-CH_2), 2.18 (app quin, 2H, J = 7.8, 7.4 9-CH_2), 1.80 (m, 2H, 10-CH_2); NMR δ_C (100 MHz, CD_3OD, 323K) 154.7 (1-C), 152.9 (19-C), 150.3 (5-C), 150.2 (6-C), 142.4 (3-C), 140.8 (21-C), 128.3 (4-C), 127.6 (20-C), 127.2 (7-C), 124.0 (C-)117.8 (2-C), 52.7 (8-C), 39.6 (11-C), 27.3 (9-C),

25.1 (10-C), MS (ES+) 567 $[M]^+$, 488 $[M\text{-}py]^+$; HRMS (ES+) $C_{19}H_{20}N_6O_3{}^{185}Re$ $[M]^+$ requires 565.1127 found 565.1130; UV/Vis (H_2O) 280 (13402), 330 (7592).

[Re(COOH-pyta)(CO)$_3$py]TFA (113)

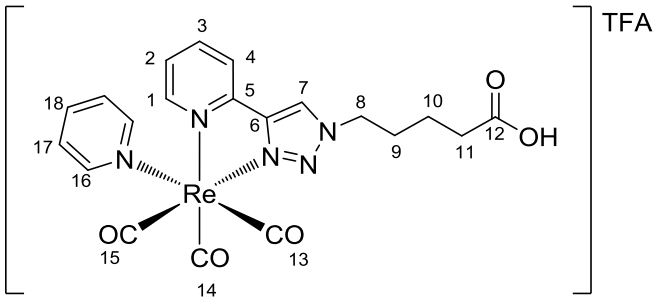

Complex 163 (43.4 mg, 0.067 mmol) was reacted with $AgBF_4$ (20.4 mg, 0.105 mmol) and pyridine (22 µl, 21.7 mg, 0.274 mmol) according to method D. The product was dissolved in methanol, (1 mL) to which NaOH solution (0.02 M, 1 mL) was added and stirred at room temperature overnight. The mixture was neutralised by dropwise addition of 0.01 M hydrochloric acid and filtered. The mixture was purified by RP-HPLC method A, t_R = 23.93 mins. Solvent was removed to give a yellow solid (31.5 mg, 85 %). NMR δ_H (400 MHz, CD_3OD, 298K) 9.30 (ddd, 1H, ^3J = 5.6, ^4J = 1.3, ^5J = 0.8, 1-C*H*), 9.02 (s, 1H, 7-C*H*), 8.48 – 8.39 (m, 2H, 19-C*H*), 8.27 (ddd, ^3J = 8.0, 7.9, ^4J = 1.3, 1H, 3-CH), 8.03 (app dt, 1H, ^3J = 7.9, ^4J = 0.9, 2-C*H*), 7.98 – 7.88 (m, 2H, 21-C*H*), 7.65 (ddd, ^3J = 6.3, ^4J = 5.6, ^5J = 1.4, 1H, 4-C*H*), 7.41 – 7.34 (m, 2H, 20-C*H*), 4.83 – 4.72 (m, 2H, 8-CH_2), 2.48 – 2.42 (m, 2H, 11-CH_2), 2.18 – 2.11 (m, 2H, 9- CH_2), 1.63 (app quin, 2H, ^3J = 7.5, 8.0, 10- CH_2); NMR δ_C (100 MHz, CD_3OD) 176.7 (12-C), 155.1 (1-C), 153.4 (19-C), 150.8 (5-C), 150.7 (6-C), 142.8 (3-C), 141.2 (21-C), 128.7 (4-C), 127.5 (20-C), 126.5 (7-C), 124.4 (2-C), 53.6 (8-C), 33.9 (11-C), 30.1 (9-C), 22.7 (10-C); MS (ES+) 597 $[M]^+$, 517 $[M\text{-}py]^+$; HRMS (ES+) $C_{20}H_{19}N_5O_5{}^{185}Re$ [M]+ requires 594.0916 found 594.0917; UV/Vis (H_2O) 280 (8086), 330 (4455).

[Re(PO(OH)$_2$-pyta)(CO)$_3$py]2TFA (114)

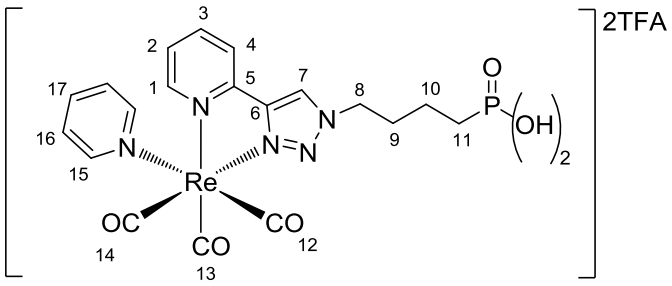

Complex **164** (39.7 mg, 0.068 mmol) $AgBF_4$ (26.5 mg, 0.136 mmol) and pyridine (22 µL, 21.7 mg, 0.274 mmol) were dissolved in THF (4 mL) and heated in a microwave reactor. The product was dissolved in dry acetonitrile, (2 mL). TMSBr (410 µL, 3.800 mmol) was added, then stirred under nitrogen at room temperature overnight. Water (1 mL) was added and the mixture was stirred for an additional 2 h. The mixture was purified by RP-HPLC method A, t_R = 22.23 mins. Fractions were lyophilised to give a yellow solid (10.8 mg, 43 %). NMR δ_H (400 MHz, CD_3OD, 298K); 9.17 (ddd, 1H, 3*J* = 5.6, ^4J = 1.2, ^5J = 0.8, 1-C*H*), 8.86 (s, 1H, 7-C*H*), 8.31 (m, 2H, 19- C*H*), 8.15 (ddd, ^3J = 7.9, 7.8, ^4J = 1.4, 1H, 3-C*H*), 8.03 (app dt, 1H, ^3J = 7.9, ^4J = 1.1, 2-C*H*), 7.89 -7.78 (m, 2H, 21-C*H*), 7.65 (ddd, ^3J = 7.6, ^4J = 5.6, ^5J = 1.4, 1H, 4-C*H*), 7.42 – 7.31 (m, 2H, 20-C*H*), 4.73 – 4.60 (t, 2H, *J* = 6.9, 8-CH_2), 4.01 (q, 2H, *J* = 7.4, 13-CH_2), 2.33 (app dt, J = 7.4, 2.3 2H, 11-CH_2), 2.09 – 1.98 (m, 2H, 9-CH_2), 1.54 (m, 2H, 10-CH_2), 1.12 (t, 3H, *J* = 7.2, 14-CH_3), MS (ES+) 632 $[M]^+$, 554 $[M\text{-py}]^+$; HRMS (ES+) $C_{19}H_{20}N_5O_6{}^{185}Re$ $[M]^+$ requires 630.0681 found 630.0681. UV/Vis (H_2O) 280 (11517), 330 (6238).

[Re(AcPut-pyta)(CO)$_3$py]TFA (112)

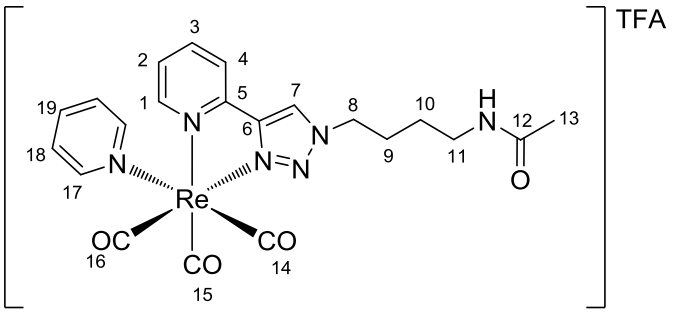

Complex 111 (36.4 mg, 0.046 mmol) was dissolved in 20 % AcOAc in DMF and stirred overnight at room temperature. The solvent was removed, and the crude solid was dissolved in water, prior to purification by RP-HPLC method A, t_R = 23.00 mins, which yielded a yellow hygroscopic solid after lyophilisation (36.4 mg, 77 %). NMR δ_H (400 MHz, CD_3OD, 298K) 9.29 (d, 1H, *J* = 5.4, 1-C*H*), 9.03 (s, 1H, 7-C*H*), 8.41 (m, 2H, 17- C*H*), 8.28 (app td, *J* = 7.8, 1.4, 3-C*H*), 8.14 (app d, 1H, *J* = 7.8, 2-C*H*), 7.93 (m, 2H, 19-C*H*), 7.76 (ddd, ^3J = 7.4, ^4J = 5.7, ^5J = 1.1, 1H, 4-C*H*), 7.41 (m, 2H, 18-CH), 4.76 (t, 2H, *J* = 7.2, 8-CH_2), 3.27 (t, 2H, J = 6.9, 11-CH_2), 2.16-2.04 (m, 2H, 9-CH_2), 1.65-1.51 (m, 2H, 10-CH_2); NMR δ_C (100 MHz, CD_3OD) 173.5 (12-C) 155.1 (1-C), 153.4 (17-C), 150.8 (5-C), 150.7 (6-C), 142.8 (3-C), 141.3 (10-C), 128.7 (2-C), 128.0 (18-C), 127.5 (C-7), 124.3 (C-4), 53.5 (8-C), 39.5 (11-C), 28.2 (C-13), 27.4 (9-C), 22.7 (10-C), MS (ES+) 609 $[M]^+$, 530 $[M\text{-}py]^+$; HRMS (ES+) $C_{21}H_{22}N_6O_4{}^{185}Re$ $[M]^+$ requires 607.1232 found 607.1232; UV/Vis (H2O) 280 (6813), 330 (3593).

[Re(AP-Put-pyta)(CO)$_3$py]3TFA (125)

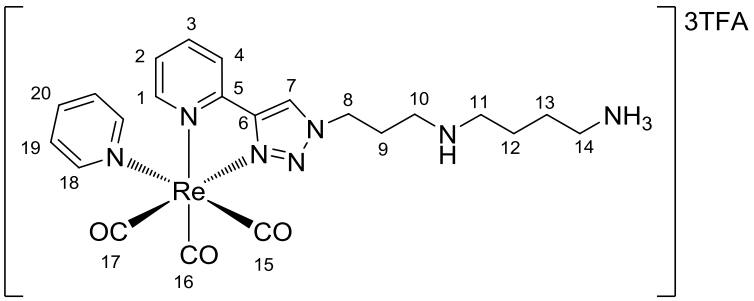

Complex **165** (19.2 mg, 0.025 mmol) was reacted with $AgBF_4$ (10.5 mg, 0.054 mmol) and pyridine (8.8 mg, 0.111 mmol) according to method D. The isolated complex was dissolved in 4M TFA in dichloromethane and stirred for 2 h at room temperature. The volatiles were removed, the crude solid was dissolved in water and filtered through a nylon membrane prior to purification by RP-HPLC method A, t_R = 19.68 mins, and lyophilised to give the title compound as a hygroscopic yellow solid (17.6 mg, 73 %). NMR δ_H (400 MHz, CD_3OD, 298K) 9.32 (ddd, 1H, *J* = 5.6, 1.4, 0.9, 1-CH), 9.11 (s, 1H, 7-CH), 8.43 (m, 2H, 18-CH), 8.30 (td, 1H, *J* = 7.8, 1.6, 3-CH), 8.19 (ddd, 1H, *J* = 7.9, 1.4, 0.9, 4-CH), 7.95 (tt, 1H, *J* = 7.5, 1.6, 20-CH), 7.79 (ddd, 1H, *J* =7.6, 5.5, 1.4, 2-CH), 7.43 (m, 2H, 19-CH), 4.86 (m, 2H, 8-CH_2), 3.24 (m, 2H, 10-CH_2), 3.14 (m, 2H, 11-CH_2), 3.00 (m, 2H, 14-CH_2), 2.55 (m, 2H, 9-CH_2), 1.82 (m, 4H, 13- and 14-CH_2). NMR δ_C (100 MHz, CD_3OD) 195.26, 193.85, (16- and 17-C), 190.72 (15-C), 161.04 (q, $^2J_{CF}$ = 36.3, $CF_3\mathbf{C}O_2^-$), 153.67 (1-C), 151.98 (18-C), 149.40 (5-C), 149.23 (6-C), 141.39 (3-C), 139.77 (20-C), 127.38 (2-C), 126.60 (19-C), 126.48 (7-C), 123.06 (4-C), 116.54 (q, $^1J_{CF}$ = 290.9, $\mathbf{C}F_3CO_2^-$), 49.39 (8-C), 46.88 (11-C), 44.42 (10-C), 38.56 (14-C), 25.98 (9-C), 24.13 (12-C), 22.86 (13-C). MS (ES+) 624 $[M]^+$, 545 $[M\text{-py}]^+$; HRMS (ES+) $C_{22}H_{27}N_7O_3{}^{187}Re$ $[M]^+$ requires 624.1732 found 624.1733.

[Re(Spm-pyta)(CO)$_3$py]4TFA (119)

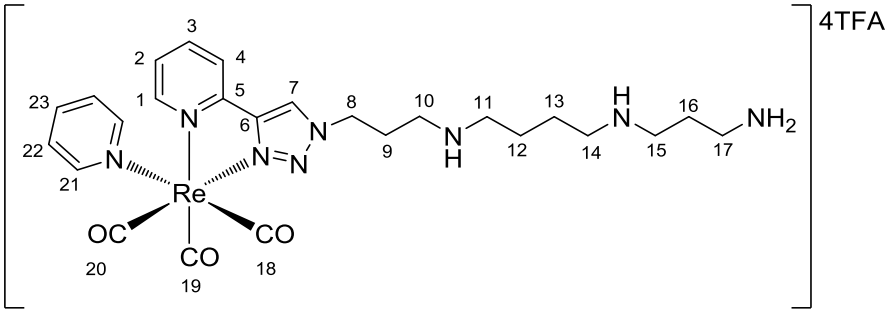

Complex **166** (146.8 mg, 0.157 mmol) was reacted with $AgBF_4$ (57.9 mg, 0.297 mmol) and pyridine (36.0 mg, 0.500 mmol) according to method D. The isolated complex was dissolved in 4M TFA in dichloromethane and stirred for 2 h at room temperature. The volatiles were removed, the crude solid was dissolved in water and filtered through a nylon membrane prior to purification by RP-HPLC method A, t_R = 19.33 mins, and lyophilised to give the title compound as a hygroscopic yellow solid (82.6 mg, 49 %). δ_H (500 MHz, CD_3OD, 323K) 9.32 (ddd, 1H, *J* = 5.6, 1.4, 0.9, 1-CH), 9.11 (s, 1H, 7-CH), 8.44 (m, 2H, 18-CH), 8.31 (dt, 1H, *J* = 7.8, 1.4, 3-CH), 8.19 (ddd, 1H, *J* = 7.8, 1.4, 0.9, 4-CH), 7.95 (tt, 1H, *J* = 7.7, 1.6, 20-CH), 7.79 (ddd, 1H, *J* =7.7, 5.6, 1.3, 2-CH), 7.43 (m, 2H, 19-CH), 4.86 (m, 2H, 8-CH_2), 3.24 (m, 2H, 10-CH_2), 3.20 - 3.05 (m, 8H, 11-, 14-, 15- and 17-CH_2), 2.55 (m, 2H, 9-CH_2), 2.11 (m, 2H, 16-CH_2), 1.86 (m, 4H, 13- and 14-CH_2). NMR δ_C (125 MHz, CD_3OD, 323K) 196.65, 195.25, (19- and 20-C), 192.11 (18-C), 162.64 (q, $^2J_{CF}$ = 36.9, $CF_3\mathbf{C}O_2^-$), 155.10 (1-C), 153.35 (21-C), 150.85 (5-C), 150.67 (6-C), 142.80 (3-C), 141.17 (23-C), 128.80 (2-C), 127.99 (22-C), 127.83 (7-C), 124.48 (4-C), 117.96 (q, $^1J_{CF}$ = 297.6, $\mathbf{C}F_3CO_2^-$), 50.88 (8-C), 48.29 (10-C), 45.92 (11-C), 45.09 (14-C), 37.92 (17-C), 27.33(9-C), 25.32 (16-C), 24.24 (12-C), 24.15 (13-C). MS (ES+) 682 $[M]^+$, 603 $[M\text{-py}]^+$; HRMS (ES+) $C_{25}H_{34}N_8O_3{}^{187}Re$ $[M]^+$ requires 681.2312 found 681.2327. UV/Vis (H_2O) 280 (28935), 327 (6739).

[Re(APSpm-pyta)(CO)$_3$py]5TFA (126)

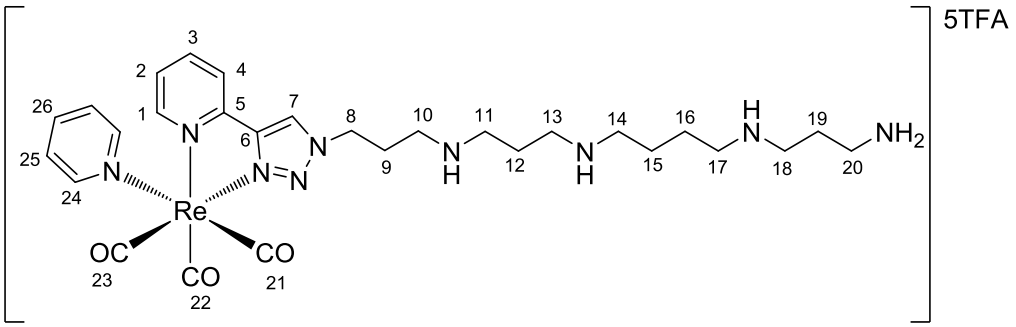

Complex **167** (43.4 mg, 0.041 mmol) was reacted with $AgBF_4$ (17.6 mg, 0.090 mmol) and pyridine (15 µL, 14.7 mg, 0.186 mmol) according to method D. The isolated complex was dissolved in 4M TFA in dichloromethane and stirred for 2 h at room temperature. The volatiles were removed, the crude solid was dissolved in water and filtered through a nylon membrane prior to purification by RP-HPLC method A, t_R = 19.25 mins, and lyophilised to give the title compound as a hygroscopic yellow solid (36.8 mg, 69 %). δ_H (400 MHz, CD_3OD, 298K) 9.32 (ddd, 1H, *J* = 5.9, 1.4, 0.9, 1-CH), 9.10 (s, 1H, 7-CH), 8.45 (m, 2H, 24-CH), 8.31 (td, 1H, *J* = 7.8, 1.5, 3-CH), 8.18 (ddd, 1H, *J* = 8.0, 1.3, 0.9, 4-CH), 7.80 (tt, 1H, *J* = 7.7, 1.6, 26-CH), 7.79 (ddd, 1H, *J* =7.7, 5.7, 1.4, 2-CH), 7.66 (m, 2H, 25-CH), 4.86 (m, 2H, 8-CH_2), 3.30 - 3.03 (m, 14H, 10-, 11-, 13-, 14-, 17-, 18- and 20-CH_2), 2.55 (m, 2H, 9- CH_2), 2.19 (m, 2H, 9- CH_2), 2.10 (m, 2H, 9- CH_2), 1.82 (m, 4H, 13- and 14-CH_2); NMR δ_C (100 MHz, CD_3OD, 298K) 195.24, 194.18 (22- and 23-C), 191.82 (21-C), 161.45 (q, $^2J_{CF}$ = 35.3, $CF_3\mathbf{C}O_2^-$), 153.71 (1-C), 152.00 (24-C), 149.41 (5-C), 149.21 (6-C), 141.34 (3-C), 139.75 (4-C), 127.38 (2-C), 126.59 (25-C), 126.44 (7-C), 123.02 (26-C), 116.54 (q, $^1J_{CF}$ = 35.3, $\mathbf{C}F_3CO_2^-$), 49.35 (8-C), 46.78 (10-C), 44.59 (11-C), 44.56 (13-C), 44.43 (14-C), 44.38 (17-C), 36.40 (18-CH_2), 25.98 (9-C), 23.97 (19-C), 22.80 (12-, 15- and 16-C); IR (solid state): ν_{CO} (cm^{-1}) 2034, 1913; MS (ES+) 738 $[M]^+$, 659 $[M\text{-}py]^+$; HRMS (ES+) $C_{28}H_{41}N_9O_3{}^{185}Re$ $[M]^+$ requires 738.2863 found 738.2862.

[Re(PEG-pyta)(CO)$_3$py]TFA (168)

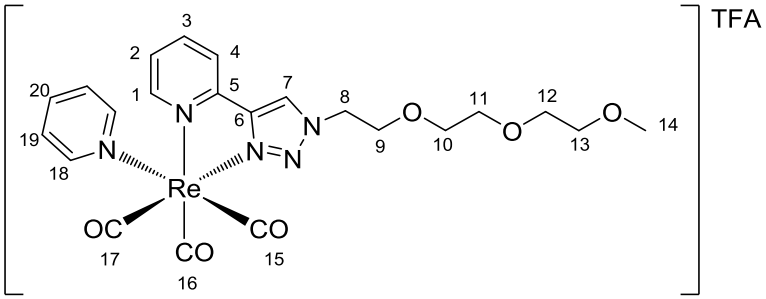

Complex **139** (32.9 mg, 0.058 mmol) was reacted with $AgBF_4$ (25.1 mg, 0.129 mmol) and pyridine (20 µL, 19.6 mg, 0.248 mmol) according to method D. The volatiles were removed, the crude solid was dissolved in water and filtered through a nylon membrane prior to purification by RP-HPLC method A, t_R = 24.83 mins, and lyophilised to give the title compound as a hygroscopic yellow solid (21.8 mg, 50 %). NMR δ_H (400 MHz, $CDCl_3$, TMS, 298K) 9.01 (ddd, 1H, *J* = 5.5, 1.7, 1,0, 1-CH), 8.96 (s, 1H, 7-CH), 8.18 (m, 2H, 18-CH), 8.14 (ddd, 1H, *J* = 8.0, 1.1, 0.9, 3-CH), 8.04 (td, 1H, *J* = 7.9, 1.4, 4-CH), 7.73 (tt, 1H, *J* = 7.8, 1.4, 20-CH), 7.57 (ddd, 1H, *J* =7.6, 5.7, 1.6, 2-CH), 7.29 (m, 2H, 19-CH), 4.74 (t, 2H, *J* = 5.9, 8-CH_2), 3.97 (m, 2H, 9-CH_2), 3.63 (m, 2H, 10-CH_2), 3.58 – 3.52 (m, 4H, 11- and 12-CH_2), 3.46 (m, 2H, 13-CH_2), 3.24 (s, 3H, 14-CH_3). NMR δ_C (100 MHz, CD_3OD) 195.74, 193.84, (16- and 17-C), 190.73 (15-C), 152.79 (1-C), 151.89 (18-C), 149.57 (5-C), 149.13 (6-C), 141.53 (3-C), 139.67 (20-C), 127.33 (2-C), 127.14 (19-C), 126.97 (7-C), 123.90 (4-C), 71.80 (8-C), 70.38 (10-, 11- and 12-C), 68.20 (9-C), 58.96 (13-C), 52.50 (14-C), MS (ES+) 642 $[M]^+$, 563 $[M\text{-py}]^+$; HRMS (ES+) $C_{22}H_{25}N_5O_6{}^{187}Re$ $[M]^+$ requires 642.1362 found 642.1363.

[Re(4-CF_3-pyta)$(CO)_3$py]4TFA (131)

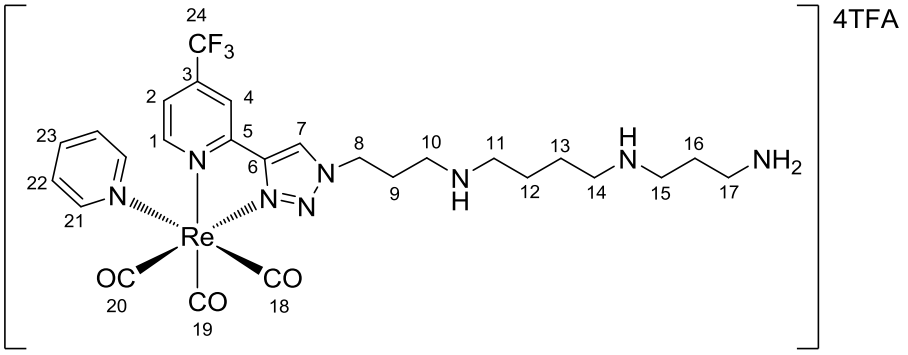

Complex **169** (43.4 mg, 0.043 mmol) was reacted with $AgBF_4$ (18.4 mg, 0.094 mmol) and pyridine (15 µl, 14.7 mg, 0.186 mmol) according to method D. The isolated complex was dissolved in 4M TFA in dichloromethane and stirred for 2 h at room temperature. The volatiles were removed, the crude solid was dissolved in water and filtered through a nylon membrane prior to purification by RP-HPLC method A, t_R = 23.78 mins, and lyophilised to give the title compound as a hygroscopic yellow solid (30.9 mg, 60 %). NMR δ_H (500 MHz, D_2O, 298K) 9.45 (br d, 1H, *J* = 5.7, 1-CH), 8.81 (s, 1H, 7-CH), 8.31 (s, 2H, 4-CH), 8.28 (d, 2H, *J* = 5.6, 21-CH), 7.93 (d, 1H, *J* = 6.3, 2-CH), 7.78 (t, 1H, *J* = 7.9, 23-CH), 7.24 (t, *J* = 6.7, 22-CH), 4.68 (m, 2H, 8-CH_2), 3.11(m, 2H, 17- CH_2), 3.09 – 2.98 (m, 8H, 10-, 11-, 14- and 15-CH_2), 2.42 (m, 2H, 9- CH_2), 2.00 (m, 4H, 16- CH_2), 3.49 - 3.42 (m, 4H, 12- and 13- CH_2); δ_C (125 MHz, D_2O, 298K), 195.51 (19-C), 194.45, 194.39 (18- and 20-C), 162.87 (q, $^2J_{CF}$ = 36.6, CF_3**C**O_2^-), 155.10 (1-C), 152.00 (21-C), 150.63 (5-C), 148.93 (6-C), 145.08 (q, $^2J_{CF}$ = 411.2, 3-C), 139.71 (20-C), 126.93 (7-C), 126.40 (22-C), 123.19 (2-CH), 119.37 (4-C), 121.25, (q, $^1J_{CF}$ = 478.5, 24-CF_3), 116.28 (q, $^1J_{CF}$ = 288.5, **C**$F_3CO_2^-$), 49.44 (8-C), 46.99 (10-C), 46.96 (14-C), 46.68 (11-C), 44.49 (15-C), 36.50 (17-C), 25.77 (9-C), 23.70 (16-C), 22.38 (12- and 13-C); δ_F (376 MHz, MeCN, 298K), -65.78, -75.48. IR (solid state): ν_{CO} (cm^{-1}) 2038, 1923; MS (ES+) 749 $[M]^+$, 670 $[M\text{-py}]^+$; HRMS (ES+) $C_{26}H_{33}N_8O_3F_3{}^{185}Re$ $[M]^+$ requires 747.2157 found 747.2157. UV/Vis (H_2O) 238 (15049), 331 (3596).

[Re(5-CF_3-pyta)$(CO)_3$py]4TFA (130)

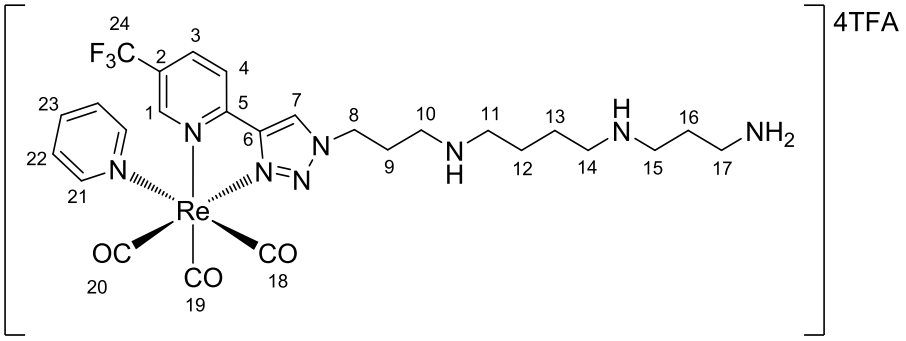

Complex **170** (55.0 mg, 0.0547 mmol) was reacted with $AgBF_4$ (24.6 mg, 0.124 mmol) and pyridine (20 µL, 19.6 mg, 0.248 mmol) according to method D. The isolated complex was dissolved in 4M TFA in dichloromethane and stirred for 2 h at room temperature. The volatiles were removed, the crude solid was dissolved in water and filtered through a nylon membrane prior to purification by RP-HPLC method A, t_R = 26.67 mins, (36.4 mg, 55 %). δ_H (500 MHz, CD_3OD, 298K) 9.52 (br s, 1H, 1-CH), 9.26 (s, 1H, 7-CH), 8.67 (dd, 1H, *J* = 8.5, 1.7, 4-CH), 8.47 (m, 2H, 21-CH), 8.41 (d, 1H, *J* = , 8.4, 3-CH), 7.96 (td, 1H, *J* = 7.6, 1.5, 23-CH), 7.45 (m, 2H, 22-CH), 4.87 (m, 2H, 8-CH_2), 4.03 - 3.89 (m, 2H), 3.26 (m, 2H, 10-CH_2), 3.19 - 3.04 (m, 8H, 11-, 14-, 15- and 17-CH_2), 2.56 (m, 2H, 9-CH_2), 2.11 (m, 2H, 16-CH_2), 1.85 (m, 4H, 12- and 13-CH_2); δ_C (125 MHz, CD_3OD, 298K) 195.51 194.45 (19- and 20-C), 194.39 (18-C), 162.87 (q, $^2J_{CF}$ = 36.6, $CF_3\mathbf{C}O_2^-$), 158.54 (1-C) 152.79 (21-C), 152.00 (5-C), 151.89 (6-C), 149.57 (3-C), 149.13 (23-C), 139.67 (23-C), 139.47, 127.34 (7-C), 127.14 (22-C), 126.98 (q, $^2J_{CF}$ = 29.6, 2-C), 123.90 (4-C), 121.25, (q, $^1J_{CF}$ = 478.5, 24-CF_3), 116.28 (q, $^1J_{CF}$ = 288.5, $\mathbf{C}F_3CO_2^-$), 49.44 (8-C), 46.99 (10-C), 46.96 (14-C), 46.68 (11-C), 44.49 (15-C), 36.50 (17-C), 25.77 (9-C), 23.70 (16-C), 22.38 (12- and 13-C); IR (solid state): ν_{CO} (cm^{-1}) 2037, 1920; MS (ES+) 749 $[M]^+$, 670 $[M\text{-py}]^+$; HRMS (ES+) $C_{26}H_{33}N_8O_3F_3{}^{185}Re$ $[M]^+$ requires 749.2157 found 749.2145. UV/Vis (H_2O) 242 (4836), 321 (1044).

[Re(5-OMe-pyta)(CO)$_3$py]4TFA (129)

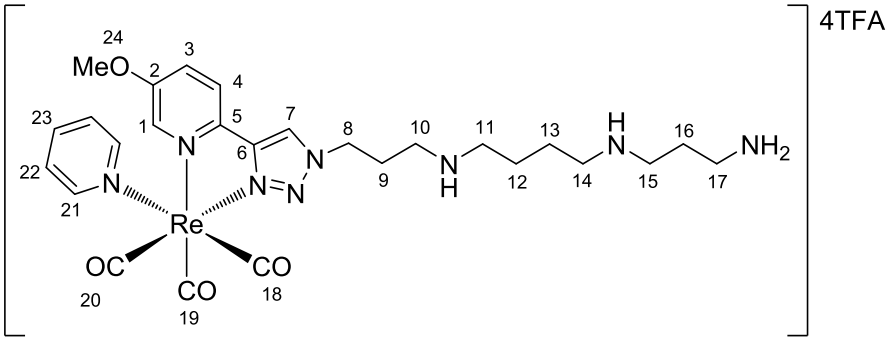

Complex **171** (20.1 mg, 0.021 mmol) was reacted with $AgBF_4$ (8.8 mg, 0.046 mmol) and pyridine (8 µL, 7.9 mg, 0.092 mmol) according to method D. The isolated complex was dissolved in 4M TFA in dichloromethane and stirred for 2 h at room temperature. The volatiles were removed, the crude solid was dissolved in water and filtered through a nylon membrane prior to purification by RP-HPLC method A, t_R = 21.66 mins, and lyophilised to give the title compound as a hygroscopic yellow solid (12.1 mg, 48 %). NMR δ_H (400 MHz, CD_3OD, 298K) 8.93 (m, 2H, 1- and7-CH), 8.45 (m, 2H, 21-CH), 8.12 (d, *J* = 8.8, 4-CH), 7.98 - 7.88 (m, 2H, 3- and 23-CH), 7.43 (m, 2H, 22-CH), 4.83 (m, 2H, 8-CH_2), 3.23 (m, 2H, 17-CH_2), 3.19 - 3.03 (m, 8H, 10-, 11-, 14- and 15-CH_2), 2.53 (m, 2H, 9-CH_2), 2.11 (m, 2H, 16-CH_2), 1.85(m, 4H, 12- and 13-CH); NMR δ_C (101 MHz, CD_3OD, 298K) 195.3027, 193.78 (19- and 20-C), 190.90 (18-C), 161.36 (q, $^2J_{CF}$ = 36.5 , $CF_3\mathbf{C}O_2^-$), 158.54 (2-C), 151. 99 (1-C), 149.31 (21-C), 142.07 (5-C), 141.26 (6-C), 139.74 (3-C), 126.57 (2-C), 124.79 (22-C), 124.61 (4-C), 123.70 (7-C), 55.98 (24-C), 49.25 (8-C), 46.80 (10- and 11-C), 44.47 (14-C), 44.43 (15-C), 36.39 (17-C), 26.01 (9-C), 23.97 (16-C), 22.88 (12-C), 22.78 (13-C); IR (solid state): ν_{CO} (cm^{-1}) 2034, 1910; MS (ES+) 749 $[M]^+$, 711; HRMS (ES+) $C_{26}H_{33}N_8O_3F_3{}^{185}Re$ $[M]^+$ requires 711.2417 found 711.2417. UV/Vis (H_2O) 258 (12640), 307 (5606).

7.7: Synthesis of Iridium(III) complexes

$[Ir(4\text{-}OMe\text{-}ppy)_2Cl]_2$ "$[Ir(papy)_2Cl]_2$" (184)

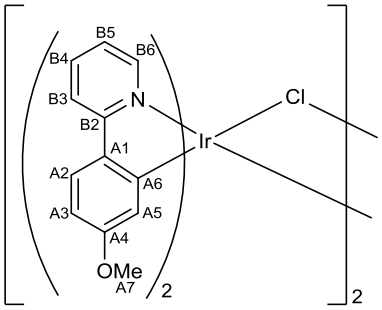

2-(4-methoxyphenyl)pyridine (98.2 mg, 0.530 mmol) and $IrCl_3.nH_2O$ (79.3 mg, 0.263 mmol) were dissolved in a 3:1 mixture of propan-2-ol and water then heated in a microwave reactor for 90 minutes at 110 °C, cooled then the reaction mixture was concentrated in vacuo, re-dissolved in DCM (30 mL) then filtered through celite. The DCM solution was washed with a 0.1 M solution of HCl (3 x 20 mL), dried over magnesium sulfate then concentrated *in vacuo*. The title compound was isolated by precipitation from dichloromethane using hexane to yield a yellow powder (302 mg, 72 %) NMR δ_H (400 MHz, CD_2Cl_2, 298K) 9.11 (ddd, 1H, *J* = 5.8, 1.6, 0.8, B6-CH), 7.72 (ddd, 1H, *J* = 7.2, 1.6, 0.8, B3-CH), 7.65 (m, 1H, B4-CH), 7.42 (d, 1H, *J* = 8.5, A2-CH), 6.67 (ddd, 1H, *J* = 7.2, 5.8, 1.8, B5-CH), 6.32 (dd, 1H, *J* = 8.5, 2.5, A3-CH), 5.26 (d, 1H, *J* = 2.5, A5-CH), 3.33 (s, 3H, A7-CH_3). NMR δ_C (100 MHz, CD_2Cl_2, 298K) 167.81 (B2-C), 159.94 (A4-C), 151.26 (B6-C), 146.97 (A1-C), 136.81 (A6-C), 136.54 (B4-C), 125.01 (A2-C), 121.22 (B5-C), 117.90 (B3-C), 114.75 (A5-C), 107.39 (A3-C), 54.42 (A7-C); MS (ES+) 643 $[Ir(papy)_2(MeCN)_2]^+$, 602 $[Ir(papy)_2(MeCN)_2]^+$, 561 $[Ir(papy)_2]^+$

General procedure E for microwave synthesis of cationic polyamine iridium complexes

Proligand (0.050 mmol) and iridium dimer (0.025 mmol) were dissolved in methanol (4 mL) and heated in a microwave reactor for 2 h at 90 °C. Reaction mixture was cooled, filtered through Celite, then the solvent was removed *in vacuo*. The complex was deprotected and volatiles were removed. The residue was taken up in water, filtered

through a nylon membrane and purified by RP-HPLC using method A, combined fractions were lyophilised.

[Ir(ppy)$_2$(Put-pyta)]2TFA "Ir-Put" (115)

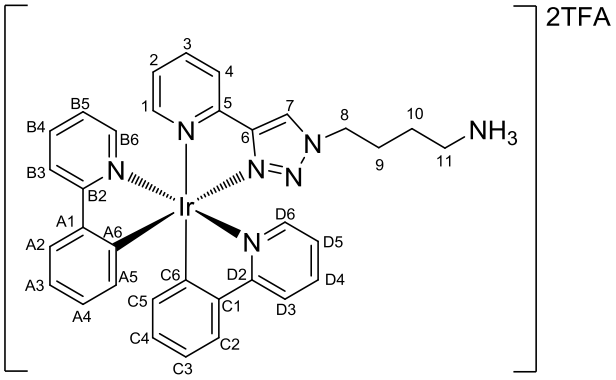

Proligand **160** (20.2 mg, 0.066 mmol) and $[Ir(ppy)_2Cl]_2$ (31.7 mg, 0.030 mmol) were reacted according to general method E. The isolated complex was dissolved in 4M TFA (3 mL) and stirred for 2 h and then volatiles were removed. The residue was taken up in water, filtered through a nylon membrane and purified by RP-HPLC using method A, t_R = 22.97 mins. Combined fractions were lyophilised to give the title compound as a yellow, hygroscopic solid, (39.7 mg, 64 %). NMR δ_H (400 MHz, CD_3OD, 298K) 9.39 (s, 1H, 7-CH), 8.50 (br s, 3H, NH_3) 8.36 (br d, 1H, *J* = 8.5, 4-CH), 7.97 (br t, 1H, *J* = 7.6, 3-CH), 7.89 (br d, 2H, J = 8.1, B3 and D3-CH), 7.79 – 7.72 (m, 3H, 1-CH, B4- and D4-CH), 7.71 – 7.61 (m, 3H, B6-, A2- and C2-CH), 7.48 (br d, 1H, *J* = 5.9, D6-CH), 7.23 (br t, 1H, *J* = 5.9, 1.4, 0.8, 2-CH), 7.08 (ddd, 1H, *J* = 7.3, 5.9, 1.1, D5-CH), 7.04 (dt, 1H, *J* = 7.6, 1.1, B5-CH), 6.32 (m, 2H, C5- and A5-CH). 4.45 (m, 2H, 8-CH_2), 3.03 (br s, 2H, 11-CH_2), 2.35 (m, 2H, 9- CH_2), 1.71 (m, 2H, 10-CH_2); NMR δ_C (100 MHz, CD_3OD, 298K) 168.20 (D2-C), 167.39 (B2-C), 161.40 (q, $^2J_{CF}$ = 29.6, $CF_3\mathbf{C}O_2$), 149.81 (A1- and C1-C), 149.73 (1-C), 149.53 (D6-C), 148.53 (C1-C), 148.38 (B6-C), 146.19 (A1-C), 143.85 (6-C), 143.66 (5-C), 139.61 (3-C), 137.98 (B4- and D4-C), 131.88 (C5-C), 131.75 (A5-C), 130.58 (A4-C), 130.02 (C4-C), 126.84 (2-C), 126.07 (7-C), 124.57 (4-C), 124.28 (D5-C), 123.50 (B5-C), 122.91 (A3-C), 122.59 (C3-C), 122.22 (A3-C), 119.42 (B3-C), 119.31 (D3-C), 116.59 (q, $^1J_{CF}$ = 295.2, $\mathbf{C}F_3CO_2$), 51.33 (8-C), 38.55 (11-C), 26.13 (9-C), 23.86 (10-C). MS (ES+) 718 $[M]^+$, HRMS (ES+) $C_{33}H_{31}N_7{}^{193}Ir$ requires 718.2270 found 718.2271.

[Ir(ppy)$_2$(APPut-pyta)]3TFA "Ir-APPut" (127)

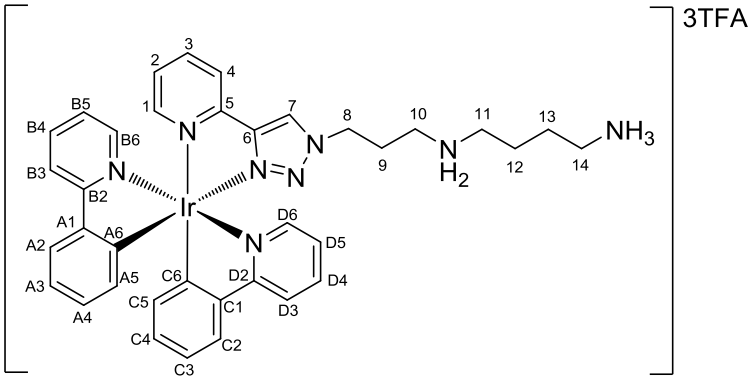

Proligand **154** (41.2 mg, 0.083 mmol) and iridium dimer (39.9 mg, 0.037 mmol) were reacted according to general method E. The isolated complex was dissolved in 4M TFA (3 mL) and stirred for 1 h and then volatiles were removed. The residue was taken up in water, filtered through a nylon membrane and purified by RP-HPLC using method A, t_R = 21.77 mins. Combined fractions were lyophilised to give the title compound as a yellow, hygroscopic solid, (75.0 mg, 81 %). NMR δ_H (400 MHz, CD_3OD, 298K) 9.19 (s, 1H, 7-CH), 8.36 (ddd, 1H, *J* = 8.0, 1.0, 0.9, 4-CH), 8.14 – 8.08 (m, 3H, 3-CH, B3- and D3-CH), 7.92 - 7.85 (m, 3H, 1-CH, B4- and D4-CH), 7.83 (br dd, 1H, *J* = 8.0, 0.8, C2-CH), 7.80 (ddd, 1H, *J* = 5.9, 1.6, 0.7, D6-CH), 7.75 (br dd, 1H, *J* = 7.8, 1.3, A2-CH), 7.66 (ddd, 1H, *J* = 5.9, 1.4, 0.8, B6-CH), 7.43 (ddd, 1H, *J* = 7.7, 5.6, 1.4, 2-CH), 7.13 (ddd, 1H, *J* = 7.4, 6.0, 1.4, D5-CH), 7.08 (ddd, 1H, *J* = 7.5, 5.8, 1.4, B5-CH), 7.04 (m, 1H, C3-CH), 6.95 (ddd, 1H, *J* = 8.5, 7.2, 1.3, A3-CH), 6.90 (dt, 1H, *J* = 7.5, 1.4, C4-CH), 6.80 (dt, 1H, *J* = 7.5, 1.4, A4-CH), 6.30 (dd, 1H, *J* = 7.7, 0.8, C5-CH), 6.27 (dd, 1H, *J* = 7.6, 0.9, A5-CH), 4.64 (m, 2H, 8-CH_2), 3.08 (m, 2H, 10- CH_2), 2.99 (m, 4H, 11- and 14- CH_2), 2.35 (m, 2H, 9- CH_2), 1.75 (m, 4H, 12- and 13- CH_2); NMR δ_C (100 MHz, CD_3OD, 298K) 168.37 (B2-C), 167.72 (D2-C), 161.27 (q, $^2J_{CF}$ = 28.2, $CF_3\mathbf{C}O_2$), 150.10 (1-C), 149.49 (C6-C), 149.44 (5-C), 149.25 (D6-C), 148.66 (6- and B6-C), 146.19 (A6 -C), 144.05 (A1-C), 144.00 (C1-C), 139.56 (3-C), 138.22 (D4-C), 138.12 (B4-C), 131.61 (A5-C), 131.25 (C5-C), 130.07 (C4-C), 129.27 (A4-C), 126.51 (2-C), 126.30 (7-C), 124.55 (C2-C), 123.97 (A2-C), 123.06 (D5-C), 122.78 (B5-C), 122.61 (4-C), 122.37 (C3-C), 121.75 (A3-C), 119.49 (B3-C), 119.30 (D3-C), 116.59 (q, $^1J_{CF}$ = 295.2, $\mathbf{C}F_3CO_2$), 48.76 (8-C), 46.97 (11-C), 44.45 (10-C), 38.55 (14-C), 25.97 (9-C), 24.13 (12-C), 22.82 (13-C). MS (ES+) 775 $[M]^+$, HRMS (ES^+) $C_{36}H_{38}N_8{}^{193}Ir$ requires 775.2849 found 775.2858.

[Ir(ppy)$_2$(Spm-pyta)]4TFA "Ir-Spm" (123)

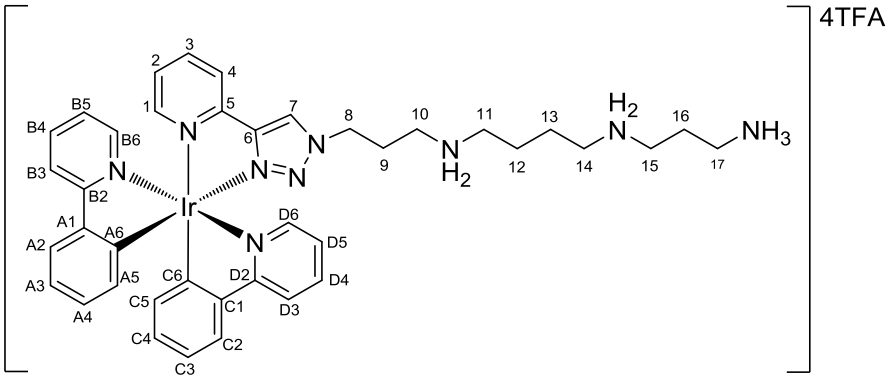

Proligand **166** (83.3 mg, 0.13 mmol) and $[Ir(ppy)_2Cl]_2$ (67.3 mg, 0.06 mmol) were reacted according to general method E. The isolated complex was dissolved in 4M TFA (3 mL) and stirred for 30 minutes and then volatiles were removed. The residue was taken up in water, filtered through a nylon membrane and purified by RP-HPLC using method A, t_R = 20.59 mins. Combined fractions were lyophilised to give the title compound as a yellow, hygroscopic solid, (49.8 mg, 63 %). δ_H (400 MHz, CD_3OD, 298K) 9.01 (s, 1H), 8.22 - 8.14 (br d, 1H, *J* = 8.1, 4-CH), 8.03 - 7.95 (m, 3H, 3-C, B3- and D3-C), 7.82 - 7.71 (m, 3H, 1-CH, B4- and D4-CH), 7.71 - 7.64 (m, 2H, D6- and C2-C), 7.62 (dd, 1H, J = 8.0, 0.8, A2-C), 7.53 (m, 1H, B6-C), 7.29 (ddd, 1H, *J* = 7.7, 5.5, 1.0, 2-CH), 7.00 (ddd, 1H, *J* = 7.4, 5.9, 1.4, D5-CH), 6.95 (ddd, 1H, *J* = 7.2, 5.6, 1.0, B5-CH), 6.91 (dt, 1H, *J* = 7.6 1.2, 1H), 6.82 (dt, *J* = 1.1, 7.5 Hz, 1H), 6.77 (dt, 1H, *J* = 7.4, 1.3, C3-CH), 6.67 (dt, 1H, *J* = 7.4, 1.3, A3-CH), 6.21 - 6.12 (m, 2H, C5- and A5-CH), 4.52 (m, 2H, 8-CH_2), 3.03 (m, 2H, 17- CH_2), 2.96 (m, 6H, 10-, 11- and 15- CH_2), 2.88 (m, 2H, 14- CH_2), 2.23 (m, 2H, 9- CH_2), 1.99 (m, 2H, 16- CH_2), 1.67 (m, 4H, 12- and 13- CH_2). δ_C (100 MHz, CD_3OD, 298K) 168.34 (B2-C), 167.68 (D2-C), 161.63 (q, $^2J_{CF}$ = 33.4, $CF_3\mathbf{C}O_2$), 150.09 (1-C), 149.48 (C6-C), 149.46 (5-C), 149.26 (D6-C), 148.65 (6- and B6-C), 146.19 (A6-C), 144.06 (C1-C), 144.01 (A1-C), 139.57 (3-C), 138.23 (C2-C), 138.14 (A2-C), 131.62 (A5-C), 131.26 (C5-C), 130.08 (C4-C), 129.29 (A4-C), 126.50 (2-C), 126.30 (7-C), 124.56 (C2-C), 123.99 (A2-C), 123.09 (D5-C), 122.80 (B5-C), 122.63 (4-C), 122.38 (C3-C), 121.78 (A3-C), 119.50 (D3-C), 119.32 (B3-C), 116.80 (q, $^1J_{CF}$ = 281.1, $\mathbf{C}F_3$), 46.90 (8-CH_2), 46.81 (11-CH_2), 46.77 (14-CH_2), 44.45 (10- and 17-CH_2), 36.42 (15-CH_2), 25.96 (9-CH_2), 23.96 (16-CH_2), 22.83 (12-CH_2), 22.78 (13-CH_2). MS (ES+) 832 $[M]^+$, HRMS (ES+) $C_{39}H_{45}N_9{}^{193}Ir$ requires 832.3427 found 832.3427. UV/Vis (H_2O) 252 (45937), 381 (4748).

[Ir(ppy)$_2$(APSpm-pyta)]5TFA "Ir-APSpm" (128)

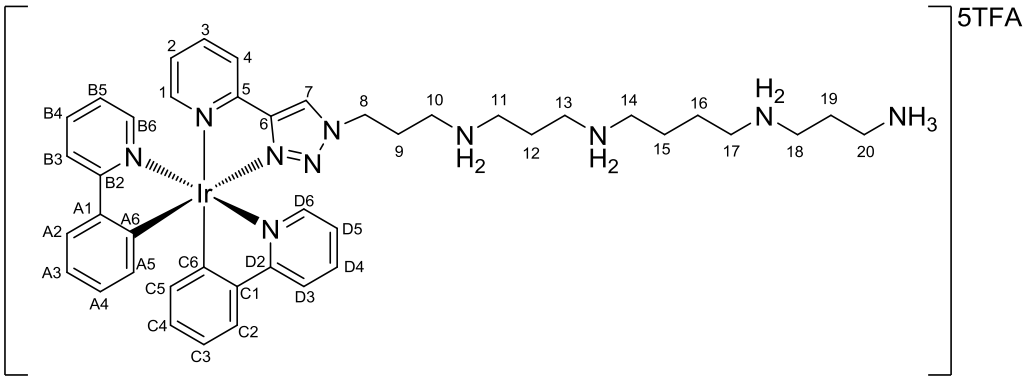

Proligand **167** (40.2 mg, 0.051 mmol) and $[Ir(ppy)_2Cl]_2$ (26.4 mg, 0.024 mmol) were reacted according to general method E. The isolated complex was dissolved in 4M TFA (3 mL) and stirred for 30 minutes and then volatiles were removed. The residue was taken up in water, filtered through a nylon membrane and purified by RP-HPLC using method A, t_R = 20.99 mins. Combined fractions were lyophilised to give the title compound as a yellow, hygroscopic solid, (54.8 mg, 73 %). δ_H (400 MHz, CD_3OD, 298K) 9.13 (s, 1H, 7-CH), 8.30 (dt, 1H, *J* = 7.7, 1.0, 4-CH), 8.17 - 8.08 (m, 3H, 3-CH, B3- and D3-CH), 7.95 - 7.85 (m, 3H, 1-CH, B4- and D4-CH), 7.83 (dd, 1H, *J* = 7.9, 1.0, C2-CH), 7.79 (ddd, 1H, *J* = 5.7, 1.5, 1.0, D6-CH), 7.75 (dd, 1H *J* = 7.8, 1.2, A2-CH), 7.66 (ddd, *J* = 5.9, 1.7, 0.7, B6-CH), 7.44 (ddd, 1H, *J* = 7.6, 5.5, 1.4, 2-CH), 7.13 (ddd, 1H, *J* = 7.4, 5.9, 1.4, D5-CH), 7.10 - 7.02 (m, 2H, B5- and C3-CH), 6.95 (ddd, 1H, *J* = 8.4, 7.4, 1.2, A3-CH), 6.90 (dt, 1H, *J* = 7.5, 1.3, C4-CH), 6.80 (dt, 1H, *J* = 7.5, 1.3, A4-CH), 6.30 (dd, 1H, *J* = 7.6, 0.8, C5-CH), 6.27 (dd, *J* = 7.7, 0.8, A5-CH), 4.64 (m, 2H, 8-CH_2), 3.20 - 3.04 (m, 14H, 10-, 11-, 13-, 14-, 17- and 20- CH_2), 2.36 (m, 2H, 18-CH_2), 2.11 (m, 4H, 12- and 19-CH_2), 1.83 (m, 4H, 15- and 16-CH_2). δ_C (100 MHz, CD_3OD, 298K) 168.38 (B2-C), 167.72 (D2-C), 161.62 (q, $^2J_{CF}$ = 35.2, $CF_3\mathbf{C}O_2$), 150.11 (1-C), 149.49 (C6-C), 149.42 (5-C), 149.25 (D6-C), 148.66 (B6-C), 148.64 (6-C), 146.16 (3-C), 144.04 (C1-C), 143.99 (A1-C), 139.55 (3-C), 138.21 (C3-C), 138.12 (A3-C), 131.61 (A5-C), 131.25 (C5-C), 130.06 (C4-C), 129.27 (A4-C), 126.51 (2-C), 126.27 (7-C), 124.54 (C2-C), 123.97 (A2-C), 123.06 (D5-C), 122.77 (B5-C), 122.60 (4-C), 122.36 (C3-C), 121.75 (A3-C), 119.48 (D3-C), 119.30 (B3-C), 116.62 (q, $^1J_{CF}$ = 291.1, $\mathbf{C}F_3CO_2$), 48.74 (8-C), 46.77 (17-C), 44.59 (11-C), 44.47 (17-C), 44.43 (11-C), 44.35 (13-C), 36.40 (20-CH), 25.96 (9-C), 23.97 (19-C), 22.77 (12-, 15- and 16-C). MS (ES+) 889 $[M]^+$, HRMS (ES+) $C_{42}H_{52}N_{10}{}^{193}Ir$ requires 889.4006 found 889.4008.

[Ir(ppy)$_2$(AcPut-pyta)]TFA "Ir-AcPut" (116)

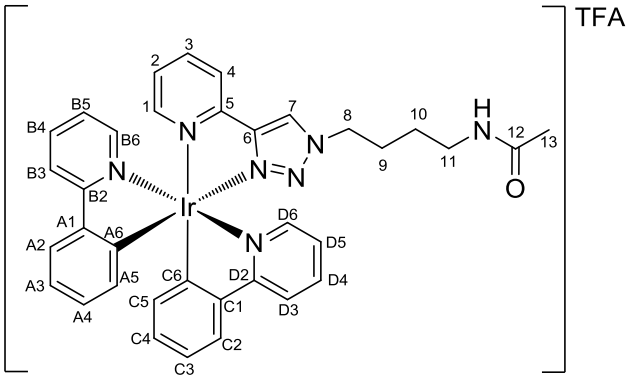

Complex **126** (18.7 mg, 0.02 mmol) was dissolved in 20 % AcOAc in dry DMF and stirred at room temperature overnight. Volatiles were removed under reduced pressure and the resulting residue was taken up in water, filtered through a nylon membrane and purified by RP-HPLC using method A, t_R = 225.51 mins. Combined fractions were lyophilised to give the title compound as a yellow, hygroscopic solid, (13.1 mg, 76 %). δ_H (500 MHz, $CDCl_3$, 298K) 9.62 (br s, 1H, 7-CH), 8.40 (br s, 1H, NH), 7.92 (m, 1H, 4-CH), 7.86 (m, 2H, B3- and D3-CH), 7.72 (m, 3H, 3-CH, B4- and D4-CH), 7.61 (m, 3H, C2-, D6- and B6-CH), 7.40 (m, H, A2-CH), 7.20 - 7.15 (m, 1H, 2-CH), 7.03 – 6.96 (m, 2H, D5- and B5-CH), 6.94 (m, 1H, C3-CH), 6.90 (m, 1H, A3-CH), 6.86 (br dt, 1H, *J* = 7.3, 1.1, C4-CH),6.82 (br dt, 1H, *J* = 7.6, 1.1, A4-CH), 6.27 (d, 1H, *J* = 7.5, C5-CH), 6.24 (d, 1H, *J* = 7.7, A5-CH), 4.39 (m, 2H, 8-CH_2), 3.17 (m, 2H, 11-CH_2), 1.94 (m, 5H, 9-CH_2 and 13-CH_3), 1.94 (s, 3H), 1.45 (m, 2H, 10-CH_2). δ_C (126 MHz, $CDCl_3$, 298K) 169.57 (12-C), 168.42 (B2-C), 167.64 (D2-C), 149.98 (1-C), 149.87 (C6-C), 149.74 (5-C), 149.34 (D6-C), 148.46 (6-C), 148.24 (B6-C), 146.09 (A6-C), 143.73 (C1-C), 143.53 (A1-C), 139.56 (3-C), 138.00 (C2-C), 137.92 (A2-C), 131.86 (A5-C), 131.76 (C5-C), 130.73 (C4-C), 130.15 (A4-C), 127.24 (2-C), 126.05 (7-C), 124.68 (C2-C), 124.35 (A2-C), 123.57 (D5-C), 123.30 (B5-C), 122.73 (4-C), 122.70 (C3-C), 122.33 (A3-C), 119.49 (D3-C), 119.43 (B3-C), 51.83 (8-C), 38.29 (11-C), 26.82 (13-C), 25.62 (9-C), 22.62 (10-C). MS (ES+) 760 $[M]^+$, HRMS (ES+) $C_{35}H_{33}N_7O^{193}Ir$ requires 760.2376 found 760.2377.

[Ir(ppy)$_2$(COOH-pyta)]TFA "Ir-COOH" (128)

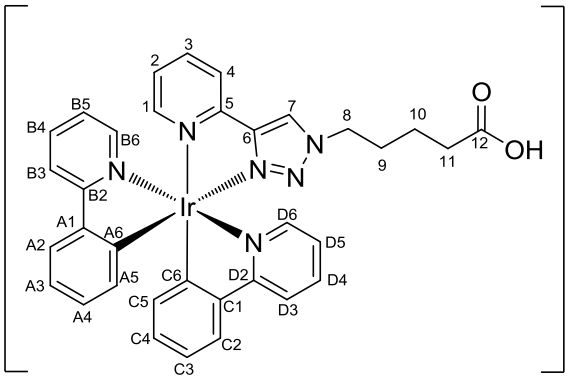

Proligand **161** (28.6 mg, 0.104 mmol) and $[Ir(ppy)_2Cl]_2$ (52.6 mg, 0.049 mmol) were reacted according to general method E. The isolated complex was dissolved in THF (3 mL) and stirred with $LiOH.H_2O$ (5.4 mg, 0.108 mmol) overnight. Volatiles were removed and the residue was taken up in water, filtered through a nylon membrane and purified by RP-HPLC using method A, t_R = 28.33 mins. Combined fractions were lyophilised to give the title compound as a yellow, hygroscopic solid, (18.7 mg, 40 %). δ_H (400 MHz, CD_3OD, 298K) 9.08 (s, 1H, 7-CH), 8.28 (br d, 1H, J = 8.0, 4-CH), 8.10 (m, 3H, 3-CH, B3- and D3-CH), 7.92 - 7.83 (m, 3H, 1-CH, B4- and D4-CH), 7.82 (dd, 1H, *J* = 7.8, 0.8, C2-CH), 7.78 (ddd, 1H, *J* = 5.8, 1.4, 0.6 D6-CH), 7.74 (dd, 1H, *J* = 7.9, 1.0, A2-CH), 7.64 (ddd, 1H, *J* = 5.7, 1.4, 0.7, B6-CH), 7.40 (ddd, 1H, *J* = 7.6, 5.6, 1.3, 2-CH), 7.17 (ddd, 1H, *J* = 7.4, 5.9, 1.4, D5-CH), 7.04 (m, 2H, B5- and C3-CH), 6.91 (m, 2H, A3- and C4-CH), 6.78 (dt, 1H, *J* = 7.5, 1.3, A4-CH), 6.33 (dd, 1H, *J* = 7.7, 1.4, C5-CH), 6.26 (dd, *J* = 7.7, 0.8, A5-CH), 4.49 (m, 2H, 8-CH_2), 2.15 (m, 2H, 11- CH_2), 1.94 (m, 2H, 9- CH_2), 1.50 (m, 2H 10- CH_2). δ_C (101 MHz, CD_3OD, 298K) 180.29 (12-C), 168.42 (B2-C), 167.67 (D2-C), 149.99 (1-C), 149.79 (C6-C), 149.78 (5-C), 149.28 (D6-C), 148.47 (B6-C), 148.43 (6-C), 146.18 (A6-C), 144.13 (A1-C), 143.96(C1-C), 139.44 (3-C), 138.15 (C2-C), 138.08 (A2-C), 131.56 (A5-C), 131.38 (C-5), 129.99 (C4-C), 129.26 (A4-C), 126.24 (7-C), 125.85 (2-C), 124.49 (C2-C), 123.99 (A2-C), 123.23 (D5-C), 122.65 (B5-C), 122.48 (4-C), 122.26 (C3-C), 121.72 (A3-C), 119.41 (D3-C), 119.31 (B3-C), 51.74 (8-C), 36.67 (11-C), 29.13 (9-C), 22.74 (10-C). MS (ES+) 815 $[M]^+$, HRMS (ES^+) $C_{35}H_{29}N_6O_2{}^{191}Ir$ requires 813.1910 found 813.1915.

[Ir(ppy)$_2$(PO(OH)$_2$-pyta)]TFA "Ir-PO(OH)$_2$" (129)

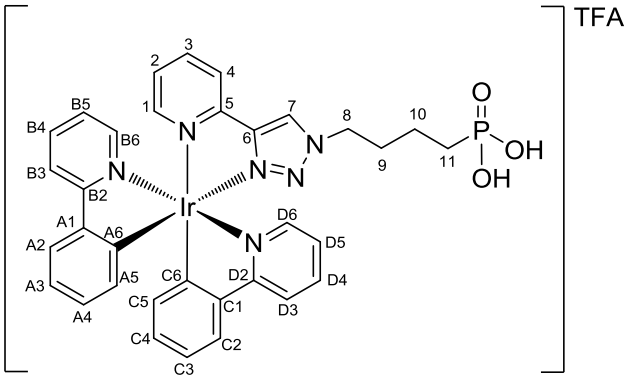

Proligand **162** (19.7 mg, 0.058 mmol) and [Ir(ppy)$_2$Cl]$_2$ (31.2 mg, 0.029 mmol) were reacted according to general method E. The isolated complex was dissolved in dry MeCN (3 mL) under an inert atmosphere to which TMSBr (50 µL, 0.380 mmol) was added dropwise via a septum at 0 °C. After the addition was complete, the mixture was warmed to ambient temperature and stirred overnight. Water (1 mL) was then added and the mixture stirred for 1 h at room temperature, then volatiles were removed *in vacuo*. The mixture was filtered through a nylon membrane and purified by RP-HPLC using method A, t_R = 24.99 mins. Combined fractions were lyophilised to give the title compound as a yellow, hygroscopic solid, (14.9 mg, 26 %). δ_H (400 MHz, CD_3OD, 298K) 8.99 (s, 1H, 7-CH), 8.17 (dt, 1H, *J* = 7.8, 1.1, 4-CH), 8.01 (m, 3H, 3-CH, B3- and D3-CH), 7.84 - 7.74 (m, 3H, 1-CH, B4- and C4-CH), 7.73 (dd, 1H, *J* = 7.8, 1.0, C2-CH), 7.68 -7.62 (m, 2H, A2- and D6-CH), 7.54 (ddd, 1H, *J* = 5.9, 1.5, 0.6, B6-CH), 7.33 (ddd, 1H, *J* = 7.7, 5.5, 1.3, 2-CH), 7.06 (ddd, 1H, *J* = 7.3, 5.9, 1.7, D5-CH), 6.99 - 6.91 (m, 2H, B5- and C3-CH), 6.85 (ddd, 1H, *J* = 7.8, 7.2, 1.0, A3-CH), 6.80 (dt, 1H, *J* = 7.4, 1.0, C4-CH), 6.70 (dt, 1H, *J* = 7.6, 1.0, A4-CH), 6.22 (dd, *J* = 7.6, 0.8, C5-CH), 6.16 (dd, 1H, *J* = 7.7, 0.8, A5-CH), 4.43 (m, 2H, 8-CH_2), 1.96 (m, 2H, 9-CH_2), 1.69 - 1.55 (m, 2H, 11-CH_2), 1.55 - 1.40 (m, 2H, 10-CH_2) δ_C (101 MHz, CD_3OD, 298K) 168.43 (B2-C), 167.74 (D2-C), 150.08 (1-C), 149.66 (C6-C), 149.62 (5-C), 149.14 (D6-C), 148.56(6-C), 148.48 (B6-C), 146.13 (A6-C), 144.07 (C1-C), 143.96 (A1-C), 139.50 (3-C), 138.17 (C2-C), 138.09 (A2-C), 131.56 (A5-C), 131.34 (C5-C), 130.04 (C4-C), 129.28 (A4-C), 126.38 (7-C), 125.82 (2-C), 124.52 (C2-C), 124.00 (A2-C), 123.17 (D5-C), 122.67 (B5-C), 122.46 (4-C), 122.32(C3-C), 121.74 (A3-C), 119.47 (D3-C), 119.32 (B3-C), 51.45 (8-C), 29.88 (9-C), 25.86 (d, $^1J_{CP}$ = 136.8, 11-C) 19.55 (10-C). δ_P (162 MHz, CD_3OD, 298K) 31.18. MS (ES+) 783 $[M]^+$, HRMS (ES^+) $C_{33}H_{31}N_6O_3P^{193}Ir$ requires 783.1824 found 783.1833.

[Ir(ppy)$_2$(PEG-pyta)]TFA "Ir-PEG" (140)

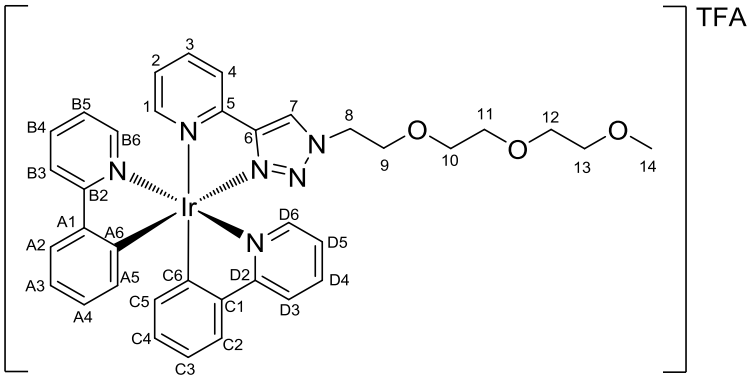

Proligand **152** (51.6 mg, 0.177 mmol) and [Ir(ppy)$_2$Cl]$_2$ (86.2 mg, 0.080 mmol) were reacted according to general method E. The residue was taken up in water, filtered through a nylon membrane and purified by RP-HPLC using method A, t_R = 29.03 mins. Combined fractions were lyophilised to give the title compound as a yellow, hygroscopic solid, (47.7 mg, 66 %). δ_H (400 MHz, CD_3OD, 298K) 9.32 (s, 1H, 7-CH), 8.37 (br d, 1H, *J* = 7.7, 4-CH), 8.06 (t, 1H, *J* = 7.3, 3-CH), 7.98 (m, 2H, B6- and D6-CH), 7.87 (d, 1H, *J* = 4.6, 1-CH), 7.73 - 7.67 (m, 2H, B4- and D4-CH), 7.97 – 7.68 (m, 3H, C2-, D6- and A2-CH), 7.56 (d, 1H, *J* = 5.8, B6-CH), 7.33 (t, 1H, *J* = 6.7, 2-CH), 7.14 – 7.00 (m, 4H, D5-, B5-, C3- and A3-CH), 6.97 (dt, 1H, *J* = 7.5, 1.4, C4-CH), 6.91 (dt, 1H, *J* = 7.5, 1.4, C4-CH), 6.35 (m, 2H, C5- and A5-CH), 4.70 (m, 2H, 8-CH_2), 3.96 (m, 2H, 8-CH_2), 3.57 - 3.50 (m, 2H, 10-CH_2), 3.50 - 3.44 (m, 4H, 11- and 12-CH_2), 3.42 - 3.38 (m, 2H, 13-CH_2), 3.31 (s, 3H, 14-CH_3). δ_C (100 MHz, CD_3OD, 298K) 168.05 (B2-C), 167.48 (D2-C), 150.24 (1-C), 149.82 (C6-C), 149.45 (5-C), 149.32 (D6-C), 148.63 (B6-C), 148.59 (6-C), 146.31 (A6-C), 143.97 (C1-C), 143.93 (A1-C), 139.59 (3-C), 138.10 (D4-C), 138.02 (B4-C), 131.91 (C5-C), 131.53 (A5-C), 130.57 (C4-C), 129.87 (A4-C), 127.55(2-C), 126.36 (7-C), 124.76(C2-C), 124.36 (A2-C), 123.37 (D5-C), 123.27 (B5-C), 123.02 (4-C), 122.73 (C3-C), 122.24 (A3-C), 119.65 (D3-C), 119.61 (B3-C), 71.79 (13-CH_2), 70.34 (10-CH_2), 70.26 (11- or 12-CH_2), 70.19 (11- or 12-CH_2), 68.27 (9-CH_2), 58.50 (14-CH_3), 52.10 (8-CH_2). MS (ES+) 793 $[M]^+$, HRMS (ES+) $C_{36}H_{36}N_6O_3{}^{193}Ir$ requires 793.2478 found 793.2479.

[Ir(ppy)$_2$(5-ClMe-PEG-pyta)]TFA "5-ClMe-IrPEG" (147)

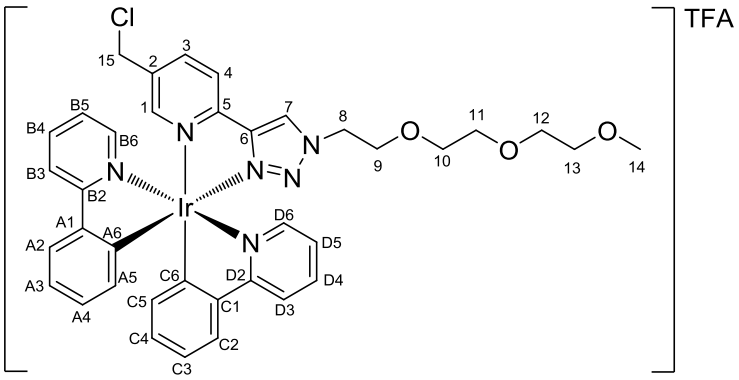

Proligand **153** (28.7 mg, 0.090 mmol) and $[Ir(ppy)_2Cl]_2$ (45.9 mg, 0.043 mmol) were reacted according to general method E. The isolated complex taken up in water, filtered through a nylon membrane and purified by RP-HPLC using method A, t_R = 27.28 mins. Combined fractions were lyophilised to give the title compound as a yellow, hygroscopic solid, (22.4 mg, 26 %). δ_H (500 MHz, $CDCl_3$, $SiMe_4$, 298K) 9.63 (br s, 1H, 7-CH), 8.53 (br d, 1H, *J* = 6.3, 4-CH), 7.95 (br d, 1H, *J* = 6.2, 3-CH), 7.90 (m, 2H, B3- and D3-CH), 7.75 (m, 2H, D4- and B4-CH), 7.65 (m, 4H, 1-, C2-, A2- and D6-CH), 7.49 (m, 1H, B6-CH), 7.08 - 7.00 (m, 2H, D5- and B5-CH), 6.98 (m, 2H, C3- and A3-CH), 6.91 (t, 1H, *J* = 7.5, C4-CH), 6.86 (t, 1H, *J* = 7.4, A4-CH), 6.33 - 6.27 (m, 2H, C5- and A5-CH), 4.64 (m, 2H, 8-CH_2), 4.29 (s, 2H, 15-CH_2), 3.91 (m, 2H, 9-CH_2), 3.66 - 3.60 (m, 2H, 10-CH_2), 3.60 - 3.53 (m, 4H, 11- and 12-CH_2), 3.50 (m, 2H, 13-CH_2), 3.32 (s, 3H, 14-CH_2). δ_C (125 MHz, $CDCl_3$, $SiMe_4$, 298K) 168.33 (B2-C), 167.64 (D2-C), 149.88 (1-C), 149.40 (C6-C), 149.22 (5-C), 148.55 (D6-C), 148.37 (B6-C), 148.20 (6-C), 146.35 (A6-C), 143.72 (C1-C), 143.59 (A1-C), 138.71(3-C), 137.90 (D4-C), 137.79 (B4-C), 131.84 (A5-C), 131.69 (C5-C), 130.68 (C4-C), 130.04 (A4-C), 128.01 (2-C), 126.25 (7-C), 124.59 (C2-C) 124.26 (A2-C)123.49 (D5-C), 123.26 (B5-C-C), 122.82 (4-C), 122.62 (C3-C), 122.19 (A3-C), 119.37 (B3-and D3-C), 71.78(13-C), 70.98 (15-C), 70.34 (11- and 12-C), 70.27 (10-C), 68.26 (9-C), 58.87 (14-C), 51.76 (8-C). MS (ES+) 840 $[M]^+$.

[Ir(ppy)$_2$(4-CF$_3$-pyta)]4TFA "4-CF$_3$-IrSpm" (134)

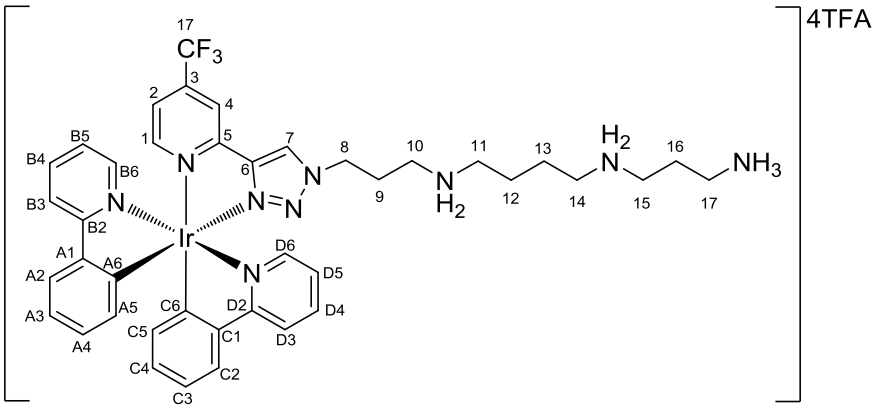

Proligand **158** (19.2 mg, 0.027 mmol) and $[Ir(ppy)_2Cl]_2$ (13.9 mg, 0.013 mmol) were reacted according to general method E. The isolated complex was dissolved in 4M TFA (3 mL) and stirred for 30 minutes and then volatiles were removed. The residue was taken up in water, filtered through a nylon membrane and purified by RP-HPLC using method A, t_R = 25.04 mins. Combined fractions were lyophilised to give the title compound as a yellow, hygroscopic solid, (15.7 mg, 84 %). δ_H (400 MHz, CD_3OD, 298K) 9.16 (bs, 1H, 7-CH), 8.59 (s, 1H, 4-CH), 8.00 (m, 3H, B3-, D3- and 1-CH), 7.83 - 7.74 (m, 2H, B4- and D4-CH), 7.72 (dd, 1H, *J* = 8.0, 0.9, C2-CH), 7.67 (dd, 1H, *J* = 5.8, 0.8, D6-CH), 7.65 - 7.59 (m, 3H, A2-, B6- and 2-CH), 7.02 (ddd, 1H, *J* = 7.3, 5.9, 1.2, D5-CH), 7.00 - 6.91 (m, 2H, B5- and C3-CH), 6.87 - 6.76 (m, 2H, A3- and C4-CH), 6.18 (dd, 1H, *J* = 7.7, 0.9, C5-CH), 6.12 (dd, 1H, *J* = 7.7, 0.9, A5-CH), 4.55 (m, 2H, 8-CH_2), 3.03 (m, 2H, 17-CH_2), 2.96 (m, 6H, 10-, 11- and 15-CH_2), 2.90 (m, 2H, 14-CH_2), 2.25 (m, 2H, 9-CH_2), 1.99 (m, 2H, 16-CH_2), 1.68 (m, 4H, 12- and 13-CH_2). δ_C (100 MHz, CD_3OD, 298K) 168.10 (B2-C), 167.58 (D2-C), 161.35 (q, $^2J_{CF}$ = 33.4, $CF_3\mathbf{C}O_2$), 151.57 (1-C), 151.22 (C6-C), 149.41 (5-C), 149.03 (D6-C), 148.72 (B6-C), 147.80 (6-C), 145.34 (A6), 144.06 (C1-C), 143.87 (A1-C), 140.39 (q, $^2J_{CF}$ = 35.2, 3-C), 138.45 (C3-C), 138.27 (A3-C), 131.46 (A5-C), 131.30 (C5-C), 130.17 (C4-C), 129.83(2-C), 129.33 (A4-C), 127.56 (7-C), 124.65 (C2-C), 124.00 (A2-C), (D5-C), 123.26 (D5-C), 122.95 (4-C), 122.63 (B5-C), 122.44 (C3-C), 121.97 (A3-C), 120.69 (q, $^1J_{CF}$ = 350.0, 17-$\mathbf{C}F_3$), 119.62 (D3-C), 119.36 (B3-C), 48.92 (8-C), 46.96 (11-C), 44.78 (14-C), 44.43 (17- and 10-C), 36.40 (15-C), 25.93 (9-C), 23.96 (16-C), 22.79 (12-C), 22.74 (13-C). δ_F (376 MHz, CD_3OD, 298K) -66.39 (s, Ar-C$\mathbf{F}_3$), -76.89 (s, $C\mathbf{F}_3CO_2^-$). MS (ES+) 960 $[M]^+$, HRMS (ES+) $C_{42}H_{48}N_9O_2F_3{}^{191}Ir$ requires 958.3489 found 958.3505. UV/Vis (H_2O) 2249 (43293), 373 (4948).

[Ir(ppy)$_2$(5-CF$_3$-pyta)]4TFA "5-CF$_3$-IrSpm" (133)

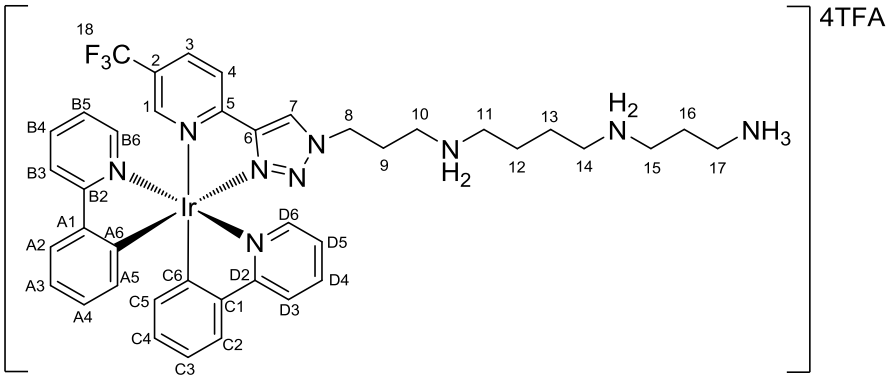

Proligand **157** (48.1 mg, 0.069 mmol) and $[Ir(ppy)_2Cl]_2$ (35.7 mg, 0.033 mmol) were reacted according to general method E. The isolated complex was dissolved in 4M TFA (3 mL) and stirred for 30 minutes and then volatiles were removed. The residue was taken up in water, filtered through a nylon membrane and purified by RP-HPLC using method A, t_R = 26.67 mins. Combined fractions were lyophilised to give the title compound as a yellow, hygroscopic solid, (25.7 mg, 55 %). δ_H (400 MHz, CD_3OD, 298K) 9.34 (s, 1H, 7-CH), 8.55 (br d, 1H, *J* = 8.2, 4-CH), 8.49 (dd, *J* = 8.4, 1.9, 3-CH), 8.18 – 8.11 (m, 2H, B3 and D3-CH), 8.09 (q, 1H, $^4J_{HF}$ = 1.0 Hz, 1-CH) 7.95 – 7.89 (m, 2H, B4 and D4-CH), 7.87 (m, 2H, C2 and D6-CH), 7.78 (m, 2H, A2 and B6-CH), 7.18 (ddd, 1H *, J* = 7.5, 5.8, 1.3, D5-CH), 7.13 (ddd, 1H *, J* = 7.5, 5.8, 1.3, B5-CH), 7.10 (td, 1H, *J* = 7.7, 1.2, C3-CH), 7.00 - 6.93 (m, 2H, A3- and D5-CH), 6.82 (dt, 1H *, J* = 7.2, 1.4, 1H, B5-CH), 6.36 (dd, 1H *, J* = 7.6, 0.8, C5-CH), 6.30 (dd, 1H, *J* = 7.6, 0.8, A5-CH), 4.76 - 4.63 (m, 2H, 8-CH_2), 3.19 (m, 2H, 17-CH_2), 3.12 (m, 6H, 10, 11 and 15-CH_2), 3.05 (m, 2H, 14-CH_2), 2.40 (m, 2H, 9-CH_2), 2.15 (m, 2H, 16-CH_2), 1.83 (m, 4H, 12 and 13-CH_2). δ_C (100 MHz, CD_3OD, 298K) 168.10 (B2-C), 167.58 (D2-C), 161.35 (q, $^2J_{CF}$ = 33.4, CF_3**C**O_2), 151.57 (1-C), 151.22 (C6-C), 149.41 (5-C), 149.03 (D6-C), 148.72 (B6-C), 147.80 (6-C), 145.34 (A6), 144.06 (C1-C), 143.87 (A1-C), 140.39 (q, $^2J_{CF}$ = 35.2, 3-C), 138.45 (C3-C), 138.27 (A3-C), 131.46 (A5-C), 131.30 (C5-C), 130.17 (C4-C), 129.83(2-C), 129.33 (A4-C), 127.56 (7-C), 124.65 (C2-C), 124.00 (A2-C), (D5-C), 123.26 (D5-C), 122.95 (4-C), 122.63 (B5-C), 122.44 (C3-C), 121.97 (A3-C), 120.69 (q, $^1J_{CF}$ = 350.0, 17-**C**F_3), 119.62 (D3-C), 119.36 (B3-C), 48.92 (8-C), 46.96 (11-C), 44.78 (14-C), 44.43 (17- and 10-C), 36.40 (15-C), 25.93 (9-C), 23.96 (16-C), 22.79 (12-C), 22.74 (13-C). δ_F (376 MHz, CD_3OD, 298K) -66.39 (s, Ar-C**F**$_3$), -76.89 (s, C**F**$_3CO_2^-$). 678 MS (ES+) 900 $[M]^+$, HRMS (ES+) $C_{40}H_{44}N_9F_3{}^{193}Ir$ requires 900.3299 found 900.3301. UV/Vis (H_2O) 251 (44141), 379 (5000).

[Ir(ppy)$_2$(5-OMe-pyta)]4TFA "5-OMe -IrSpm" (132)

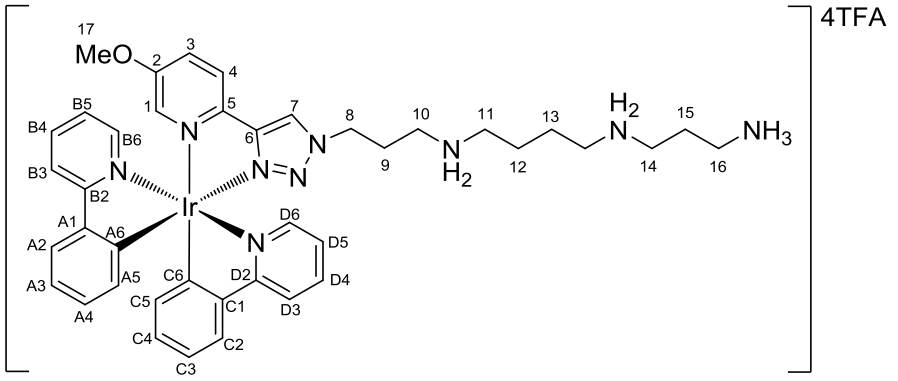

Proligand **160** (39.6 mg, 0.058 mmol) and [Ir(ppy)$_2$Cl]$_2$ (30.1 mg, 0.028 mmol) were reacted according to general method E. The isolated complex was dissolved in 4M TFA (3 mL) and stirred for 30 minutes and then volatiles were removed. The residue was taken up in water, filtered through a nylon membrane and purified by RP-HPLC using method A, t_R = 22.96 mins. Combined fractions were lyophilised to give the title compound as a yellow, hygroscopic solid, (22.2 mg, 29 %). δ_H (400 MHz, CD_3OD, 298K) 8.86 (s, 1H, 7-CH), 8.12 (d, 1H, *J* = 8.8, 4-CH), 8.00 (m, 2H, B3- and D3-CH), 7.83 – 7.74 (m, 2H, B4- and D4-CH), 7.73 (d, 1H, *J* = 7.8, C2-CH), 7.69 (d, 1H, *J* = 5.1, D6-H), 7.67 - 7.56 (m, 3H, 3-, A2- and B6-CH), 7.38 (d, 1H, *J* = 2.5, 1-CH), 7.03 (ddd, 1H, *J* = 7.6, 5.8, 1.2, D5-CH), 7.01 - 6.91 (m, 2H, B5- and C3-CH), 6.87 - 6.77 (m, 2H, A3- and C4-CH), 6.69 (dt, 1H, J = 7.4, 0.9, A4-CH), 6.20 (m, 2H, C5- and A5-CH), 4.51 (m, 2H, 8-CH_2), 3.05 (m, 2H, 17-CH_2), 2.98 (m, 6H, 10-, 11- and 15- CH_2), 2.23 (m, 2H, 14- CH_2), 2.90 (m, 2H, 9- CH_2), 2.01 (m, 2H,16- CH_2), 1.68 (br m, 4H, 12- and 13- CH_2). δ_C (101 MHz, CD_3OD, 298K) 168.31 (B2-C), 167.67 (D2-C), 161.55 (q, $^2J_{CF}$ = 34.9, $CF_3\mathbf{C}O_2^-$), 158.11 (1-C), 149.68 (C6-C), 149.25 (D6-C), 148.65 (B6- and 6-C), 148.54 (5-C), 146.09 (A-6), 144.16 (C1-C), 144.01 (A1-C), 141.57 (3-C), 138.33 (2-C), 138.25 (D4-C), 138.09 (B4-C), 131.65 (A5-C), 131.30 (C5-C), 130.06 (C4-C), 129.25 (A4-C), 124.51 (C2-C), 123.97 (A2-C), 123.16 (4-C), 123.10 (D5-C), 122.80 (B5-C), 122.43 (C3-C), 121.72 (A3-C), 119.51 (B3-C), 119.25 (D3-C), 55.31 (18-C), 48.62 (8-C), 46.81 (11-C), 46.76 (14-C), 44.44 (10- and 17-C), 36.40 (15-C), 25.98 (9-C), 23.97 (16-C), 22.83 (12-C), 22.78 (13-C). MS (ES+) 863 $[M]^+$, HRMS (ES+) $C_{40}H_{48}N_9O^{193}Ir$ requires 863.3611 found 863.3584. UV/Vis (H_2O) 258 (53061), 379 (4362).

[Ir(4-OMe-ppy)$_2$(Spm-pyta)]4TFA "Ir(papy)$_2$Spm" (135)

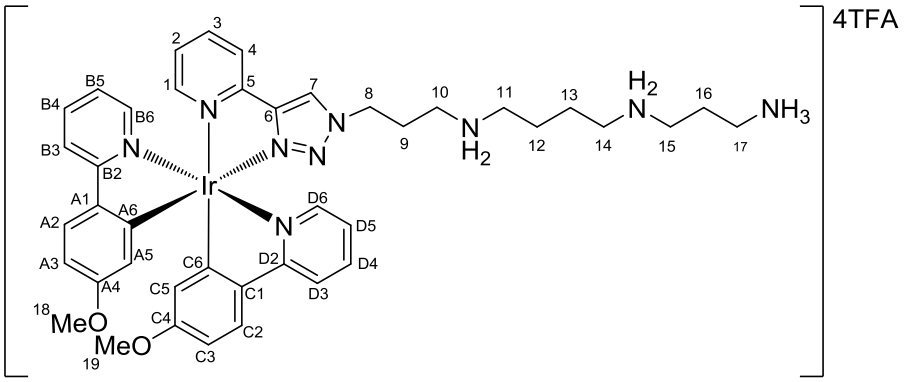

Proligand **166** (28.1 mg, 0.044 mmol) and $[Ir(papy)_2Cl]_2$ (22.9 mg, 0.021 mmol) were reacted according to general method E. The isolated complex was dissolved in 4M TFA (3 mL) and stirred for 30 minutes and then volatiles were removed. The residue was taken up in water, filtered through a nylon membrane and purified by RP-HPLC using method A, t_R = 24.97 mins. Combined fractions were lyophilised to give the title compound as a yellow, hygroscopic solid, (27.3 mg, 48 %). δ_H (400 MHz, CD_3OD, 298K) 9.00 (s, 1H, 7-CH), 8.17 (dt, 1H, *J* = 7.7, 0.9, 4-CH), 7.98 (dt, 1H, *J* = 7.7, 1.7, 3-CH), 7.86 - 7.79 (m, 3H, 1-, B3- and D3-CH), 7.71 - 7.65 (m, 2H, B4- and D4-CH), 7.62 (d, 1H, *J* = 8.7, C2-CH), 7.58 (ddd, 1H, *J* = 1.0, 5.8 Hz, D6-CH), 7.55 (d, *J* = 8.7, A2-CH), 7.45 (ddd, 1H, *J* = 5.8, 1.3, 0.6, B6-CH), 7.31 (ddd, 1H, *J* = 7.7, 5.5, 1.3, 2-CH), 6.90 (ddd, 1H, *J* = 7.3, 5.9, 1.4, D5-CH), 6.85 (ddd, 1H, *J* = 7.3, 5.9, 1.4, B5-CH), 6.50 (dd, 1H, *J* = 8.7, 2.5, C3-CH), 6.42 (dd, 1H, *J* = 8.6, 2.5, A3-CH), 5.65 (d, 1H, *J* = 2.6, C5-CH), 5.64 (d, 1H, *J* = 2.6, A5-CH), 4.52 (m, 2H, 8-CH_2), 3.43 (s, 3H, 19-CH_3), 3.40 (s, 3H, 18-CH_3), 3.03 (m, 2H, 17-CH_2), 2.96 (m, 6H, 10-, 11- and 15-CH_2), 2.89 (m, 2H, 14-CH_2), 2.24 (m, 2H, 9-CH_2), 1.99 (m, 2H, 16-CH_2), 1.74 - 1.60 (m, 4H, 12- and 13-CH_2); δ_C (101 MHz, CD_3OD, 298K) 168.14 (B2-C), 167.52 (D2-C), 161.43 (q $^2J_{CF}$ = 29.2, $CF_3\mathbf{C}O_2^-$), 161.26 (C4-C), 160.63 (A4-C), 151.81 (C6-C), 150.14 (1-C), 149.45 (5-C), 148.95 (D6-C), 148.63 (6-C), 148.60 (A6-C), 148.36 (B6-C), 139.53 (3-C), 137.99 (D4-C), 137.89 (B4-C), 136.93 (A1-C), 136.78 (C1-C), 126.53 (2-C), 126.25 (7-C), 126.22 (C2-C), 125.57 (A2-C), 122.57 (4-C), 121.71 (D5-C), 121.45 (B5-C), 116.65 (q, $^1J_{CF}$ = 295.34, $\mathbf{C}F_3CO_2^-$), 116.43 (A5-C), 116.12 (C5-C), 107.90 (C3-C), 107.50 (A3-C), 53.79 (19-C), 53.71 (18-C), 48.79 (8-C), 46.74 (11-C), 46.83 (14-C), 44.44 (17- and 10-C), 36.41 (15-C), 25.98 (9-C), 23.96 (16-C), 22.84 (13-C), 22.78 (12-C). MS (ES+) 892 $[M]^+$, HRMS (ES+) $C_{41}H_{49}N_9O_2{}^{193}Ir$ requires 892.3638 found 892.3638. UV/Vis (H_2O) 274 (43203), 379 (6826).

[Ir(4-OMe-ppy)$_2$(4CF$_3$-Spm pyta)]4TFA "Ir(papy)$_2$4-CF$_3$-Spm" (136)

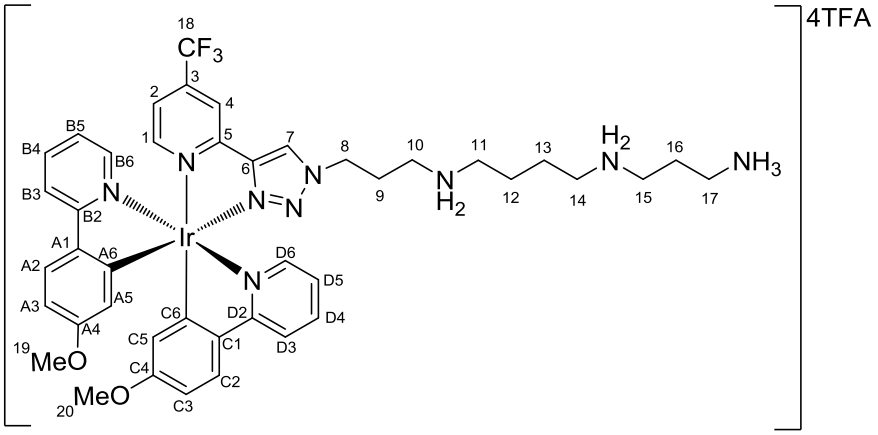

Proligand **158** (38.4 mg, 0.047 mmol) and $[Ir(papy)_2Cl]_2$ (26.9 mg, 0.025 mmol) were reacted according to general method E. The isolated complex was dissolved in 4M TFA (3 mL) and stirred for 30 minutes and then volatiles were removed. The residue was taken up in water, filtered through a nylon membrane and purified by RP-HPLC using method A, t_R = 25.60 mins. Combined fractions were lyophilised to give the title compound as a yellow, hygroscopic solid, (25.9mg, 70 %). δ_H (400 MHz, CD_3OD, 298K) 9.15 (s, 1H, 7-CH), 8.58 (m, 1H, 4-CH), 8.07 (d, 1H, *J* = 5.8, 1-CH), 7.92 - 7.80 (m, 2H B3- and D3-CH), 7.76 - 7.68 (m, 2H, B5- and D5-CH), 7.68 - 7.64 (m, 2H, 2- and C2-CH), 7.61 -7.56 (m, D6- and A2-CH), 7.52 (ddd, 1H, *J* = 5.9, 1.2, 0.6, B6-H), 6.92 (ddd, 1H, *J* = 6.6, 5.9, 1.4Hz, D5-CH), 6.88 (ddd, 1H, *J* = 7.4, 5.8, 1.3, B5-CH), 6.55 (dd, 1H, *J* = 8.9, 2.6, C3-CH), 6.46 (dd, 1H, *J* = 8.6, 2.6 Hz, A3-CH), 5.66 (d, 1H, *J* = 2.5, 1H, C5-CH), 5.61 (d, 1H, *J* = 2.5, A5-CH), 4.56 (m, 2H, 8-CH_2), 3.46 (s, 3H, 20-CH_3), 3.43 (s, 3H, 19-CH_3,) 3.03 (m, 2H, 17- CH_2), 2.96 (m, 6H, 10-, 11- and 14- CH_2), 2.90 (m, 2H, 15- CH_2), 2.26 (m, 2H, 9- CH_2), 1.99 (m, 2H, 16- CH_2), 1.68 (m, 4H, 12- and 3- CH_2); δ_C (101 MHz, CD_3OD, 298K) 167.91 (B2-C), 167.45 (D2-C), 161.61 (C4-C), 161.11, (q, $^2J_{CF}$ = 34.6, $CF_3\mathbf{C}O_2^-$), 160.66 (A4-C), 151.65 (1-C), 151.17 (5-C), 149.84 (D6-C), 149.05 (B6-C), 148.86 (q, $^2J_{CF}$ = 345.2, 3-C) (B6-C), 147.79 (6-C), 147.69 (A6-C), 140.43 (C6-C), 138.24 (D4-C), 138.06 (B4-C), 136.78 and 136.73 (A1- and C1-C) 127.50 (7-C), 126.35 (2-C), 125.60 (C2-C), 125.54 (A2-C), 121.87 (D5-C), 121.61 (B5-C), 118.93 (4-C), 118.65 (D3- and B3-C), 117.52 (q, $^1J_{CF}$ = 265.3, 18-CF_3), 116.65 (q, $^1J_{CF}$ = 289.63, $\mathbf{C}F_3CO_2^-$), 116.32 (A5-C), 116.20 (C5-C), 108.13 (C3-C), 107.67 (A3-C), 53.83 (20-C), 53,75 (19-C), 48.95 (8-C), 46.81 (11- and 14-C), 44.46 (17- and 10-C), 36.36 (15-C), 25.96 (9-C), 23.97 (16-C), 22.82 (12-C), 22.76 (13-C); δ_F (376

MHz, CD_3OD, 298K) δ = -66.44 (Ar-CF_3), -76.94 -76.80 (TFA). MS (ES+) 959 $[M]^+$, HRMS (ES^+) $C_{42}H_{48}N_9O_2F_3{}^{193}Ir$ requires 960.3512 found 960.3508. UV/Vis (H_2O) 271 (39749), 374 (7056).

7.8: Platinum complexes

Pt[(Put-pyta)Cl_2] "$PtCl_2$-Put" (1)

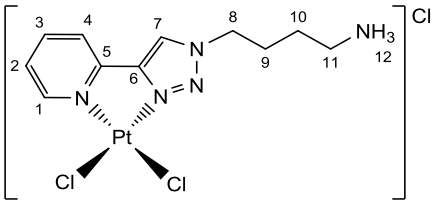

Proligand **137** (62.1 mg, 0.098 mmol) and [$Pt(DMSO)_2Cl_2$] (42.4 mg, 0.100 mmol) were dissolved in nitromethane (5 mL) and heated to reflux overnight under a nitrogen atmosphere in the dark. Solvent was evaporated under reduced pressure. The solid was purified by flash column chromatography eluting with 10 % MeOH in DCM and combined fractions were evaporated to dryness. The complex was stirred in 4M TFA in DCM for 2h. Solvent was removed under reduced pressure and passed through a short column containing Dowex 1X2 chloride resin, eluent was lyophilised to yield the title compound as a yellow solid (23.4 mg, 46 %). NMR $δ_H$ (400 MHz, d_6-DMSO, 298 K) 9.37 (br d, 1H, 1-C*H*), 9.30 (s, 1H, 7-C*H*), 8.38 (dt, ^3J = 8.0, ^4J = 1.5, 1H, 3-C*H*), 7.86 (br d, 1H, ^3J = 7.6, 4-C*H*), 7.79 (br s, 3H, 12-NH_3), 7.75 (ddd, 1H, ^3J = 7.4, 6.2, ^4J = 1.4, 2-CH), 4.63 (t, 1H, *J* = 7.0, 8-CH_2), 2.86 (m, 2H, 11-CH_2), 1.99 (m, 2H, 9-CH_2), 1.60 (m, 2H, 10-CH_2); MS (ES+) 484 $[M+H]^+$.

Pt[(Spm-pyta)Cl_2] "$PtCl_2$-Spm" (182)

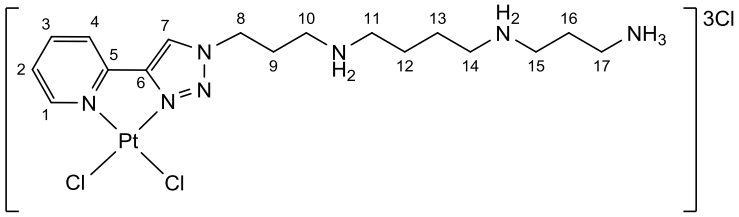

Method 1 (via $Pt(DMSO)_2Cl_2$)

Proligand **138** (62.1 mg, 0.093 mmol) and $[Pt(DMSO)_2Cl_2]$ (42.4 mg, 0.100 mmol) were dissolved in nitromethane (5 mL) and heated to reflux overnight under a nitrogen atmosphere in the dark. Solvent was evaporated under reduced pressure. The solid was purified by flash column chromatography eluting with 10 % MeOH in DCM and combined fractions were evaporated to dryness. The complex was stirred in 4M TFA in DCM for 2h. Solvent was removed under reduced pressure and passed through a short column containing Dowex 1X2 chloride resin, eluent was lyophilised to yield the title compound as a yellow solid (37.7 mg, 56 %).

Method 2 (via $K_2[PtCl_2]$)

Proligand **166** (58.8 mg, 0.093 mmol) and $K_2[PtCl_4]$ (39.3 mg, 0.095 mmol) were dissolved in nitromethane (5 mL) and heated to reflux overnight under a nitrogen atmosphere in the dark. Solvent was evaporated under reduced pressure. The solid was purified by flash column chromatography eluting with 10 % MeOH in DCM and combined fractions were evaporated to dryness. The complex was stirred in 4M TFA in DCM for 2h. Solvent was removed under reduced pressure and passed through a short column containing Dowex 1X2 chloride resin, eluent was lyophilised to yield the title compound as a yellow solid (26.6 mg, 41 %).

NMR δ_H (400 MHz, D_20, 298 K) δ = 8.84 (s, 1H, 7-CH), 8.67 (d, 1H, *J* = 5.1, 1-CH), 7.99 (t, 1H, *J* = 7.4, 3-CH), 7.86 (d, 1H, *J* = 7.4, 4-CH), 7.32 (t, 1H, *J* = 6.7, 2-CH), 4.66 (m, 2H, 8-CH_2), 3.31 (m, 2H, 17-CH_2), 3.26 - 3.12 (m, 8H, 10-, 11-, 14- and 15- CH_2), 2.54 (m, 2H, 9-CH_2), 2.14 (m, 2H, 16- CH_2), 1.85 (m, 4H, 12- and 13-CH_2). MS (ES+) 598 $[M+H]^+$, HRMS (ES^+) $C_{17}H_{30}N_7{}^{35}Cl^{195}Pt$ requires 598.1573 found 598.1683 (isotope pattern match).

7.9: Peptide Synthesis

GGK-Ir (185)

The peptide was synthesised manually using Fmoc-SPPS on a 0.15 mmol scale using Rink amide resin (0.47 mmol/g). Resin was swollen prior to use in DMF for 1 h. The Fmoc protecting group was removed with a solution of 20 % piperidine (v/v) in DMF for 15 mins at room temperature. Resin was thoroughly washed with DMF (3 x 3 mL), MeOH (3 x 3 mL) and DCM (3 x 3 mL) then excess solvent removed under a positive pressure of nitrogen. Fmoc-Gly-OH (5 eq with respect to the resin) was dissolved in DMF to give a working concentration of 0.05M. HCTU (5 eq) and DIEA as a 2M solution in NMP, (10 eq) were added and the solution was left to react for 10 minutes. The activated amino acid was added to the resin and agitated gently for 1 h at room temperature, after which the resin was filtered and washed with DMF (3 x 3 mL), MeOH (3 x 3 mL) and DCM (3 x 3 mL). The resin was capped with 20 % (v/v) acetic anhydride in DMF for 1 h at room temperature, after which the resin was thoroughly washed (*as previously described). 20 % piperidine (v/v) in DMF was then used to remove the Fmoc protecting group (15 mins at room temperature), then the resin was washed*. These steps were repeated using Fmoc-Gly-OH and Fmoc-Lys(Boc)-OH to complete the sequence, and the terminal Fmoc group was cleaved with 20 % piperidine in DMF. The iridium complex [4-CF_3-IrCOOH]PF_6 (**174**) (27.7 mg, 0.028 mmol) was dissolved in dry DMF to which DIC (3.6 mg, 0.028 mmol) and NHS (3.3 mg, 0.029 mmol) were added. The mixture was stirred at room temperature for 1 h, then added to 50 mg of the resin with 4 uL of Et_3N and stirred overnight at room temperature. The peptide was cleaved from the resin using 95 % TFA with 2.5 % TES and 2.5 % water (3 h at room temperature). The filtrate was dropped into ice-cold diethyl ether and centrifuged. The supernatant was decanted, and the pelleted peptide dried under a steady stream of nitrogen. The crude peptide was dissolved in 10% acetonitrile in water, filtered through a nylon membrane and purified by RP-HPLC using method A, t_R = 25.14 mins. MS (ES+) 1056 $[M]^+$, HRMS (ES+) $C_{45}H_{48}N_{11}O_4F_3{}^{193}Ir$ requires 1056.3472 found 1056.3507.

7.10: *In Vitro* Studies

General considerations.

A549 cells (ATCC) were a gift from Dr Lynne Howells, University of Leicester, A2780 and A2780-cis cells were purchased from Sigma and the polyamine deficient cell lines CHO-MG, A549-R and H157-R cells were a gift from Prof Robert Cassero, John Hopkins School of Medicine. All cell lines were cultured in RPMI 1640 medium with phenol red indicator supplemented with 10 % foetal bovine serum (Gibco). RPMI medium without phenol red was used for imaging experiments. Sterile phosphate buffered saline (PBS) without Ca^{2+} or Mg^{2+} ions was used to wash cells, and trypsin-EDTA was used to dissociate cells from the culture flask, (Gibco). Lysotracker™ and MitoTracker™, (Molecular probes, Invitrogen) were used to label cells, and slides were mounted using Prolong antifade (Invitrogen).

7.10.1: Cell Culture

(N.B. This method describes the procedure using T-75 flasks, the method may be adapted to other flask sizes by referring to table 8.1)

All reagents were prewarmed to 37 °C in a water bath prior to use. Medium was aspirated, and cells rinsed with 2 x 5 ml PBS. 3 mL 0.05 % trypsin-EDTA was added to the flask and incubated at 37 °C for 3 minutes. The flask was tapped firmly to dislodge cells, and 3 mL fresh medium was added, and the cell suspension centrifuged. The supernatant was decanted and discarded, and cells were suspended in 10 mL of fresh medium. 1 mL of this suspension was transferred to a fresh flask containing 10 mL fresh warm medium. The flask was returned to the incubator and allowed to grow to 70 % confluence before passaging (approximately 2 days).

Culture vessel	Seeding density / cells x 10^6	Cells at Confluence / cells x 10^6	Vol of TE /mL	Vol of medium / mL
4 well slide	0.05	0.2	0.5	0.7
35 mm dish	0.3	1.2	1	1.6
6 well plate	0.3	1.2	2	3 - 5
T-25 flask	0.7	2.8	3	3 - 5
T-75 flask	2.1	8.4	5	8 - 15
T-160 flask	4.6	18.4	10	15 - 30

***Table 7.1**: Cell culture conditions.*

7.10.2: Thawing frozen cells

Frozen cells were removed from liquid nitrogen storage and immediately placed into an incubator at 37 °C until just melted. Under aseptic conditions, cells were transferred into a centrifuge tube containing 10 mL prewarmed medium. Cells were centrifuged at 1500 rpm for 5 minutes, after which the supernatant was decanted into sterilising solution. The cell pellet was resuspended in 10 mL fresh, prewarmed RPMI medium containing 10 % FBS and transferred to a T75 culture flask. Cells were incubated at 37 °C in an atmosphere containing 5 % CO_2 until they reached 70 % confluence (approx. 2 days) and passaged twice before use.

7.10.3: Cryopreservation

Cells were grown to 80 % confluence in a T-160 flask prior to harvesting for cryopreservation. Cell medium was decanted, and cells washed twice with PBS. Cells were dissociated using 10 mL 0.05 % trypsin-EDTA (as described in section 8.9.1), then centrifuged at 1500 rpm for 5 minutes. The supernatant was decanted, and the cell pellet resuspended in 5 mL freezing medium (10 % tissue culture grade DMSO in FBS). 500 µL aliquots of the cell suspension were transferred into sterile cryovials. Cells were cooled for 2 h in a freezer (- 20°C) then stored at - 80 °C overnight before permanent storage in liquid nitrogen.

7.10.4: Poly-D-lysine coating glassware

5 mg sterile poly-D-lysine (average Mr 30000 -70000) was dissolved in 100 mL sterile tissue culture grade water to give a working solution of 50 µg/mL. Glass surfaces to be coated were rinsed with sterile water (x 3) prior to coating with poly-D-lysine (PDL) solution (for volumes see table below). The culture vessels were sealed and placed into an incubator at 37 °C for 30 minutes. PDL solution was aspirated and the surface washed with sterile water (x 3) and left to dry in a laminar flow hood for 2 h.

Culture vessel	Volume / µL
4 well chamber slide	700 per well
35 mm dish	400
Coverslips in 6 well plate	1000 per well

***Table 7.2**: Volume of PDL coating solution to use for different culture chambers*

7.10.5: Preparing cells for confocal microscopy

4-well chambers

Approximately 5 x 10^4 cells in 350 µL phenol red free medium were pipetted into each channel of a 4-well chamber slide. Cells were incubated at 37 °C, 5% CO_2 overnight to ensure they were attached to the slide before treatment with complexes. Complexes were dissolved in phenol red free medium to give a 2x concentration solution, (typically 50 µM for Ir complexes). 350 µL of the complex solution was added to the well and incubated for the required time. Prior to imaging, medium was aspirated and replaced with fresh medium without complexes.

35 mm dishes

Approximately 1 x 10^5 cells in 400 µL phenol red free medium were applied to the inner well of a 35 mm dish. Cells were incubated at 37 °C, 5% CO_2 for 2 h to ensure they were attached to the dish. After cells had attached, an additional 600 µL of phenol red free medium was added to the dish and returned to the incubator overnight. Complexes were dissolved in medium to give a 2x concentration solution, (typically 50 µM for Ir complexes). 1 mL of the complex solution was added to the dish and incubated for the required time. Prior to imaging, medium was aspirated and replaced with fresh buffer without complexes.

7.10.6: Fixing cells

Sterile PBS (160 mL) was heated with stirring to 60 °C, to which paraformaldehyde (8 g) was added. 1M NaOH was added dropwise until the paraformaldehyde dissolved. The solution was cooled to room temperature, filtered and the pH adjusted to approximately 7.4 using 1M HCl. The solution was stored for up to one month in the refrigerator.

Fixing cells grown on coverslips

Medium was aspirated, cells were rinsed with twice with PBS and incubated at 37 °C, 5% CO_2 with 4% formaldehyde solution for 15 minutes. The formaldehyde solution was removed and discarded in bleach. Cells were rinsed with a further 3 portions of PBS, before being mounted on microscope slide with ProLong Gold antifade mountant and sealed with clear nail varnish.

Fixing cells in chamber slides or dishes.

Medium was aspirated, cells were rinsed with twice with PBS (using the volume of medium suggested in table 7.1) and incubated at 37 °C, 5% CO_2 with 4% formaldehyde solution for 15 minutes. The formaldehyde solution was then removed and discarded. Cells were rinsed with a further 3 portions of PBS, then a final portion of PBS was left in the dish and the lid was replaced for imaging.

7.10.7: Labelling cells

8.9.7.1: MitoTracker™ Deep Red

Stock solutions were made by adding cell culture grade DMSO to 50 µg lyophillised MitoTracker™ powder to give a concentration of 1 mM. Aliquots were stored at -20°C until required. Working solutions of 250 nM were prepared using prewarmed phenol red free medium as diluent. To label cells, growth medium was aspirated and replaced with the MitoTracker™ solution. Cells were returned to the incubator for 30 minutes, after which time the MitoTracker™ solution was aspirated, and cells gently washed with PBS (x 3) before cells were fixed with PFA.

8.9.7.2: Lysotracker™ Deep Red FM

Lysotracker™ Deep Red is supplied as a 1 mM stock solution in DMSO. Recommended working concentrations are 50 – 75 nM, with an incubation time of 30 minutes to 2 h; when used at 50 nM and incubated with cells for 30 minutes.

7.10.8: Viability assay

A2780 and A2780-cis cells (Sigma) were cultured in RPMI 1640 medium supplemented with 2mM Glutamine and 10% FCS. The cisplatin resistant A2780 Cis cells were continuously cultured in the presence of 2 μM cisplatin to maintain a resistant phenotype. Following routine cell culture, cells were harvested and counted, then diluted to give a cell suspension with a concentration of 4 x 10^5 cells/mL. 50 μL of cell suspension was added to each well in a 96 well plate. 50 μL freshly prepared drug solution (2 x concentrated) in PBS were added to each well.

Cells were plated at 2 x 10^5cells/mL in 96 well plates and exposed to different concentrations of cisplatin or derivatives for 72h before assessment of viability using CellTiterGlo (Promega).

Chapter 8 References

1 C. W. Tabor and H. Tabor, *Annu. Rev. Biochem.*, 1984, **53**, 749–790.

2 A. E. Pegg and R. A. Casero, *Methods Mol. Biol.*, 2011, **720**, 3–35.

3 L. Brieger, *Weitere Untersuchungen über Ptomaine*, August Hirschwald, Berlin, 1885.

4 H. W. Dudley, M. C. Rosenheim and O. Rosenheim, *Biochem. J.*, 1924, **18**, 1263–72.

5 H. W. Dudley, O. Rosenheim and W. W. Starling, *Biochem. J.*, 1926, **20**, 1082–94.

6 H. W. Dudley, O. Rosenheim and W. W. Starling, *Biochem. J.*, 1927, **21**, 97–103.

7 E. Herbst and E. Snell, *J. Biol. Chem.*, 1949, **181**, 47–54.

8 R. G. Ham, *Biochem. Biophys. Res. Commun.*, 1963, **14**, 34–38.

9 A. E. Pegg, *Biochem. J.*, 1986, **234**, 249–62.

10 H. Tabor, *Biochemistry*, 1962, **1**, 496–501.

11 T. J. Thomas, U. B. Gunnia and T. Thomas, *J. Biol. Chem.*, 1991, **266**, 6137–6141.

12 T. Thomas, M. A. Gallo, C. M. Klinge and T. J. Thomas, *J. Steroid Biochem. Mol. Biol.*, 1995, **54**, 89–99.

13 H. S. Basu, M. C. Sturkenboom, J. G. Delcros, P. P. Csokan, J. Szollosi, B. G. Feuerstein and L. J. Marton, *Biochem. J.*, 1992, **282 (Pt 3)**, 723–7.

14 K. Igarashi and K. Kashiwagi, *Biochem. Biophys. Res. Commun.*, 2000, **271**, 559–64.

15 K. Igarashi and K. Kashiwagi, *IUBMB Life*, 2015, **67**, 160–169.

16 K. Igarashi and K. Kashiwagi, *J. Biochem.*, 2006, **139**, 11–6.

17 A. Pasini, C. M. Caldarera and E. Giordano, *Amino Acids*, 2014, **46**, 595–603.

18 M. A. Desiderio, S. Mattei, G. Biondi and M. P. Colombo, *Biochem. J.*, 1993, **293 (Pt 2)**, 475–9.

19 C. A. Hobbs, B. A. Paul and S. K. Gilmour, *Exp. Cell Res.*, 2003, **290**, 427–436.

20 P. R. Libby and J. S. Bertram, *Arch. Biochem. Biophys.*, 1980, **201**, 359–361.

21 E. Gutierrez, B.-S. Shin, C. J. Woolstenhulme, J.-R. Kim, P. Saini, A. R. Buskirk and T. E. Dever, *Mol. Cell*, 2013, **51**, 35–45.

22 M. H. Park, *J. Biochem.*, 2006, **139**, 161–9.

23 T. E. Dever, E. Gutierrez and B.-S. Shin, *Crit. Rev. Biochem. Mol. Biol.*, 2014, **49**, 413–425.

24 J. Mager, *Biochim. Biophys. Acta*, 1959, **36**, 529–531.

25 C. W. Tabor, *J. Bacteriol.*, 1962, **83**, 1101–11.

26 F. Schuber, *Biochem. J.*, 1989, **260**, 1–10.

27 R. F. Coburn, *J. Cell. Physiol.*, 2009, **221**, 544–551.

28 K. Williams, *Biochem. J.*, 1997, **325**, 289–97.

29 K. Williams, C. Romano, M. A. Dichter and P. B. Molinoff, *Life Sci.*, 1991, **48**, 469–498.

30 D. Bowie and M. L. Mayer, *Neuron*, 1995, **15**, 453–462.

31 M. Salvi and A. Toninello, *Biochim. Biophys. Acta - Biomembr.*, 2004, **1661**, 113–124.

32 K. Ahmed, S. A. Goueli and H. G. Williams-Ashman, *Adv. Enzyme Regul.*, 1986, **25**, 401–421.

33 D. F. Qi, R. C. Schatzman, G. J. Mazzei, R. S. Turner, R. L. Raynor, S. Liao and J. F. Kuo, *Biochem. J.*, 1983, **213**, 281–8.

34 S. M. Oredsson, *Biochem. Soc. Trans.*, 2004, **31**, 366–370.

35 R. M. Ray, C. Li, S. Bhattacharya, A. P. Naren and L. R. Johnson, *Cell. Signal.*, 2012, **24**, 931–42.

36 P. Savarin, A. Barbet, S. Delga, V. Joshi, L. Hamon, J. Lefevre, S. Nakib, J.-P. De Bandt, C. Moinard, P. A. Curmi and D. Pastré, *Biochem. J.*, 2010, **430**, 151–159.

37 G. Z. Sowa, D. S. Cannell, A. J. Liu and E. Reisler, *J. Phys. Chem. B*, 2006, **110**, 22279–22284.

38 K. Igarashi and K. Kashiwagi, *Int. J. Biochem. Cell Biol.*, 2010, **42**, 39–51.

39 J. L. Mitchell, G. G. Judd, A. Bareyal-Leyser and S. Y. Ling, *Biochem. J.*, 1994, **299**, 19–22.

40 S. L. Nowotarski, P. M. Woster and R. A. Casero, *Expert Rev. Mol. Med.*, 2013, **15**, e3.

41 A. E. Pegg, *Essays Biochem.*, 2009, **46**, 25–45.

42 U. K. B. Roy, N. S. Rial, K. L. Kachel and E. W. Gerner, *Mol. Carcinog.*, 2008, **47**, 538–53.

43 U. Regenass, G. Caravatti, H. Mett, J. Stanek, P. Schneider, M. Müller, A. Matter, P. Vertino and C. W. Porter, *Cancer Res.*, 1992, **52**, 4712–8.

44 D. D. Von Hoff, *Ann. Oncol. Off. J. Eur. Soc. Med. Oncol.*, 1994, **5**, 487–93.

45 R. A. Casero and A. E. Pegg, *Biochem. J.*, 2009, **421**, 323–38.

46 Y. Wang, L. Xiao, A. Thiagalingam, B. D. Nelkin and R. A. Casero, *J. Biol. Chem.*, 1998, **273**, 34623–30.

47 R. A. Casero and A. E. Pegg, *FASEB J.*, 1993, **7**, 653–61.

48 A. Pledgie-Tracy, M. Billam, A. Hacker, M. D. Sobolewski, P. M. Woster, Z. Zhang, R. A. Casero and N. E. Davidson, *Cancer Chemother. Pharmacol.*, 2010, **65**, 1067–81.

49 D. P. Dowling, L. Di Costanzo, H. A. Gennadios and D. W. Christianson, *Cell. Mol. Life Sci.*, 2008, **65**, 2039–55.

50 Y. Wang, W. Devereux, P. M. Woster, T. M. Stewart, A. Hacker and R. A. Casero, *Cancer Res.*, 2001, **61**, 5370–3.

51 J. L. A. Mitchell, T. K. Thane, J. M. Sequeira and R. Thokala, *Biochem. Soc. Trans.*, 2007, **35**, 318–321.

52 T. Uemura, D. E. Stringer, K. A. Blohm-Mangone and E. W. Gerner, *Am. J. Physiol. Gastrointest. Liver Physiol.*, 2010, **299**, G517-22.

53 K. Igarashi and K. Kashiwagi, *Plant Physiol. Biochem.*, 2010, **48**, 506–12.

54 N. Seiler and F. Dezeure, *Int. J. Biochem.*, 1990, **22**, 211–218.

55 R. J. Bergeron, Y. Feng, W. R. Weimar, J. S. McManis, H. Dimova, C. Porter, B. Raisler and O. Phanstiel, *J. Med. Chem.*, 1997, **40**, 1475–94.

56 P. H. M. Hoet and B. Nemery, *Am. J. Physiol. Cell. Mol. Physiol.*, 2000, **278**, L417–L433.

57 S. M. Aziz*, M. Yatin, D. R. Worthen, D. W. Lipke and P. A. Crooks, *J. Pharm. Biomed. Anal.*, 1998, **17**, 307–320.

58 P. M. Cullis, R. E. Green, L. Merson-Davies and N. Travis, *Chem. Biol.*, 1999, **6**, 717–729.

59 D. Soulet, L. Covassin, M. Kaouass, R. Charest-Gaudreault, M. Audette and R. Poulin, *Biochem. J.*, 2002, **367**, 347–57.

60 M. Belting, S. Persson and L. A. Fransson, *Biochem. J.*, 1999, **338 (Pt 2)**, 317–23.

61 K. Ding, S. Sandgren, K. Mani, M. Belting and L. A. Fransson, *J. Biol. Chem.*, 2001, **276**, 46779–91.

62 T. Uemura, D. E. Stringer, K. A. Blohm-Mangone and E. W. Gerner, *Am. J. Physiol. Gastrointest. Liver Physiol.*, 2010, **299**, G517-22.

63 E. YAMADA, *J. Biophys. Biochem. Cytol.*, 1955, **1**, 445–58.

64 J. Couet, M. M. Belanger, E. Roussel and M.-C. Drolet, *Adv. Drug Deliv. Rev.*, 2001, **49**, 223–235.

65 M. Bastiani and R. G. Parton, *J. Cell Sci.*, 2010, **123**, 3831–6.

66 L. Johannes, R. G. Parton, P. Bassereau and S. Mayor, *Nat. Rev. Mol. Cell Biol.*, 2015, **16**, 311–321.

67 R. M. Ray, C. Li, S. Bhattacharya, A. P. Naren and L. R. Johnson, *Cell. Signal.*, 2012, **24**, 931–42.

68 A. A. Abdulhussein and H. M. Wallace, *Amino Acids*, 2014, **46**, 655–60.

69 K. Igarashi and K. Kashiwagi, *Polyamine transport in bacteria and yeast*, 1999, vol. 344.

70 K. Kashiwagi, A. Kuraishi, H. Tomitori, A. Igarashi, K. Nishimura, A. Shirahata and K. Igarashi, *J. Biol. Chem.*, 2000, **275**, 36007–36012.

71 A. E. Busch, S. Quester, J. C. Ulzheimer, S. Waldegger, V. Gorboulev, P. Arndt, F. Lang and H. Koepsell, *J. Biol. Chem.*, 1996, **271**, 32599–604.

72 M. Sala-Rabanal, D. C. Li, G. R. Dake, H. T. Kurata, M. Inyushin, S. N. Skatchkov and C. G. Nichols, *Mol. Pharm.*, 2013, **10**, 1450–1458.

73 T. N. Winter, W. F. Elmquist and C. A. Fairbanks, *Mol. Pharm.*, 2011, **8**, 133–42.

74 M. Aouida, R. Poulin and D. Ramotar, *J. Biol. Chem.*, 2010, **285**, 6275–84.

75 J. Chadwick, M. Jones, A. E. Mercer, P. A. Stocks, S. A. Ward, B. K. Park and P. M. O'Neill, *Bioorg. Med. Chem.*, 2010, **18**, 2586–97.

76 J. S. Mcmanis, W. R. Weimar, K. M. Schreier, F. Gao, Q. Wu, J. Ortiz-ocasio, G. R. Luchetta, C. Porter and J. R. T. Vinsont, *J. Med. Chem.*, 1995, **38**, 2278–2285.

77 C. J. Bergeron, H. S. Basu, L. J. Marton, D. F. Deen, M. Pellarin and B. G. Feuerstein, *Cancer Chemother. Pharmacol.*, 1995, **36**, 411–417.

78 R. J. Bergeron, J. S. McManis, W. R. Weimar, K. Schreier, F. Gao, Q. Wu, J. Ortiz-Ocasio, G. R. Luchetta, C. Porter and J. R. T. Vinson, *J. Med. Chem.*, 1995, **38**, 2278–2285.

79 C. W. Porter, J. Miller and R. J. Bergeron, *Cancer Res.*, 1984, **44**, 126–128.

80 A. Muth, M. Madan, J. J. Archer, N. Ocampo, L. Rodriguez and O. Phanstiel, *J. Med. Chem.*, 2014, **57**, 348–63.

81 C. Wang, J. G. Delcros, J. Biggerstaff and O. Phanstiel IV, *J. Med. Chem.*, 2003, **46**, 2672–2682.

82 E. M. Sevick-Muraca, *Annu. Rev. Med.*, 2012, **63**, 217–231.

83 E. Damiani and H. M. Wallace, in *Methods in Molecular Biology*, Humana Press, New York, NY, 2018, vol. 1694, pp. 469–488.

84 T. Uemura and E. W. Gerner, in *Methods in molecular biology (Clifton, N.J.)*, 2011, vol. 720, pp. 339–348.

85 G. M. Cohen, P. M. Cullis, J. A. Hartley, A. Mather, M. C. R. Symons and R. T. Wheelhouse, *J. Chem. Soc. Chem. Commun.*, 1992, 298.

86 K. Strømgaard, L. S. Jensen and S. B. Vogensen, *Toxicon*, 2005, **45**, 249–254.

87 R. D. Verschoyle, P. Carthew, J. L. Holley, P. Cullis and G. M. Cohen, *Cancer Lett.*, 1994, **85**, 217–222.

88 O. N. Kostopoulou, E. C. Kouvela, G. E. Magoulas, T. Garnelis, I. Panagoulias, M. Rodi, G. Papadopoulos, A. Mouzaki, G. P. Dinos, D. Papaioannou and D. L. Kalpaxis, *Nucleic Acids Res.*, 2014, **42**, 8621–34.

89 X. Shu, M. Linet, R. Gao, Y. Gao, L. Brinton, F. Jin and J. Fraumeni, *Lancet*, 1987, **330**, 934–937.

90 K. Hoshino, E. Momiyama, K. Yoshida, K. Nishimura, S. Sakai, T. Toida, K. Kashiwagi and K. Igarashi, *J. Biol. Chem.*, 2005, **280**, 42801–8.

91 F. Mouawad, A. Gros, B. Rysman, C. Bal-Mahieu, C. Bertheau, S. Horn, T. Sarrazin, E. Lartigau, D. Chevalier, C. Bailly, A. Lansiaux and S. Meignan, *Oral Oncol.*, 2014, **50**, 113–9.

92 B. Thibault, E. Clement, G. Zorza, S. Meignan, J.-P. Delord, B. Couderc, C. Bailly, F. Narducci, I. Vandenberghe, A. Kruczynski, N. Guilbaud, P. Ferré and J.-P. Annereau, *Cancer Lett.*, 2016, **370**, 10–18.

93 J.-P. Annereau, V. Brel, C. Dumontet, Y. Guminski, T. Imbert, M. Broussas, S. Vispé, S. Bréand, N. Guilbaud, J.-M. Barret and C. Bailly, *Leuk. Res.*, 2010, **34**, 1383–9.

94 F. Dai, H. He, X. Xu, S. Chen, C. Wang, C. Feng, Z. Tian, H. Dong and S. Xie, *Bioorg. Chem.*, 2018, **77**, 16–24.

95 C. Fidanzi-Dugas, B. Liagre, G. Chemin, A. Perraud, C. Carrion, C.-Y. Couquet, R. Granet, V. Sol and D. Y. Léger, *Biochim. Biophys. Acta - Gen. Subj.*, 2017, **1861**, 1676–1690.

96 S. Phillips, University of Leicester, 2014.

97 D. Russell and S. H. Snyder, *Proc. Natl. Acad. Sci. U. S. A.*, 1968, **60**, 1420–7.

98 A. Tabib and U. Bachrach, *Int. J. Biochem. Cell Biol.*, 1999, **31**, 1289–1295.

99 A. C. Goodwin, C. E. Destefano Shields, S. Wu, D. L. Huso, X. Wu, T. R. Murray-Stewart, A. Hacker-Prietz, S. Rabizadeh, P. M. Woster, C. L. Sears, R. A. Casero and Jr., *Proc. Natl. Acad. Sci. U. S. A.*, 2011, **108**, 15354–9.

100 N. Babbar and R. A. Casero, *Cancer Res.*, 2006, **66**, 11125–30.

101 D. H. Russell, *Life Sci.*, 1973, **13**, 1635–1647.

102 D. H. Russell, B. G. M. Durie and S. E. Salmon, *Lancet*, 1975, **306**, 797–799.

103 B. G. M. Durie, S. E. Salmon and D. H. Russell, *Cancer Res.*, 1977, **37**, 214–221.

104 A. Arruabarrena-Aristorena, A. Zabala-Letona and A. Carracedo, .

105 D. Hanahan and R. A. Weinberg, *Cell*, 2011, **144**, 646–74.

106 H. M. Wallace, A. V Fraser and A. Hughes, *Biochem. J.*, 2003, **376**, 1–14.

107 Y. Huang, A. Pledgie, E. Rubin, L. J. Marton, P. M. Woster, S. Sukumar, R. A. Casero and N. E. Davidson, *Cancer Biol. Ther.*, 2005, **4**, 1006–13.

108 J. Y. Wang, M. J. Viar, J. Li, H. J. Shi, S. A. McCormack and L. R. Johnson, *Am. J. Physiol. Liver Physiol.*, 1997, **272**, G713–G720.

109 R. M. Newman, A. Mobascher, U. Mangold, C. Koike, S. Diah, M. Schmidt, D. Finley and B. R. Zetter, *J. Biol. Chem.*, 2004, **279**, 41504–11.

110 T. Thomas and T. J. Thomas, *Cancer Res.*, 1994, **54**, 1077–1084.

111 P. Savarin, A. Barbet, S. Delga, V. Joshi, L. Lo¨ıc Hamon, J. Lefevre, S. Nakib, J.-P. De Bandt, C. Moinard, P. A. Curmi, D. Pastré and P. Pastré, *Biochem. J*, 2010, **430**, 151–159.

112 L. Chamaillard, V. Catros-Quemener, J. G. Delcros, J. Y. Bansard, R. Havouis, D. Desury, A. Commeurec, N. Genetet and J. P. Moulinoux, *Br. J. Cancer*, 1997, **76**, 365–70.

113 Y. Zhao, D. Cheng, S. Wang and J. Zhu, *Nucleic Acids Res.*, 2014, **42**, 10385–98.

114 P. Celano, S. B. Baylin and R. A. Casero, *J. Biol. Chem.*, 1989, **264**, 8922–8927.

115 S.-H. Kim, J. Roszik, E. A. Grimm and S. Ekmekcioglu, *Front. Oncol.*, 2018, **8**, 67.

116 L. M. Coussens and Z. Werb, *Nature*, 2002, **420**, 860–7.

117 N. Babbar, T. Murray-Stewart and R. A. Casero, *Biochem. Soc. Trans.*, 2007, **35**, 300–304.

118 J. Satriano, *Amino Acids*, 2004, **26**, 321–9.

119 K. Soda, *J. Exp. Clin. Cancer Res.*, 2011, **30**, 95.

120 V. L. J. L. Thijssen, F. Poirier, L. G. Baum and A. W. Griffioen, *Blood*, 2007, **110**, 2819–27.

121 M. Takigawa, M. Enomoto, Y. Nishida, H. O. Pan, A. Kinoshita and F. Suzuki, *Cancer Res.*, 1990, **50**, 4131–8.

122 P. A. J. Muller and K. H. Vousden, *Nat. Cell Biol.*, 2013, **15**, 2–8.

123 D. L. Kramer, S. Vujcic, P. Diegelman, J. Alderfer, J. T. Miller, J. D. Black, R. J. Bergeron and C. W. Porter, *Cancer Res.*, 1999, **59**, 1278–1286.

124 S. Bhattacharya, R. M. Ray and L. R. Johnson, *Cell. Signal.*, 2009, **21**, 509–22.

125 D. Reisman, N. B. Elkind, B. Roy, J. Beamon and V. Rotter, *Cell Growth Differ.*, 1993, **4**, 57–65.

126 R. G. Schipper, L. C. Penning and A. A. J. Verhofstad, *Semin. Cancer Biol.*, 2000, **10**, 55–68.

127 N. Seiler and F. Raul, *J. Cell. Mol. Med.*, **9**, 623–42.

128 B. Brüne, P. Hartzell, P. Nicotera and S. Orrenius, *Exp. Cell Res.*, 1991, **195**, 323–329.

129 L. Li, J. N. Rao, X. Guo, L. Liu, R. Santora, B. L. Bass and J.-Y. Wang, *Am. J. Physiol. Physiol.*, 2001, **281**, C941–C953.

130 D. Marinkovic, T. Marinkovic, E. Kokai, T. Barth, P. Möller and T. Wirth, *Nucleic Acids Res.*, 2004, **32**, 5368–78.

131 T. P. Forshell, S. Rimpi and J. A. Nilsson, *Cancer Prev. Res. (Phila).*, 2010, **3**, 140–7.

132 R. Sever and J. S. Brugge, *Cold Spring Harb. Perspect. Med.*, , DOI:10.1101/cshperspect.a006098.

133 F. Stark, J. Pfannstiel, I. Klaiber and T. Raabe, *Cell. Signal.*, 2011, **23**, 876–882.

134 J. Luo, B. D. Manning and L. C. Cantley, *Cancer Cell*, 2003, **4**, 257–62.

135 V. Rajeeve, W. Pearce, M. Cascante, B. Vanhaesebroeck and P. R. Cutillas, *Biochem. J.*, 2013, **450**, 619–28.

136 J. R. Lakowicz, *Principles of fluorescence spectroscopy*, 2006.

137 V. Fernández-Moreira, F. L. Thorp-Greenwood and M. P. Coogan, *Chem. Commun. (Camb).*, 2010, **46**, 186–202.

138 K. A. King and R. J. Watts, *J. Am. Chem. Soc.*, 1987, **109**, 1589–1590.

139 M. G. Colombo, A. Hauser and H. U. Gudel, *Inorg. Chem.*, 1993, **32**, 3088–3092.

140 D. L. Davies, M. P. Lowe, K. S. Ryder, K. Singh and S. Singh, *Dalt. Trans.*, 2011, **40**, 1028–1030.

141 K. Hasan, A. K. Bansal, I. D. W. Samuel, C. Roldán-Carmona, H. J. Bolink and E. Zysman-Colman, *Sci. Rep.*, , DOI:10.1038/srep12325.

142 A. F. Henwood and E. Zysman-Colman, *Chem. Commun.*, 2017, **53**, 807–826.

143 K. K. W. Lo, J. S. W. Chan, C. K. Chung, V. W. H. Tsang and N. Zhu, *Inorganica Chim. Acta*, 2004, **357**, 3109–3118.

144 T. Huang, Q. Yu, S. Liu, W. Huang and Q. Zhao, *Dalt. Trans.*, 2018, **47**, 7628–7633.

145 Z. Yan, J. Wang, Y. Zhang, S. Zhang, J. Qiao and X. Zhang, *Chem. Commun.*, 2018, **54**, 9027–9030.

146 Y. You, S. Lee, T. Kim, K. Ohkubo, W.-S. Chae, S. Fukuzumi, G.-J. Jhon, W. Nam and S. J. Lippard, *J. Am. Chem. Soc.*, 2011, **133**, 18328–18342.

147 K. Y. Zhang, P. Gao, G. Sun, T. Zhang, X. Li, S. Liu, Q. Zhao, K. K. W. Lo and W. Huang, *J. Am. Chem. Soc.*, 2018, **140**, 7827–7834.

148 Y. Chen, T. W. Rees, L. Ji and H. Chao, *Curr. Opin. Chem. Biol.*, 2018, **43**, 51–57.

149 K. Qiu, Y. Chen, T. W. Rees, L. Ji and H. Chao, *Coord. Chem. Rev.*, 2019, 378, 66–86.

150 C.-K. Koo, L. K.-Y. So, K.-L. Wong, Y.-M. Ho, Y.-W. Lam, M. H.-W. Lam, K.-W. Cheah, C. C.-W. Cheng and W.-M. Kwok, *Chem. - A Eur. J.*, 2010, **16**, 3942–3950.

151 B. Wang, Y. Liang, H. Dong, T. Tan, B. Zhan, J. Cheng, K. K.-W. Lo, Y. W. Lam and S. H. Cheng, *ChemBioChem*, 2012, **13**, 2729–2737.

152 K. Qiu, Y. Liu, H. Huang, C. Liu, H. Zhu, Y. Chen, L. Ji, H. Chao, F.-T. Luo, H. Liu and H. Chao, *Dalt. Trans.*, 2016, **45**, 16144–16147.

153 R. Horobin, F. Rashid-Doubell, J. Pediani and G. Milligan, *Biotech. Histochem.*, 2013, **88**, 440–460.

154 J. S. Nam, M.-G. Kang, J. Kang, S.-Y. Park, S. J. C. Lee, H.-T. Kim, J. K. Seo, O.-H. Kwon, M. H. Lim, H.-W. Rhee and T.-H. Kwon, *J. Am. Chem. Soc.*, 2016, **138**, 10968–10977.

155 Q. Zhang, X. Lu, H. Wang, X. Tian, A. Wang, H. Zhou, J. Wu and Y. Tian, *Chem. Commun.*, 2018, **54**, 3771–3774.

156 K. Vellaisamy, G. Li, C.-N. Ko, H.-J. Zhong, S. Fatima, H.-Y. Kwan, C.-Y. Wong, W.-J. Kwong, W. Tan, C.-H. Leung and D.-L. Ma, *Chem. Sci.*, 2018, **9**, 1119–1125.

157 J. R. Shewring, A. J. Cankut, L. K. McKenzie, B. J. Crowston, S. W. Botchway, J. A. Weinstein, E. Edwards and M. D. Ward, *Inorg. Chem.*, 2017, **56**, 15259–15270.

158 C. Caporale and M. Massi, *Coord. Chem. Rev.*, 2018, 363, 71–91.

159 M. P. Coogan and V. Fernández-Moreira, *Chem. Commun. (Camb).*, 2014, **50**, 384–99.

160 V. Fernández-Moreira, F. L. Thorp-Greenwood, A. J. Amoroso, J. Cable, J. B. Court, V. Gray, A. J. Hayes, R. L. Jenkins, B. M. Kariuki, D. Lloyd, C. O. Millet, C. F. Williams and M. P. Coogan, *Org. Biomol. Chem.*, 2010, **8**, 3888–901.

161 K. A. Stephenson, J. Zubieta, S. R. Banerjee, M. K. Levadala, L. Taggart, L. Ryan, N. McFarlane, D. R. Boreham, K. P. Maresca, J. W. Babich and J. F. Valliant, *Bioconjug. Chem.*, 2003, **15**, 128–36.

162 K. A. Stephenson, S. R. Banerjee, T. Besanger, O. O. Sogbein, M. K. Levadala, N. McFarlane, J. A. Lemon, D. R. Boreham, K. P. Maresca, J. D. Brennan, J. W. Babich, J. Zubieta and J. F. Valliant, *J. Am. Chem. Soc.*, 2004, **126**, 8598–8599.

163 T. U. Connell, D. J. Hayne, U. Ackermann, H. J. Tochon-Danguy, J. M. White and P. S. Donnelly, *J. Labelled Comp. Radiopharm.*, 2014, **57**, 262–9.

164 Q. Nadeem, Y. Shen, M. F. Warsi, G. Nasar, M. A. Qadir and R. Alberto, *J. Label. Compd. Radiopharm.*, 2017, **60**, 394–400.

165 J. B. Arterburn, C. Corona, K. V. Rao, K. E. Carlson and J. A. Katzenellenbogen, *J. Org. Chem.*, 2003, **68**, 7063–70.

166 C. Neto, M. C. Oliveira, L. Gano, F. Marques, T. Thiemann and I. Santos, *J. Inorg. Biochem.*, 2012, **111**, 1–9.

167 S. Pesnel, Y. Guminski, A. Pillon, S. Lerondel, T. Imbert, N. Guilbaud, A. Kruczynski, C. Bailly and A. Le Pape, *Eur. J. Nucl. Med. Mol. Imaging*, 2011, **38**, 1832–1841.

168 R. G. Balasingham, M. P. Coogan, F. L. Thorp-Greenwood, G. Prencipe, L. D'Alfonso, I. Zanoni, C. Baldoli, S. Maiorana, G. D'Alfonso, E. Licandro, I. Santos, J. Zubieta and J. F.

Valliant, *Dalt. Trans.*, 2011, **40**, 11663.

169 S. Banerjee, E. B. Veale, C. M. Phelan, S. A. Murphy, G. M. Tocci, L. J. Gillespie, D. O. Frimannsson, J. M. Kelly and T. Gunnlaugsson, *Chem. Soc. Rev.*, 2013, 42, 1601–1618.

170 E. E. Langdon-Jones, N. O. Symonds, S. E. Yates, A. J. Hayes, D. Lloyd, R. Williams, S. J. Coles, P. N. Horton and S. J. A. Pope, *Inorg. Chem.*, 2014, **53**, 3788–3797.

171 E. E. Langdon-Jones, C. F. Williams, A. J. Hayes, D. Lloyd, S. J. Coles, P. N. Horton, L. M. Groves and S. J. A. Pope, *Eur. J. Inorg. Chem.*, 2017, **2017**, 5279–5287.

172 M. Obata, A. Kitamura, A. Mori, C. Kameyama, J. A. Czaplewska, R. Tanaka, I. Kinoshita, T. Kusumoto, H. Hashimoto, M. Harada, Y. Mikata, T. Funabiki and S. Yano, *Dalton Trans.*, 2008, 3292–300.

173 H. C. Bertrand, S. Clède, R. Guillot, F. Lambert and C. Policar, *Inorg. Chem.*, 2014, **53**, 6204–23.

174 W. K. C. Lo, G. S. Huff, J. R. Cubanski, A. D. W. Kennedy, C. J. McAdam, D. A. McMorran, K. C. Gordon and J. D. Crowley, *Inorg. Chem.*, 2015, **54**, 1572–87.

175 C. Orvig and M. J. Abrams, *Chem. Rev.*, 1999, **99**, 2201–4.

176 J. Minigh, in *xPharm: The Comprehensive Pharmacology Reference*, 2011, vol. 36, pp. 1–6.

177 I. Ott and R. Gust, *Arch. Pharm. (Weinheim).*, 2007, **340**, 117–126.

178 U. Ndagi, N. Mhlongo and M. E. Soliman, *Drug Des. Devel. Ther.*, 2017, **11**, 599–616.

179 P. Zhang and P. J. Sadler, *J. Organomet. Chem.*, 2017, **839**, 5–14.

180 S. Medici, M. Peana, V. M. Nurchi, J. I. Lachowicz, G. Crisponi and M. A. Zoroddu, *Coord. Chem. Rev.*, 2014, **284**, 329–350.

181 N. D. Eljack, H.-Y. M. Ma, J. Drucker, C. Shen, T. W. Hambley, E. J. New, T. Friedrich and R. J. Clarke, *Metallomics*, 2014, **6**, 2126–2133.

182 N. J. Wheate, S. Walker, G. E. Craig and R. Oun, *Dalt. Trans.*, 2010, **39**, 8113.

183 L. Kelland, *Nat. Rev. Cancer*, 2007, **7**, 573–584.

184 F. I. Raynaud, F. E. Boxall, P. M. Goddard, I. Raynaud, M. Goddard and E. Boxall, *Cancer Res.*, 1997, **3**, 2063–2074.

185 V. Novohradsky, I. Zanellato, C. Marzano, J. Pracharova, J. Kasparkova, D. Gibson, V. Gandin, D. Osella and V. Brabec, *Sci. Rep.*, 2017, **7**, 3751.

186 V. Novohradsky, L. Zerzankova, J. Stepankova, O. Vrana, R. Raveendran, D. Gibson, J. Kasparkova and V. Brabec, *J. Inorg. Biochem.*, 2014, **140**, 72–79.

187 S. Dhar and S. J. Lippard, *Proc. Natl. Acad. Sci. U. S. A.*, 2009, **106**, 22199–204.

188 E. Petruzzella, R. Sirota, I. Solazzo, V. Gandin and D. Gibson, *Chem. Sci.*, 2018, **9**, 4299–4307.

189 E. Petruzzella, J. P. Braude, J. R. Aldrich-Wright, V. Gandin and D. Gibson, *Angew. Chemie Int. Ed.*, 2017, **56**, 11539–11544.

190 M. Van Beusichem and N. Farrell, *Inorg. Chem.*, 1992, **31**, 634–639.

191 N. Farrell, *Adv. DNA Seq. Agents*, 1996, **2**, 187–216.

192 A. T. Porter, J. C. Blasko, P. D. Grimm, S. M. Reddy and H. Ragde, *CA. Cancer J. Clin.*, 1995, **45**, 165–178.

193 Z. Liu, A. Habtemariam, A. M. Pizarro, S. A. Fletcher, A. Kisova, O. Vrana, L. Salassa, P. C. A. Bruijnincx, G. J. Clarkson, V. Brabec and P. J. Sadler, *J. Med. Chem.*, 2011, **54**, 3011–3026.

194 P. Štarha, Z. Trávníček, B. Drahoš, R. Herchel and Z. Dvořák, *Appl. Organomet. Chem.*, 2018, **32**, e4246.

195 J. Li, L. Guo, Z. Tian, M. Tian, S. Zhang, K. Xu, Y. Qian and Z. Liu, *Dalt. Trans.*, 2017, **46**, 15520–15534.

196 Z. Liu, I. Romero-Canelón, A. Habtemariam, G. J. Clarkson and P. J. Sadler, *Organometallics*, 2014, **33**, 5324–5333.

197 L.-J. Liu, B. He, J. A. Miles, W. Wang, Z. Mao, W. I. Che, J.-J. Lu, X.-P. Chen, A. J. Wilson, D.-L. Ma, C.-H. Leung, L.-J. Liu, B. He, J. A. Miles, W. Wang, Z. Mao, W. I. Che, J.-J. Lu, X.-P. Chen, A. J. Wilson, D.-L. Ma, C.-H. Leung, L.-J. Liu, B. He, J. A. Miles, W. Wang, Z. Mao, W. I. Che, J.-J. Lu, X.-P. Chen, A. J. Wilson, D.-L. Ma and C.-H. Leung, *Oncotarget*, 2016, **7**, 13965–13975.

198 S. Sperandio, I. de Belle and D. E. Bredesen, *Proc. Natl. Acad. Sci. U. S. A.*, 2000, **97**, 14376–81.

199 J.-J. Cao, C.-P. Tan, M.-H. Chen, N. Wu, D.-Y. Yao, X.-G. Liu, L.-N. Ji and Z.-W. Mao, *Chem. Sci.*, 2017, **8**, 631–640.

200 J. Wang, X. Hou, Z. Zhao, H. Bo and Q. Chen, *Inorg. Chem. Commun.*, 2016, **67**, 40–43.

201 L. He, K.-N. Wang, Y. Zheng, J.-J. Cao, M.-F. Zhang, C.-P. Tan, L.-N. Ji and Z.-W. Mao, *Dalt. Trans.*, 2018, **47**, 6942–6953.

202 R. Schibli and P. A. Schubiger, *Eur. J. Nucl. Med. Mol. Imaging*, 2002, **29**, 1529–42.

203 S. Prakash, M. J. Went and P. J. Blower, *Nucl. Med. Biol.*, 1996, **23**, 543–549.

204 F. Zobi, O. Blacque, R. K. O. Sigel and R. Alberto, *Inorg. Chem.*, 2007, **46**, 10458–10460.

205 F. Zobi, B. Spingler, T. Fox and R. Alberto, *Inorg. Chem.*, 2003, **42**, 2818–2820.

206 T. A. Oriskovich, P. S. White and H. H. Thorp, *Inorg. Chem.*, 1995, **34**, 1629–1631.

207 M. Kaplanis, G. Stamatakis, V. D. Papakonstantinou, M. Paravatou-Petsotas, C. A. Demopoulos and C. A. Mitsopoulou, *J. Inorg. Biochem.*, 2014, **135**, 1–9.

208 K. M. Knopf, B. L. Murphy, S. N. Macmillan, J. M. Baskin, M. P. Barr, E. Boros and J. J. Wilson, *J. Am. Chem. Soc.*, 2017, **139**, 14302–14314.

209 V. W. W. Yam, K. K. W. Lo, K. K. Cheung and R. Y. C. Kong, *J. Chem. Soc. Chem. Commun.*, 1995, 1191–1193.

210 H. D. Stoeffler, N. B. Thornton, S. L. Temkin and K. S. Schanze, *J. Am. Chem. Soc.*, 1995, **117**, 7119–7128.

211 V. Wing-Wah Yam, K. Kam-Wing Lo, K.-K. Cheung and R. Yuen-Chong Kong, *J. Chem. Soc. Dalt. Trans.*, 1997, 2067–2072.

212 F. L. Thorp-Greenwood, M. P. Coogan, L. Mishra, N. Kumari, G. Rai and S. Saripella, *New J. Chem.*, 2012, **36**, 64–72.

213 J. Yang, J. X. Zhao, Q. Cao, L. Hao, D. Zhou, Z. Gan, L. N. Ji and Z. W. Mao, *ACS Appl. Mater. Interfaces*, 2017, **9**, 13900–13912.

214 S. Imstepf, V. Pierroz, R. Rubbiani, M. Felber, T. Fox, G. Gasser and R. Alberto, *Angew. Chem. Int. Ed. Engl.*, 2016, **55**, 2792–5.

215 J. Ho, W. Y. Lee, K. J. T. Koh, P. P. F. Lee and Y.-K. Yan, *J. Inorg. Biochem.*, 2013, **119**, 10–20.

216 E. D. Sternberg, D. Dolphin and C. Brückner, *Tetrahedron*, 2003, **54**, 4151–4202.

217 M. J. Davies, *Biochem. Biophys. Res. Commun.*, 2003, **305**, 761–70.

218 L. K. McKenzie, I. V Sazanovich, E. Baggaley, M. Bonneau, V. Guerchais, J. A. G. Williams, J. A. Weinstein and H. E. Bryant, *Chemistry*, 2017, **23**, 234–238.

219 J. Fong, K. Kasimova, Y. Arenas, P. Kaspler, S. Lazic, A. Mandel and L. Lilge, *Photochem. Photobiol. Sci.*, 2015, **14**, 2014–2023.

220 L. K. McKenzie, I. V. Sazanovich, E. Baggaley, M. Bonneau, V. Guerchais, J. A. G. Williams, J. A. Weinstein and H. E. Bryant, *Chem. - A Eur. J.*, 2017, **23**, 234–238.

221 F. Borgia, R. Giuffrida, E. Caradonna, M. Vaccaro, F. Guarneri and S. P. Cannavò, *Biomedicines*, 2018, **6**, 12.

222 F.-X. Wang, M.-H. Chen, Y.-N. Lin, H. Zhang, C.-P. Tan, L.-N. Ji and Z.-W. Mao, *ACS Appl. Mater. Interfaces*, 2017, **9**, 42471–42481.

223 S. Bonnet, *Dalt. Trans.*, 2018, **47**, 10330–10343.

224 R. E. Mahnken, M. A. Billadeau, E. P. Nikonowicz and H. Morrison, *J. Am. Chem. Soc.*, 1992, **114**, 9253–9265.

225 F. S. Mackay, J. A. Woods, P. Heringová, J. Kaspárková, A. M. Pizarro, S. A. Moggach, S. Parsons, V. Brabec and P. J. Sadler, *Proc. Natl. Acad. Sci. U. S. A.*, 2007, **104**, 20743–8.

226 M. A. Gonzales and P. K. Mascharak, *J. Inorg. Biochem.*, 2014, **133**, 127–135.

227 I. Chakraborty, J. Jimenez, W. M. C. Sameera, M. Kato and P. K. Mascharak, *Inorg. Chem.*, 2017, **56**, 2863–2873.

228 R. Vanhoutte, J. P. Kahler, S. Martin, S. van Veen and S. H. L. Verhelst, *ChemBioChem*, 2018, **19**, 907–911.

229 B. Ganem, *Acc. Chem. Res.*, 1982, **15**, 290–298.

230 R. J. Bergeron, *Acc. Chem. Res.*, 1986, **19**, 105–113.

231 V. Kuksa, R. Buchan and P. Kong Thoo Lin, *Synthesis (Stuttg).*, **2000**, 1189–1207.

232 D. Xu, K. Prasad, O. Repic and T. J. Blacklock, *Tetrahedron Lett.*, 1995, **36**, 7357–7360.

233 K. E. Krakowiak and J. S. Bradshaw, *Synth. Commun.*, 1998, **28**, 3451–3459.

234 G. E. Magoulas, T. Tsigkou, L. Skondra, M. Lamprou, P. Tsoukala, V. Kokkinogouli, E. Pantazaka, D. Papaioannou, C. M. Athanassopoulos and E. Papadimitriou, *Bioorg. Med. Chem.*, 2017, **25**, 3756–3767.

235 P. M. Cullis, L. Merson-Davies and R. Weaver, *J. Am. Chem. Soc.*, 1995, **117**, 8033–8034.

236 A. Q. Siddiqui, L. Merson-Davies and P. M. Cullis, *J. Chem. Soc. Perkin Trans. 1*, 1999, 3243–3252.

237 D. Soulet, B. Gagnon, S. Rivest, M. Audette and R. Poulin, *J. Biol. Chem.*, 2004, **279**, 49355–66.

238 J. M. Harris, E. C. Struck, M. G. Case, M. S. Paley, M. Yalpani, J. M. Van Alstine and D. E. Brooks, *J. Polym. Sci. Polym. Chem. Ed.*, 1984, **22**, 341–352.

239 D. Villemin, F. Simeon, H. Decreus and P.-A. Jaffres, *Phosphorus. Sulfur. Silicon Relat. Elem.*, 1998, **133**, 209–213.

240 P. Jansa, A. Holý, M. Dračinský, O. Baszczyňski, M. Česnek and Z. Janeba, *Green Chem.*, 2011, **13**, 882–888.

241 K. Sonogashira, Y. Tohda and N. Hagihara, *Tetrahedron Lett.*, 1975, **16**, 4467–4470.

242 R. Chinchilla and C. Nájera, *Chem. Soc. Rev.*, 2011, 40, 5084–5121.

243 H. A. Dieck and F. R. Heck, *J. Organomet. Chem.*, 1975, **93**, 259–263.

244 M. R. an der Heiden, H. Plenio, S. Immel, E. Burello, G. Rothenberg and H. C. J. Hoefsloot, *Chem. - A Eur. J.*, 2008, **14**, 2857–2866.

245 C. He, J. Ke, H. Xu and A. Lei, *Angew. Chemie Int. Ed.*, 2013, **52**, 1527–1530.

246 A. D'Amora, L. Fanfoni, D. Cozzula, N. Guidolin, E. Zangrando, F. Felluga, S. Gladiali, F. Benedetti and B. Milani, *Organometallics*, 2010, **29**, 4472–4485.

247 B. U. W. Maes, S. Verbeeck, T. Verhelst, A. Ekomié, N. Von Wolff, G. Lefèvre, E. A. Mitchell and A. Jutand, *Chem. - A Eur. J.*, 2015, **21**, 7858–7865.

248 M. Wolff, L. Munoz, A. François, C. Carrayon, A. Seridi, N. Saffon, C. Picard, B. Machura and E. Benoist, *Dalt. Trans.*, 2013, **42**, 7019–7031.

249 C. W. Tornøe, C. Christensen and M. Meldal, *J. Org. Chem.*, 2002, **67**, 3057–3064.

250 V. V Rostovtsev, L. G. Green, V. V Fokin and K. B. Sharpless, *Angew. Chem. Int. Ed. Engl.*, 2002, **41**, 2596–9.

251 B. C. Boren, S. Narayan, L. K. Rasmussen, L. Zhang, H. Zhao, Z. Lin, G. Jia and V. V. Fokin, *J. Am. Chem. Soc.*, 2008, **130**, 8923–8930.

252 H. C. Kolb, M. G. Finn and K. B. Sharpless, *Angew. Chem. Int. Ed. Engl.*, 2001, **40**, 2004–2021.

253 B. T. Worrell, J. A. Malik and V. V Fokin, *Science*, 2013, **340**, 457–60.

254 P. Appukkuttan, W. Dehaen, V. V Fokin and E. Van der Eycken, *Org. Lett.*, 2004, **6**, 4223–5.

255 N. Khoukhi, M. Vaultier and R. Carrié, *Tetrahedron*, 1987, **43**, 1811–1822.

256 F. Aguilar, R. Crebelli, A. Di Domenico, B. Dusemund, M. J. Frutos, P. Galtier, D. Gott, U. Gundert-Remy, C. Lambré, J.-C. Leblanc, O. Lindtner, P. Moldeus, A. Mortensen, P. Mosesso, D. Parent-Massin, A. Oskarsson, I. Stankovic, I. Waalkens-Berendsen, R. A. Woutersen, M. Wright, M. Younes, P. E. Boon, D. Chrysafidis, R. Gürtler, D. Marzin and P. Tobback, *EFSA J.*, 2016, **13**, 4087.

257 N. Smith, M. Greaves, R. Jewell, M. Perry, M. Stocks and J. Stonehouse, *Synlett*, 2009, **2009**, 1391–1394.

258 H. S. G. Beckmann and V. Wittmann, *Org. Lett.*, 2007, **9**, 1–4.

259 N. Fischer, E. D. Goddard-Borger, R. Greiner, T. M. Klapötke, B. W. Skelton and J. Stierstorfer, *J. Org. Chem.*, 2012, **77**, 1760–4.

260 P. T. Nyffeler, C. H. Liang, K. M. Koeller and C. H. Wong, *J. Am. Chem. Soc.*, 2002, **124**, 10773–10778.

261 M. Nonoyama, *Bull. Chem. Soc. Jpn.*, 1974, **47**, 767–768.

262 D. L. Davies, M. P. Lowe, K. S. Ryder, K. Singh and S. Singh, *Dalt. Trans.*, 2011, **40**, 1028–1030.

263 S. Lamansky, P. Djurovich, D. Murphy, F. Abdel-Razzaq, R. Kwong, I. Tsyba, M. Bortz, B. Mui, R. Bau and M. E. Thompson, *Inorg. Chem.*, 2001, **40**, 1704–1711.

264 F. A. Palocsay and J. V. Rund, *Inorg. Chem.*, 1969, **8**, 524–528.

265 M. P. Lowe, D. Parker, O. Reany, S. Aime, M. Botta, G. Castellano, E. Gianolio and R. Pagliarin, *J. Am. Chem. Soc.*, 2001, **123**, 7601–7609.

266 G. D. Kishore Kumar, D. Saenz, G. L. Lokesh and A. Natarajan, *Tetrahedron Lett.*, 2006, **47**, 6281–6284.

267 T. Uemura, D. E. Stringer, K. A. Blohm-Mangone and E. W. Gerner, *Am. J. Physiol. Gastrointest. Liver Physiol.*, 2010, **299**, G517-22.

268 K. K.-W. Lo, K. Y. Zhang and S. P.-Y. Li, *Eur. J. Inorg. Chem.*, 2011, **2011**, 3551–3568.

269 P. A. Scattergood and P. I. P. Elliott, *Dalt. Trans.*, 2017, 46, 16343–16356.

270 L. D. Ramos, H. M. da Cruz and K. P. Morelli Frin, *Photochem. Photobiol. Sci.*, 2017, **16**, 459–466.

271 B. S. Uppal, R. K. Booth, N. Ali, C. Lockwood, C. R. Rice and P. I. P. Elliott, *Dalton Trans.*, 2011, **40**, 7610–6.

272 W. K. C. Lo, G. S. Huff, J. R. Cubanski, A. D. W. Kennedy, C. J. McAdam, D. A. McMorran, K. C. Gordon and J. D. Crowley, *Inorg. Chem.*, 2015, **54**, 1572–1587.

273 Y. You and W. Nam, *Chem. Soc. Rev.*, 2012, **41**, 7061.

274 A. F. Henwood and E. Zysman-Colman, *Top. Curr. Chem.*, 2016, **374**, 36.

275 T. U. Connell, D. J. Hayne, U. Ackermann, H. J. Tochon-Danguy, J. M. White and P. S. Donnelly, *J. Label. Compd. Radiopharm.*, 2014, **57**, 262–269.

276 C. B. Anderson, A. B. S. Elliott, J. E. M. Lewis, C. J. McAdam, K. C. Gordon and J. D. Crowley, *Dalt. Trans.*, 2012, **41**, 14625–14632.

277 T. U. Connell, J. M. White, T. A. Smith and P. S. Donnelly, *Inorg. Chem.*, 2016, **55**, 2776–2790.

278 M. Mydlak, C. Bizzarri, D. Hartmann, W. Sarfert, G. Schmid and L. De Cola, *Adv. Funct. Mater.*, 2010, **20**, 1812–1820.

279 M. Felici, P. Contreras-Carballada, J. M. M. Smits, R. J. M. Nolte, R. M. Williams, L. De

Cola, M. C. Feiters, M. Felici, P. Contreras-Carballada, J. M. M. Smits, R. J. M. Nolte, R. M. Williams, L. De Cola and M. C. Feiters, *Molecules*, 2010, **15**, 2039–2059.

280 E. Orselli, R. Q. Albuquerque, P. M. Fransen, R. Fröhlich, H. M. Janssen and L. De Cola, *J. Mater. Chem.*, 2008, **18**, 4579.

281 P. A. Scattergood, A. Sinopoli and P. I. P. Elliott, *Coord. Chem. Rev.*, 2017, 350, 136–154.

282 J. C. Deaton and F. N. Castellano, in *Iridium(III) in Optoelectronic and Photonics Applications*, John Wiley & Sons, Ltd, Chichester, UK, 2017, pp. 1–69.

283 U. Resch-Genger and K. Rurack, *Pure Appl. Chem.*, 2013, **85**, 2005–2013.

284 C. Würth, M. Grabolle, J. Pauli, M. Spieles and U. Resch-Genger, *Nat. Protoc.*, 2013, **8**, 1535–1550.

285 D. F. Eaton, *Pure Appl. Chem.*, 1988, **60**, 1107–1114.

286 Y. Sun and C. Turro, *Inorg. Chem.*, 2010, **49**, 5025–5032.

287 E. Abbe, *Arch. für Mikroskopische Anat.*, 1873, **9**, 413–418.

288 *Patent*, 1957.

289 S. Inoué, in *Handbook of Biological Confocal Microscopy*, Springer US, Boston, MA, 1995, pp. 1–17.

290 B. W. Graf and S. A. Boppart, in *Methods in molecular biology (Clifton, N.J.)*, 2010, vol. 591, pp. 211–227.

291 M. Göppert-Mayer, *Ann. Phys.*, 2009, **18**, 466–479.

292 W. Denk, J. H. Strickler and W. W. Webb, *Science*, 1990, **248**, 73–6.

293 W. BECKER, *J. Microsc.*, 2012, **247**, 119–136.

294 E. Ruska, *Rev. Mod. Phys.*, 1987, **59**, 627–638.

295 P. de Boer, J. P. Hoogenboom and B. N. G. Giepmans, *Nat. Methods*, 2015, **12**, 503–513.

296 J. R. Shewring, A. J. Cankut, L. K. McKenzie, B. J. Crowston, S. W. Botchway, J. A. Weinstein, E. Edwards and M. D. Ward, *Inorg. Chem.*, 2017, **56**, 15259–15270.

297 R. Van Noorden, *Nature*, 2014, **514**, 286–286.

298 S. W. Hell and J. Wichmann, *Opt. Lett.*, 1994, **19**, 780–2.

299 T. A. Klar, S. Jakobs, M. Dyba, A. Egner and S. W. Hell, *Proc. Natl. Acad. Sci. U. S. A.*, 2000, **97**, 8206–10.

300 E. Betzig, G. H. Patterson, R. Sougrat, O. W. Lindwasser, S. Olenych, J. S. Bonifacino, M. W. Davidson, J. Lippincott-Schwartz and H. F. Hess, *Science (80-.).*, 2006, **313**, 1642–1645.

301 M. J. Rust, M. Bates and X. Zhuang, *Nat. Methods*, 2006, **3**, 793–796.

302 H. Shroff, C. G. Galbraith, J. A. Galbraith, H. White, J. Gillette, S. Olenych, M. W. Davidson and E. Betzig, *Proc. Natl. Acad. Sci. U. S. A.*, 2007, **104**, 20308–13.

303 T. Ha and P. Tinnefeld, *Annu. Rev. Phys. Chem.*, 2012, **63**, 595–617.

304 G. Drummen, Drummen and G. P. C., *Molecules*, 2012, **17**, 14067–14090.

305 T. Ha and P. Tinnefeld, *Annu. Rev. Phys. Chem.*, 2012, **63**, 595–617.

306 D. Axelrod, D. E. Koppel, J. Schlessinger, E. Elson and W. W. Webb, *Biophys. J.*, 1976, **16**, 1055–1069.

307 G. A. Dunn, I. M. Dobbie, J. Monypenny, M. R. Holt and D. Zicha, *J. Microsc.*, 2002, **205**, 109–112.

308 N. B. Cole, C. L. Smith, N. Sciaky, M. Terasaki, M. Edidin and J. Lippincott-Schwartz, *Science*, 1996, **273**, 797–801.

309 Y. Guminski, M. Grousseaud, S. Cugnasse, V. Brel, J.-P. Annereau, S. Vispé, N. Guilbaud, J.-M. Barret, C. Bailly and T. Imbert, *Bioorg. Med. Chem. Lett.*, 2009, **19**, 2474–7.

310 K. Y. Zhang, H.-W. Liu, M.-C. Tang, A. W.-T. Choi, N. Zhu, X.-G. Wei, K.-C. Lau and K. K.-W. Lo, *Inorg. Chem.*, 2015, **54**, 6582–6593.

311 J. S. Nam, M.-G. Kang, J. Kang, S.-Y. Park, S. J. C. Lee, H.-T. Kim, J. K. Seo, O.-H. Kwon, M. H. Lim, H.-W. Rhee and T.-H. Kwon, *J. Am. Chem. Soc.*, 2016, **138**, 10968–10977.

312 S.-F. Huang, H.-Z. Sun, G.-G. Shan, F.-S. Li, Q.-Y. Zeng, K.-Y. Zhao and Z.-M. Su, *Dye. Pigment.*, 2017, **139**, 524–532.

313 K. Y. Zhang and K. K.-W. Lo, *Inorg. Chem.*, 2009, **48**, 6011–6025.

314 K. Qiu, H. Huang, B. Liu, Y. Liu, Z. Huang, Y. Chen, L. Ji and H. Chao, *ACS Appl. Mater. Interfaces*, 2016, **8**, 12702–12710.

315 S. Moromizato, Y. Hisamatsu, T. Suzuki, Y. Matsuo, R. Abe and S. Aoki, *Inorg. Chem.*, 2012, **51**, 12697–12706.

316 F.-X. Wang, M.-H. Chen, X.-Y. Hu, R.-R. Ye, C.-P. Tan, L.-N. Ji and Z.-W. Mao, *Sci. Rep.*, 2016, **6**, 38954.

317 T. L. Byers and A. E. Pegg, *Am J Physiol Cell Physiol*, 1989, **257**, C545-553.

318 M. Belting, K. Mani, M. Jönsson, F. Cheng, S. Sandgren, S. Jonsson, K. Ding, J.-G. Delcros and L.-A. Fransson, *J. Biol. Chem.*, 2003, **278**, 47181–9.

319 D. Shao, L. Xiao, H.-C. Ha and R. A. Casero, *J. Cell. Physiol.*, 1996, **166**, 43–48.

320 Y. K. Yoon, H. P. Kim, S. W. Han, D. Y. Oh, S. A. Im, Y. J. Bang and T. Y. Kim, *Mol. Carcinog.*, 2010, **49**, 353–362.

321 T. Mosmann, *J. Immunol. Methods*, 1983, **65**, 55–63.

322 R. D. Petty, L. A. Sutherland, E. M. Hunter and I. A. Cree, *J. Biolumin. Chemilumin.*, 1995, **10**, 29–34.

323 L. Kangas, M. Grönroos and A. L. Nieminen, *Med. Biol.*, 1984, **62**, 338–43.

324 D.-W. Shen, L. M. Pouliot, M. D. Hall and M. M. Gottesman, *Pharmacol. Rev.*, 2012, **64**, 706–21.

325 S. Ishida, J. Lee, D. J. Thiele and I. Herskowitz, *Proc. Natl. Acad. Sci. U. S. A.*, 2002, **99**, 14298–302.

326 S. B. Howell, R. Safaei, C. A. Larson and M. J. Sailor, *Mol. Pharmacol.*, 2010, **77**, 887–894.

327 R. Tummala, P. Diegelman, S. M. Fiuza, L. A. E. Batista de Carvalho, M. P. M. Marques, D.

L. Kramer, K. Clark, S. Vujcic, C. W. Porter and L. Pendyala, *Oncol. Rep.*, 2010, **24**, 15–24.

328 K. M. Knopf, B. L. Murphy, S. N. Macmillan, J. M. Baskin, M. P. Barr, E. Boros and J. J. Wilson, *J. Am. Chem. Soc.*, 2017, **139**, 14302–14314.

329 K. Yin Zhang, K. Ka-Shun Tso, M. W. Louie, H. W. Liu and K. Kam-Wing Lo, *Organometallics*, 2013, **32**, 5098–5102.

330 K. Yin Zhang, K. Ka-Shun Tso, M. W. Louie, H. W. Liu and K. Kam-Wing Lo, *Organometallics*, 2013, **32**, 5098–5102.

331 K. O. Piletska, K. V. Domasevitch, A. N. Gusev, V. F. Shul'gin and A. V. Shtemenko, *Polyhedron*, 2015, **102**, 699–704.

332 E. Orselli, G. S. Kottas, A. E. Konradsson, P. Coppo, R. Fröhlich, L. De Cola, A. Van Dijken, M. Büchel and H. Börner, *Inorg. Chem.*, 2007, **46**, 11082–11093.

333 K. A. Phillips, T. M. Stonelake, P. N. Horton, S. J. Coles, A. J. Hallett, S. P. O'Kell, J. M. Beames and S. J. A. Pope, *J. Organomet. Chem.*, 2019, **893**, 11–20.

334 T. Yoshihara, M. Hosaka, M. Terata, K. Ichikawa, S. Murayama, A. Tanaka, M. Mori, H. Itabashi, T. Takeuchi and S. Tobita, *Anal. Chem.*, 2015, **87**, 2710–2717.

335 Y. Hirakawa, K. Mizukami, T. Yoshihara, I. Takahashi, P. Khulan, T. Honda, I. Mimura, T. Tanaka, S. Tobita and M. Nangaku, *Kidney Int.*, 2018, **93**, 1483–1489.

336 S. Takizawa, K. Shimada, Y. Sato and S. Murata, *Inorg. Chem.*, 2014, **53**, 2983–2995.

337 S. Tobita and T. Yoshihara, *Curr. Opin. Chem. Biol.*, 2016, **33**, 39–45.

338 G. T. Potter, G. C. Jayson, G. J. Miller and J. M. Gardiner, *J. Org. Chem.*, 2016, **81**, 3443–3446.

Chapter 9 : Appendices

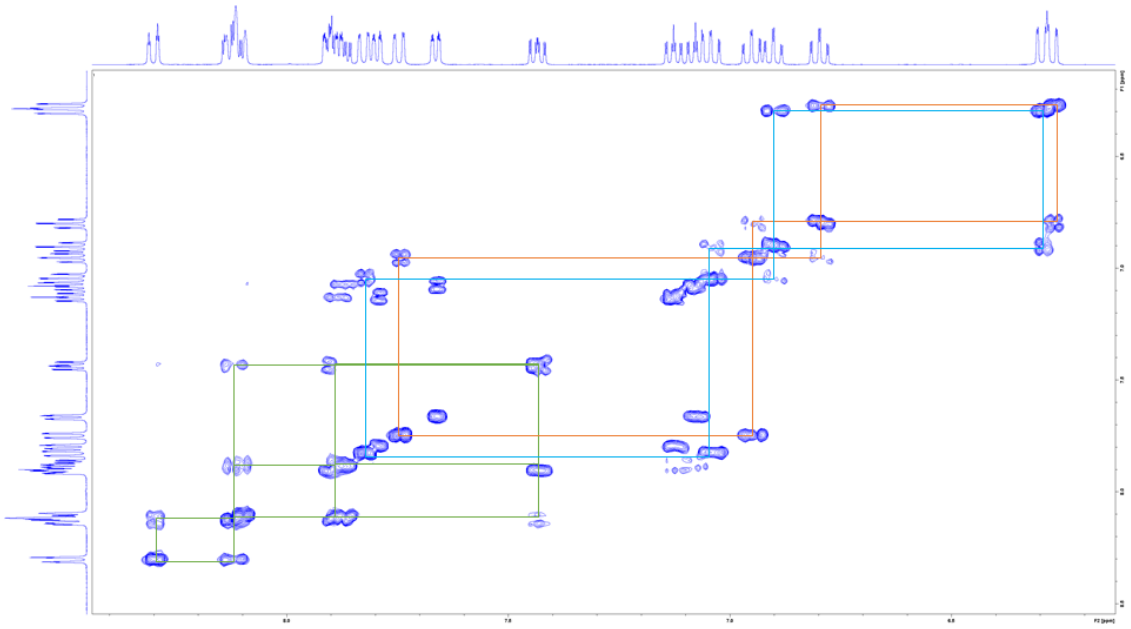

***Figure 9.1**: 1H COSY spectrum (400 MHz, CD_3OD, 298 K) of $Ir(ppy)_2Spm$-pyta (**134**) showing correlations of the ppy phenyl ring systems (in blue and orange) and the pyta pyridine ring (in green).*

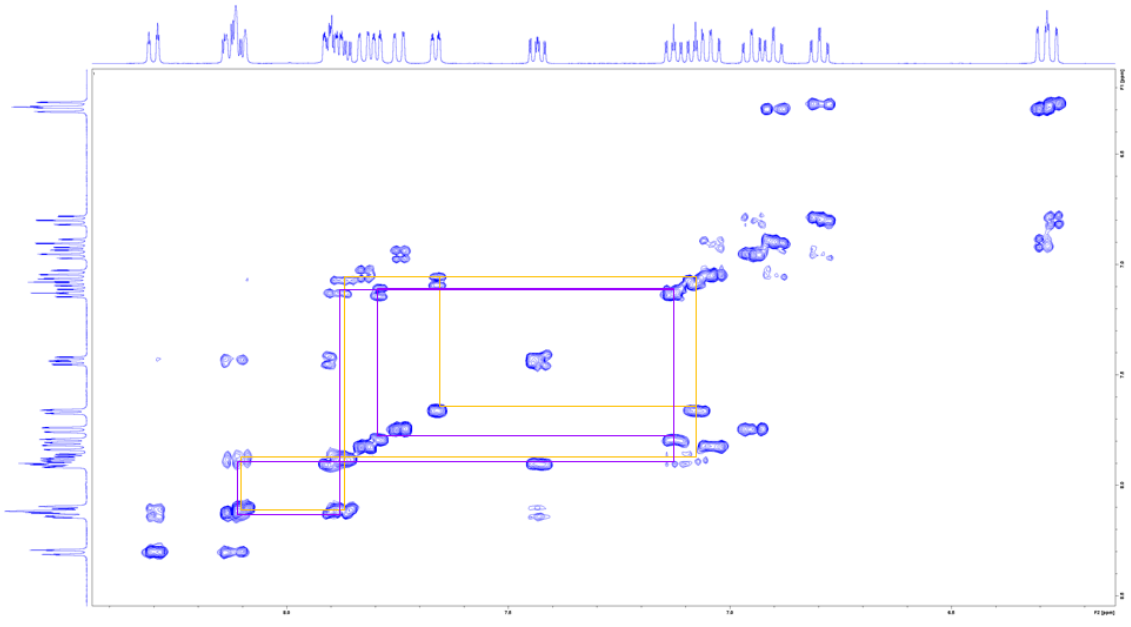

***Figure 9.2:** 1H COSY spectrum (400 MHz, CD_3OD, 298 K) of $Ir(ppy)_2Spm$-pyta (**134**) showing correlations of the ppy phenyl rings.*

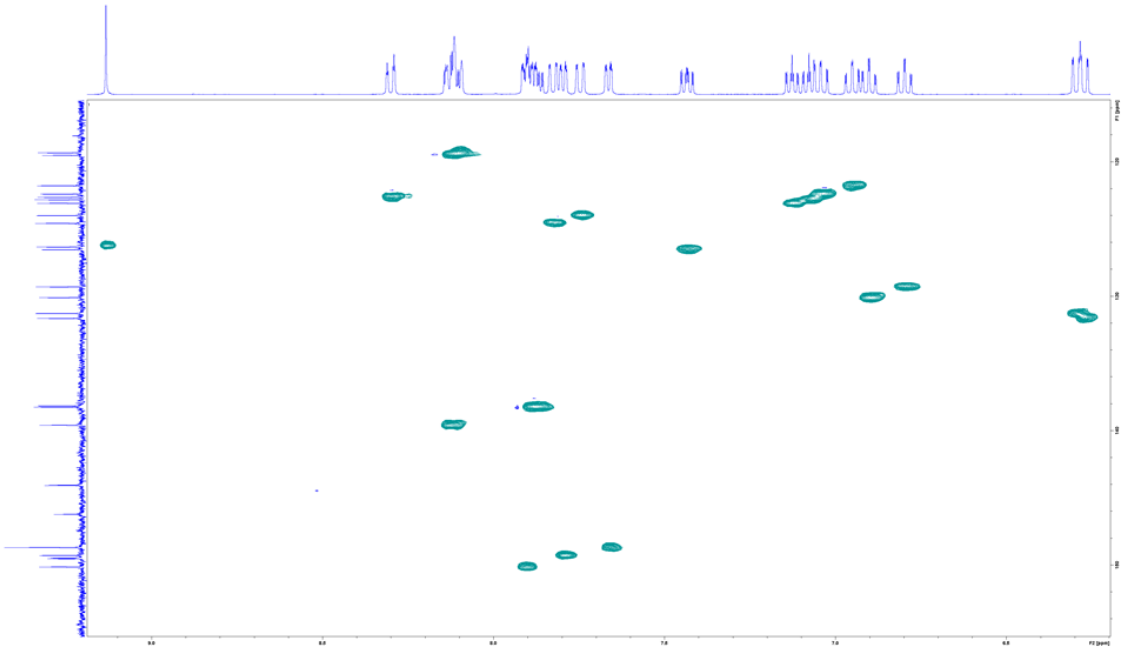

***Figure 9.3**: HSQC spectrum (400 MHz, CD_3OD, 298 K) of Ir(ppy)2Spm-pyta (**134**).*

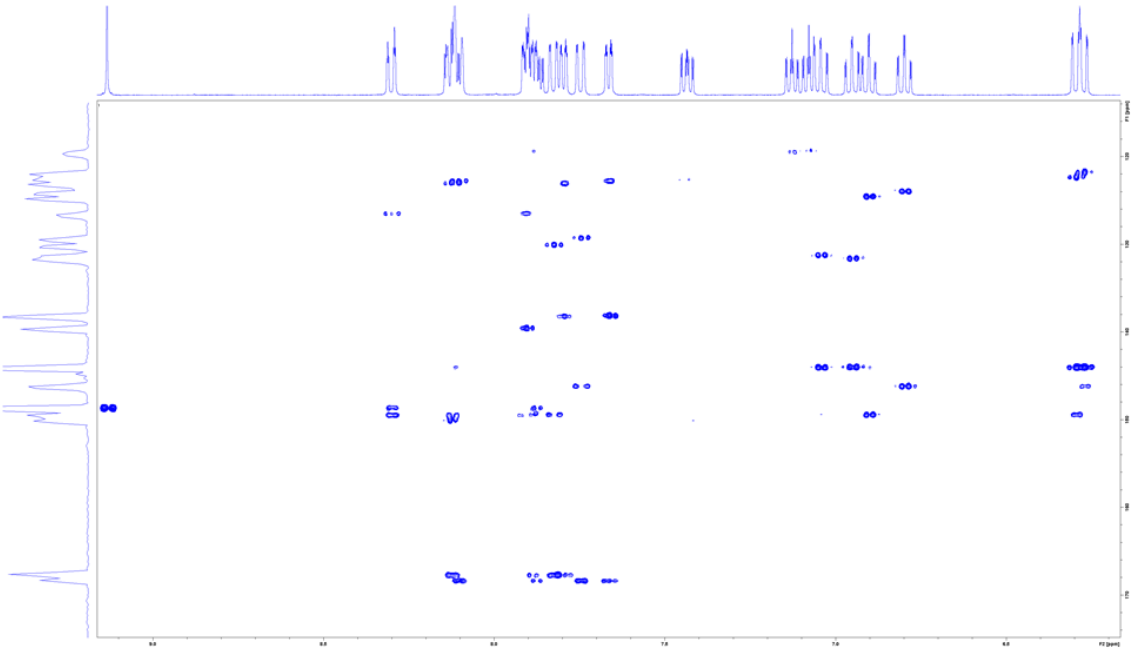

***Figure 9.4**: HMBC spectrum (400 MHz, CD_3OD, 298 K) of Ir(ppy)2Spm-pyta (**134**).*

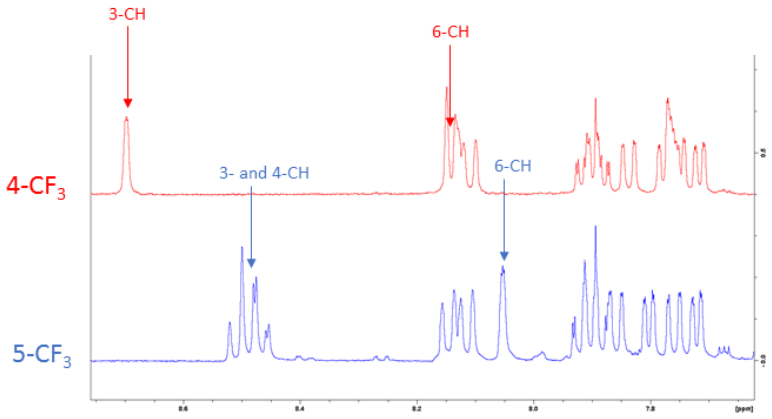

***Figure 9.5**: Comparison of the : 1H NMR spectra (400 MHz, CD_3OD, 298 K) of 5- and 4- CF_3 substituted $Ir(ppy)_2pyta$ complexes (**146** and **147**).*

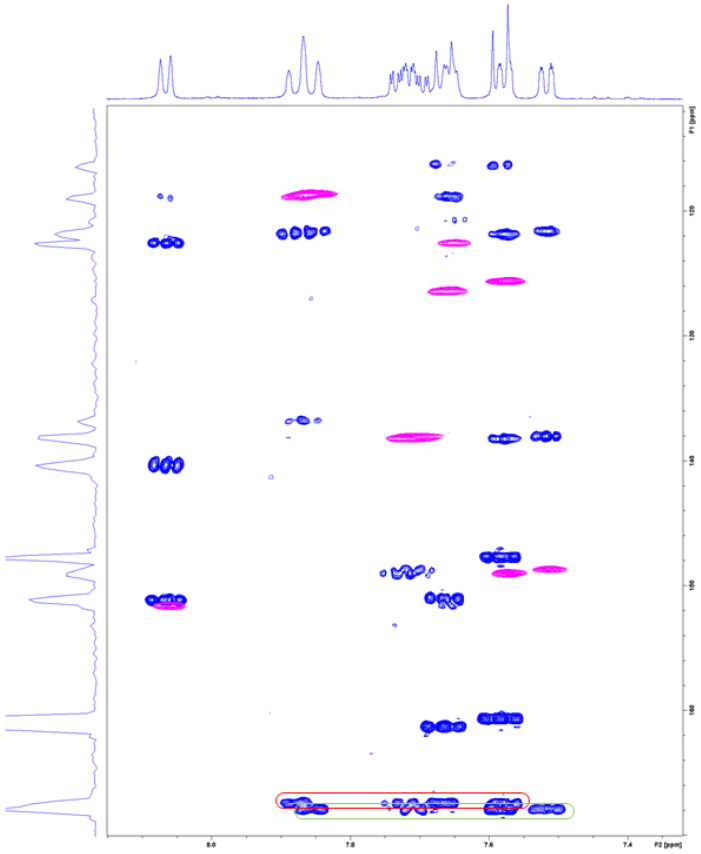

***Figure 9.6:** Superimposed HSQC and HMBC NMR spectra (400 MHz, CD_3OD, 298 K), of complex **149**, ($Ir(papy)_2$4-CF_3-pyta) showing key peaks used to identify connectivity of each phenyl and pyridyl ring system.*

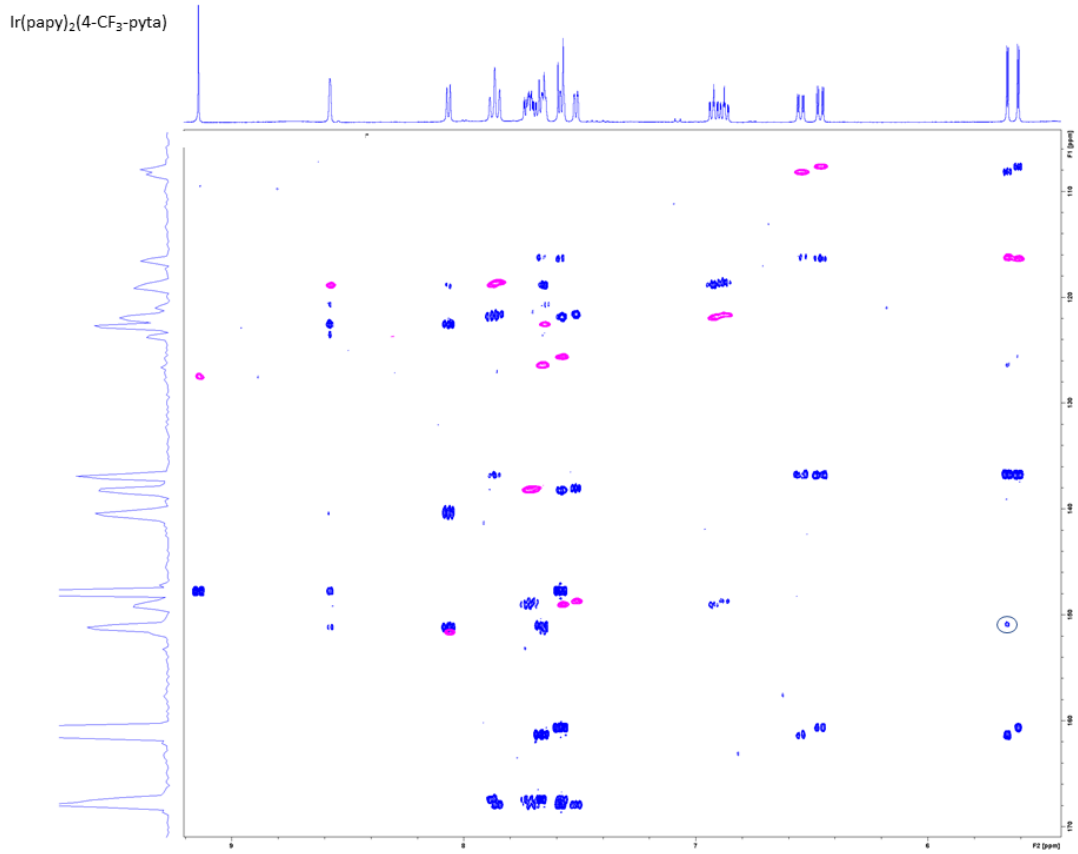

***Figure 9.7**: Superimposed HSQC and HMBC NMR spectra (400 MHz, CD_3OD, 298 K) of complex **149**, ($Ir(papy)_2$4-CF_3-pyta) showing key peak used to identify connectivity to the pyta ligand.*